The quest for broad-spectrum coronavirus inhibitors

Lima Leite Ogando, N.S.

The quest for broad-spectrum coronavirus inhibitors

Natacha Sofia Lima Leite Ogando

Colophon

PhD Thesis, Leiden University, 2021

Thesis The research described in this thesis was performed at Leiden University Medical Center, Department of Medical Microbiology, Leiden, The Netherlands

Funding The work presented in this thesis was supported by the Marie Skłodowska-Curie ETN European Training Network 'ANTIVIRALS' (EU grant agreement no. 642434) , the SCORE project (EU Horizon 2020 program, grant agreement 101003627), and the #wakeuptocorona crowdfunding initiative of the Leiden University Fund (LUF) and LUMC Bontius Foundation.

Layout Natacha S. Ogando

Cover Natacha S. Ogando

Print Proefschriftmaken (www.proefschriftmaken.nl)

ISBN/EAN 978-94-6423-444-2

The quest for broad-spectrum coronavirus inhibitors

Proefschrift

ter verkrijging van

de graad van doctor aan de Universiteit Leiden,

op gezag van rector magnificus prof. dr. ir. H. Bijl,

volgens besluit van het college voor promoties

te verdedigen op dinsdag 12 oktober 2021

klokke 15:00

door

Natacha Sofia Lima Leite Ogando

geboren te Sé Porto, Portugal

In 1988

Promotor: Prof. dr. E. J. Snijder

Co-promotor: Dr. C. C. Posthuma

Leden van de promotiecommissie:

Prof. dr. M. Roestenberg

Prof. dr. A.E. Gorbalenya

Prof. dr. F.J.M. van Kuppeveld (Universiteit Utrecht)

Prof. dr. B. Coutard (Universiteit van Aix-Marseille, Frankrijk)

“We keep moving forward, opening new doors, and doing new things, because we’re curious and curiosity keeps leading us down new paths.”

(Walt Disney; in the ending credits of the movie “Meet the Robinsons”, 2007)

Table of contents

CHAPTER I

General introduction and Thesis outline

GENERAL INTRODUCTION

The word “quest” originates from the Latin *quaerere*. Since the 1300s, *quaerere* has evolved with the Medieval Latin, Middle English and Modern English languages and gave rise to the words “question” (from the imperative *quaere*) and “quest” (from the past participle *quaesitus*). In the 15th century, “quest” was applied as “a search”, and later was defined as “a number of events that occur to find” or ”achieve something in the end”. Many are the examples of quests featured by writers such as John Ronald Reuel Tolkien in his master piece “The Lord of the Rings”. A quest has several components: a subject, a means to an end, challenges along the journey, at least one motif and an aim. Here, I will describe all the elements of my scientific pursuit, “The quest for broad-spectrum coronavirus inhibitors”, step by step, but not in a particular order.

The discovery of Coronaviruses - Walk the line (of history)

In 1996, the order *Nidovirales* was established by the International Committee on Taxonomy of viruses (ICTV) and united two families of positive-strand RNA viruses infecting vertebrates, *Coronaviridae* and *Arteriviridae* [1, 2]. Through the years, in particular following the advent of next-generation sequencing technologies and the conversion of virus taxonomy into a classification based on phylogeny, the nidovirus order expanded to (currently) 14 different families with many of them including only a single species [3]. The name ‘nidovirus’ was derived from a prominent common feature, the production of a nested set of subgenomic (sg) RNAs that share identical 5’- and/or 3’-terminal sequences with the genomic RNA (nest in Latin is *nidus*) [4, 5]. Additional common properties of nidoviruses are: a positive-sense, non-segmented linear RNA genome with a size ranging from 12-41 kb packaged into enveloped virions; a conserved genome organization including a large replicase in the 5’-proximal part of the genome; the presence of seven replicase domains that are critical to control genome replication and expression of viral proteins, 3C-like protease (3CLpro), RNA dependent RNA polymerase (RdRp), nidovirus RdRp-associated nucleotidyltransferase (NiRAN), Zinc-binding domain (ZBD), Helicase (HEL), transmembrane domain 2 (TM2) and transmembrane domain 3 (TM3); a conserved genome expression mechanism involving production of at least one subgenomic mRNA species; and the encoding of large polyproteins, with the one of the planarian secretory cell nidovirus (PSCNV) being exceptionally long, 13,556 amino acids (aa) [1, 5-10]. On the other hand, between the nidovirus families there are major differences in number, type and sizes of the viral proteins that make up the virus particle, resulting in variations in the morphology of the nucleocapsid and virion: spherical [11], rod-shaped [12], spherular with crown-like projections [13] or elongated rod-shaped [11, 14].

The best-studied family within the order *Nidovirales* is the family *Coronaviridae*, which currently incorporates the subfamilies *Letovirinae* and *Orthocoronavirinae*. The latter subfamily consists of four genera: *Alphacoronavirus*, *Betacoronavirus*, *Gammacoronavirus* and *Deltacoronavirus* [15]. Some coronavirus (CoV) are important pathogens that challenge human public health or are of veterinary and economic interest. Whereas alphacoronaviruses and betacoronaviruses seem to exclusively target human and other mammalian host species, such as pigs, bats, cats and dogs, gammacoronaviruses and deltacoronaviruses infect a broader range of hosts including avian species (Table 1).

The first report on CoVs dates back to 1931, when a new acute and fatal respiratory disease in 2- and 3-year old chicken was described [16]. Only later, the microorganism responsible for this pathology, avian infectious bronchitis virus (IBV), was isolated using filtration techniques [17] and imaged by electron microscopy [13]. Subsequently, transmissible gastroenteritis virus (TGEV; [18]) in 1946 and murine hepatitis virus (MHV; [19]) in 1949 were isolated from swine and mice, respectively. The first full-length CoV genome sequence was reported for IBV in 1987 [20], followed by that of MHV a few years later [21, 22]. In 1965, the first human coronavirus, named B814, was isolated from a typical case of common cold and was cultured in human embryonic tracheal and nasal organ cultures [23]. A year later, a strain called 229E was isolated from students of Chicago University and cultured in human embryo kidney cells [24]. In order to study these viruses and fulfill Koch's postulates, healthy adult volunteers were inoculated with cultured virus. Curiously, in these studies the number of paper handkerchiefs used per day was taken as a marker for CoV infection [25]. In 1967, human CoV (HCoV) OC43 (OC stands for organ culture) was isolated from patient material and used for the first serological studies where serum of OC43-infected patients was tested for antibodies that would cross react with HCoV-229E [26]. Later, in 2003, HCoV-NL63 was isolated from a 7-months old child in the Netherlands (NL) [27, 28] and in 2004 HCoV-HKU1 was discovered in a 71-year-old Chinese man admitted to a Hong Kong (HK) hospital [29].

To date, only seven CoVs infecting humans have been characterized in cell culture, and all belong to the *Alphacoronavirus* and *Betacoronavirus* genera (Table 1). Four endemic human CoVs (HCoVs 229E, NL63, OC43 and HKU1) circulate annually and are associated with mild respiratory illness (common cold; [30]). The other three are zoonotic and (highly) pathogenic CoVs that emerged in the last two decades and were/are the cause of severe outbreaks in the human population: in 2002-2003, severe acute respiratory syndrome CoV (SARS-CoV; [31]) emerged in South East Asia; since 2012, and probably earlier too, Middle East respiratory syndrome CoV (MERS-CoV; [32, 33]) is causing small outbreaks in the Middle East; and severe

acute respiratory syndrome CoV 2 (SARS-CoV-2) is the cause of the on-going COVID-19 pandemic and was first discovered in December 2019 in Wuhan, China [34]).

Based on the abundant occurrence of related viruses in bat species, bats have been suspected to be a major CoV reservoir that has possibly given rise to several of the CoVs found in humans [35, 36]. In contrast, the detection of HCoV-HKU1 in rodents, the description of close relatives of HCoV-OC43 in rodents and phylogenetic analysis of their lineage (βCoV lineage A) suggest rodents as the possible original reservoir of these two viruses [37-40]. In general, peridomestic mammals may serve as intermediate hosts of CoVs. In the case of MERS-CoV and SARS-CoV, transmission to humans was attributed to an intermediate host species: dromedary camels [41] and civet cats [42], respectively. The origin of SARS-CoV-2 is still under investigation: it remains unclear if the epidemic was derived from a direct spillover of the virus from bats, or if a yet unknown intermediate host played a role [43]. Since 2003, the risk of another zoonotic CoV spillover into the human population has been predicted based (among others) on surveillance studies in which several SARS-like and MERS-like CoV sequences were extracted from bats [44, 45]. For example, the SARS-CoV-2 genome presents a high level of sequence identity (96.3%) with the bat CoV RaTG13 [46], while MERS-CoV is closely related to the bat CoVs HKU4 and HKU5 [33]. Various mutations and recombination events in different regions of the genomes of these zoonotic CoVs, mainly involving structural and accessory proteins, were identified and hypothesized to have contributed to cross-species transmission (reviewed in [47]). Furthermore, several human-related, pathogen-related and climate/environment-related factors (presumably) have promoted the dissemination of these viruses among humans worldwide. These factors include the easy access to international air travel and the exponential growth of the human population [48].

The recurrent spillovers of CoVs from animal reservoirs to humans, along with their ability to cross species barriers, indicate that future zoonotic transmission events are likely. This threat stresses the importance of studying zoonotic CoVs to understand their replication, control their spread and, ultimately, be prepared for the possible emergence of a new zoonotic virus. Preparedness for large outbreaks requires investments in prevention and surveillance programs, the development of vaccine platforms and the quest for broad-spectrum antiviral drugs. The main goal of this thesis project was to find inhibitors of CoV replication/infection. During the first 4 years of my work, the focus was on studying MERS-CoV, until February 2020, when SARS-CoV-2 took the world by surprise.

Table 1- Coronavirus and associated diseases

		Virus		Host	Respiratory inf.	Enteric inf.	Hepatitis	Neurologic inf.
Genus	α	canine coronavirus	CCoV	Dog		X		
		feline enteric coronavirus	FeCoV	Cat		X		
		feline infectious peritonitis virus	FIPV	Cat	X	X	X	X
		human coronavirus 229E	HCoV-229E	Human	X			
		human coronavirus NL63	HCoV-NL63	Human	X			
		porcine epidemic diarrhea virus	PEDV	Pig		X		X
		rabbit coronavirus	RbCoV	Rabbit		X		
		transmissible gastroenteritis virus	TGEV	Pig	X	X		
	β	bovine coronavirus	BCoV	Bovine	X	X		
		equine coronavirus	EqCoV	Horse		X		X
		human coronavirus HKU1	HCoV-HKU1	Human	X			
		human coronavirus OC43	HCoV-OC43	Human	X			
		Middle East respiratory syndrome coronavirus	MERS-CoV	Camels, Human	X	X		
		mouse hepatitis virus	MHV	Mouse, rat	X	X	X	X
		porcine hemagglutinating encephalomyelitis virus	PHEV	Pig	X	X		X
		rat coronavirus	RCoV	Rat	X			
		severe acute respiratory syndrome coronavirus	SARS-CoV	Civet cat, Human	X	X		
		severe acute respiratory syndrome coronavirus 2	SARS-CoV-2	Human, other?	X	X		
	γ	infectious bronchitis virus	IBV	Chicken	X		X	
		Beluga whale coronavirus	BwCoV	Beluga whale	X			
		pheasant coronavirus	PhCoV	Pheasant		X		
		turkey coronavirus	TuCoV	Turkey	X	X		
	δ	porcine deltacoronavirus	PDCoV	Pig		X		

Inf., infection; Adapted from [49]. α, *Alphacoronavirus;* β, *Betacoronavirus;* γ, *Gammacoronavirus;* δ, *Deltacoronavirus*

Human diseases caused by Coronavirus infection – (Keep) Five feet apart

Transmission of HCoVs to susceptible hosts occurs mainly by the respiratory or fecal-oral routes of infection, with viral replication starting in epithelial cells. Each year, endemic HCoVs (229E, NL63, OC43 and HKU1) account for 15-30% of upper respiratory tract infections, mainly in the common high-risk groups: newborns, elderly people and individuals presenting comorbidities (reviewed in [50] and [49]). All of these HCoVs are distributed globally. Most of the infected people develop mild disease with common cold-like symptoms including fever, headache, malaise, sore throat and cough. The peak of disease symptoms is observed 3 to 4 days after infection and symptoms last for 7 days on average, up to a maximum of 18 days. Furthermore, HCoV-NL63 has been associated with acute laryngotracheitis (croup [51]). To date, only a few life-threatening infections with HCoV-229E have been reported in immunocompromised patients [52, 53]. Based on natural infections and studies involving healthy volunteers, reinfection with these HCoVs is relatively frequent, which suggests that infection does not provide long-lasting protective immunity [54].

In general, the pathogenic zoonotic CoVs, SARS-CoV, SARS-CoV-2 and MERS-CoV, can cause more severe disease that can progress into an atypical pneumonia after infecting the upper and lower respiratory tract. These CoVs have an incubation period from 1 up to 14 days with symptoms appearing typically between 3 and 7 days after infection. Patients present cold/flu-like symptoms, sometimes also with gastrointestinal manifestations such as watery diarrhea. The 2003 SARS-CoV outbreak was largely confined to Southern China and the Hong Kong region, affecting around eight thousand people (confirmed cases) with a fatality rate of about 10% [31, 55]. Early on, via international air travel, this pathogen was spread to 29 countries and regions. Human-to-human transmissions of SARS-CoV was mainly associated with hospital and household settings and human super-spreading events [56]. During this outbreak (in 2002/2003), the low number of asymptomatic infections facilitated the identification and isolation of infected people, followed by the implementation of strict quarantine protocols. Consequently, eradication of SARS-CoV was achieved in a relatively short period of time, around 6-8 months after the first cases [57]. SARS-CoV infection caused lower respiratory tract disease that could evolve into an atypical pneumonia characterized by acute respiratory distress syndrome (ARDS), which results in alveolar damage and oedema in the patients' lungs. Health follow-up of SARS-CoV survivors showed that after one year there was a fully recovery from the physical illness [58]. However, many patients reported concentration problems and psychological limitations.

During the on-going pandemic of SARS-CoV-2, more than 140 million cases (until April 2021) have been reported worldwide, with a case fatality rate of around 2%, corresponding to more

than 2.6 million deaths. The high number of asymptomatic SARS-CoV-2 infections (estimated to be one third of the cases) and easy human-to-human transmission through droplets and aerosols facilitated the spread of the virus (reviewed in [59]). Severity and prevalence of disease has been correlated with gender, age, obesity and the presence of other risk factors such as diabetes, immune- and hormonal-associated diseases [60-63]. The majority of people infected with SARS-CoV-2 develop mild or moderate coronavirus disease 2019 (COVID-19). Approximately, 5% of the COVID-19 patients experience severe symptoms, resulting in a need for intensive care including supplemental oxygen and mechanical ventilation. Strikingly, loss of smell (anosmia) is reported in many cases and it is due to viral replication in the sinonasal epithelium [64, 65]. For both SARS-CoV-2 and SARS-CoV infections, a triphasic pattern of disease is observed starting with mild respiratory and systemic symptoms (reviewed .in [60]). The second phase is characterized by viral pneumonia derived from increased viral replication, and a third phase by the onset of an immunological and inflammatory response [66, 67]. Interestingly, children apparently are less susceptible to develop COVID-19, although in rare cases a multisystem inflammatory syndrome similar to Kawasaki disease was reported [68]. Still under evaluation, neurologic manifestations including impaired consciousness and acute cerebrovascular disease have been reported after patients recover from severe COVID-19, which raises some concerns about the future, taking into account the number of people affected by this disease. Furthermore, recent studies have described that, following asymptomatic or symptomatic SARS-CoV-2 infection, some individuals have prolonged/persistent symptoms for months, like fatigue, breathlessness, myalgia and insomnia, together referred to as Long COVID [69-71].

In 2012, MERS-CoV was first isolated from a 60-year-old patient from Saudi Arabia [32]. Since then, a series of small(er) outbreaks resulted in more than 2,500 confirmed cases with a 36% fatality rate. Concomitant with the seroprevalence of MERS-CoV antibodies in human populations across Saudi Arabian provinces, evidence of widespread infections of dromedary camels and asymptomatic human infections project a higher number of infections in humans than the actual known epidemiology [72-75]. Frequently, in 50-89% of MERS patients, mechanical ventilation is needed [76]. Inefficient human-to-human transmission and association of virus spread to close interactions between human and camels, crowded health care settings or closed family households contributed to a lower incidence of MERS-CoV cases (reviewed on [77]). Until now, 27 countries reported cases of MERS-CoV-infection, with 80% of infections occurring in Saudi Arabia. Although clinical features closely resemble those of SARS-CoV infections, many patients developed acute renal failure [32], ARDS, septic shock and multiorgan failure, resulting in higher fatality rate for MERS [78, 79].

In most cases, human CoV infections are not readily identified by clinical diagnosis because they usually cause mild disease and their symptoms cannot be easily distinguished from other respiratory tract infections (like those with rhinoviruses and influenza viruses). Early diagnosis has been critical to isolate infected people and avoid viral spread, during outbreaks and the on-going pandemic. Current diagnostics tools include detection of nucleic acid, antibodies or viral antigens and virus isolation/culture. Differential diagnosis through real time qPCR has been the standard method (with great sensitivity) to detect different CoVs in nasal swabs, saliva, gargling, sputum, deep tracheal aspirate, bronchoalveolar lavage or stool samples, and distinguish them from other respiratory pathogens (reviewed in [80-82]). Serological tests can determine the presence of IgM and IgG anti-CoV antibodies while antigen tests can detect the presence of CoV proteins like spike and nucleocapsid. These types of tests are predominantly used as retrospective diagnosis, or for the evaluation of immune responses to therapies and vaccination or for epidemiologic studies. Virus isolation is not routinely performed for diagnostic purposes, but it is essential to obtain isolates for characterization of specific pathogens and to support the development of its research, including therapeutic agents and vaccines. It can also be performed from nasal swabs, sputum and bronchial/alveolar lavage, although not always efficiently [83]. For surveillance purposes, NGS and subsequent quick data sharing are currently a good practice between clinicians, scientists and healthcare institutions to monitor virus evolution and attempt to control spread of new variants within and between countries/continents. Given the lack of effective anti-CoV drugs and yet unclear efficacy of vaccination campaigns against SARS-CoV-2, a lot of countries continue to impose or recommend the use of face masks and implement physical distancing guidelines similar to those used during the SARS-CoV outbreak in 2002/2003. In majority of cases, more restrictive measures were adopted like local or national lockdowns, implementation of a curfew to reduce public circulation and quarantine of symptomatic people with the intention to control the spread of this infectious agent.

The Coronavirus replication cycle - The perks of being a Coronavirus

Electron microscopy shows CoVs as roundish packed particles, with a diameter of approximately 100-125 nm, that have a surface layer of club-shaped projections [13]. These spikes (S) are homotrimers of a class I fusion glycoprotein, which are embedded in the viral envelope and provide a crown-like appearance, in Latin *corona* (Fig. 1A). As for all viruses, the CoV replication cycle can be divided in different steps: attachment and entry, uncoating, translation, genome replication, assembly and release. For attachment of virions to the cells, CoVs may use both proteinaceous and sialoglycan-based receptors (reviewed in [84]). The

binding to proteinaceous receptors is mediated through a specific receptor-binding domain (RBD) exposed at the surface of S1, one of the two subunits of S.

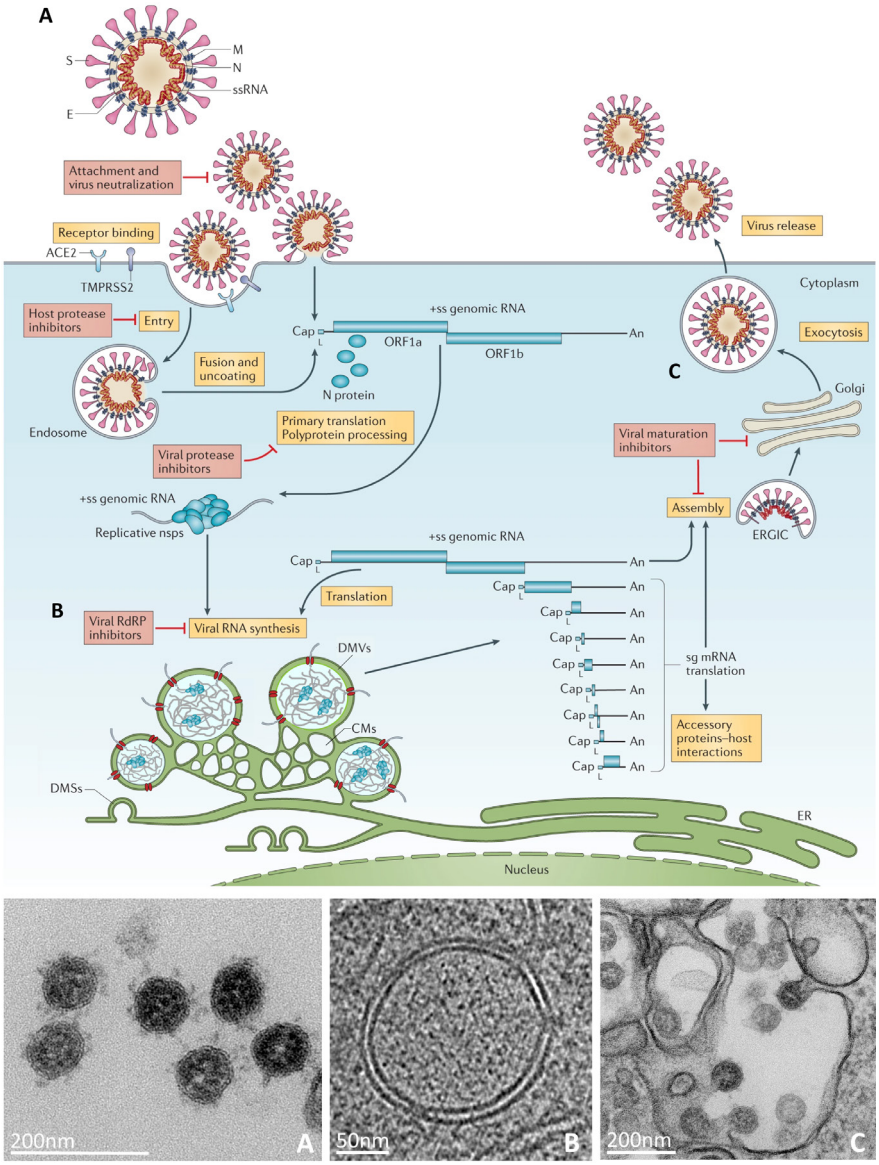

Fig. 1- Schematic representation of the coronavirus particle and replication cycle. At the bottom, electron micrographs of Vero E6 cells infected with SARS-CoV at 10 h p.i. and 8h p.i., respectively, showing extracellular viral particles (A) and virion assembly (C). Tomographic slice (7 nm thick) of a prefixed SARS-CoV-2-induced DMV with molecular pores embedded in its membrane (B). Images were used and adapted with permission from [85-87].

For several CoVs, the host cell receptor has been identified: aminopeptidase N (APN; for most of *Alphacoronavirus* such as HCoV-229E [88], TGEV [89] and porcine epidemic diarrhea virus, PEDV [90]), angiotensin-converting enzyme 2 (ACE2; for HCoV-NL63 [91], SARS-CoV [92] and SARS-CoV-2 [34, 93]), dipeptidyl peptidase 4 (DPP4; for MERS-CoV [94]) and murine carcinoembryonic antigen-related adhesion molecule (CEACAM; MHV [95]). Different CoVs from the four genera may use carbohydrates like sialic acids or sialosides as the main receptor (like BCoV and OC43), as attachment co-factors (TGEV and FeCoV) or as an alternative receptor to bind to the cells (presumably MERS-CoV) [96-99]. With the exception of MHV, the N-terminal domain of S1 mediates this interaction. The receptor specificity determines CoV tropism and, may contribute to pathogenicity taking into consideration the cellular receptor expression and tissue distribution in the host. In order to bind to the receptor, the S protein needs to be activated by proteolytic cleavage into two subunits, S1 and S2. A first cleavage occurs between S1 and S2 subunit resulting in a conformational change of the S protein, after which a second site is cleaved which is located within S2 subunit. This results in exposure of the so-called fusion peptide that mediates the fusion of the viral envelope with the host cell membrane. The timing of cleavage of the S glycoprotein is dependent on the virus species and is considered a barrier to zoonotic coronavirus transmission [100]. Both S cleavages can be accomplished by different host cellular proteases such as cathepsin L during endosomal entry, or by transmembrane protease serine (TMPRSS) 2, 6 and 11D at the plasma membrane [93, 101, 102]. For some CoVs, like MERS-CoV, S protein activation can be achieved by furin protease activity during virus egress, thus preparing the virus to infect the next cell [103, 104]. In contrast, the SARS-CoV S glycoprotein is likely cleaved only during virus entry while SARS-CoV-2 is thought to use different routes for S protein activation [105].

Following attachment, entry of viruses into the cells can occur via two pathways: release of viral genome into the cytosol after fusion of the viral envelope with the plasma membrane at the cell surface; or alternatively, virions can be taken up by endocytosis. In the latter case, acidification of the endosomal microenvironment results in fusion of viral and endosomal membrane, and subsequently, release of the viral genome into the cytoplasm (Fig. 1).

Remarkably, CoVs possess one of the largest known positive-sense RNA genomes (~30 kb) equipped with heavily structured untranslated regions at each end, a 5’ cap structure and a 3’ poly-A tail. Two thirds of the CoV genome are occupied by two large (briefly overlapping) open reading frames (ORF), ORF1a and ORF1b. The 3’-proximal third of the genome incorporates a series of ORFs that encode for the structural proteins [S protein, envelope protein (E), membrane protein (M), and nucleoprotein (N)], and the so-called accessory proteins. In the cytoplasm, ORF1a and ORF1b are translated by host ribosomes into the large replicase

polyprotein 1a (pp1a) and pp1ab. Proteins encoded by ORF1a are produced in larger quantities than those encoded by ORF1b due to a -1 programmed ribosomal frameshift that directs part of the ribosomes from ORF1a into ORF1b during genome translation [106, 107]. Subsequently, the replicase polyproteins are processed into 16, or in the case of *Gammacoronavirus* (like IBV) 15 individual non-structural proteins (nsps). This process is driven by 1 or 2 papain-like proteases (PL^{pro}) and a chymotrypsin-like or main protease ($3CL^{pro}$ or M^{pro}) that reside in nsp3 and nsp5, respectively. Most of the polyprotein cleavages are performed by M^{pro} [108]. During the three decades that have passed since the first CoV genome sequences were obtained, enzymatic activities have been attributed to various nsps (reviewed in [85, 109, 110]) such as: RNA-dependent RNA polymerase (RdRp; nsp12), helicase (HEL; nsp13), exoribonuclease (ExoN; nsp14); methyltransferases (nsp14 and nsp16) and endoribonuclease (EndoU; nsp15). ORF1a mainly encodes proteins that perform proteolytic processing (PL^{pro} and M^{pro}), provide the necessary supporting functions for formation of replication organelles (RO), and supply co-factors for RNA-synthesizing enzymes. On the other hand, ORF1b encodes nsps that perform core enzymatic functions involved in RNA synthesis, fidelity control and post-transcriptional RNA modifications. Both ORFs encode nsps with accessory functions presumably involved in interactions with the host (nsp1) and host immune evasion (PL^{pro}, ADRP, EndoU and others). The 3'ORF proteins include the structural proteins and proteins that (presumably) modulate virus-host interactions or are associated with virulence (reviewed in [111, 112]).

Most of the nsps assemble into the viral replication and transcription complex (RTC) that uses positive strand genomic RNA (gRNA) as template for the replication of new gRNA and transcription of sub-genomic (sg) mRNAs through subgenome-length negative-strand intermediates. For certain CoVs, nsp1 is involved in modulation of the host cell translation machinery by interacting with the 40S ribosomal subunit [113, 114]. Following the expression of nsps, viral ROs are formed, probably triggered by the membrane association of specific nsps that have hydrophobic domains (nsp3, nsp4, nsp6). This leads to the abundant formation of paired membranes and double-membrane vesicles (DMVs) for which the endoplasmic reticulum (ER) is the likely membrane donor [115, 116]. The double-membrane vesicles (DMVs) have been identified as the site of viral RNA synthesis [116, 117] and they may provide a suitable micro-environment for viral RNA synthesis. Recently, it was discovered that, these DMV membranes contain hexameric molecular pores, including the large nsp3 subunit, that connect the DMV interior with the cytosol, where viral mRNA translation and packaging need to occur ([87]; Fig. 1B). Although further research is needed, this suggests that the pore may serve to export viral RNA from the DMVs, and perhaps also for the import of metabolites and

protein factors needed for RNA synthesis. Hypothetically, on the one hand, these double-membrane structures may concentrate the NTPs, RNAs and proteins necessary for RNA synthesis and, on the other, hide viral replication products, such as double-stranded RNA intermediates, from detection by the host's innate immune system [116].

Similar to all + RNA viruses, CoV RNA synthesis alternates between negative and positive strand RNA, with the nsp12-RdRp being the centerpiece of the RTC, together with its co-factors nsp7 and nsp8 [118, 119]. Associated with this complex is the nsp13-helicase to unwind dsRNA in a 5' to 3' direction [120-122] and nsp14-ExoN which can excise mismatching nucleotides incorporated in the RNA chain, thus serving as a proof-reading enzyme that improves the fidelity of RNA synthesis ([123-127] and reviewed in **chapter III** of this thesis). Besides the synthesis of copies of the full-length gRNA, the transcription process involves discontinuous minus strand RNA synthesis to produce subgenome-length minus strand RNAs that serve as the template for mRNA production [128, 129]. Along the CoVs genome, there are short conserved sequences known as transcription-regulating sequences (TRSs) located upstream of most of the 3' ORFs (body TRS) and near the genome's 5'-end (leader TRS). In a unique process, during negative-strand synthesis, the viral RdRp may stop at a body TRS and reinitiate synthesis at the TRS leader of the positive sense template [129, 130]. Base-pairing between leader and body TRS determines the stability of TRS duplexes. In the end, a set of negative-strand templates that possess a poly-uridylate tail and an anti-leader sequence are produced. Most of the sg mRNAs are polycistronic and their abundance controls the amount of the corresponding structural and accessory proteins relative to each other and to the nsps [131]. Generally, only the 5'-located ORF, which is absent in the following shorter sgRNA, is translated into protein [132].

Ultimately, two essential modifications are introduced on both sg- and genomic mRNA to mimic cellular mRNAs: a cap-1 structure at the 5' end and a polyadenylate tail at the 3' end. The capping mechanism involves four sequential reactions performed by the nsp13 RNA triphosphatase (TPase; [133]); a RNA guanylyltransferase (GTase), still to be defined/ characterized; and two methyltransferases, the nsp14 (guanine-N7)-methyltransferase (N7-MTase; [134]) and the nsp16 2'-O-methyltransferase (2'O-MTase; [135]). The 5' cap-structure is important for translation as it is recognized by eIF4E, which is part of the pre-initiation complex that mediates the binding of ribosomes to mRNAs [136]. After sg mRNA synthesis, structural and accessory proteins are translated in the cytoplasm. The S, E and M proteins, the viral envelop components, are inserted into the ER and transit to the site of virion assembly, the ER-to-Golgi intermediate compartment (ERGIC). Moreover, newly made full-length gRNA is packaged by the cytosolic N protein (forming RNPs) and buds into the ERGIC. This results in

viral particles with a host cell-derived envelope containing the viral M, E and S transmembrane structural proteins ([137, 138]; Fig. 1C). In the end, virions are secreted from the infected cell by exocytosis. Recently, it has been suggested that egress of MHV and SARS-CoV-2 viral particles from intracellular environment may (also) occur via the lysosomal trafficking pathway [139]. In this way, virions may induce deacidification of lysosomes, and therefore avoid degradation of viral particles.

Coronavirus inhibitors - The good, the bad and the ugly

Despite all research efforts to create either prophylactic (prevent infection) or therapeutic (treat infection) options, there is no registered antiviral drug against any HCoV. One exception is remdesivir, which was authorized by health authorities for emergency use in United States, Japan and Europe for the treatment of hospitalized adult and pediatric patients with suspected or laboratory confirmed COVID-19. However, only modest clinical efficacy and no impact on the survival of COVID-19 patients treated with remdesivir was observed in a recent WHO trial [140] as also reported by others [141-144], probably due to the fact that the drug is usually administered to patients in a late(r) stage of serious COVID-19 disease. Based on the promising results of some small clinical trials performed in 2020, favipiravir has been also licensed for emergency use in certain countries including Japan, Russia, Malaysia, India and Thailand for the treatment of COVID-19 patients [145]. However, in some of these countries, it still remains under regulatory review.

Thus far, driven forward by the COVID-19 pandemic, vaccine development has by far outpaced antiviral drug discovery. The majority of vaccine development strategies is based on using the S protein as an antigen to elicit a potent neutralizing antibody response. Antibodies generated against S protein in recovered SARS patients are immunodominant and long-lasting in humans and animals [146-148]. Approaches previously used to develop CoV vaccines included DNA plasmids, nanoparticles, virus-like particles, viral vector preparations using adenovirus or vaccinia virus as platforms encoding viral antigens, chemically inactivated virus and live attenuated virus (reviewed in [149, 150]). In 2020, innovative solutions using mRNA technology resulted in the fast-track development and production of FDA-approved vaccines (reviewed in [151]). Although, no vaccines against SARS and MERS have been approved and most of them did not progress beyond Phase I clinical trials, four vaccines have now (March 2021) been approved for use against COVID-19 by the European Medicines Agency (EMA). These include mRNA vaccines encoding the S protein of SARS-CoV-2 from Pfizer/BioNTech and Moderna, and adenovirus-vectored vaccines encoding the SARS-CoV-2 spike glycoprotein from AstraZeneca and Janssen/Johnson & Johnson. Based on results in countries with

advanced vaccination programs, like Israel and the United Kingdom, vaccination clearly reduces severe disease and the number of hospitalizations. However, the impact on preventing transmission between humans and re-infection of vaccinated people is still under evaluation. It is also too early to know how long the protection derived from vaccination would last. Moreover, the circulation of new SARS-CoV-2 variants worldwide, carrying multiple mutations in the S protein, may affect the vaccine efficacy. Therefore, for a number of reasons, it remains critical to also pursue antiviral drug development for CoVs. Social and economic factors, including compliance by the public and cost-effective production/distribution, play an important role in successful vaccination campaigns, especially to achieve the threshold necessary to obtain herd-immunity. Moreover, not all individuals can receive vaccination such as young children, immunocompromised patients and other risk groups or vaccination may be less efficient. In such cases, antiviral therapy can provide treatment of illness at the onset of symptoms, and/or when vaccination-induced protection is incomplete. Antiviral drugs can be designed to target different viral components with broad-spectrum activity against multiple or perhaps all CoVs (pan-coronaviral activity). If already developed and tested, antiviral could be administered at the onset of a future outbreak of a novel CoV, when specific vaccines will again not be available immediately.

Strategies for anti-CoV drug design and screening

To identify potential virus inhibitors different approaches can be used: structure-based drug design using crystal structures or structure models of a target, and enzyme-based or infected cell-based high-throughput screening (HTS) campaigns. The computer-aided approaches can contribute to the (*in silico)* design of inhibitors targeting a specific site/pocket of a viral protein, and to predict its potential inhibitory effect. Understanding structure-activity relationships can help to improve compounds by designing new analogues or derivatives. Subsequently, enzymatic assays and/or infected cell-based assays should follow to obtain proof of activity. The viral load reduction assays with different read-outs, such as quantification of viral genomes or progeny titers, or measuring a reduction of virus-induced cytopathology, provide information on the antiviral activity of compounds. In parallel, cytotoxicity of compounds should be evaluated in non-infected control cells, by directly or indirectly measuring concentrations of cellular metabolites. Selection of resistant mutants obtained by culturing virus in the presence of increasing concentrations of compound can give insights about the compound's target and potential mode of action. To evaluate the specificity of an inhibitor and explore target inhibition, biochemical assays can be developed. These approaches are used to identify candidate drug compounds that can be broadly classified as

direct-acting antivirals, targeting viral components (Fig. 1), or host-directed antivirals, targeting host factors important for viral replication.

Instead of designing new molecules, particularly when a new pathogen emerges, the testing of antiviral drugs registered for use to treat other viral infections or the screening of libraries with drugs approved for treatment of other diseases can be used to try to repurpose already marketed drugs. The advantage of the repurposing approach is the available knowledge of the drug's pharmacodynamic and pharmacokinetic properties, as well as any potential side effects of the compound. Moreover, repurposing can substantially reduce the time and investments commonly required for drug design/development. Thus far, most compounds developed against RNA viruses are direct-acting antivirals. Usually, therapeutics with different targets are combined in order to minimize the chances of the rapid development of drug resistance, which is commonly associated with the high mutation rate and potential for rapid adaptation of RNA viruses [78]. When developing therapies, one should take into consideration the potential cytotoxicity or other undesirable side effects of drugs potentially affecting cellular processes/pathways. Therefore, it is critical to balance specificity and efficiency during drug development. The ultimate goal is to identify broad-spectrum inhibitors that can target multiple current and future emerging CoVs. So far, treatment options for human CoV infections and derived diseases can be divided into the following categories: neutralizing antibodies, entry/fusion inhibitors, viral protease inhibitors, inhibitors of viral RNA synthesis (predominantly nucleoside analogues), and immunomodulators.

Entry inhibitors

One step of virus cycle replication that can be targeted with inhibitors is the entry of the virus into host cells. This can be achieved, for example, by inhibiting receptor binding, preventing conformational changes in the S protein needed for fusion activity, or modulating the catalytic activity of cellular proteases that are needed to cleave the S protein to achieve successful viral entry. For this purpose, antibody-containing convalescent plasma can be obtained from recovered patients and administered to newly infected patients, which resulted in a viral load reduction. Similar results were observed for treatment of SARS-CoV [152, 153], MERS-CoV [154, 155] and SARS-CoV-2 [156] infections when corresponding convalescent plasma was used. Most of the antibodies in convalescent plasma target epitopes on the RBD region of the S1 subunit, inhibiting S binding to the cellular receptor. As the amount of antibodies that can be obtained by extraction from blood of patients (convalescent plasma) is low, the production of recombinant human antibodies was developed as an alternative, which is based on immunization of transgenic mice and the cloning of variable regions or immortalization of

convalescent S protein-specific antibody-producing B cells [157]. Besides, monoclonal antibodies obtained by immunization of animals with viral antigens have shown high specificity and neutralization activity against different CoVs (reviewed in [158]) including SARS-CoV-2 [159].

Since the emergence of SARS-CoV in 2003, some laboratories have developed strategies to block the fusion step during CoV entry by targeting the heptad repeat 1 (HR1) and HR2 domains in the S2 subunit of the S protein. These regions play a key role in viral entry, by interacting with each other to form structures (six-helical bundle) that will bring viral and cellular membranes close together for fusion [160-162]. Although, this type of compounds is still under evaluation, a recently developed lipopeptide based on this concept was demonstrated to have pan-coronaviral inhibitory activity against the pseudotypes of 6 different CoVs [160, 163].

Another strategy to interfere with viral entry is to inhibit S protein cleavage by cellular proteases at the cell surface (TMPRSS2 inhibitors) or within endosomes (Cathepsin B and L inhibitors). Camostat mesylate is a synthetic serine protease inhibitor with broad-spectrum antiviral activity against SARS-CoV, SARS-CoV-2, MERS-CoV and HCoV-229E in cell-based assays. It also improves survival of SARS-CoV-infected mice [164-167]. Interestingly, only when used in combination with E-64d, an inhibitor of cathepsin B/L, complete inhibition of SARS-CoV-2 replication was observed [164]. This suggests that different entry routes can be exploited by SARS-CoV-2 [168]. As an alternative to camostat, nafamostat has been reported to efficiently inhibit SARS-CoV-2 entry at low nanomolar concentrations in lung-derived human Calu-3 cells and is currently under evaluation in clinical trials with COVID-19 patients. Compounds that prevent endosomal acidification, like ammonium chloride and the FDA-approved anti-malaria drug chloroquine/hydroxychloroquine, were also reported to have an inhibitory effect in cell culture and/or in animal models during MERS-CoV, SARS-CoV and SARS-CoV-2 infections [169-171]. However, other reports demonstrated that the inhibitory effect of this compound against SARS-CoV-2 was dependent on the cell line used [168]. Moreover, clinical trials revealed inefficiency of hydroxychloroquine to reduce the SARS-CoV-2 load in patients, which suggests that inhibition of the endosomal pathway is dispensable for efficient viral infection (revised on [172]).

In cell culture, suramin, another well-studied antiparasitic drug, has been shown to have antiviral activity against SARS-CoV-2 [173] and other RNA viruses such as Zika virus (ZIKV), chikungunya virus and herpes simplex virus type 1 [174-178]. Follow-up studies in animal models have been started to evaluate potential routes of administration. This is one of the drug repurposing efforts made in the course of the SARS-CoV-2 pandemic [179].

Viral protease inhibitors

Most proteins that are involved in viral replication are potential targets for drug design or development. Since the ORF1a-encoded viral proteases are indispensable for CoV replication, M^{pro} and PL^{pro} have both been targeted using synthetic small-molecule or peptide-like inhibitors and natural molecules, especially after SARS-CoV-2 emerged [180]. This includes known inhibitors for other proteases and newly designed inhibitors targeting the active-site of CoV proteases or other protein regions important for folding and stability. Based on the crystal structures available [180, 181], targeted screenings have been performed with part of the compounds being further characterized using enzymatic and cell-based approaches [182-185]. Structural differences between SARS- and MERS-CoV PL^{pro} account for the narrow-spectrum activity of inhibitors, whereas the high conservation of key M^{pro} residues involved in substrate recognition promotes the activity of inhibitors against multiple CoVs, at least *in vitro* [184, 186]. However, despite the amount of *in silico* and *in vitro* screenings, only a few compounds have been tested *in* animal models. Compound GC376, an M^{pro} inhibitor, demonstrated high potency against FIPV with capacity to reverse disease progression of severely ill cats [187]. Interestingly, this compound and some of its derivatives presented high affinity to proteases of other CoVs, including MERS-CoV, SARS-CoV and SARS-CoV-2. Two other compounds, designated 11a and 11b, exhibited efficient antiviral activity against SARS-CoV-2 in cell culture and good pharmacokinetics in animal models [188, 189]. The compound PF-00835231 displayed broad antiviral activity against different CoV subgenera at low nanomolar to picomolar concentrations and is now in Phase I clinical trials for COVID-19 treatment [190, 191]. Furthermore, combinations of protease and RdRp inhibitors have been tested against SARS-CoV-2 replication to prevent viral resistance [190].

Nucleoside analogues

In order to develop broad-spectrum antivirals, targeting the virus-encoded polymerase of different RNA viruses (such as hepatitis C virus (HCV), HIV, Ebola, Zika and influenza) has been a key strategy. The compounds used mainly are nucleoside analogues that can compete with endogenous cellular nucleoside pools for being incorporated into the RNA chain during its synthesis. Subsequently, elongation of the RNA chain can be abrogated or the introduction of mismatches can lead to an enhanced mutation rate, potentially resulting in 'error catastrophe' and reduced viral fitness [126, 192, 193]. As indicated before, lately, the most-studied nucleoside analogue with anti-CoV activity has been remdesivir, a prodrug of a monophosphoramidate adenosine analogue with efficient inhibitory activity against different HCoVs and other RNA viruses in cell culture and animal models [171, 194-197]. Other drugs

like favipiravir (T-705), N4-hydroxycytidine (NHC), ribavirin, sofosbuvir, AT-511, BCX4430, mycophenolic acid and penciclovir have been explored as alternatives *in vitro*, *in vivo* and in clinical trials. However, poor efficiency and severe side effects were associated with administration of ribavirin alone or in combination with interferon (IFN) α or IFN-β when tested in SARS and MERS patients (reviewed in [78]), presumably due to the high doses used [198-200]. Therefore, no clinical trials using solely ribavirin were pursued for COVID-19 patients. Nevertheless, this compound has been used to understand mechanistic properties of the CoV RTC *in vivo* [126] and *in vitro* [123, 201]. Efficient incorporation of favipiravir into RNA chains leads to an increased mutation frequency *in vitro* as observed with influenza, coxsackie and Ebola virus [202-204]. However, high concentrations of this compound are needed to have an inhibitory effect in CoV-infected cells. Sofosbuvir, a licensed therapy against HCV since 2015, displayed a high binding energy to the SARS-CoV-2 nsp12-nsp7-nsp8 RNA polymerase complex *in vitro* and abrogated RNA chain elongation [201, 205]. Despite the poor efficiency of sofosbuvir to protect cells against SARS-CoV-2-induced cytopathic effects [206], this compound currently is under investigation in animal models and clinical trials. The newest promising antiviral drug against CoVs is NHC, with proven inhibitory effect against different RNA viruses including HCV [207], Ebola [208] and VEEV [209], and betacoronaviruses in human airway cell cultures and mice [210, 211]. As it can be administered orally, NHC is a good candidate for HCoVs and it is currently awaiting clinical trials (mentioned in [212]). The pro-drug of this compound (EIDD-2801) is expected to act as a mutagen (more selective than 5-fluoro-uracil, 5-FU) that can be used prophylactically [213] and therapeutically [214].

Other viral protein targets

Several computational docking, *in vitro* and cell-based screening assays have been performed to find potential inhibitors of CoV enzymes encoded like the helicase, exoribonuclease and methyltransferases. Helicase inhibitors, that affect the unwinding and ATPase activities have been identified through compound screening [215]. Bananins and SSYA10-001 were demonstrated to be broad-spectrum CoV inhibitors at low micromolar concentrations [120, 216, 217]. A few small molecules were reported to inhibit the SARS-CoV nsp14 and nsp16 methyltransferases, such as S-adenosyl-l-homocysteine, sinefungin and aurintricarboxylic acid *in vitro* [218-222]. When testing these compounds in infected-cell assays, low efficiency and poor specificity was observed.

So far, of the CoV structural proteins, besides the S protein, only the E protein that is involved in viral assembly, morphogenesis and virulence in animal models can be efficiently blocked by small-molecule inhibitors. Hexamethylene amiloride is hypothesized to interfere with the ion

channel activity of the E viroporin of SARS-CoV, HCoV-229E and some animal CoVs [223, 224]. In order to target this and other non-structural, structural and accessory proteins, the use of RNA interference (RNAi) that complement mRNA strands for degradation in infected cells have been studied. Still, this mechanism reveals a narrow spectrum and needs investment on optimal delivery to be approved for use in humans [225, 226].

Host factor-targeting inhibitors

Targeting host factors that can modulate viral replication, which takes place in the cytoplasm, has also been explored as a strategy for drug design/development. CoVs employ different mechanisms to disguise their presence from pathogen recognition receptors by interacting with molecules involved in innate immune responses or by compartmentalizing their activities in host-derived platforms (DMVs, RO and ERGIC). During CoV replication, type I IFN production is limited or delayed in most infected cell types, like human airway cells, fibroblasts, and organoids [227-230]. Interestingly, CoVs are susceptible to different types of IFN treatment *in vitro*. Therefore, treatment involving the direct administration of IFN or molecules that can stimulate IFN production, such as corticosteroids, poly-I:C (synthetic analogue of dsRNA) and nitazoxanide, have been widely tested. Recombinant type I IFN inhibits SARS-CoV, MERS-CoV and SARS-CoV-2 replication in infected cells [231-233], with the latter being more sensitive to lower concentrations of IFN-α [86]. Surprisingly, no significant effect on the clinical outcome was observed with IFN-α2a, IFN-α2b or IFN-β-1a treatment or in combination therapies with ribavirin or with lopinavir-ritonavir when administered to SARS or MERS patients (reviewed in [78]). Reports on poly-I:C (commercially named Hitonol) demonstrated increased survival rates when administered 21 days up to 24 hours before infection of mice with a lethal dose of SARS-CoV [234, 235]. Besides being a potential prophylactic option, it could be used as therapeutic treatment if given early in infection. Nitazoxanide is a synthetic nitrothiazolyl-salicylamide that induces IFN-α and IFN-β production with broad-spectrum activity against different RNA viruses including human and animal CoVs [171, 236, 237]. However, its activity against human-pathogenic CoVs has yet to be fully determined in animal or clinical studies [238].

Corticosteroids such as dexamethasone were widely used during the SARS-CoV epidemics. Some studies reported a positive impact on the oxygenation index [239, 240], while others claimed that it resulted in prolonged viremia and had serious side effects [241, 242]. As a consequence, it was used as a last resource in the treatment of MERS patients [79]. In the case of SARS-CoV-2, it has been considered as a standard of care for COVID-19 patients with severe disease and who required mechanical ventilation [243, 244]. Overall, despite the

potency of IFN and its modulators as antiviral agents, it needs to be taken into consideration that it can potentially contribute to prolongation of viral clearance, boosting the inflammatory response and consequently aggravate the associated (serious) side effects when administered late in infection, i.e. phase 3 of SARS-CoV-2 infection, cytokine storm.

CoVs can modify intracellular membranes, and hide their RTCs within double membrane vesicles where dsRNA replication intermediates are produced [115, 116, 245]. Compounds like K22 can inhibit DMV formation of a broad-range of human and animal CoVs in cell culture [246, 247]. Although, resistance culturing of HCoV-229E in presence of K22 resulted in the appearance of nsp6 mutations and suggested a potential mode of action of this inhibitor, no further studies were performed to pursue its mechanism of action nor was it explored further as an antiviral strategy.

THESIS OUTLINE

The main focus of this thesis is the search for compounds with an inhibitory effect against coronaviruses, mainly MERS-CoV. In **chapter I**, a brief introduction to the general molecular and structural biology of CoVs is provided. The importance of the quest for inhibitors against these agents is emphasized by describing the pathogenesis and epidemiology of CoVs.

In the past decades, a lot of the studies in our laboratory have been dedicated to the fundamental biology of virus replication, using *enzymatic and cell-based assays*. Frequently, this was done in collaboration with other departments or institutes that shared their expertise in different fields, e.g. electron microscopy, proteomics or structural biology. The emergence of SARS-CoV-2, during the course of this project, obliged us to apply our skills to investigate this new agent. Part of this teamwork was the development of a toolbox to study the replication kinetics, rapid adaptation and cytopathology of SARS-CoV-2 in cell culture, which is described in **chapter II.**

Analysis of CoV genomes highlights the conservation of certain domains and proteins across the members of this family. In order to develop broad-spectrum therapies against these viruses, it is important to understand the role of essential viral enzymes. In **chapter III**, the knowledge regarding the RTC, in particular focusing on nsp14 and its 3'-to-5' exoribonuclease (ExoN) activity is reviewed. The importance of this enzyme in CoV replication has been mainly studied using ExoN knockout mutants of MHV and SARS-CoV. ExoN mutants of both these viruses are viable but attenuated, and display an increased accumulation of mutations in their genome. Surprisingly, corresponding MERS-CoV and SARS-CoV-2 ExoN knockout mutants were not viable, as described in **chapter IV.** This highlights an unknown but critical role of nsp14 in CoV replication in cell culture, besides its presumed function as a proofreading enzyme. The nsp14 is a bi-functional replicase subunit that contains an N-terminal ExoN domain and a C-terminal N7-MTase domain. Structural analysis of SARS-CoV nsp14 demonstrated that the N7-Mtase has a structure that distinguishes this methyltransferase from the common viral and cellular Rossman-fold enzymes. In **chapter V**, residues presumably involved in N7-MTase activity were identified using computational analysis of the nsp14 structure and sequence of different β-CoVs. Next, selected residues were mutated to alanine and we evaluated the impact of these substitutions on nsp14 enzymatic activities and on viral replication/viability. This functional analysis provides insights into the pocket regions of nsp14 that could be targeted for drug design and the development of N7-MTase inhibitors.

Over the past years, many compounds were tested in our laboratory to check their potential inhibitory effect against CoVs. Different classes of inhibitors, which presumably targeted viral components directly or indirectly, affected host-virus interactions, or modulated host

responses before or during infection, were analyzed in cell-based assays. **Chapter VI** shows that 6',6'-difluoro-aristeromycin (DFA) blocks MERS-CoV replication in different human and non-human cell lines at low-micromolar concentrations. Insights into the potential mode of action of this promising nucleoside analogue were sought using cell-based assays and resistance culturing.

In **Chapter VII,** voclosporin (VCS), a host factor-targeting compound, was evaluated as a SARS-CoV-2 inhibitor. This compound can be used as a therapeutic alternative for cyclosporin A (CsA), tacrolimus (TAC) and other immunomodulators used in transplant patients, to whom certain treatments used for control of viral infection cannot be administered. In cell-based assays, VCS could inhibit SARS-CoV-2 load in Calu-3 cells more efficiently than TAC and with similar potency as CsA. This suggests that this compound should be evaluated in clinical trials for patients undergoing this type of therapy as a substitute of CsA or TAC as it can further suppress SARS-CoV-2 replication.

Finally, in **chapter VIII,** the findings described in this thesis are discussed in the context of our existing knowledge about anti-CoV research, and the problems that remain to be solved. Additionally, new discoveries related to the CoV RTC are summarized and discussed.

REFERENCES

1. den Boon, J.A., et al., *Equine arteritis virus is not a togavirus but belongs to the coronaviruslike superfamily.* J Virol, 1991. **65**(6): p. 2910-20.
2. Cavanagh, D., *Nidovirales: a new order comprising Coronaviridae and Arteriviridae.* Arch Virol, 1997. **142**(3): p. 629-33.
3. Siddell, S.G., et al., *Additional changes to taxonomy ratified in a special vote by the International Committee on Taxonomy of Viruses (October 2018).* Arch Virol, 2019. **164**(3): p. 943-946.
4. van Vliet, A.L., et al., *Discontinuous and non-discontinuous subgenomic RNA transcription in a nidovirus.* EMBO J, 2002. **21**(23): p. 6571-80.
5. Cowley, J.A., et al., *Gill-associated virus of Penaeus monodon prawns: an invertebrate virus with ORF1a and ORF1b genes related to arteri- and coronaviruses.* J Gen Virol, 2000. **81**(Pt 6): p. 1473-84.
6. Nga, P.T., et al., *Discovery of the first insect nidovirus, a missing evolutionary link in the emergence of the largest RNA virus genomes.* PLoS Pathog, 2011. **7**(9): p. e1002215.
7. Lauber, C., et al., *The footprint of genome architecture in the largest genome expansion in RNA viruses.* PLoS Pathog, 2013. **9**(7): p. e1003500.
8. Zirkel, F., et al., *An insect nidovirus emerging from a primary tropical rainforest.* mBio, 2011. **2**(3): p. e00077-11.
9. Saberi, A., et al., *A planarian nidovirus expands the limits of RNA genome size.* PLoS Pathog, 2018. **14**(11): p. e1007314.
10. Gulyaeva, A.A. and A.E. Gorbalenya, *A nidovirus perspective on SARS-CoV-2.* Biochem Biophys Res Commun, 2020.
11. Snijder, E.J. and J.J. Meulenberg, *The molecular biology of arteriviruses.* J Gen Virol, 1998. **79 (Pt 5)**: p. 961-79.
12. Spann, K.M., Vickers, J.E., Lester, R.J.G., *Lymphoid organ virus of Penaeus-Monodon from Australia.* Diseases of Aquatic Organisms, 1995. **23**: p. 127-134.
13. Berry, D.M., et al., *The Structure of Infectious Bronchitis Virus.* Virology, 1964. **23**: p. 403-7.
14. Weiss, M., F. Steck, and M.C. Horzinek, *Purification and partial characterization of a new enveloped RNA virus (Berne virus).* J Gen Virol, 1983. **64 (Pt 9)**: p. 1849-58.
15. Adams, M.J., et al., *Ratification vote on taxonomic proposals to the International Committee on Taxonomy of Viruses (2016).* Arch Virol, 2016. **161**(10): p. 2921-49.
16. Schalk, A.a.H., M.C. , *An apparenly new respiratory disease of baby chicks.* Journal of the American Veterinary Medical Association, 1931. **78**: p. 413-423.
17. Beach, J.R.a.S., O. W. , *A filterable virus, distinct from that of laryngotracheitis, the cause of a respiratory disease of chickens.* Poultry Science, 1939. **15**: p. 199-215.
18. Doyle, L.P. and L.M. Hutchings, *A transmissible gastroenteritis in pigs.* J Am Vet Med Assoc, 1946. **108**: p. 257-9.
19. Cheever, F.S., J.B. Daniels, and et al., *A murine virus (JHM) causing disseminated encephalomyelitis with extensive destruction of myelin.* J Exp Med, 1949. **90**(3): p. 181-210.
20. Boursnell, M.E., et al., *Completion of the sequence of the genome of the coronavirus avian infectious bronchitis virus.* J Gen Virol, 1987. **68 (Pt 1)**: p. 57-77.

21. Lee, H.J., et al., *The complete sequence (22 kilobases) of murine coronavirus gene 1 encoding the putative proteases and RNA polymerase.* Virology, 1991. **180**(2): p. 567-82.
22. Pachuk, C.J., et al., *Molecular cloning of the gene encoding the putative polymerase of mouse hepatitis coronavirus, strain A59.* Virology, 1989. **171**(1): p. 141-8.
23. Tyrrell, D.A. and M.L. Bynoe, *Cultivation of a Novel Type of Common-Cold Virus in Organ Cultures.* Br Med J, 1965. **1**(5448): p. 1467-70.
24. Hamre, D. and J.J. Procknow, *A new virus isolated from the human respiratory tract.* Proc Soc Exp Biol Med, 1966. **121**(1): p. 190-3.
25. Bradburne, A.F., M.L. Bynoe, and D.A. Tyrrell, *Effects of a "new" human respiratory virus in volunteers.* Br Med J, 1967. **3**(5568): p. 767-9.
26. McIntosh, K., et al., *Antigenic relationships among the coronaviruses of man and between human and animal coronaviruses.* J Immunol, 1969. **102**(5): p. 1109-18.
27. Pyrc, K., et al., *Genome structure and transcriptional regulation of human coronavirus NL63.* Virol J, 2004. **1**: p. 7.
28. Fouchier, R.A., et al., *A previously undescribed coronavirus associated with respiratory disease in humans.* Proc Natl Acad Sci U S A, 2004. **101**(16): p. 6212-6.
29. Lau, S.K., et al., *Coronavirus HKU1 and other coronavirus infections in Hong Kong.* J Clin Microbiol, 2006. **44**(6): p. 2063-71.
30. van der Hoek, L., *Human coronaviruses: what do they cause?* Antivir Ther, 2007. **12**(4 Pt B): p. 651-8.
31. Ksiazek, T.G., et al., *A novel coronavirus associated with severe acute respiratory syndrome.* N Engl J Med, 2003. **348**(20): p. 1953-66.
32. Zaki, A.M., et al., *Isolation of a novel coronavirus from a man with pneumonia in Saudi Arabia.* N Engl J Med, 2012. **367**(19): p. 1814-1820.
33. van Boheemen, S., et al., *Genomic characterization of a newly discovered coronavirus associated with acute respiratory distress syndrome in humans.* MBio, 2012. **3**(6): p. e00473-12.
34. Zhou, P., et al., *A pneumonia outbreak associated with a new coronavirus of probable bat origin.* Nature, 2020. **579**(7798): p. 270-273.
35. de Wit, E., et al., *SARS and MERS: recent insights into emerging coronaviruses.* Nat Rev Microbiol, 2016. **14**(8): p. 523-34.
36. Drexler, J.F., V.M. Corman, and C. Drosten, *Ecology, evolution and classification of bat coronaviruses in the aftermath of SARS.* Antiviral Res, 2014. **101**: p. 45-56.
37. Corman, V.M., et al., *Hosts and Sources of Endemic Human Coronaviruses.* Adv Virus Res, 2018. **100**: p. 163-188.
38. Vijgen, L., et al., *Evolutionary history of the closely related group 2 coronaviruses: porcine hemagglutinating encephalomyelitis virus, bovine coronavirus, and human coronavirus OC43.* J Virol, 2006. **80**(14): p. 7270-4.
39. Lau, S.K., et al., *Discovery of a novel coronavirus, China Rattus coronavirus HKU24, from Norway rats supports the murine origin of Betacoronavirus 1 and has implications for the ancestor of Betacoronavirus lineage A.* J Virol, 2015. **89**(6): p. 3076-92.
40. Jacomy, H., et al., *Human coronavirus OC43 infection induces chronic encephalitis leading to disabilities in BALB/C mice.* Virology, 2006. **349**(2): p. 335-46.

41. Reusken, C.B., et al., *Middle East respiratory syndrome coronavirus neutralising serum antibodies in dromedary camels: a comparative serological study.* Lancet Infect Dis, 2013. **13**(10): p. 859-66.
42. Song, H.D., et al., *Cross-host evolution of severe acute respiratory syndrome coronavirus in palm civet and human.* Proc Natl Acad Sci U S A, 2005. **102**(7): p. 2430-5.
43. Lam, T.T., et al., *Identifying SARS-CoV-2 related coronaviruses in Malayan pangolins.* Nature, 2020.
44. Menachery, V.D., et al., *A SARS-like cluster of circulating bat coronaviruses shows potential for human emergence.* Nat Med, 2015. **21**(12): p. 1508-13.
45. Hu, B., et al., *Discovery of a rich gene pool of bat SARS-related coronaviruses provides new insights into the origin of SARS coronavirus.* PLoS Pathog, 2017. **13**(11): p. e1006698.
46. Li, X., et al., *Evolutionary history, potential intermediate animal host, and cross-species analyses of SARS-CoV-2.* J Med Virol, 2020.
47. Letko, M., et al., *Bat-borne virus diversity, spillover and emergence.* Nat Rev Microbiol, 2020. **18**(8): p. 461-471.
48. Cascio, A., et al., *The socio-ecology of zoonotic infections.* Clin Microbiol Infect, 2011. **17**(3): p. 336-42.
49. Masters, P.S., Perlman, S., *Coronaviridae*, in *Fields' Virology*, H.P. Knipe DM, Cohen JI , et al (Eds), Editor. 2013, Lippincott Williams & Wilkins: Philadelphia. p. 825-858.
50. Weiss, S.R. and S. Navas-Martin, *Coronavirus pathogenesis and the emerging pathogen severe acute respiratory syndrome coronavirus.* Microbiol Mol Biol Rev, 2005. **69**(4): p. 635-64.
51. van der Hoek, L., et al., *Croup is associated with the novel coronavirus NL63.* PLoS Med, 2005. **2**(8): p. e240.
52. Pene, F., et al., *Coronavirus 229E-related pneumonia in immunocompromised patients.* Clin Infect Dis, 2003. **37**(7): p. 929-32.
53. Folz, R.J. and M.A. Elkordy, *Coronavirus pneumonia following autologous bone marrow transplantation for breast cancer.* Chest, 1999. **115**(3): p. 901-5.
54. van der Hoek, L., *SARS-CoV-2 Re-infections: Lessons from Other Coronaviruses.* Med (N Y), 2020. **1**(1): p. 23-28.
55. Zhong, N.S., et al., *Epidemiology and cause of severe acute respiratory syndrome (SARS) in Guangdong, People's Republic of China, in February, 2003.* Lancet, 2003. **362**(9393): p. 1353-8.
56. Yu, I.T., et al., *Evidence of airborne transmission of the severe acute respiratory syndrome virus.* N Engl J Med, 2004. **350**(17): p. 1731-9.
57. Leung, G.M., et al., *SARS-CoV antibody prevalence in all Hong Kong patient contacts.* Emerg Infect Dis, 2004. **10**(9): p. 1653-6.
58. Tansey, C.M., et al., *One-year outcomes and health care utilization in survivors of severe acute respiratory syndrome.* Arch Intern Med, 2007. **167**(12): p. 1312-20.
59. Jayaweera, M., et al., *Transmission of COVID-19 virus by droplets and aerosols: A critical review on the unresolved dichotomy.* Environ Res, 2020. **188**: p. 109819.
60. Jamilloux, Y., et al., *Should we stimulate or suppress immune responses in COVID-19? Cytokine and anti-cytokine interventions.* Autoimmun Rev, 2020. **19**(7): p. 102567.

61. Garg, S., et al., *Hospitalization Rates and Characteristics of Patients Hospitalized with Laboratory-Confirmed Coronavirus Disease 2019 - COVID-NET, 14 States, March 1-30, 2020.* MMWR Morb Mortal Wkly Rep, 2020. **69**(15): p. 458-464.
62. Richardson, S., et al., *Presenting Characteristics, Comorbidities, and Outcomes Among 5700 Patients Hospitalized With COVID-19 in the New York City Area.* JAMA, 2020. **323**(20): p. 2052-2059.
63. Epidemiology Working Group for Ncip Epidemic Response, C.C.f.D.C. and Prevention, *[The epidemiological characteristics of an outbreak of 2019 novel coronavirus diseases (COVID-19) in China].* Zhonghua Liu Xing Bing Xue Za Zhi, 2020. **41**(2): p. 145-151.
64. Torabi, A., et al., *Proinflammatory Cytokines in the Olfactory Mucosa Result in COVID-19 Induced Anosmia.* ACS Chem Neurosci, 2020. **11**(13): p. 1909-1913.
65. Butowt, R. and C.S. von Bartheld, *Anosmia in COVID-19: Underlying Mechanisms and Assessment of an Olfactory Route to Brain Infection.* Neuroscientist, 2020: p. 1073858420956905.
66. Siddiqi, H.K. and M.R. Mehra, *COVID-19 illness in native and immunosuppressed states: A clinical-therapeutic staging proposal.* J Heart Lung Transplant, 2020. **39**(5): p. 405-407.
67. Gralinski, L.E. and R.S. Baric, *Molecular pathology of emerging coronavirus infections.* J Pathol, 2015. **235**(2): p. 185-95.
68. Levin, M., *Childhood Multisystem Inflammatory Syndrome - A New Challenge in the Pandemic.* N Engl J Med, 2020. **383**(4): p. 393-395.
69. Huang, C., et al., *6-month consequences of COVID-19 in patients discharged from hospital: a cohort study.* Lancet, 2021. **397**(10270): p. 220-232.
70. Nalbandian, A., et al., *Post-acute COVID-19 syndrome.* Nat Med, 2021.
71. Halpin, S., R. O'Connor, and M. Sivan, *Long COVID and chronic COVID syndromes.* J Med Virol, 2021. **93**(3): p. 1242-1243.
72. El-Kafrawy, S.A., et al., *Enzootic patterns of Middle East respiratory syndrome coronavirus in imported African and local Arabian dromedary camels: a prospective genomic study.* Lancet Planet Health, 2019. **3**(12): p. e521-e528.
73. Muller, M.A., et al., *Presence of Middle East respiratory syndrome coronavirus antibodies in Saudi Arabia: a nationwide, cross-sectional, serological study.* Lancet Infect Dis, 2015. **15**(6): p. 629.
74. Penttinen, P.M., et al., *Taking stock of the first 133 MERS coronavirus cases globally--Is the epidemic changing?* Euro Surveill, 2013. **18**(39).
75. Memish, Z.A., A.I. Zumla, and A. Assiri, *Middle East respiratory syndrome coronavirus infections in health care workers.* N Engl J Med, 2013. **369**(9): p. 884-6.
76. Paules, C.I., H.D. Marston, and A.S. Fauci, *Coronavirus Infections-More Than Just the Common Cold.* JAMA, 2020. **323**(8): p. 707-708.
77. Al-Tawfiq, J.A. and Z.A. Memish, *Drivers of MERS-CoV transmission: what do we know?* Expert Rev Respir Med, 2016. **10**(3): p. 331-338.
78. Zumla, A., et al., *Coronaviruses - drug discovery and therapeutic options.* Nat Rev Drug Discov, 2016. **15**(5): p. 327-47.
79. Zumla, A., D.S. Hui, and S. Perlman, *Middle East respiratory syndrome.* Lancet, 2015. **386**(9997): p. 995-1007.
80. Wang, W., et al., *Detection of SARS-CoV-2 in Different Types of Clinical Specimens.* JAMA, 2020. **323**(18): p. 1843-1844.

81. Woo, P.C., K.Y. Yuen, and S.K. Lau, *Epidemiology of coronavirus-associated respiratory tract infections and the role of rapid diagnostic tests: a prospective study.* Hong Kong Med J, 2012. **18 Suppl 2**: p. 22-4.
82. Yan, Y., L. Chang, and L. Wang, *Laboratory testing of SARS-CoV, MERS-CoV, and SARS-CoV-2 (2019-nCoV): Current status, challenges, and countermeasures.* Rev Med Virol, 2020. **30**(3): p. e2106.
83. Wolfel, R., et al., *Virological assessment of hospitalized patients with COVID-2019.* Nature, 2020. **581**(7809): p. 465-469.
84. Millet, J.K., J.A. Jaimes, and G.R. Whittaker, *Molecular diversity of coronavirus host cell entry receptors.* FEMS Microbiol Rev, 2020.
85. V'Kovski, P., et al., *Coronavirus biology and replication: implications for SARS-CoV-2.* Nat Rev Microbiol, 2020.
86. Ogando, N.S., et al., *SARS-coronavirus-2 replication in Vero E6 cells: replication kinetics, rapid adaptation and cytopathology.* J Gen Virol, 2020.
87. Wolff, G., et al., *A molecular pore spans the double membrane of the coronavirus replication organelle.* Science, 2020.
88. Yeager, C.L., et al., *Human aminopeptidase N is a receptor for human coronavirus 229E.* Nature, 1992. **357**(6377): p. 420-2.
89. Delmas, B., et al., *Aminopeptidase N is a major receptor for the entero-pathogenic coronavirus TGEV.* Nature, 1992. **357**(6377): p. 417-20.
90. Li, B.X., J.W. Ge, and Y.J. Li, *Porcine aminopeptidase N is a functional receptor for the PEDV coronavirus.* Virology, 2007. **365**(1): p. 166-72.
91. Hofmann, H., et al., *Human coronavirus NL63 employs the severe acute respiratory syndrome coronavirus receptor for cellular entry.* Proc Natl Acad Sci U S A, 2005. **102**(22): p. 7988-93.
92. Li, W., et al., *Angiotensin-converting enzyme 2 is a functional receptor for the SARS coronavirus.* Nature, 2003. **426**(6965): p. 450-4.
93. Hoffmann, M., et al., *The novel coronavirus 2019 (2019-nCoV) uses the SARS-coronavirus receptor ACE2 and the cellular protease TMPRSS2 for entry into target cells.* bioRxiv, 2020.
94. Raj, V.S., et al., *Dipeptidyl peptidase 4 is a functional receptor for the emerging human coronavirus-EMC.* Nature, 2013. **495**(7440): p. 251-254.
95. Williams, R.K., G.S. Jiang, and K.V. Holmes, *Receptor for mouse hepatitis virus is a member of the carcinoembryonic antigen family of glycoproteins.* Proc Natl Acad Sci U S A, 1991. **88**(13): p. 5533-6.
96. Peng, G., et al., *Crystal structure of bovine coronavirus spike protein lectin domain.* J Biol Chem, 2012. **287**(50): p. 41931-8.
97. Li, W., et al., *Identification of sialic acid-binding function for the Middle East respiratory syndrome coronavirus spike glycoprotein.* Proc Natl Acad Sci U S A, 2017. **114**(40): p. E8508-E8517.
98. Schultze, B., et al., *Transmissible gastroenteritis coronavirus, but not the related porcine respiratory coronavirus, has a sialic acid (N-glycolylneuraminic acid) binding activity.* J Virol, 1996. **70**(8): p. 5634-7.
99. Tortorici, M.A., et al., *Structural basis for human coronavirus attachment to sialic acid receptors.* Nat Struct Mol Biol, 2019. **26**(6): p. 481-489.

100. Menachery, V.D., et al., *Trypsin Treatment Unlocks Barrier for Zoonotic Bat Coronavirus Infection.* J Virol, 2020. **94**(5).
101. Kawase, M., et al., *Simultaneous treatment of human bronchial epithelial cells with serine and cysteine protease inhibitors prevents severe acute respiratory syndrome coronavirus entry.* J Virol, 2012. **86**(12): p. 6537-45.
102. Shirato, K., M. Kawase, and S. Matsuyama, *Wild-type human coronaviruses prefer cell-surface TMPRSS2 to endosomal cathepsins for cell entry.* Virology, 2018. **517**: p. 9-15.
103. Millet, J.K. and G.R. Whittaker, *Host cell entry of Middle East respiratory syndrome coronavirus after two-step, furin-mediated activation of the spike protein.* Proc Natl Acad Sci U S A, 2014. **111**(42): p. 15214-9.
104. Coutard, B., et al., *The spike glycoprotein of the new coronavirus 2019-nCoV contains a furin-like cleavage site absent in CoV of the same clade.* Antiviral Res, 2020. **176**: p. 104742.
105. Shang, J., et al., *Cell entry mechanisms of SARS-CoV-2.* Proc Natl Acad Sci U S A, 2020. **117**(21): p. 11727-11734.
106. Firth, A.E. and I. Brierley, *Non-canonical translation in RNA viruses.* J Gen Virol, 2012. **93**(Pt 7): p. 1385-1409.
107. Irigoyen, N., et al., *High-Resolution Analysis of Coronavirus Gene Expression by RNA Sequencing and Ribosome Profiling.* PLoS Pathog, 2016. **12**(2): p. e1005473.
108. Snijder, E.J., et al., *Unique and conserved features of genome and proteome of SARS-coronavirus, an early split-off from the coronavirus group 2 lineage.* J Mol Biol, 2003. **331**(5): p. 991-1004.
109. Snijder, E.J., E. Decroly, and J. Ziebuhr, *The Nonstructural Proteins Directing Coronavirus RNA Synthesis and Processing.* Adv Virus Res, 2016. **96**: p. 59-126.
110. Perlman, S. and J. Netland, *Coronaviruses post-SARS: update on replication and pathogenesis.* Nat Rev Microbiol, 2009. **7**(6): p. 439-50.
111. Liu, D.X., et al., *Accessory proteins of SARS-CoV and other coronaviruses.* Antiviral Res, 2014. **109**: p. 97-109.
112. Narayanan, K., C. Huang, and S. Makino, *SARS coronavirus accessory proteins.* Virus Res, 2008. **133**(1): p. 113-21.
113. Schubert, K., et al., *SARS-CoV-2 Nsp1 binds the ribosomal mRNA channel to inhibit translation.* Nat Struct Mol Biol, 2020. **27**(10): p. 959-966.
114. Lokugamage, K.G., et al., *Middle East Respiratory Syndrome Coronavirus nsp1 Inhibits Host Gene Expression by Selectively Targeting mRNAs Transcribed in the Nucleus while Sparing mRNAs of Cytoplasmic Origin.* J Virol, 2015. **89**(21): p. 10970-81.
115. Knoops, K., et al., *SARS-coronavirus replication is supported by a reticulovesicular network of modified endoplasmic reticulum.* PLoS Biol, 2008. **6**(9): p. e226.
116. Snijder, E.J., et al., *A unifying structural and functional model of the coronavirus replication organelle: Tracking down RNA synthesis.* PLoS Biol, 2020. **18**(6): p. e3000715.
117. Klein, S., et al., *SARS-CoV-2 structure and replication characterized by in situ cryo-electron tomography.* Nat Commun, 2020. **11**(1): p. 5885.
118. Kirchdoerfer, R.N. and A.B. Ward, *Structure of the SARS-CoV nsp12 polymerase bound to nsp7 and nsp8 co-factors.* Nat Commun, 2019. **10**(1): p. 2342.
119. Hillen, H.S., et al., *Structure of replicating SARS-CoV-2 polymerase.* Nature, 2020. **584**(7819): p. 154-156.

120. Adedeji, A.O., et al., *Severe acute respiratory syndrome coronavirus replication inhibitor that interferes with the nucleic acid unwinding of the viral helicase.* Antimicrob Agents Chemother, 2012. **56**(9): p. 4718-28.
121. Seybert, A., et al., *The human coronavirus 229E superfamily 1 helicase has RNA and DNA duplex-unwinding activities with 5'-to-3' polarity.* RNA, 2000. **6**(7): p. 1056-68.
122. Chen, J., et al., *Structural Basis for Helicase-Polymerase Coupling in the SARS-CoV-2 Replication-Transcription Complex.* Cell, 2020. **182**(6): p. 1560-1573 e13.
123. Ferron, F., et al., *Structural and molecular basis of mismatch correction and ribavirin excision from coronavirus RNA.* Proc Natl Acad Sci U S A, 2018. **115**(2): p. E162-E171.
124. Ma, Y., et al., *Structural basis and functional analysis of the SARS coronavirus nsp14-nsp10 complex.* Proc Natl Acad Sci U S A, 2015. **112**(30): p. 9436-9441.
125. Minskaia, E., et al., *Discovery of an RNA virus 3'->5' exoribonuclease that is critically involved in coronavirus RNA synthesis.* Proc Natl Acad Sci U S A, 2006. **103**(13): p. 5108-5113.
126. Smith, E.C., et al., *Coronaviruses lacking exoribonuclease activity are susceptible to lethal mutagenesis: evidence for proofreading and potential therapeutics.* PLoS Pathog, 2013. **9**(8): p. e1003565.
127. Graepel, K.W., et al., *Proofreading-deficient coronaviruses adapt for increased fitness over long-term passage without reversion of exoribonuclease-inactivating mutations.* MBio, 2017. **8**(6): p. e01503-01517.
128. Sawicki, S.G. and D.L. Sawicki, *A new model for coronavirus transcription.* Adv Exp Med Biol, 1998. **440**: p. 215-9.
129. Pasternak, A.O., W.J. Spaan, and E.J. Snijder, *Nidovirus transcription: how to make sense...?* J Gen Virol, 2006. **87**(Pt 6): p. 1403-21.
130. Sawicki, S.G. and D.L. Sawicki, *Coronaviruses use discontinuous extension for synthesis of subgenome-length negative strands.* Adv Exp Med Biol, 1995. **380**: p. 499-506.
131. Baric, R.S. and B. Yount, *Subgenomic negative-strand RNA function during mouse hepatitis virus infection.* J Virol, 2000. **74**(9): p. 4039-46.
132. Viehweger, A., et al., *Direct RNA nanopore sequencing of full-length coronavirus genomes provides novel insights into structural variants and enables modification analysis.* Genome Res, 2019. **29**(9): p. 1545-1554.
133. Ivanov, K.A. and J. Ziebuhr, *Human coronavirus 229E nonstructural protein 13: characterization of duplex-unwinding, nucleoside triphosphatase, and RNA 5'-triphosphatase activities.* J Virol, 2004. **78**(14): p. 7833-8.
134. Chen, Y., et al., *Functional screen reveals SARS coronavirus nonstructural protein nsp14 as a novel cap N7 methyltransferase.* Proc Natl Acad Sci U S A, 2009. **106**(9): p. 3484-3489.
135. Decroly, E., et al., *Coronavirus nonstructural protein 16 is a cap-0 binding enzyme possessing (nucleoside-2'O)-methyltransferase activity.* J Virol, 2008. **82**(16): p. 8071-84.
136. von der Haar, T., et al., *The mRNA cap-binding protein eIF4E in post-transcriptional gene expression.* Nat Struct Mol Biol, 2004. **11**(6): p. 503-11.
137. de Haan, C.A., et al., *Coronavirus particle assembly: primary structure requirements of the membrane protein.* J Virol, 1998. **72**(8): p. 6838-50.
138. de Haan, C.A., H. Vennema, and P.J. Rottier, *Assembly of the coronavirus envelope: homotypic interactions between the M proteins.* J Virol, 2000. **74**(11): p. 4967-78.

139. Ghosh, S., et al., *beta-Coronaviruses Use Lysosomes for Egress Instead of the Biosynthetic Secretory Pathway.* Cell, 2020. **183**(6): p. 1520-1535 e14.
140. Consortium, W.H.O.S.T., et al., *Repurposed Antiviral Drugs for Covid-19 - Interim WHO Solidarity Trial Results.* N Engl J Med, 2021. **384**(6): p. 497-511.
141. Beigel, J.H., K.M. Tomashek, and L.E. Dodd, *Remdesivir for the Treatment of Covid-19 - Preliminary Report. Reply.* N Engl J Med, 2020. **383**(10): p. 994.
142. Goldman, J.D., et al., *Remdesivir for 5 or 10 Days in Patients with Severe Covid-19.* N Engl J Med, 2020. **383**(19): p. 1827-1837.
143. Wang, Y., et al., *Remdesivir in adults with severe COVID-19: a randomised, double-blind, placebo-controlled, multicentre trial.* Lancet, 2020. **395**(10236): p. 1569-1578.
144. Dyer, O., *Covid-19: Remdesivir has little or no impact on survival, WHO trial shows.* BMJ, 2020. **371**: p. m4057.
145. Joshi, S., et al., *Role of favipiravir in the treatment of COVID-19.* Int J Infect Dis, 2021. **102**: p. 501-508.
146. Qiu, M., et al., *Antibody responses to individual proteins of SARS coronavirus and their neutralization activities.* Microbes Infect, 2005. **7**(5-6): p. 882-9.
147. Li, Y., et al., *A humanized neutralizing antibody against MERS-CoV targeting the receptor-binding domain of the spike protein.* Cell Res, 2015. **25**(11): p. 1237-49.
148. Tang, X.C., et al., *Identification of human neutralizing antibodies against MERS-CoV and their role in virus adaptive evolution.* Proc Natl Acad Sci U S A, 2014. **111**(19): p. E2018-26.
149. Zumla, A., et al., *Vaccine against Middle East respiratory syndrome coronavirus.* Lancet Infect Dis, 2019. **19**(10): p. 1054-1055.
150. Li, Y.D., et al., *Coronavirus vaccine development: from SARS and MERS to COVID-19.* J Biomed Sci, 2020. **27**(1): p. 104.
151. Krammer, F., *SARS-CoV-2 vaccines in development.* Nature, 2020. **586**(7830): p. 516-527.
152. Cheng, Y., et al., *Use of convalescent plasma therapy in SARS patients in Hong Kong.* Eur J Clin Microbiol Infect Dis, 2005. **24**(1): p. 44-6.
153. Yeh, K.M., et al., *Experience of using convalescent plasma for severe acute respiratory syndrome among healthcare workers in a Taiwan hospital.* J Antimicrob Chemother, 2005. **56**(5): p. 919-22.
154. Jiang, L., et al., *Potent neutralization of MERS-CoV by human neutralizing monoclonal antibodies to the viral spike glycoprotein.* Sci Transl Med, 2014. **6**(234): p. 234ra59.
155. Ying, T., et al., *Exceptionally potent neutralization of Middle East respiratory syndrome coronavirus by human monoclonal antibodies.* J Virol, 2014. **88**(14): p. 7796-805.
156. Casadevall, A., M.J. Joyner, and L.A. Pirofski, *A Randomized Trial of Convalescent Plasma for COVID-19-Potentially Hopeful Signals.* JAMA, 2020. **324**(5): p. 455-457.
157. Coughlin, M.M. and B.S. Prabhakar, *Neutralizing human monoclonal antibodies to severe acute respiratory syndrome coronavirus: target, mechanism of action, and therapeutic potential.* Rev Med Virol, 2012. **22**(1): p. 2-17.
158. Shanmugaraj, B., et al., *Perspectives on monoclonal antibody therapy as potential therapeutic intervention for Coronavirus disease-19 (COVID-19).* Asian Pac J Allergy Immunol, 2020. **38**(1): p. 10-18.
159. Wang, C., et al., *A human monoclonal antibody blocking SARS-CoV-2 infection.* Nat Commun, 2020. **11**(1): p. 2251.

160. Xia, S., et al., *Inhibition of SARS-CoV-2 (previously 2019-nCoV) infection by a highly potent pan-coronavirus fusion inhibitor targeting its spike protein that harbors a high capacity to mediate membrane fusion.* Cell Res, 2020. **30**(4): p. 343-355.
161. Xia, S., et al., *Fusion mechanism of 2019-nCoV and fusion inhibitors targeting HR1 domain in spike protein.* Cell Mol Immunol, 2020. **17**(7): p. 765-767.
162. de Vries, R.D., et al., *Intranasal fusion inhibitory lipopeptide prevents direct-contact SARS-CoV-2 transmission in ferrets.* Science, 2021. **371**(6536): p. 1379-1382.
163. Xia, S., et al., *A pan-coronavirus fusion inhibitor targeting the HR1 domain of human coronavirus spike.* Sci Adv, 2019. **5**(4): p. eaav4580.
164. Hoffmann, M., et al., *SARS-CoV-2 Cell Entry Depends on ACE2 and TMPRSS2 and Is Blocked by a Clinically Proven Protease Inhibitor.* Cell, 2020. **181**(2): p. 271-280 e8.
165. Shirato, K., M. Kawase, and S. Matsuyama, *Middle East respiratory syndrome coronavirus infection mediated by the transmembrane serine protease TMPRSS2.* J Virol, 2013. **87**(23): p. 12552-61.
166. Zhou, Y., et al., *Protease inhibitors targeting coronavirus and filovirus entry.* Antiviral Res, 2015. **116**: p. 76-84.
167. Bertram, S., et al., *TMPRSS2 activates the human coronavirus 229E for cathepsin-independent host cell entry and is expressed in viral target cells in the respiratory epithelium.* J Virol, 2013. **87**(11): p. 6150-60.
168. Hoffmann, M., et al., *Chloroquine does not inhibit infection of human lung cells with SARS-CoV-2.* Nature, 2020. **585**(7826): p. 588-590.
169. Vincent, M.J., et al., *Chloroquine is a potent inhibitor of SARS coronavirus infection and spread.* Virol J, 2005. **2**: p. 69.
170. de Wilde, A.H., et al., *Screening of an FDA-approved compound library identifies four small-molecule inhibitors of Middle East respiratory syndrome coronavirus replication in cell culture.* Antimicrob Agents Chemother, 2014. **58**(8): p. 4875-84.
171. Wang, M., et al., *Remdesivir and chloroquine effectively inhibit the recently emerged novel coronavirus (2019-nCoV) in vitro.* Cell Res, 2020. **30**(3): p. 269-271.
172. Kashour, Z., et al., *Efficacy of chloroquine or hydroxychloroquine in COVID-19 patients: a systematic review and meta-analysis.* J Antimicrob Chemother, 2021. **76**(1): p. 30-42.
173. Salgado-Benvindo, C., et al., *Suramin Inhibits SARS-CoV-2 Infection in Cell Culture by Interfering with Early Steps of the Replication Cycle.* Antimicrob Agents Chemother, 2020. **64**(8).
174. Albulescu, I.C., et al., *Suramin inhibits Zika virus replication by interfering with virus attachment and release of infectious particles.* Antiviral Res, 2017. **143**: p. 230-236.
175. Albulescu, I.C., et al., *Suramin inhibits chikungunya virus replication through multiple mechanisms.* Antiviral Res, 2015. **121**: p. 39-46.
176. Garson, J.A., et al., *Suramin blocks hepatitis C binding to human hepatoma cells in vitro.* J Med Virol, 1999. **57**(3): p. 238-42.
177. Tan, C.W., et al., *Polysulfonate suramin inhibits Zika virus infection.* Antiviral Res, 2017. **143**: p. 186-194.
178. Yahi, N., et al., *Suramin inhibits binding of the V3 region of HIV-1 envelope glycoprotein gp120 to galactosylceramide, the receptor for HIV-1 gp120 on human colon epithelial cells.* J Biol Chem, 1994. **269**(39): p. 24349-53.
179. Li, G. and E. De Clercq, *Therapeutic options for the 2019 novel coronavirus (2019-nCoV).* Nat Rev Drug Discov, 2020. **19**(3): p. 149-150.

180. Roe, M.K., et al., *Targeting novel structural and functional features of coronavirus protease nsp5 (3CL(pro), M(pro)) in the age of COVID-19.* J Gen Virol, 2021.
181. Cannalire, R., et al., *Targeting SARS-CoV-2 Proteases and Polymerase for COVID-19 Treatment: State of the Art and Future Opportunities.* J Med Chem, 2020.
182. Coelho, C., et al., *Biochemical screening for SARS-CoV-2 main protease inhibitors.* PLoS One, 2020. **15**(10): p. e0240079.
183. Jin, Z., et al., *Structure of M(pro) from SARS-CoV-2 and discovery of its inhibitors.* Nature, 2020. **582**(7811): p. 289-293.
184. Yang, H., et al., *Design of wide-spectrum inhibitors targeting coronavirus main proteases.* PLoS Biol, 2005. **3**(10): p. e324.
185. Amin, S.A., et al., *Protease targeted COVID-19 drug discovery: What we have learned from the past SARS-CoV inhibitors?* Eur J Med Chem, 2021. **215**: p. 113294.
186. Ren, Z., et al., *The newly emerged SARS-like coronavirus HCoV-EMC also has an "Achilles' heel": current effective inhibitor targeting a 3C-like protease.* Protein Cell, 2013. **4**(4): p. 248-50.
187. Kim, Y., et al., *Reversal of the Progression of Fatal Coronavirus Infection in Cats by a Broad-Spectrum Coronavirus Protease Inhibitor.* PLoS Pathog, 2016. **12**(3): p. e1005531.
188. Dai, W., et al., *Structure-based design of antiviral drug candidates targeting the SARS-CoV-2 main protease.* Science, 2020. **368**(6497): p. 1331-1335.
189. Zhang, L., et al., *alpha-Ketoamides as Broad-Spectrum Inhibitors of Coronavirus and Enterovirus Replication: Structure-Based Design, Synthesis, and Activity Assessment.* J Med Chem, 2020. **63**(9): p. 4562-4578.
190. Boras, B., et al., *Discovery of a Novel Inhibitor of Coronavirus 3CL Protease as a Clinical Candidate for the Potential Treatment of COVID-19.* bioRxiv, 2020.
191. de Vries, M., et al., *Comparative study of a 3CL (pro) inhibitor and remdesivir against both major SARS-CoV-2 clades in human airway models.* bioRxiv, 2020.
192. Crotty, S., C.E. Cameron, and R. Andino, *RNA virus error catastrophe: direct molecular test by using ribavirin.* Proc Natl Acad Sci U S A, 2001. **98**(12): p. 6895-900.
193. Eigen, M., *Error catastrophe and antiviral strategy.* Proc Natl Acad Sci U S A, 2002. **99**(21): p. 13374-13376.
194. Agostini, M.L., et al., *Coronavirus Susceptibility to the Antiviral Remdesivir (GS-5734) Is Mediated by the Viral Polymerase and the Proofreading Exoribonuclease.* MBio, 2018. **9**(2).
195. Gordon, C.J., et al., *The antiviral compound remdesivir potently inhibits RNA-dependent RNA polymerase from Middle East respiratory syndrome coronavirus.* J Biol Chem, 2020.
196. Tchesnokov, E.P., et al., *Mechanism of Inhibition of Ebola Virus RNA-Dependent RNA Polymerase by Remdesivir.* Viruses, 2019. **11**(4).
197. Sheahan, T.P., et al., *Broad-spectrum antiviral GS-5734 inhibits both epidemic and zoonotic coronaviruses.* Sci Transl Med, 2017. **9**(396).
198. Al-Tawfiq, J.A., et al., *Ribavirin and interferon therapy in patients infected with the Middle East respiratory syndrome coronavirus: an observational study.* Int J Infect Dis, 2014. **20**: p. 42-6.

199. Shalhoub, S., et al., *IFN-alpha2a or IFN-beta1a in combination with ribavirin to treat Middle East respiratory syndrome coronavirus pneumonia: a retrospective study.* J Antimicrob Chemother, 2015. **70**(7): p. 2129-32.
200. Omrani, A.S., et al., *Ribavirin and interferon alfa-2a for severe Middle East respiratory syndrome coronavirus infection: a retrospective cohort study.* Lancet Infect Dis, 2014. **14**(11): p. 1090-1095.
201. Elfiky, A.A., *Ribavirin, Remdesivir, Sofosbuvir, Galidesivir, and Tenofovir against SARS-CoV-2 RNA dependent RNA polymerase (RdRp): A molecular docking study.* Life Sci, 2020. **253**: p. 117592.
202. Shannon, A., et al., *Favipiravir strikes the SARS-CoV-2 at its Achilles heel, the RNA polymerase.* bioRxiv, 2020.
203. Vanderlinden, E., et al., *Distinct Effects of T-705 (Favipiravir) and Ribavirin on Influenza Virus Replication and Viral RNA Synthesis.* Antimicrob Agents Chemother, 2016. **60**(11): p. 6679-6691.
204. Furuta, Y., et al., *In vitro and in vivo activities of anti-influenza virus compound T-705.* Antimicrob Agents Chemother, 2002. **46**(4): p. 977-81.
205. Chien, M., et al., *Nucleotide Analogues as Inhibitors of SARS-CoV-2 Polymerase, a Key Drug Target for COVID-19.* J Proteome Res, 2020. **19**(11): p. 4690-4697.
206. Liu, S., et al., *Evaluation of 19 antiviral drugs against SARS-CoV-2 Infection.* bioRxiv, 2020: p. 2020.04.29.067983.
207. Reynard, O., et al., *Identification of a New Ribonucleoside Inhibitor of Ebola Virus Replication.* Viruses, 2015. **7**(12): p. 6233-40.
208. Stuyver, L.J., et al., *Ribonucleoside analogue that blocks replication of bovine viral diarrhea and hepatitis C viruses in culture.* Antimicrob Agents Chemother, 2003. **47**(1): p. 244-54.
209. Urakova, N., et al., *beta-d-N (4)-Hydroxycytidine Is a Potent Anti-alphavirus Compound That Induces a High Level of Mutations in the Viral Genome.* J Virol, 2018. **92**(3).
210. Sheahan, T.P., et al., *An orally bioavailable broad-spectrum antiviral inhibits SARS-CoV-2 in human airway epithelial cell cultures and multiple coronaviruses in mice.* Sci Transl Med, 2020. **12**(541).
211. Agostini, M.L., et al., *Small-Molecule Antiviral beta-d-N (4)-Hydroxycytidine Inhibits a Proofreading-Intact Coronavirus with a High Genetic Barrier to Resistance.* J Virol, 2019. **93**(24).
212. Robson, F., et al., *Coronavirus RNA Proofreading: Molecular Basis and Therapeutic Targeting.* Mol Cell, 2020. **79**(5): p. 710-727.
213. Wahl, A., et al., *SARS-CoV-2 infection is effectively treated and prevented by EIDD-2801.* Nature, 2021.
214. Cox, R.M., J.D. Wolf, and R.K. Plemper, *Therapeutically administered ribonucleoside analogue MK-4482/EIDD-2801 blocks SARS-CoV-2 transmission in ferrets.* Nat Microbiol, 2021. **6**(1): p. 11-18.
215. Kao, R.Y., et al., *Identification of novel small-molecule inhibitors of severe acute respiratory syndrome-associated coronavirus by chemical genetics.* Chem Biol, 2004. **11**(9): p. 1293-9.
216. Tanner, J.A., et al., *The adamantane-derived bananins are potent inhibitors of the helicase activities and replication of SARS coronavirus.* Chem Biol, 2005. **12**(3): p. 303-11.

217. Adedeji, A.O., et al., *Evaluation of SSYA10-001 as a replication inhibitor of severe acute respiratory syndrome, mouse hepatitis, and Middle East respiratory syndrome coronaviruses.* Antimicrob Agents Chemother, 2014. **58**(8): p. 4894-8.
218. Bouvet, M., et al., *In vitro reconstitution of SARS-coronavirus mRNA cap methylation.* PLoS Pathog, 2010. **6**(4): p. e1000863.
219. He, R., et al., *Potent and selective inhibition of SARS coronavirus replication by aurintricarboxylic acid.* Biochem Biophys Res Commun, 2004. **320**(4): p. 1199-203.
220. Jin, X., et al., *Characterization of the guanine-N7 methyltransferase activity of coronavirus nsp14 on nucleotide GTP.* Virus Res, 2013. **176**(1-2): p. 45-52.
221. Aouadi, W., et al., *Binding of the Methyl Donor S-Adenosyl-l-Methionine to Middle East Respiratory Syndrome Coronavirus 2'-O-Methyltransferase nsp16 Promotes Recruitment of the Allosteric Activator nsp10.* J Virol, 2017. **91**(5).
222. Aouadi, W., et al., *Toward the identification of viral cap-methyltransferase inhibitors by fluorescence screening assay.* Antiviral Res, 2017. **144**: p. 330-339.
223. Wilson, L., P. Gage, and G. Ewart, *Hexamethylene amiloride blocks E protein ion channels and inhibits coronavirus replication.* Virology, 2006. **353**(2): p. 294-306.
224. Pervushin, K., et al., *Structure and inhibition of the SARS coronavirus envelope protein ion channel.* PLoS Pathog, 2009. **5**(7): p. e1000511.
225. Akerstrom, S., A. Mirazimi, and Y.J. Tan, *Inhibition of SARS-CoV replication cycle by small interference RNAs silencing specific SARS proteins, 7a/7b, 3a/3b and S.* Antiviral Res, 2007. **73**(3): p. 219-27.
226. He, M.L., et al., *Development of interfering RNA agents to inhibit SARS-associated coronavirus infection and replication.* Hong Kong Med J, 2009. **15**(3 Suppl 4): p. 28-31.
227. Chan, R.W., et al., *Tropism of and innate immune responses to the novel human betacoronavirus lineage C virus in human ex vivo respiratory organ cultures.* J Virol, 2013. **87**(12): p. 6604-14.
228. Kindler, E., et al., *Efficient replication of the novel human betacoronavirus EMC on primary human epithelium highlights its zoonotic potential.* mBio, 2013. **4**(1): p. e00611-12.
229. Kindler, E., et al., *Early endonuclease-mediated evasion of RNA sensing ensures efficient coronavirus replication.* PLoS Pathog, 2017. **13**(2): p. e1006195.
230. Xia, H., et al., *Evasion of Type I Interferon by SARS-CoV-2.* Cell Rep, 2020. **33**(1): p. 108234.
231. de Wilde, A.H., et al., *MERS-coronavirus replication induces severe in vitro cytopathology and is strongly inhibited by cyclosporin A or interferon-alpha treatment.* J Gen Virol, 2013. **94**(Pt 8): p. 1749-60.
232. Paragas, J., et al., *Interferon alfacon1 is an inhibitor of SARS-corona virus in cell-based models.* Antiviral Res, 2005. **66**(2-3): p. 99-102.
233. Zheng, B., et al., *Potent inhibition of SARS-associated coronavirus (SCOV) infection and replication by type I interferons (IFN-alpha/beta) but not by type II interferon (IFN-gamma).* J Interferon Cytokine Res, 2004. **24**(7): p. 388-90.
234. Kumaki, Y., et al., *Prophylactic and therapeutic intranasal administration with an immunomodulator, Hiltonol((R)) (Poly IC:LC), in a lethal SARS-CoV-infected BALB/c mouse model.* Antiviral Res, 2017. **139**: p. 1-12.
235. Zhao, J., et al., *Intranasal treatment with poly(I*C) protects aged mice from lethal respiratory virus infections.* J Virol, 2012. **86**(21): p. 11416-24.

236. Rossignol, J.F., *Nitazoxanide: a first-in-class broad-spectrum antiviral agent.* Antiviral Res, 2014. **110**: p. 94-103.
237. Rossignol, J.F., *Nitazoxanide, a new drug candidate for the treatment of Middle East respiratory syndrome coronavirus.* J Infect Public Health, 2016. **9**(3): p. 227-30.
238. Rocco, P.R.M., et al., *Early use of nitazoxanide in mild Covid-19 disease: randomised, placebo-controlled trial.* Eur Respir J, 2021.
239. Jia, W.D., et al., *[Dose of glucocorticosteroids in the treatment of severe acute respiratory syndrome].* Nan Fang Yi Ke Da Xue Xue Bao, 2009. **29**(11): p. 2284-7.
240. Sung, J.J., et al., *Severe acute respiratory syndrome: report of treatment and outcome after a major outbreak.* Thorax, 2004. **59**(5): p. 414-20.
241. Lee, N., et al., *Effects of early corticosteroid treatment on plasma SARS-associated Coronavirus RNA concentrations in adult patients.* J Clin Virol, 2004. **31**(4): p. 304-9.
242. Lee, D.T., et al., *Factors associated with psychosis among patients with severe acute respiratory syndrome: a case-control study.* Clin Infect Dis, 2004. **39**(8): p. 1247-9.
243. Huang, C., et al., *Clinical features of patients infected with 2019 novel coronavirus in Wuhan, China.* Lancet, 2020. **395**(10223): p. 497-506.
244. Raju, R., et al., *Therapeutic role of corticosteroids in COVID-19: a systematic review of registered clinical trials.* Futur J Pharm Sci, 2021. **7**(1): p. 67.
245. Weber, F., et al., *Double-stranded RNA is produced by positive-strand RNA viruses and DNA viruses but not in detectable amounts by negative-strand RNA viruses.* J Virol, 2006. **80**(10): p. 5059-64.
246. Lundin, A., et al., *Targeting membrane-bound viral RNA synthesis reveals potent inhibition of diverse coronaviruses including the middle East respiratory syndrome virus.* PLoS Pathog, 2014. **10**(5): p. e1004166.
247. Rappe, J.C.F., et al., *Antiviral activity of K22 against members of the order Nidovirales.* Virus Res, 2018. **246**: p. 28-34.

CHAPTER II

SARS-coronavirus-2 replication in Vero E6 cells: replication kinetics, rapid adaptation and cytopathology

Natacha S. Ogando[1], Tim J. Dalebout[1], Jessika C. Zevenhoven-Dobbe[1], Ronald W. A. L. Limpens[2], Yvonne van der Meer[1], Leon Caly[3], Julian Druce[3], Jutte J. C. de Vries[4], Marjolein Kikkert[1], Montserrat Bárcena[2], Igor Sidorov[1] and Eric J. Snijder[1]

[1] Molecular Virology Laboratory, Department of Medical Microbiology, Leiden University Medical Center, Leiden, the Netherlands

[2] Section Electron Microscopy, Department of Cell and Chemical Biology, Leiden University Medical Center, Leiden, the Netherlands

[3] Virus Identification Laboratory, Victorian Infectious Diseases Reference Laboratory, Royal Melbourne Hospital, at the Peter Doherty Institute for Infection and Immunity, Victoria, 3000, Australia

[4] Clinical Microbiology Laboratory, Department of Medical Microbiology, Leiden University Medical Center, Leiden, the Netherlands

Published in Journal of General Virology
doi.org/10.1099/jgv.0.001453

ABSTRACT

The sudden emergence of severe acute respiratory syndrome coronavirus 2 (SARS-CoV-2) at the end of 2019 from the Chinese province of Hubei and its subsequent pandemic spread highlight the importance of understanding the full molecular details of coronavirus infection and pathogenesis. Here, we compared a variety of replication features of SARS-CoV-2 and SARS-CoV and analysed the cytopathology caused by the two closely related viruses in the commonly used Vero E6 cell line. Compared to SARS-CoV, SARS-CoV-2 generated higher levels of intracellular viral RNA, but strikingly about 50-fold less infectious viral progeny was recovered from the culture medium. Immunofluorescence microscopy of SARS-CoV-2-infected cells established extensive cross-reactivity of antisera previously raised against a variety of nonstructural proteins, membrane and nucleocapsid protein of SARS-CoV. Electron microscopy revealed that the ultrastructural changes induced by the two SARS viruses are very similar and occur within comparable time frames after infection. Furthermore, we determined that the sensitivity of the two viruses to three established inhibitors of coronavirus replication (Remdesivir, Alisporivir and chloroquine) is very similar, but that SARS-CoV-2 infection was substantially more sensitive to pre-treatment of cells with pegylated interferon alpha. An important difference between the two viruses is the fact that - upon passaging in Vero E6 cells - SARS-CoV-2 apparently is under strong selection pressure to acquire adaptive mutations in its spike protein gene. These mutations change or delete a putative furin-like cleavage site in the region connecting the S1 and S2 domains and result in a very prominent phenotypic change in plaque assays.

INTRODUCTION

For the first time in a century, societies and economies worldwide have come to a near-complete standstill due to a pandemic outbreak of a single RNA virus. This virus, the severe acute respiratory syndrome coronavirus 2 (SARS-CoV-2) [1] belongs to the coronavirus (CoV) family, which is thought to have given rise to zoonotic introductions on multiple occasions during the past centuries. Coronaviruses are abundantly present in mammalian reservoir species, including bats [2], and should now be recognized definitively as a continuous zoonotic threat with the ability to cause severe human disease and explosive pandemic transmission.

To date, seven CoVs that can infect humans have been identified, which segregate into two classes. On the one hand, there are four endemic human CoVs (HCoVs), the first of which were identified in the 1960's, annually causing a substantial number of common colds [3, 4]. On the other hand, we now know of (at least) three zoonotic CoVs that recently have caused outbreaks in the human population: severe acute respiratory syndrome coronavirus (SARS-CoV) [5, 6] in 2002-2003, Middle East respiratory syndrome-coronavirus (MERS-CoV) [7, 8] since 2012 (and probably earlier) and the current pandemic SARS-CoV-2 [9, 10]. The latter agent emerged near Wuhan (People's Republic of China) in the fall of 2019 and its animal source is currently under investigation [11-13]. Transmission to humans of SARS-CoV and MERS-CoV was attributed to civet cats [14] and dromedary camels [15], respectively, although both species may have served merely as an intermediate host due to their close contact with humans. All three zoonotic CoVs belong to the genus *Betacoronavirus*, which is abundantly represented among the CoVs that circulate in the many bat species on this planet [2, 16-19]. The genetic diversity of bat CoVs and their phylogenetic relationships with the four known endemic HCoVs (OC43, HKU1, 229E and NL63; the latter two being *Alphacoronavirus*) suggests that also these may have their evolutionary origins in bat hosts, for most of them probably centuries ago [20].The potential of multiple CoVs from different genera to cross species barriers had been predicted and documented previously [2, 16-19, 21, 22], but regrettably was not taken seriously enough to invest more extensively in prophylactic and therapeutic solutions that could have contributed to rapidly containing an outbreak of the current magnitude.

Compared to other RNA viruses, CoVs possess an unusually large positive-sense RNA genome with a size ranging from 26 to 34 kilobases [23]. The CoV genome is single-stranded and its 5'-proximal two-thirds encode for the large and partially overlapping replicase polyproteins pp1a and pp1ab (4,000-4,500 and 6,700-7,200 amino acids long, respectively), with the latter being a C-terminally extended version of the former that results from ribosomal frameshifting. The replicase polyproteins are processed into 16 cleavage products (non-structural proteins,

nsps) by two internal proteases, the papain-like protease (PL^{pro}) in nsp3 and the 3C-like or 'main' protease (M^{pro}) in nsp5 [24]. Specific trans-membrane nsps (nsp3, 4 and 6) then cooperate to transform intracellular membranes into a viral replication organelle (RO) [25] that serves to organize and execute CoV RNA synthesis, which entails genome replication and the synthesis of an extensive nested set of subgenomic mRNAs. The latter are used to express the genes present in the 3'-proximal third of the genome, which encode the four common CoV structural proteins (spike (S), envelope (E), membrane (M) and nucleocapsid (N) protein) and the 'so-called' accessory protein genes, most of which are thought to be involved in the modulation of host responses to CoV infection [26]. The CoV proteome includes a variety of potential targets for drug repurposing or *de novo* development of specific inhibitors of e.g. viral entry (S protein) or RNA synthesis [27]. The latter process depends on a set of enzymatic activities [24] including an RNA-dependent RNA polymerase (RdRp; in nsp12), RNA helicase (in nsp13), two methyltransferases involved in mRNA capping (a guanine-N7-methyltransferase in nsp14 and a nucleoside-2'-O-methyltransferase in nsp16) and a unique exoribonuclease (ExoN, in nsp14) that promotes the fidelity of the replication of the large CoV genome [28]. Other potential drug targets are the transmembrane proteins that direct the formation of the viral RO, several less well characterised enzymatic activities and a set of smaller nsps (nsp7-10) that mainly appear to serve as cofactors/modulators of other nsps.

The newly emerged SARS-CoV-2 was rapidly identified as a CoV that is relatively closely related to the 2003 SARS-CoV [9, 29, 30].The two genome sequences are about ~80% identical and the organization of open reading frames is essentially the same. The overall level of amino acid sequence identity of viral proteins ranges from about 65% in the least conserved parts of the S protein to about 95% in the most conserved replicative enzyme domains, prompting the coronavirus study group of the International Committee on the Taxonomy of Viruses to classify the new agent within the species *Severe acute respiratory syndrome-related coronavirus*, which also includes the 2003 SARS-CoV [1]. The close phylogenetic relationship also implies that much of our knowledge of SARS-CoV molecular biology, accumulated over the past 17 years, can probably be translated to SARS-CoV-2. Many reports posted over the past months have described such similarities, including the common affinity of the two viruses for the angiotensin-converting enzyme 2 (ACE2) receptor [9, 31]. This receptor is abundantly expressed in Vero cells (African green monkey kidney cells). Since 2003, Vero cells have been used extensively for SARS-CoV research in cell culture-based infection models by many laboratories, including our own.

We set out to establish the basic features of SARS-CoV-2 replication in Vero cells and compare it to the Frankfurt-1 SARS-CoV isolate from 2003 [32, 33] . When requesting virus isolates

(February 2020), and in spite of the rapidly emerging public health crisis, we were confronted - not for the first time - with administrative hurdles and discussions regarding the alleged 'ownership' of virus isolates cultured from (anonymous) clinical samples. From a biological and evolutionary point of view, this would seem a strangely anthropocentric consideration, but it ultimately forced us to reach out across the globe to Australian colleagues in Melbourne. After checking our credentials and completing a basic material transfer agreement, they provided us (within one week) with their first SARS-CoV-2 isolate (originally named 2019-nCoV/Victoria/1/2020 and subsequently renamed BetaCoV/Australia/VIC01/2020; [34], which will be used throughout this study. Until now, this isolate has been provided to 17 other laboratories worldwide to promote the rapid characterization of SARS-CoV-2, in this critical time of lockdowns and other preventive measures to avoid a collapse of public health systems. In this report, we describe a comparative study of the basic replication features of SARS-CoV and SARS-CoV-2 in Vero E6 cells, including growth kinetics, virus titres, plaque phenotype and an analysis of intracellular viral RNA and protein synthesis. Additionally, we analysed infected cells by light and electron microscopy, and demonstrated cross-reactivity of 13 available SARS-CoV-specific antisera (recognising 10 different viral proteins) with their SARS-CoV-2 counterparts. Finally, we established the conditions for a medium-throughput assay to evaluate basic antiviral activity and assessed the impact of some known CoV inhibitors on SARS-CoV-2 replication. In addition to many anticipated similarities, our results also established some remarkable differences between the two viruses that warrant further investigation. One of them is the rapid evolution - during virus passaging in Vero cells - of a specific region of the SARS-CoV-2 S protein that contains the so-called furin-like cleavage site.

RESULTS

Rapid adaptation of SARS-CoV-2 BetaCoV/Australia/VIC01/2020 during passaging in Vero E6 cells

SARS-CoV-2 isolate BetaCoV/Australia/VIC01/2020 was received as a stock derived from two consecutive passages in Vero/hSLAM cells [34]. The virus was then propagated two more times at low m.o.i.in Vero E6 cells, in which it caused a severe cytopathic effect (CPE). We also attempted propagation in HuH7 cells, using the same amount of virus or a ten-fold larger inoculum, but did not observe any cytopathology after 72 h (data not shown). At 24 h p.i., immunofluorescence microscopy revealed infection of only a small percentage of the HuH7 cells, without any clear spread to other cells occurring in the next 48 h. We therefore conclude that infection of HuH7 cells does not lead to a productive SARS-CoV-2 infection and deemed this cell line unsuitable for further SARS-CoV-2 studies.

The infectivity titre of the Leiden-p2 stock grown in Vero E6 cells was analysed by plaque assay, after which we noticed a mixed plaque phenotype (~1:3 ratio of small versus large (plaques; data not shown) while a virus titre of 7 x 10^6 PFU/ml was calculated. To verify the identity and genome sequence of the SARS-CoV-2/p2 virus stock, we isolated genomic RNA from culture supernatant and applied next-generation sequencing (NGS; see methods for details). The resulting consensus sequence was found to be identical to the sequence previously deposited in GenBank (accession number MT007544.1) [34], with one exception. Compared to the SARS-CoV-2 GenBank reference sequence (NC_045512.3) [35] and other field isolates [29], isolate BetaCoV/Australia/VIC01/2020 exhibits >99.9% sequence identity. In addition to synonymous mutations in the nsp14-coding sequence (U19065 to C) and S protein gene (U22303 to G), ORF3a contains a single non-synonymous mutation (G26144 to U). Strikingly, the 3' untranslated region (UTR) contains a 10-nt deletion (nt 29750-29759; CGAUCGAGUG) located 120 nt upstream of the genomic 3' end, which is not present in other SARS-CoV-2 isolates described thus far (>670 SARS-CoV2 sequences present in GenBank on April 17, 2020).

In about 71% of the 95,173 p2 NGS reads covering this position, we noticed a G23607 to A mutation encoding an Arg682 to Gln substitution near the so-called S1/S2 cleavage site of the viral S protein (see Discussion), with the other 29% of the reads being wild-type sequence. As this ratio approximated the observed relative proportions between large and small plaques, we performed a plaque assay on the p1 virus stock (Fig. 1a, leftmost well) and picked multiple plaques of each size, which were passaged three times in Vero E6 cells while monitoring their plaque phenotype. Interestingly, for several of the small-plaque virus clones (like S5; Fig. 1a) we observed rapid conversion to a mixed or large-plaque phenotype during these three passages, while large-plaque virus clones (like L8) stably retained their plaque phenotype (Fig. 1a). NGS analysis of the genome of a large-plaque p1 virus (L8p1) revealed that >99% of the reads in the S1/S2 cleavage site region contained the G23607 to A mutation described above. No other mutations were detected in the genome, thus clearly linking the Arg682 to Gln substitution in the S protein to the large-plaque phenotype observed for the L8p1 virus.

Next, we also analysed the genomes of the p1, p2 and p3 viruses derived from a small-plaque (S5) that was picked. This virus clone retained its small-plaque phenotype during the first passage (Fig. 1a; S5p1), but began to yield an increasing proportion of large(r) plaques during subsequent passages. Sequencing of S5p2 (Fig. 1b) revealed a variety of low-frequency reads with mutations near the S1/S2 cleavage site motif (aa 681-687; PRRAR↓SV), with G23607 to A (specifying the Arg682 to Gln substitution) again being the dominant one (in ~2.1% of the reads covering nt 23,576 to 23,665 of the genome). At lower frequencies single-nucleotide

changes specifying Arg682 to Trp and Arg683 to Leu substitutions were also detected. Furthermore, a 10-aa deletion (residues 679-688) that erases the S1/S2 cleavage site region was discovered, as well as a 5-aa deletion (residues 675-679) immediately preceding that region. The amount of large plaques increased substantially upon the next passage, with NGS revealing the prominent emergence of the mutants containing the 10-aa deletion or the Arg682 to Gln point mutation (~22% and ~12% of the reads, respectively), and yet other minor variants with mutations in the PRRAR↓SV sequence being discovered. Taken together these data clearly link the large-plaque phenotype of SARS-CoV-2 to the acquisition of mutations in this particular region of the S protein, which apparently provides a strong selective advantage during passaging in Vero E6 cells.

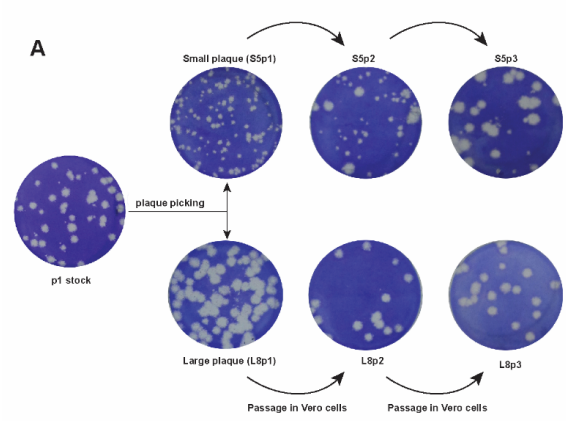

B

672-ASYQTQTNSPRRAR↓SVASQSIIAYTMSLGA-702

Mutation in furin-like cleavage site region	p2 stock	S5p1	S5p2	S5p3	L8p1
Wild type	44.4%	100%	93.9%	56.5%	13.2%
R682Q	48.3%		2.1%	11.6%	86.8%
R682W	3.8%		1.5%	4.3%	
R682P				1.7%	
R683L			0.9%	1.5%	
R685L	1.4%				
R685P	0.8%				
675-679ΔQTQTN	1.5%		0.8%	2.2%	
679-688ΔNSPRRARSVA			0.7%	22.3%	

Fig. 1. Rapid evolution of SARS-CoV-2 during passaging in Vero E6 cells. (a) Outline of a plaque picking experiment that was initiated when the p2 stock of SARS-CoV-2 Australia/VIC01/2020 showed remarkable plaque heterogeneity on Vero E6 cells (leftmost well). Following a plaque assay of the p1 virus stock, small and large plaques were picked and these virus clones were passaged three times in Vero E6 cells, while their plaque phenotype was monitored. In contrast to the large plaque viruses (example L8; bottom row), the plaque phenotype of the small plaque viruses (example S5; top row) rapidly evolved within these 3 passages. (b) Evolution/adaptation of the S protein gene during Vero E6 passaging. Overview of NGS data obtained for the p2 stock, S5p1/p2/p3 and S8p1 in the S1/S2 region of the SARS-CoV-2 S protein gene that encodes the so-called furin-like cleavage site. The analysis was based on NGS reads spanning nt 23,576 to 23,665 of the SARS-CoV genome (see Methods for details) and their translation in the S protein open reading frame. Deletions are indicated with Δ followed by the affected amino acid residues.

Comparative kinetics of SARS-CoV and SARS-CoV-2 replication in Vero E6 cells

To our knowledge, a detailed comparison of SARS-CoV-2 and SARS-CoV replication kinetics in cell culture has not been reported so far. Therefore, we infected Vero E6 cells with the SARS-CoV-2/p2 virus stock at high m.o.i. to analyse viral RNA synthesis and the release of infectious viral progeny (Fig. 2a). This experiment was performed using 4 replicates per time point and for comparison we included the SARS-CoV Frankfurt-1 isolate [36], which has been used in our laboratory since 2003. During the early stages of infection (until 8 h p.i.), the growth curves of the two viruses were similar, but subsequently cells infected with SARS-CoV clearly produced more infectious progeny (about 50-fold more) than SARS-CoV-2-infected cells, with both viruses reaching their plateau by about 14 h p.i. As shown in Fig. 2b, despite its transition to a mainly large-plaque phenotype, the largest SARS-CoV-2/p3 plaques were still substantially smaller than those obtained with SARS-CoV Frankfurt-1.

In parallel, we analysed the kinetics of viral RNA synthesis by isolating intracellular viral RNA, subjecting it to agarose gel electrophoresis and visualizing the various viral mRNA species by in-gel hybridization with a ^{32}P-labeled oligonucleotide probe recognizing a fully conserved 19-nt sequence located 30 nt upstream of the 3' end of both viral genomes (Fig. 3a). This revealed the anticipated presence of the genomic RNA and eight subgenomic mRNAs, together forming the well-known 5'- and 3'- coterminal nested set of transcripts required for full CoV genome expression.

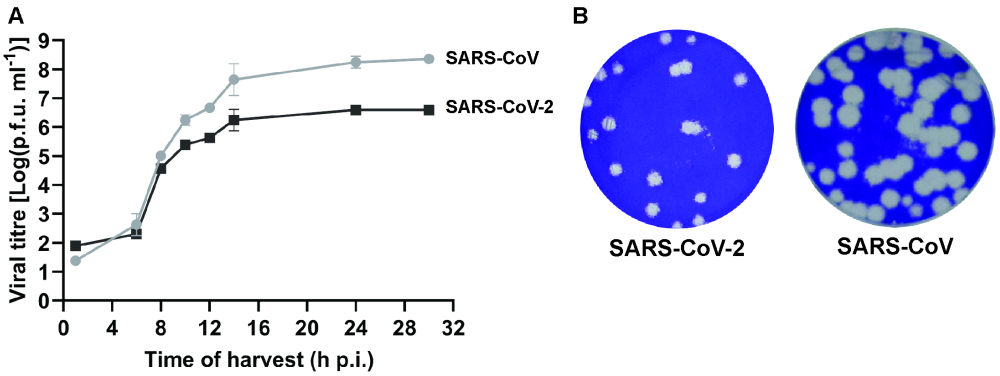

Fig. 2. Comparison of SARS-CoV-2 and SARS-CoV replication kinetics in Vero E6 cells.
(a) Growth curve showing the release of infectious viral progeny into the medium of infected Vero E6 cells (m.o.i. 3), as determined by plaque assay (n = 4; mean ± sd is presented). (b) . Comparison of SARS-CoV-2 Australia/VIC01/2020 and SARS-CoV Frankfurt-1 plaque phenotype in Vero E6 cells.

In general, for both viruses, the accumulation of viral RNAs followed the growth curves depicted in Fig. 2a. The relative abundance of the individual RNAs was determined using the 12, 14 and 24 h p.i. samples (averages presented in Fig. 3b) and found to be largely similar, with the exception of SARS-CoV-2 mRNAs 7 and 8, which accumulated to about 4- and 2-fold higher levels, respectively. Strikingly, in spite of the ultimately lower yield of infectious viral progeny, SARS-CoV-2 RNA synthesis was detected earlier and reached an overall level exceeding that of SARS-CoV. Overall, we conclude that in Vero E6 cells, SARS-CoV-2 produces levels of intracellular RNA that are at least comparable to those of SARS-CoV, although this does not translate into the release of equal amounts of infectious viral progeny (Fig. 2a).

Cross-reactivity of antisera previously raised against SARS-CoV targets

To be able to follow virus replication in SARS-CoV-2-infected cells more closely, we explored cross-reactivity of a variety of antisera previously raised against SARS-CoV targets, in particular a variety of nsps. In an earlier study, many of those were found to cross-react also with the corresponding MERS-CoV targets [37], despite the relatively large evolutionary distance between MERS-CoV and SARS-CoV. Based on the much closer relationship with SARS-CoV-2, similar or better cross-reactivity of these SARS-CoV reagents was expected, which was explored using immunofluorescence microscopy.

Indeed, most antisera recognizing SARS-CoV nsps that were tested (nsp3, nsp4, nsp5, nsp8, nsp9, nsp13, nsp15) strongly cross-reacted with the corresponding SARS-CoV-2 target (Fig. 4 and Table 1), the exception being a polyclonal nsp6 rabbit antiserum. Likewise, both a polyclonal rabbit antiserum and mouse monoclonal antibody recognizing the N protein cross-reacted strongly (Fig. 4b and Table 1). The same was true for a rabbit antiserum raised against a C-terminal peptide of the SARS-CoV M protein (Fig 4e). Labelling patterns were essentially identical to those previously documented for SARS-CoV [38, 39] , with nsps accumulating in the perinuclear region of infected cells, where the elaborate membrane structures of the viral ROs are formed (Fig. 4a, c, d). Punctate structures in the same area of the cell were labelled using an antibody recognizing double-stranded RNA (dsRNA), which presumably recognizes replicative intermediates of viral RNA synthesis [39, 40]. The N protein signal was diffusely cytosolic (Fig. 4b), whereas the M protein labelling predominantly showed the expected localization to the Golgi complex (Fig. 4e), where the protein is known to accumulate [41].

A

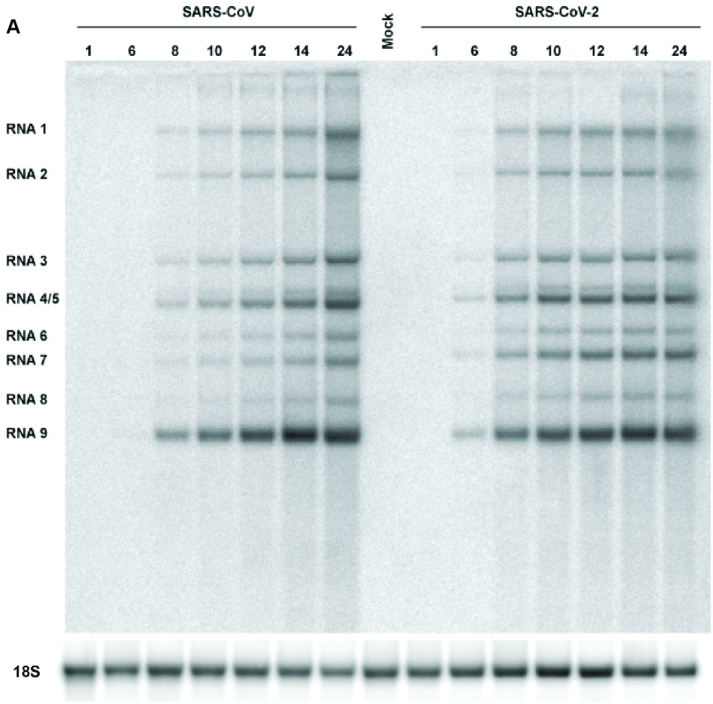

B

RNA	Size (kb) of SARS-CoV-2 mRNA	Abundance (%)	
		SARS-CoV	SARS-CoV-2
1	29.9	6.0	5.1
2	8.4	4.0	3.5
3	4.5	7.2	6.9
4	3.7	1.9	2.0
5	3.4	14.2	18.0
6	2.9	2.0	2.5
7	2.5	3.5	13.7
8	2.0	1.1	2.3
9	1.7	60.0	45.9

Fig. 3. Kinetics of SARS-CoV-2 and SARS-CoV RNA synthesis in infected Vero E6 cells.(a) Hybridization analysis of viral mRNAs isolated from SARS-CoV-2- and SARS-CoV-infected Vero E6 cells, separated in an agarose gel and probed with a radiolabelled oligonucleotide recognizing the genome and subgenomic mRNAs of both viruses. Subsequently, the gel was re-hybridized to a probe specific for 18S ribosomal RNA, which was used as a loading control. (b) Analysis of the relative abundance of each of the SARS-CoV-2 and SARS-CoV transcripts. Phosphorimager quantification was performed for the bands of the samples isolated at 12, 14 and 24 h p.i., which yielded essentially identical relative abundances. The table shows the average of these three measurements. SARS-CoV-2 mRNA sizes were calculated on the basis of the position of the leader and body transcription-regulatory sequences (ACGAAC) in the viral genome [42, 43]

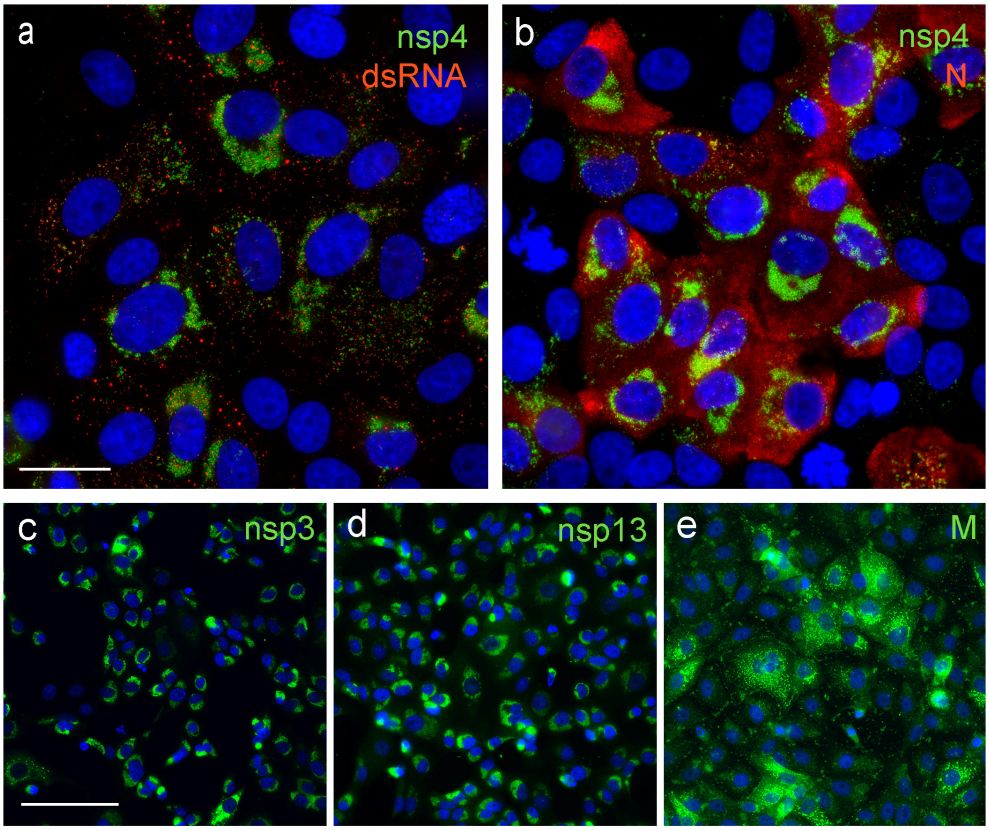

Fig. 4. Cross-reactivity of antisera raised against SARS-CoV structural and non-structural proteins. Selected antisera previously raised against SARS-CoV nsps and structural proteins cross-react with corresponding SARS-CoV-2 proteins. SARS-CoV-2-infected Vero E6 cells (m.o.i. of 0.3) were fixed at 12 or 24 h p.i. For immunofluorescence microscopy, cells were (double)labelled with (a) a rabbit antiserum recognising nsp4 and a mouse mAb recognising dsRNA; (b) anti-nsp4 rabbit serum and a mouse mAb directed against the N protein; (c-e) rabbit antisera recognising against nsp3, nsp13 and the M protein, respectively. Nuclear DNA was stained with Hoechst 33258. Bar is 25 µm for a and b; 100 µm for c, d and e.

Ultrastructural characterization of SARS-CoV-2-infected cells

We next used electron microscopy to investigate the ultrastructural changes that SARS-CoV-2 induces in infected cells, and focused on the membranous replication organelles (ROs) that support viral RNA synthesis and on the assembly and release of new virions (Fig. 5). Compared to mock-infected control cells (Fig. 5a-b), various distinct membrane alterations were observed in cells infected with either SARS-CoV or SARS-CoV-2 (Fig. 5c-j). At 6 h p.i., larger

regions with membrane alterations were found particularly in cells infected with SARS-CoV-2 (data not shown), which may align with the somewhat faster onset of intracellular RNA synthesis in SARS-CoV2-infected Vero E6 cells (Fig. 3a). From 8 h p.i onwards, SARS-CoV- and SARS-CoV-2-infected cells appeared more similar (Fig. 5c-f and 5g-j). Double-membrane vesicles (DMVs) were the most prominent membrane alteration up to this stage (Fig. 5d-e and and 5h-i, asterisks). In addition, convoluted membranes [39] were readily detected in SARS-CoV-infected cells, while zippered ER [25, 44, 45] appeared to be the predominant structure in SARS-CoV-2-infected cells (Fig. 5e and 5i, white arrowheads). As previously described for SARS-CoV [39], SARS-CoV-2-induced DMVs also appeared to fuse through their outer membrane, giving rise to vesicle packets that increased in numbers as infection progressed (Fig 5f and 5k, white asterisks). Virus budding near the Golgi apparatus, presumably into smooth membranes of the ER-Golgi intermediate compartment (ERGIC) [38, 46, 47], was frequently observed at 8 h p.i. (Fig. 5k-l and 5o-p). This step is followed by transport to the plasma membrane and release of virus particles into extracellular space. By 10 h p.i., released progeny virions were abundantly detected around all infected cells (Fig. 5m-n and 5q-r). Interestingly, whereas spikes were clearly present on SARS-CoV progeny virions, a relatively large proportion of SARS-CoV-2 particles seemed to carry few or no visible spike projections on their surface, perhaps suggesting a relatively inefficient incorporation of spike proteins into SARS-CoV-2 virions. This could potentially reduce the yield of infectious particles and may contribute to the lower progeny titres obtained for this virus (Fig. 2a).

Table 1- SARS-CoV-specific antisera used and their cross-reactivity with corresponding SARS-CoV-2 targets.

SARS-CoV antiserum	function of target	antigen type	antibody type	IFA signal*	reference
nsp3 (DGD7)	transmembrane replicase protein, containing PL^{pro}	bacterial expression product	rabbit polyclonal	++	[41]
nsp4 (FGQ4)	transmembrane replicase protein	synthetic peptide	rabbit polyclonal	++	[48]
nsp5 (DUE5)	M^{pro}	bacterial expression product	rabbit polyclonal	+	[41]
nsp6 (GBZ7)	transmembrane replicase protein	synthetic peptide	rabbit polyclonal	-	[48]
nsp8 (DUK4)	RNA polymerase co-factor	bacterial expression product	rabbit polyclonal	++	[41]
nsp8 (39-12)	RNA polymerase co-factor	bacterial expression product	mouse monoclonal	++	unpublished
nsp9 (HLJ5)	RNA-binding protein	synthetic peptide	rabbit polyclonal	++	unpublished
nsp13 (CQS2)	RNA helicase	synthetic peptide	rabbit polyclonal	++	[41]
nsp15 (HLT5)	endoribonuclease	bacterial expression product	rabbit polyclonal	+	unpublished
nsp15 (BGU6)	endoribonuclease	synthetic peptide	rabbit polyclonal	+	[41]
M (EKU9)	membrane protein	synthetic peptide	rabbit polyclonal	+	[41]
N (JUC3)	nucleocapsid protein	bacterial expression product	rabbit polyclonal	+	[37]
N (46-4)	nucleocapsid protein	bacterial expression product	mouse monoclonal	++	[49]

* ++, strongly positive; +, positive; -, negative.

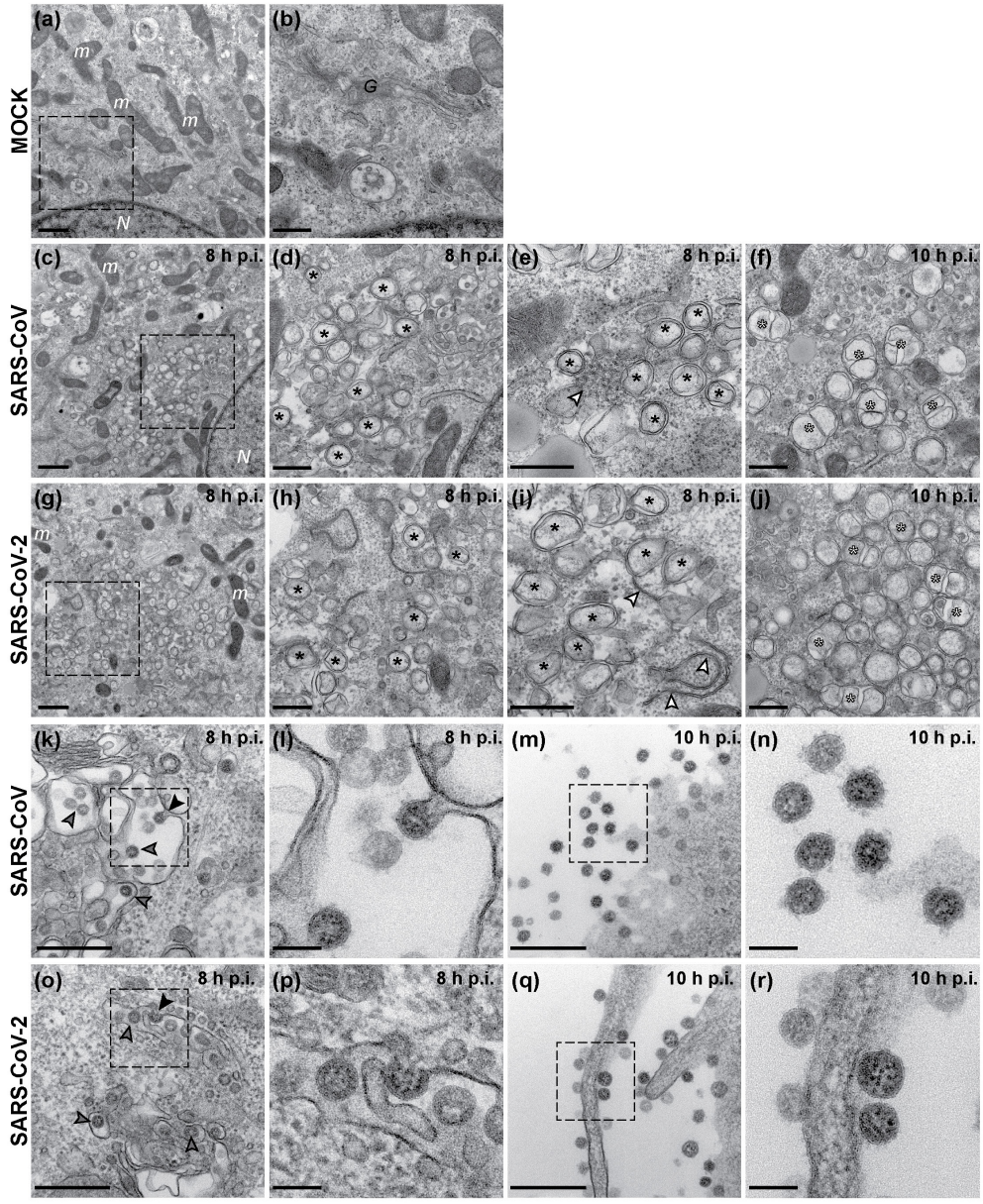

Fig. 5. Visualisation of SARS-CoV-2 and SARS-CoV infection by electron microscopy.

Electron micrographs of Vero E6 cells infected with either SARS-CoV-2 or SARS-CoV at the indicated time points (c-j). Images from a mock-infected cell are included for comparison (a-b). (c-j) Regions containing viral replication organelles. These virus-induced structures accumulated in large clusters in the perinuclear region by 8 h p.i. (c, g, boxed regions enlarged in d and h, respectively). These regions primarily contained DMVs (d-e, h-i, black asterisks). Additionally, virus-induced convoluted

membranes (e, white arrowhead) were observed in SARS-CoV infection, whereas zippered ER (i, white arrowheads) appeared to be more common in SARS-CoV-2-infected cells. At 10 h p.i., vesicle packets (f, j, white asterisks), which seem to arise by fusion of two or more DMVs through their outer membrane, became abundant in the RO regions. (k-r) Examples of virion assembly and release in infected cells. Virus particles budding into membranes of the ERGIC (k-l, o-p, arrowheads). The black arrowheads in the boxed areas highlight captured budding events, enlarged in l and p. Subsequently, virus particles are transported to the plasma membrane which, at 10 h p.i., is surrounded by a large number of released virions (m, q, boxed areas enlarged in n and r, respectively). N, nucleus; m, mitochondria; G, Golgi apparatus. Scale bars: 1 µm (a, c, g); 500 nm (b, d-f, h-j, k, m, o, q); 100 nm (l, n, p, r).

Establishing a CPE-based assay to screen compounds for anti-SARS-CoV-2 activity

In order to establish and validate a CPE-based assay to identify potential inhibitors of SARS-CoV-2 replication, we selected four previously identified inhibitors of CoV replication: Remdesivir [50, 51], chloroquine [52, 53], Alisporivir [54, 55] and pegylated interferon alpha (PEG-IFN-α) [37, 56]. Cells were infected at low m.o.i. to allow for multiple cycles of replication. After three days, a colorimetric cell viability assay [57] was used to measure drug toxicity and inhibition of virus replication in mock- and virus-infected cells, respectively. With the exception of PEG-IFN-α, the inhibition of virus replication by the compounds tested and the calculated half-maximal effective concentrations (EC_{50}) were similar for SARS-CoV and SARS-CoV-2. For Remdesivir, we obtained higher EC_{50} values for SARS-CoV-2 and SARS-CoV (6.2 ±1.3 and 4.5 ±1.1µM, respectively; Fig. 6a) than previously reported by others, but this may be explained by technical differences like a longer assay incubation time (72 h instead of 48 h) and the use of a different read-out (cell viability instead of qRT-PCR or viral load). Based on the obtained half maximal cytotoxic concentration (CC_{50}) values of >100 µM, a selectivity index >22.5 was calculated. Chloroquine potently blocked virus infection at low-micromolar concentrations, with an EC_{50} value of 2.3 ± 1.1 µM for both viruses (CC_{50} >100 µM, SI >45.5; Fig. 6b). Alisporivir, a known inhibitor of different groups of RNA viruses, was previously found to effectively reduce the production of CoV progeny. In this study, we measured EC_{50} values of 4.9 ± 1.3 and 4.3 ± 1.0 µM for SARS-CoV-2 and SARS-CoV, respectively (Fig. 6c; CC_{50}>100 µM, SI >20). Treatment with PEG-IFN-α completely inhibited replication of SARS-CoV-2, even at the lowest dose of 7.8 ng/ml (Fig. 6d). In line with previous results [37, 56], SARS-CoV was much less sensitive to PEG-IFN-α treatment, yielding only partial inhibition at all concentrations tested (from 7.8 to 1000 ng/ml). Overall, we conclude that Vero E6 cells provide a suitable basis to perform antiviral compound screening and select the most promising hits for in-depth mechanistic studies and further development.

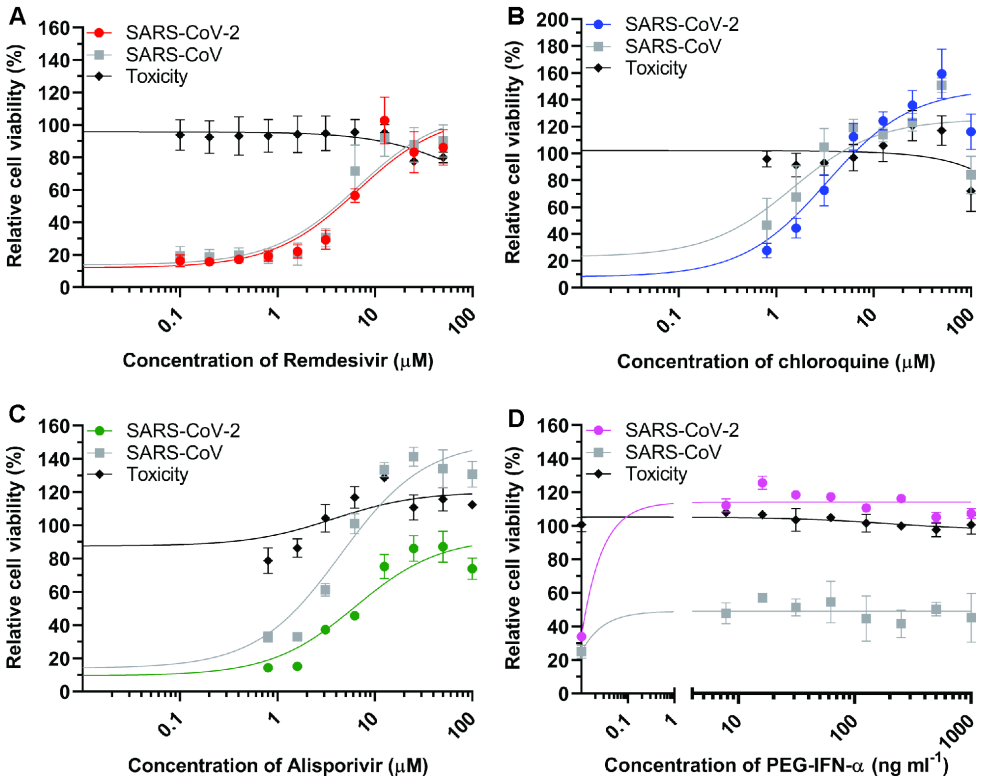

Fig. 6. Assay to screen for compounds that inhibit SARS-CoV-2 replication.

Inhibition of SARS-CoV-2 replication (coloured symbols and curves) was tested in Vero E6 cells by developing a CPE-reduction assay and evaluating several previously identified inhibitors of SARS-CoV, which was included for comparison (grey symbols and curves). For each compound a two-fold serial dilution series in the low-micromolar range was tested; (a) Remdesivir, (b) chloroquine, (c) Alisporivir and (d) pegylated interferon alpha-2. Cell viability was assayed using the CellTiter 96® Aqueous One Solution cell proliferation assay (MTS assay). Compound toxicity (solid line) was evaluated in parallel using mock-infected, compound-treated cells. The graphs show the results of 3 independent experiments, each performed using quadruplicate samples (mean ± SD are shown). A non-linear regression analysis was applied.

DISCUSSION

In this report, we describe a comparative analysis of the replication features of SARS-CoV-2 and SARS-CoV in Vero E6 cells, one of the most commonly used cell lines for studying these two viruses. In contrast to the stable phenotype exhibited by SARS-CoV during our 17 years of working with this virus in these cells, SARS-CoV-2 began to exhibit remarkable phenotypic variation in plaque assays within a few passages after its isolation from clinical samples (Fig.

1a). In addition to the BetaCoV/Australia/VIC01/2020 isolate used in this study, similar observations were made for a variety of other clinical isolates (data not shown). To establish the genetic basis for the observed plaque size heterogeneity, small and large plaques were picked and the resulting virus clones were passaged repeatedly and analysed using NGS. The consensus sequences obtained for S5p1 and L8p1, which differed by a single nucleotide substitution in the S protein gene, clearly established that a single S protein mutation (Arg682 to Gln) was responsible for the observed plaque size difference. This mutation is localized near the so-called furin-like S1/S2 cleavage site (Fig. 1b) [58] in the S protein [59]. This sequence constitutes a (potential) processing site that is present in a subset of CoVs (including SARS-CoV-2 and MERS-CoV) but is lacking in others, like SARS-CoV and certain bat CoVs [58, 60]. This polybasic motif (PRRAR↓SV, in SARS-CoV-2) can be recognized by intracellular furin-like proteases during viral egress and its cleavage is thought to prime the S protein for fusion and entry [61], which also requires a second cleavage event to occur at the downstream S2' cleavage site [58]. In general, the presence of the furin-like cleavage site does not appear to be critical for successful CoV infection. Using pseudotyped virions carrying mutant S proteins of SARS-CoV [62] or SARS-CoV-2 [63], it was shown that its presence minimally impacts S protein functionality. In the SARS-CoV S protein, an adjacent sequence that is conserved across CoVs can be cleaved by other host proteases like cathepsin L or TMPRSS2 [64-66], thus providing an alternative pathway to trigger viral entry. Possibly, this pathway is also employed by our Vero E6-cell adapted SARS-CoV-2 mutants that have lost the furin-like cleavage site, like clone L8p1 and multiple variants encountered in S5p3 (Fig. 1a). These variants contain either single point mutations or deletions of 5 to 10 aa (Fig. 1b), resembling variants recently reported by other laboratories [30, 67, 68]. Interestingly similar changes were also observed in some clinical SARS-CoV-2 isolates that had not been passaged in cell culture [67]. It is currently being investigated why mutations that inactivate the furin-like cleavage site provide such a major selective advantage during SARS-CoV-2 passaging in Vero E6 cells and how this translates into the striking large-plaque phenotype documented in this paper.

An additional remarkable feature confirmed by our re-sequencing of the BetaCoV/Australia/VIC01/2020 isolate of SARS-CoV-2 is the presence of a 10-nt deletion in the 3' UTR of the genome [34]. Screening of other available SARS-CoV-2 genome sequences indicated that the presence of this deletion apparently is unique for this particular isolate, and likely represents an additional adaptation acquired during cell culture passaging. This deletion maps to a previously described "hypervariable region" in the otherwise conserved 3' UTR, and in particular to the so-called s2m motif [69] that is conserved among CoVs and also found in several other virus groups [70, 71]. The s2m element has been implicated in the binding of

host factors to viral RNAs, but its exact function has remained enigmatic thus far. Strikingly, for the mouse hepatitis coronavirus the entire hypervariable region (including s2m) was found to be dispensable for replication in cell culture, but highly relevant for viral pathogenesis in mice [69]. Although the impact of this deletion for SARS-CoV-2 remains to be studied in more detail, these previous data suggest that this mutation need not have a major impact on SARS-CoV-2 replication in Vero E6 cells. This notion is also supported by the fact that the results of our antiviral screening assays (Fig. 6) correlate well with similar studies performed with other SARS-CoV-2 isolates [51, 72, 73]. Clearly, this could be different for *in vivo* studies, for which it would probably be better to rely on SARS-CoV-2 isolates not carrying this deletion in their 3' UTR.

Vero E6 cells are commonly used to isolate, propagate and study SARS-CoV-like viruses as they support viral replication to high titres [74-78]. This may be due to a high expression level of the ACE-2 receptor [79] that is used by both SARS-CoV-2 and SARS-CoV [9] and/or the fact that they lack the ability to produce interferon [80, 81]. It will be interesting to evaluate whether there is a similarly strong selection pressure to adapt the S1/S2 region of the S protein when SARS-CoV-2 is passaged in other cell types. Such studies are currently in progress in our laboratory and already established that HuH7 cells may be a poor choice, despite the fact that they were used for virus propagation [9, 82] and antiviral screening in other studies [51, 83]. Immunolabelling of infected HuH7 cells (data not shown) revealed non-productive infection of only a small fraction of the cells and a general lack of cytopathology. While other cell lines are being evaluated, the monitoring of the plaque phenotype (plaque size and homogeneity) as illustrated above may provide a quick and convenient method to assess the composition of SARS-CoV-2 stocks propagated in Vero E6 cells, at least where it concerns the evolution of the S1/S2 region of the S protein.

Given the ongoing SARS-CoV-2 pandemic, the detailed characterization of its replication cycle is an important step in understanding the molecular biology of the virus and defining potential targets for inhibitors of replication. The cross-reacting antisera described in this study (Table 1) will be a useful tool during such studies. In general, the subcellular localization of viral nsps and structural proteins (Fig. 4) and the ultrastructural changes associated with RO formation (Fig. 5) were very similar for the two viruses. We also observed comparable replication kinetics for SARS-CoV-2 and SARS-CoV in Vero E6 cells, although clearly lower final infectivity titres were measured for SARS-CoV-2 (~50-fold lower; Fig. 2). Nevertheless, RNA synthesis could be detected somewhat earlier for SARS-CoV-2 and the overall amount of viral RNA produced exceeded that produced by SARS-CoV (Fig. 3). This may be indicative of certain assembly or maturation problems or of virus-host interactions that are different in the case of SARS-CoV-

2. These possibilities merit further investigation, in particular since our preliminary EM studies suggested intriguing differences with SARS-CoV regarding the abundance of spikes on the surface of freshly released SARS-CoV-2 particles (Fig. 5n and 5r).

Our analysis of SARS-CoV-2 subgenomic mRNA synthesis revealed an increased relative abundance of mRNAs 7 and 8 (~4- and ~2-fold, respectively) in comparison to SARS-CoV. Mechanistically, these differences do not appear to be caused by extended base pairing possibilities of the transcription regulatory sequences that direct the synthesis of these two mRNAs [24]. As in SARS-CoV, mRNA7 of SARS-CoV-2 encodes for two proteins, the ORF7a and ORF7b proteins, with the latter presumably being expressed following leaky ribosomal scanning [32]. Upon ectopic expression, the ORF7a protein has been reported to induce apoptosis via a caspase-dependent pathway [84] and/or to be involved in cell cycle arrest [85]. The ORF7b product is a poorly studied integral membrane protein that has (also) been detected in virions [86]. When ORF7a/b or ORF7a were deleted from the SARS-CoV genome, there was a minimal impact on the kinetics of virus replication *in vitro* in different cell lines, including Vero cells, and *in vivo* using mice. In another study, however, partial deletion of SARS-CoV ORF7b was reported to provide a replicative advantage in CaCo-2 and HuH7 cells, but not in Vero cells [87].

The SARS-CoV ORF8 protein is membrane-associated and able to induce endoplasmic reticulum stress [88, 89], although it has not been characterised in great detail in the context of viral infection. Soon after the emergence of SARS-CoV in 2003, a conspicuous 29-nt (out-of-frame) deletion in ORF8 was noticed in late(r) human isolates, but not in early human isolates and SARS-like viruses obtained from animal sources [90-92]. Consequently, loss of ORF8 function was postulated to reflect an adaptation to the human host. The re-engineering of an intact ORF8, using a reverse genetics system for the SARS-CoV Frankfurt-1 isolate, yielded a virus with strikingly enhanced (up to 23-fold) replication properties in multiple systems [93] . Clearly, it remains to be established whether the increased synthesis of mRNAs 7 and 8 is a general feature of SARS-CoV-2 isolates, and this indeed also translates into higher expression levels of the accessory proteins encoded by ORFs 7a, 7b and 8. If confirmed, these differences definitely warrant an in-depth follow-up analysis as CoV accessory proteins in general have been shown to be important determinants of virulence. They may thus be relevant for our understanding of the wide spectrum of respiratory disease symptoms observed in COVID-19 patients [94].

Based on the close ancestral relationship between SARS-CoV-2 and SARS-CoV [95], one might expect that the patterns and modes of interaction with host antiviral defence mechanisms would be similar. However, our experiments with type I interferon treatment of Vero E6 cells

(Fig. 6) revealed a clear difference, with SARS-CoV-2 being considerably more sensitive than SARS-CoV, as also observed by other laboratories [73]. Essentially, SARS-CoV-2 replication could be inhibited by similarly low concentrations of PEG-IFN-alpha-2a that inhibit MERS-CoV replication in cell culture [37]. Taken together, our data suggest that SARS-CoV-2 is less able to counteract a primed type I IFN response than SARS-CoV [73, 96].

Previously identified inhibitors of CoV replication were used to further validate our cell-based assay for SARS-CoV-2 inhibitor screening. These compounds inhibited replication at similar low-micromolar concentrations and in a similar dose-dependent manner as observed for SARS-CoV (Fig. 6). Remdesivir is a prodrug of an adenosine analogue developed by Gilead Sciences. It was demonstrated to target the CoV RNA polymerase and act as a chain terminator [97-99]. The clinical efficacy of Remdesivir is still being evaluated and, after some first encouraging results [100], worldwide compassionate use trials are now being conducted. Likewise, hydroxychloroquine and chloroquine have been labelled as potential "game changers" and are being evaluated for treatment of severe COVID-19 patients [101]. Both compounds have been used to treat malaria and amebiasis [102], until drug-resistant *Plasmodium* strains emerged [103]. These compounds can be incorporated into endosomes and lysosomes, raising the pH inside these intracellular compartments, which in turn may lead to defects in protein degradation and intracellular trafficking [65, 104]. An alternative hypothesis to explain their anti-SARS-CoV activity is based on their impact on glycosylation of the ACE2 receptor that is used by SARS-CoV [53]. Finally, as expected, the non-immunosuppressive cyclosporin A analogue Alisporivir inhibited SARS-CoV-2 replication, as demonstrated previously for SARS-CoV and MERS-CoV [55]. Although the exact mode of action of this inhibitor is unclear, it is thought to modulate CoV interactions with members of the cyclophilin family [105]. Unfortunately, all of these *in vitro* antiviral activities should probably be classified as modest, emphasizing the urgency of large-scale drug repurposing and discovery programmes that target SARS-CoV-2 and coronaviruses at large.

METHODS

Cell and virus culture

Vero E6 cells and HuH7 cells were grown as described previously [37]. SARS-CoV-2 isolate Australia/VIC01/2020 (GeneBank ID: MT007544.1; [34]) was derived from a positively-testing nasopharyngeal swab in Melbourne, Australia, and was propagated twice in Vero/hSLAM cells, before being shared with other laboratories. In Leiden, the virus was passaged two more times at low multiplicity of infection (m.o.i.) in Vero E6 cells to obtain a working stock (p2 stock) that was used in all experiments. SARS-CoV isolate Frankfurt 1 [36] was used to

compare growth kinetics and other features with SARS-CoV-2. Infection of Vero E6 cells was carried out in phosphate-buffered saline (PBS) containing 50 µg/ml DEAE-dextran and 2% fetal calf serum (FCS; Bodinco). The inoculum was added to the cells for 1 h at 37°C, after which cells were washed twice with PBS and maintained in Eagle's minimal essential medium (EMEM; Lonza) with 2% FCS, 2mM L-glutamine (PAA) and antibiotics (Sigma). Viral titres were determined by plaque assay in Vero E6 cells as described previously [106]. For plaque picking, plaque assays were performed using our p1 stock, while using an overlay containing 1% of agarose instead of Avicel (RC-581; FMC Biopolymer). Following neutral red staining, small and large plaques were picked and used to inoculate a 10-cm^2 dish of Vero E6 cells containing 2 ml of EMEM-2%FCS medium, yielding p1 virus. After 48 h, 200 µl of the culture supernatant was used to infect the next dish of cells (p2), a step that was repeated one more time to obtain p3 virus. All work with live SARS-CoV and SARS-CoV-2 was performed in biosafety laboratory level 3 facilities at Leiden University Medical Center, the Netherlands.

Analysis of intracellular viral RNA and protein synthesis

Isolation of intracellular RNA was performed by lysing infected cell monolayers with TriPure isolation reagent (Roche Applied Science) according to the manufacturer's instructions. After purification and ethanol precipitation, intracellular RNA samples were loaded onto a 1.5% agarose gel containing 2.2 M formaldehyde, which was run overnight at low voltage in MOPS buffer (10 mM MOPS (sodium salt) (pH 7), 5 mM sodium acetate, 1 mM EDTA). Dried agarose gels were used for direct detection of viral mRNAs by hybridization with a ^{32}P-labeled oligonucleotide probe (5'-CACATGGGGATAGCACTAC-3') that is complementary to a fully conserved sequence located 30 nucleotides upstream of the 3' end of the genome as well as all subgenomic mRNAs produced by SARS-CoV-2 and SARS-CoV. After hybridization, RNA bands were visualised and quantified by phosphorimaging using a Typhoon-9410 variable mode scanner (GE Healthcare) and ImageQuant TL software (GE Healthcare). In order to verify the amount of RNA loaded, a second hybridization was performed using a ^{32}P-labeled oligonucleotide probe recognizing 18S ribosomal RNA (5'-GATCCGAGGGCCTCACTAAAC-3'). Protein lysates were obtained by lysing infected cell monolayers in 4x Laemmli sample buffer and were analysed by semi-dry Western blotting onto Hybond 0.2µM polyvinylidene difluoride (PVDF) membrane (GE Healthcare). Membranes were incubated with rabbit antisera diluted in PBS with 0.05% Tween-20 containing 5% dry milk (Campina). Primary antibodies were detected with a horseradish peroxidase-conjugated swine anti-rabbit IgG antibody (Dako) and protein bands were visualised using Clarity Western Blot substrate (Biorad) and detected using an Advanced Q9 Alliance imager (Uvitec Cambridge).

Next-generation sequencing and bioinformatics analysis

SARS-CoV-2 genomic RNA was isolated from cell culture supernatants using TriPure isolation reagent (Roche Applied Science) and purified according to manufacturer's instructions. The total amount of RNA in samples was measured using a Qubit fluorometer and RNA High Sensitivity kit (Thermo Fisher Scientific). For next-generation sequencing (NGS) library preparation, RNA (25-100 ng) was mixed with random oligonucleotide primers using the NEBNext® First Strand Synthesis Module kit for Illumina® (NEB) and incubated for 10 min at 94°C. NGS of samples was performed by a commercial service provider (GenomeScan, Leiden, the Netherlands) while including appropriate quality controls after each step of the procedure. Sequencing was performed using a NovaSeq 6000 Sequencing System (Illumina). Subsequently, sequencing reads were screened for the presence of human (GRCh37.75), mouse (GRCm38.p4), E. coli MG1655 (EMBL U00096.2), phiX (RefSeq NC_001422.1) and common vector sequences (UniVec and ChlSab1.1). Prior to alignment, reads were trimmed to remove adapter sequences and filtered for sequence quality. The remaining reads were mapped to the SARS-CoV-2 GenBank reference sequence (NC_045512.2; [35]). Data analysis was performed using Bowtie 2 [107]. Raw NGS data sets for each virus sample analysed in this study are deposited in NCBI Bioproject and available under the following link: http://www.ncbi.nlm.nih.gov/bioproject/628043. Only SARS-CoV-2-specific reads were included in these data files.

To study evolution/adaptation of the S protein gene, we performed an in-depth analysis of reads covering the S1/S2 region of the S protein gene. This was done for the p2 stock and for the four virus samples of the plaque picking experiment shown in Fig. 1a. First, all reads spanning nt 23,576 to 23,665 of the SARS-CoV-2 genome were selected. Next, reads constituting less than 1% of the total number of selected reads were excluded from further analysis. The remaining number of reads were 3,860 (p2 stock), 1,924 (S5p1), 2,263 (S5p2), 4,049 (S5p3) and 3,323 (L8p1). These reads were translated in the S protein open reading frame and the resulting amino acid sequences were aligned, grouped on the basis of containing the same mutations/deletions in the S1/S2 region and ranked by frequency of occurrence (Fig. 1b).

Antisera and immunofluorescence microscopy

The SARS-CoV-specific rabbit or mouse antisera/antibodies used in this study are listed in Table 1. Most antisera were described previously (see references in Table 1), with the exception of three rabbit antisera recognizing SARS-CoV nsps 8, 9 and 15. These were raised using full-length $(His)_6$-tagged bacterial expression products (nsp8 and nsp15) or a synthetic

peptide (nsp9, aa 4209-4230 of SARS-CoV pp1a), which were used to immunize New Zealand white rabbits as described previously [49, 108]. Cross-reactivity of antisera to SARS-CoV-2 targets was evaluated microscopically by immunofluorescence assay (IFA) and for some antisera (nsp3 and N protein) also by Western blot analysis. Double-stranded RNA was detected using mouse monoclonal antibody J2 from Scicons [109].

Cells were grown on glass coverslips and infected as described above [110]. At 12, 24, 48 or 72 h p.i., cells were fixed overnight at 4°C using 3% paraformaldehyde in PBS (pH 7.4). Cells were washed with PBS containing 10 mM glycine and permeabilized with 0.1% Triton X-100 in PBS. Cells were incubated with antisera diluted in PBS containing 5% FCS. Secondary antibodies used were an Alexa488-conjugated goat anti-rabbit IgG antibody (Invitrogen), a Cy3-conjugated donkey anti-mouse IgG antibody (Jackson ImmunoResearch Laboratories) and an Alexa488-conjugated goat anti-mouse IgG antibody (Invitrogen). Nuclei were stained with 1 µg/ml Hoechst 33258 (ThermoFischer). Samples were embedded using Prolong Gold (Life Technologies) and analysed with a Leica DM6B fluorescence microscope using LASX software.

Electron microscopy

Vero E6 cells were grown on TC treated Cell Star dishes (Greiner Bio-One) and infected at an m.o.i. of 3, or mock-infected. Cells were fixed after 6, 8 and 10 h p.i. for 30 min at room temperature with freshly prepared 2% (vol/vol) glutaraldehyde in 0.1 M cacodylate buffer (pH 7.4) and then stored overnight in the fixative at 4°C. The samples were then washed with 0.1 M cacodylate buffer, treated for 1 hour with 1% (wt/vol) OsO4 at 4°C, washed with 0.1 M cacodylate buffer and Milli-Q water, and stained with 1% (wt/vol) uranyl acetate in Milli-Q water. After a new washing step, samples were dehydrated in increasing concentrations of ethanol (70%, 80%, 90%,100%), embedded in epoxy resin (LX-112, Ladd Research) and polymerized at 60°C. Sections (100 nm thick) were collected on mesh-100 copper EM grids covered with a carbon-coated Pioloform layer and post-stained with 7% (wt/vol) uranyl acetate and Reynold's lead citrate. The samples were examined in a Twin transmission electron microscope (Thermo Fisher Scientific (formerly FEI)) operated at 120 kV and images were collected with a OneView 4k high-frame rate CMOS camera (Gatan).

Compounds and antiviral screening assay

A 10-mM stock of Remdesivir (HY-104077; MedChemexpress) was dissolved in DMSO and stored at -80°C in aliquots for single use. Alisporivir was kindly provided by DebioPharm (Dr. Grégoire Vuagniaux, Lausanne, Switzerland; [111]) and a 20-mM stock was dissolved in 96%

ethanol and stored at -20°C in aliquots for single use. A 20-mM chloroquine stock (C6628; Sigma) was dissolved in PBS and stored at -20°C in aliquots for single use. Pegylated interferon alpha-2a (PEG-IFN-α; Pegasys, 90 mcg, Roche) was aliquoted and stored at room temperature until further use. Vero E6 cells were seeded in 96-well flat bottom plates in 100 µl at a density of 10,000 cells/well and grown overnight at 37°C. Two-fold serial dilutions of compounds were prepared in EMEM with 2% FCS and 50 µl was added to the cells 30 min prior to infection. Subsequently, half of the wells were infected with 300 PFU each of SARS-CoV or SARS-CoV-2 in order to evaluate inhibition of infection, while the other wells were used to in parallel monitor the (potential) cytotoxicity of compound treatment. Each compound concentration was tested in quadruplicate and each assay plate contained the following controls: no cells (background control), cells only treated with medium (mock infection for normalization), infected/untreated cells and infected/solvent-treated cells (infection control). At 3 days p.i., 20 µL/well of CellTiter 96 Aqueous Non-Radioactive Cell Proliferation reagent (Promega) was added and plates were incubated for 2 h at 37°C. Reactions were stopped and virus inactivated by adding 30 µl of 37% formaldehyde. Absorbance was measured using a monochromatic filter in a multimode plate reader (Envision; Perkin Elmer). Data was normalized to the mock-infected control, after which EC_{50} and CC_{50} values were calculated with Graph-Pad Prism 7.

AUTHORS AND CONTRIBUTORS

NO, JD, MK, MB, IS and ES conceptualised the study. NO, TD, JZ, RL, YM and LC performed experimental work and contributed to analysis of the results and preparation of figures. NO, LC, JD, JV, IS and ES performed NGS and were involved in the bioinformatics analysis of the data. NO and ES wrote the manuscript, with input from all authors. All authors agreed to the submission of this work to the *Journal of General Virology*.

CONFLICTS OF INTEREST

The authors declare that there are no conflicts of interest.

FUNDING INFORMATION

None.

ACKNOWLEDGEMENTS

We thank various GenomeScan staff members for the pleasant and swift collaboration that facilitated the NGS and data analysis of the first SARS-CoV-2 samples. We are grateful to all members of the sections Research and Clinical Microbiology of the LUMC Department of Medical Microbiology for their collaborative support and dedication during the current pandemic situation. In particular, we thank Linda Boomaars, Peter Bredenbeek, Ien Dobbelaar, Martijn van Hemert, Sebenzile Myeni, Tessa Nelemans, Esther Quakkelaar, Ali Tas, Sjaak van Voorden and Gijsbert van Willigen for their technical or administrative support, constructive discussions and/or scientific input.

DEDICATION

This work is dedicated to the loving memory of José Manuel Ogando Fernandes Pereira (72) and María de los Ángeles Martín San Martín (93) who succumbed to SARS-CoV-2 infection on March 27 and 28, 2020.

REFERENCES

1. Coronaviridae Study Group of the International Committee on Taxonomy of, V., *The species Severe acute respiratory syndrome-related coronavirus: classifying 2019-nCoV and naming it SARS-CoV-2.* Nat Microbiol, 2020. **5**(4): p. 536-544.
2. Li, X., et al., *Bat origin of a new human coronavirus: there and back again.* Sci China Life Sci, 2020. **63**(3): p. 461-462.
3. McIntosh, K., et al., *Coronavirus infection in acute lower respiratory tract disease of infants.* J Infect Dis, 1974. **130**(5): p. 502-7.
4. Pyrc, K., B. Berkhout, and L. van der Hoek, *Identification of new human coronaviruses.* Expert Rev Anti Infect Ther, 2007. **5**(2): p. 245-53.
5. Ksiazek, T.G., et al., *A novel coronavirus associated with severe acute respiratory syndrome.* N Engl J Med, 2003. **348**(20): p. 1953-66.
6. Peiris, J.S., et al., *Coronavirus as a possible cause of severe acute respiratory syndrome.* Lancet, 2003. **361**(9366): p. 1319-25.
7. Zaki, A.M., et al., *Isolation of a novel coronavirus from a man with pneumonia in Saudi Arabia.* N Engl J Med, 2012. **367**(19): p. 1814-20.
8. van Boheemen, S., et al., *Genomic characterization of a newly discovered coronavirus associated with acute respiratory distress syndrome in humans.* mBio, 2012. **3**(6).
9. Zhou, P., et al., *A pneumonia outbreak associated with a new coronavirus of probable bat origin.* Nature, 2020. **579**(7798): p. 270-273.
10. Munster, V.J., et al., *A novel coronavirus emerging in China - key questions for impact assessment.* N Engl J Med, 2020. **382**(8): p. 692-694.
11. Li, X., et al., *Evolutionary history, potential intermediate animal host, and cross-species analyses of SARS-CoV-2.* J Med Virol, 2020.
12. Lam, T.T., et al., *Identifying SARS-CoV-2 related coronaviruses in Malayan pangolins.* Nature, 2020.
13. Andersen, K.G., et al., *The proximal origin of SARS-CoV-2.* Nature Medicine, 2020.
14. Song, H.D., et al., *Cross-host evolution of severe acute respiratory syndrome coronavirus in palm civet and human.* Proc Natl Acad Sci U S A, 2005. **102**(7): p. 2430-5.
15. Reusken, C.B., et al., *Middle East respiratory syndrome coronavirus neutralising serum antibodies in dromedary camels: a comparative serological study.* Lancet Infect Dis, 2013. **13**(10): p. 859-66.
16. Ge, X.Y., et al., *Isolation and characterization of a bat SARS-like coronavirus that uses the ACE2 receptor.* Nature, 2013. **503**(7477): p. 535-8.
17. Menachery, V.D., et al., *A SARS-like cluster of circulating bat coronaviruses shows potential for human emergence.* Nat Med, 2015. **21**(12): p. 1508-13.
18. Hu, B., et al., *Discovery of a rich gene pool of bat SARS-related coronaviruses provides new insights into the origin of SARS coronavirus.* PLoS Pathog, 2017. **13**(11): p. e1006698.
19. Cui, J., F. Li, and Z.L. Shi, *Origin and evolution of pathogenic coronaviruses.* Nat Rev Microbiol, 2019. **17**(3): p. 181-192.
20. Corman, V.M., et al., *Evidence for an Ancestral Association of Human Coronavirus 229E with Bats.* J Virol, 2015. **89**(23): p. 11858-70.

21. Li, W., et al., *Broad receptor engagement of an emerging global coronavirus may potentiate its diverse cross-species transmissibility.* Proc Natl Acad Sci U S A, 2018. **115**(22): p. E5135-E5143.
22. Zhou, P., et al., *Fatal swine acute diarrhoea syndrome caused by an HKU2-related coronavirus of bat origin.* Nature, 2018. **556**(7700): p. 255-258.
23. Nga, P.T., et al., *Discovery of the first insect nidovirus, a missing evolutionary link in the emergence of the largest RNA virus genomes.* PLoS Pathog, 2011. **7**(9): p. e1002215.
24. Snijder, E.J., E. Decroly, and J. Ziebuhr, *The Nonstructural Proteins Directing Coronavirus RNA Synthesis and Processing.* Adv Virus Res, 2016. **96**: p. 59-126.
25. Snijder, E.J., et al., *A unifying structural and functional model of the coronavirus replication organelle: tracking down RNA synthesis.* bioRxiv, 2020.
26. Narayanan, K., C. Huang, and S. Makino, *SARS coronavirus accessory proteins.* Virus Res, 2008. **133**(1): p. 113-21.
27. Li, G. and E. De Clercq, *Therapeutic options for the 2019 novel coronavirus (2019-nCoV).* Nat Rev Drug Discov, 2020. **19**(3): p. 149-150.
28. Ogando, N.S., et al., *The curious case of the nidovirus exoribonuclease: its role in RNA synthesis and replication fidelity.* Front Microbiol, 2019. **10**: p. 1813.
29. Lu, R., et al., *Genomic characterisation and epidemiology of 2019 novel coronavirus: implications for virus origins and receptor binding.* Lancet, 2020. **395**(10224): p. 565-574.
30. Wu, F., et al., *A new coronavirus associated with human respiratory disease in China.* Nature, 2020. **579**(7798): p. 265-269.
31. Hoffmann, M., et al., *The novel coronavirus 2019 (2019-nCoV) uses the SARS-coronavirus receptor ACE2 and the cellular protease TMPRSS2 for entry into target cells.* bioRxiv, 2020.
32. Snijder, E.J., et al., *Unique and conserved features of genome and proteome of SARS-coronavirus, an early split-off from the coronavirus group 2 lineage.* J Mol Biol, 2003. **331**(5): p. 991-1004.
33. Thiel, V., et al., *Mechanisms and enzymes involved in SARS coronavirus genome expression.* J Gen Virol, 2003. **84**(Pt 9): p. 2305-2315.
34. Caly L, D.J., Roberts J, Bond K, Tran T, Kostecki R, Yoga Y, Naughton W, Taiaroa G, Seemann T, Schultz, Howden B, Korman T, Lewin S, Williamson D, Catton M, *Isolation and rapid sharing of the 2019 novel coronavirus (SAR-CoV-2) from the first diagnosis of COVID-19 in Australia.* the medical journal of australia, 2020.
35. Wu, F., et al., *Complete genome characterisation of a novel coronavirus associated with severe human respiratory disease in Wuhan, China.* bioRxiv, 2020.
36. Drosten, C., et al., *Identification of a novel coronavirus in patients with severe acute respiratory syndrome.* N Engl J Med, 2003. **348**(20): p. 1967-76.
37. de Wilde, A.H., et al., *MERS-coronavirus replication induces severe in vitro cytopathology and is strongly inhibited by cyclosporin A or interferon-alpha treatment.* J Gen Virol, 2013. **94**(Pt 8): p. 1749-1760.
38. Stertz, S., et al., *The intracellular sites of early replication and budding of SARS-coronavirus.* Virology, 2007. **361**(2): p. 304-15.
39. Knoops, K., et al., *SARS-coronavirus replication is supported by a reticulovesicular network of modified endoplasmic reticulum.* PLoS Biol, 2008. **6**(9): p. e226.

40. Weber, F., et al., *Double-stranded RNA is produced by positive-strand RNA viruses and DNA viruses but not in detectable amounts by negative-strand RNA viruses.* J Virol, 2006. **80**(10): p. 5059-64.
41. Snijder, E.J., et al., *Ultrastructure and origin of membrane vesicles associated with the severe acute respiratory syndrome coronavirus replication complex.* J Virol, 2006. **80**(12): p. 5927-40.
42. Sawicki, S.G. and D.L. Sawicki, *Coronaviruses use discontinuous extension for synthesis of subgenome-length negative strands.* Adv Exp Med Biol, 1995. **380**: p. 499-506.
43. Xu, J., et al., *Genome organization of the SARS-CoV.* Genomics Proteomics Bioinformatics, 2003. **1**(3): p. 226-35.
44. Maier, H.J., et al., *Infectious bronchitis virus generates spherules from zippered endoplasmic reticulum membranes.* mBio, 2013. **4**(5): p. e00801-13.
45. Doyle, N., et al., *The Porcine Deltacoronavirus Replication Organelle Comprises Double-Membrane Vesicles and Zippered Endoplasmic Reticulum with Double-Membrane Spherules.* Viruses, 2019. **11**(11).
46. Tooze, J., S. Tooze, and G. Warren, *Replication of coronavirus MHV-A59 in sac- cells: determination of the first site of budding of progeny virions.* Eur J Cell Biol, 1984. **33**(2): p. 281-93.
47. Goldsmith, C.S., et al., *Ultrastructural characterization of SARS coronavirus.* Emerg Infect Dis, 2004. **10**(2): p. 320-6.
48. van Hemert, M.J., et al., *SARS-coronavirus replication/transcription complexes are membrane-protected and need a host factor for activity in vitro.* PLoS Pathog, 2008. **4**(5): p. e1000054.
49. Fang, Y., et al., *Production and characterization of monoclonal antibodies against the nucleocapsid protein of SARS-CoV.* Adv Exp Med Biol, 2006. **581**: p. 153-6.
50. Agostini, M.L., et al., *Coronavirus Susceptibility to the Antiviral Remdesivir (GS-5734) Is Mediated by the Viral Polymerase and the Proofreading Exoribonuclease.* MBio, 2018. **9**(2).
51. Wang, M., et al., *Remdesivir and chloroquine effectively inhibit the recently emerged novel coronavirus (2019-nCoV) in vitro.* Cell Res, 2020. **30**(3): p. 269-271.
52. Keyaerts, E., et al., *In vitro inhibition of severe acute respiratory syndrome coronavirus by chloroquine.* Biochem Biophys Res Commun, 2004. **323**(1): p. 264-8.
53. Vincent, M.J., et al., *Chloroquine is a potent inhibitor of SARS coronavirus infection and spread.* Virol J, 2005. **2**: p. 69.
54. Carbajo-Lozoya, J., et al., *Human coronavirus NL63 replication is cyclophilin A-dependent and inhibited by non-immunosuppressive cyclosporine A-derivatives including Alisporivir.* Virus Res, 2014. **184**: p. 44-53.
55. de Wilde, A.H., et al., *Alisporivir inhibits MERS- and SARS-coronavirus replication in cell culture, but not SARS-coronavirus infection in a mouse model.* Virus Res, 2017. **228**: p. 7-13.
56. Haagmans, B.L., et al., *Pegylated interferon-alpha protects type 1 pneumocytes against SARS coronavirus infection in macaques.* Nat Med, 2004. **10**(3): p. 290-3.
57. Riss, T.L., et al., *Cell Viability Assays*, in *Assay Guidance Manual*, G.S. Sittampalam, et al., Editors. 2004: Bethesda (MD).

58. Coutard, B., et al., *The spike glycoprotein of the new coronavirus 2019-nCoV contains a furin-like cleavage site absent in CoV of the same clade.* Antiviral Res, 2020. **176**: p. 104742.
59. Izaguirre, G., *The Proteolytic Regulation of Virus Cell Entry by Furin and Other Proprotein Convertases.* Viruses, 2019. **11**(9).
60. Zhou, P., et al., *Discovery of a novel coronavirus associated with the recent pneumonia outbreak in humans and its potential bat origin.* bioRxiv, 2020.
61. Millet, J.K. and G.R. Whittaker, *Host cell entry of Middle East respiratory syndrome coronavirus after two-step, furin-mediated activation of the spike protein.* Proc Natl Acad Sci U S A, 2014. **111**(42): p. 15214-9.
62. Follis, K.E., J. York, and J.H. Nunberg, *Furin cleavage of the SARS coronavirus spike glycoprotein enhances cell-cell fusion but does not affect virion entry.* Virology, 2006. **350**(2): p. 358-69.
63. Walls, A.C., et al., *Structure, Function, and Antigenicity of the SARS-CoV-2 Spike Glycoprotein.* Cell, 2020. **181**(2): p. 281-292 e6.
64. Bosch, B.J., W. Bartelink, and P.J. Rottier, *Cathepsin L functionally cleaves the severe acute respiratory syndrome coronavirus class I fusion protein upstream of rather than adjacent to the fusion peptide.* J Virol, 2008. **82**(17): p. 8887-90.
65. Burkard, C., et al., *Coronavirus cell entry occurs through the endo-/lysosomal pathway in a proteolysis-dependent manner.* PLoS Pathog, 2014. **10**(11): p. e1004502.
66. Huang, I.C., et al., *SARS coronavirus, but not human coronavirus NL63, utilizes cathepsin L to infect ACE2-expressing cells.* J Biol Chem, 2006. **281**(6): p. 3198-203.
67. Liu, Z., et al., *Identification of a common deletion in the spike protein of SARS-CoV-2.* bioRxiv, 2020.
68. Davidson, A.D., et al., *Characterisation of the transcriptome and proteome of SARS-CoV-2 using direct RNA sequencing and tandem mass spectrometry reveals evidence for a cell passage induced in-frame deletion in the spike glycoprotein that removes the furin-like cleavage site.* bioRxiv, 2020.
69. Goebel, S.J., et al., *A hypervariable region within the 3' cis-acting element of the murine coronavirus genome is nonessential for RNA synthesis but affects pathogenesis.* J Virol, 2007. **81**(3): p. 1274-87.
70. Stammler, S.N., et al., *A conserved RNA pseudoknot in a putative molecular switch domain of the 3'-untranslated region of coronaviruses is only marginally stable.* RNA, 2011. **17**(9): p. 1747-59.
71. Rangan, R., I.N. Zheludev, and R. Das, *RNA genome conservation and secondary structure in SARS-CoV-2 and SARS-related viruses.* bioRxiv, 2020.
72. Choy, K.T., et al., *Remdesivir, lopinavir, emetine, and homoharringtonine inhibit SARS-CoV-2 replication in vitro.* Antiviral Res, 2020. **178**: p. 104786.
73. Lokugamage, K.G., C. Schindewolf, and V.D. Menachery, *SARS-CoV-2 sensitive to type I interferon pretreatment.* bioRxiv, 2020.
74. Banerjee, A., et al., *Isolation, sequence, infectivity and replication kinetics of SARS-CoV-2.* bioRxiv, 2020.
75. Matsuyama, S., et al., *Enhanced isolation of SARS-CoV-2 by TMPRSS2-expressing cells.* Proc Natl Acad Sci U S A, 2020.

76. Tseng, C.T., et al., *Apical entry and release of severe acute respiratory syndrome-associated coronavirus in polarized Calu-3 lung epithelial cells.* J Virol, 2005. **79**(15): p. 9470-9.
77. Mossel, E.C., et al., *Exogenous ACE2 expression allows refractory cell lines to support severe acute respiratory syndrome coronavirus replication.* J Virol, 2005. **79**(6): p. 3846-50.
78. Kaye, M., *SARS-associated coronavirus replication in cell lines.* Emerg Infect Dis, 2006. **12**(1): p. 128-33.
79. Gillim-Ross, L., et al., *Discovery of novel human and animal cells infected by the severe acute respiratory syndrome coronavirus by replication-specific multiplex reverse transcription-PCR.* J Clin Microbiol, 2004. **42**(7): p. 3196-206.
80. De Clercq, E., W.E. Stewart, 2nd, and P. De Somer, *Studies on the mechanism of the priming effect of interferon on interferon production by cell cultures exposed to poly(rI)-poly(rC).* Infect Immun, 1973. **8**(3): p. 309-16.
81. Emeny, J.M. and M.J. Morgan, *Regulation of the interferon system: evidence that Vero cells have a genetic defect in interferon production.* J Gen Virol, 1979. **43**(1): p. 247-52.
82. Zhu, N., et al., *A Novel Coronavirus from Patients with Pneumonia in China, 2019.* N Engl J Med, 2020. **382**(8): p. 727-733.
83. Rothan, H., et al., *The FDA-approved gold drug Auranofin inhibits novel coronavirus (SARS-COV-2) replication and attenuates inflammation in human cells.* bioRxiv, 2020.
84. Tan, Y.J., et al., *Overexpression of 7a, a protein specifically encoded by the severe acute respiratory syndrome coronavirus, induces apoptosis via a caspase-dependent pathway.* J Virol, 2004. **78**(24): p. 14043-7.
85. Yuan, X., et al., *SARS coronavirus 7a protein blocks cell cycle progression at G0/G1 phase via the cyclin D3/pRb pathway.* Virology, 2006. **346**(1): p. 74-85.
86. Schaecher, S.R., J.M. Mackenzie, and A. Pekosz, *The ORF7b protein of severe acute respiratory syndrome coronavirus (SARS-CoV) is expressed in virus-infected cells and incorporated into SARS-CoV particles.* J Virol, 2007. **81**(2): p. 718-31.
87. Pfefferle, S., et al., *The SARS-coronavirus-host interactome: identification of cyclophilins as target for pan-coronavirus inhibitors.* PLoS Pathog, 2011. **7**(10): p. e1002331.
88. Sung, S.C., et al., *The 8ab protein of SARS-CoV is a luminal ER membrane-associated protein and induces the activation of ATF6.* Virology, 2009. **387**(2): p. 402-13.
89. Shi, C.S., et al., *SARS-Coronavirus Open Reading Frame-8b triggers intracellular stress pathways and activates NLRP3 inflammasomes.* Cell Death Discov, 2019. **5**: p. 101.
90. Chinese, S.M.E.C., *Molecular evolution of the SARS coronavirus during the course of the SARS epidemic in China.* Science, 2004. **303**(5664): p. 1666-9.
91. Guan, Y., et al., *Isolation and characterization of viruses related to the SARS coronavirus from animals in southern China.* Science, 2003. **302**(5643): p. 276-8.
92. Lau, S.K., et al., *Severe Acute Respiratory Syndrome (SARS) Coronavirus ORF8 Protein Is Acquired from SARS-Related Coronavirus from Greater Horseshoe Bats through Recombination.* J Virol, 2015. **89**(20): p. 10532-47.
93. Muth, D., et al., *Attenuation of replication by a 29 nucleotide deletion in SARS-coronavirus acquired during the early stages of human-to-human transmission.* Sci Rep, 2018. **8**(1): p. 15177.

94. Fu, Y., Y. Cheng, and Y. Wu, *Understanding SARS-CoV-2-Mediated Inflammatory Responses: From Mechanisms to Potential Therapeutic Tools.* Virol Sin, 2020.
95. Chan, J.F., et al., *Genomic characterization of the 2019 novel human-pathogenic coronavirus isolated from a patient with atypical pneumonia after visiting Wuhan.* Emerg Microbes Infect, 2020. **9**(1): p. 221-236.
96. Falzarano, D., et al., *Inhibition of novel beta coronavirus replication by a combination of interferon-alpha2b and ribavirin.* Sci Rep, 2013. **3**: p. 1686.
97. Gordon, C.J., et al., *The antiviral compound remdesivir potently inhibits RNA-dependent RNA polymerase from Middle East respiratory syndrome coronavirus.* J Biol Chem, 2020.
98. Yin, W., et al., *Structural Basis for the Inhibition of the RNA-Dependent RNA Polymerase from SARS-CoV-2 by Remdesivir.* bioRxiv, 2020.
99. Shannon, A., et al., *Remdesivir and SARS-CoV-2: structural requirements at both nsp12 RdRp and nsp14 Exonuclease active-sites.* Antiviral Res, 2020: p. 104793.
100. Holshue, M.L., et al., *First Case of 2019 Novel Coronavirus in the United States.* N Engl J Med, 2020. **382**(10): p. 929-936.
101. Kim, A.H.J., et al., *A Rush to Judgment? Rapid Reporting and Dissemination of Results and Its Consequences Regarding the Use of Hydroxychloroquine for COVID-19.* Ann Intern Med, 2020.
102. Yao, X., et al., *In Vitro Antiviral Activity and Projection of Optimized Dosing Design of Hydroxychloroquine for the Treatment of Severe Acute Respiratory Syndrome Coronavirus 2 (SARS-CoV-2).* Clin Infect Dis, 2020.
103. Wellems, T.E. and C.V. Plowe, *Chloroquine-resistant malaria.* J Infect Dis, 2001. **184**(6): p. 770-6.
104. Al-Bari, M.A., *Chloroquine analogues in drug discovery: new directions of uses, mechanisms of actions and toxic manifestations from malaria to multifarious diseases.* J Antimicrob Chemother, 2015. **70**(6): p. 1608-21.
105. de Wilde, A.H., et al., *Cyclophilins and cyclophilin inhibitors in nidovirus replication.* Virology, 2018. **522**: p. 46-55.
106. van den Worm, S.H., et al., *Reverse genetics of SARS-related coronavirus using vaccinia virus-based recombination.* PLoS One, 2012. **7**(3): p. e32857.
107. Langmead, B. and S.L. Salzberg, *Fast gapped-read alignment with Bowtie 2.* Nat Methods, 2012. **9**(4): p. 357-9.
108. Snijder, E.J., A.L. Wassenaar, and W.J. Spaan, *Proteolytic processing of the replicase ORF1a protein of equine arteritis virus.* J Virol, 1994. **68**(9): p. 5755-64.
109. Schonborn, J., et al., *Monoclonal antibodies to double-stranded RNA as probes of RNA structure in crude nucleic acid extracts.* Nucleic Acids Res, 1991. **19**(11): p. 2993-3000.
110. van der Meer, Y., et al., *Localization of mouse hepatitis virus nonstructural proteins and RNA synthesis indicates a role for late endosomes in viral replication.* J Virol, 1999. **73**(9): p. 7641-57.
111. Coelmont, L., et al., *Debio 025, a cyclophilin binding molecule, is highly efficient in clearing hepatitis C virus (HCV) replicon-containing cells when used alone or in combination with specifically targeted antiviral therapy for HCV (STAT-C) inhibitors.* Antimicrob Agents Chemother, 2009. **53**(3): p. 967-76.

CHAPTER III

The curious case of the nidovirus exoribonuclease: its role in RNA synthesis and replication fidelity

Natacha S. Ogando[1], Francois Ferron[2,3], Etienne Decroly[2], Bruno Canard[2], Clara C. Posthuma[1] & Eric J. Snijder[1]

[1]Department of Medical Microbiology, Leiden University Medical Center, Leiden, The Netherlands
[2]Architecture et Fonction des Macromolécules Biologiques, Centre National de la Recherche Scientifique, Aix-Marseille Université, Marseille, France.
[3] European Virus Bioinformatics Center, Leutragraben 1, 07743 Jena, Germany.

Published in Frontiers in Microbiology, section Virology
doi.org/10.3389/fmicb.2019.01813

ABSTRACT

Among RNA viruses, the order Nidovirales stands out for including viruses with the largest RNA genomes currently known. Nidoviruses employ a complex RNA-synthesizing machinery comprising a variety of non-structural proteins (nsps). One of the postulated drivers of the expansion of nidovirus genomes is the presence of a proofreading 3'-to-5' exoribonuclease (ExoN) belonging to the DEDDh family. ExoN may enhance the fidelity of RNA synthesis by correcting nucleotide incorporation errors made by the RNA-dependent RNA polymerase. Here, we review our current understanding of ExoN evolution, structure, and function. Most experimental data are derived from studies of the ExoN domain of coronaviruses (CoVs), which were triggered by the bioinformatics-based identification of ExoN in the genome of severe acute respiratory syndrome coronavirus (SARS-CoV) and its relatives in 2003. Although convincing data supporting the proofreading hypothesis have been obtained, from biochemical assays and studies with CoV mutants lacking ExoN functionality, the features of ExoN from most other nidovirus families remain to be characterized. Remarkably, viable ExoN knockout mutants were obtained only for two CoVs, mouse hepatitis virus (MHV) and SARS-CoV, whose RNA synthesis and replication kinetics were mildly affected by the lack of ExoN function. In several other CoV species, ExoN inactivation was not tolerated and knockout mutants could not be rescued when launched using a reverse genetics system. This suggests that ExoN is also critical for primary viral RNA synthesis, a property that poorly matches the profile of an enzyme that would merely boost long-term replication fidelity. In CoVs, ExoN resides in a bifunctional replicase subunit (nsp14) whose C-terminal part has (N7-guanine)-methyltransferase activity. The crystal structure of SARS-CoV nsp14 has shed light on the interplay between these two domains, and on nsp14's interactions with nsp10, a co-factor that strongly enhances ExoN activity in in vitro assays. Further elucidation of the structure-function relationships of ExoN and its interactions with other (viral and/or host) members of the CoV replication machinery will be key to understanding the enzyme's role in viral RNA synthesis and pathogenesis, and may contribute to the design of new approaches to combat emerging nidoviruses.

INTRODUCTION

RNA viruses typically exhibit a high mutation frequency. This intrinsic biological property facilitates rapid adaptation of the virus to changing circumstances, a major contributor to the frequent outbreaks of mutated or newly emerging RNA viruses in humans, livestock, and other host organisms. The poor fidelity of RNA virus genome replication is attributed primarily to the fact that errors made by the viral RNA-dependent RNA polymerase (RdRp) go uncorrected. This lack of proofreading results in 'quasispecies' populations of closely related viral genomes that are subject to continuous natural selection. As the accumulation of an excessive number of deleterious mutations can result in 'error catastrophe', the low fidelity of their replication is thought to have restricted genome size, which for most RNA virus families is (well) below 15 kilobases [1-3]. This evolutionary trade-off between RNA virus genome size, replication fidelity, and adaptive capacity has been explored both from a fundamental perspective and in the context of antiviral drug development [4]. The balance between quasispecies diversity and viral fitness appears to be easily disturbed, suggesting that RNA viruses in general may operate close to their error threshold [5-7]. Clearly, in the absence of countermeasures to reduce the overall error rate, similar issues would be expected upon the significant expansion of RNA virus genome size.

The largest RNA genomes currently known are all found in the order *Nidovirales*, an order of positive-stranded RNA (+RNA) viruses that includes the coronavirus (CoV) family as its best-studied taxon. Recent nidovirus additions [8, 9] have increased the known upper limit of RNA genome size from just above 30 kb (for most CoVs) to more than 41 kb in a nidovirus identified in a planarian host, which was named planarian secretory cell nidovirus (PSCNV) [9]. About 15 years ago, during the in-depth bioinformatics analysis of the genome and proteome of the severe acute respiratory syndrome coronavirus (SARS-CoV), Alexander Gorbalenya and co-workers identified a 3'-5' exoribonuclease (ExoN) signature sequence in a domain embedded in the replicase polyprotein of CoVs and other nidoviruses with a similarly large RNA genome, and speculated about its role as a proofreading enzyme in the evolution of such large nidovirus genomes [10]. Shortly after this ground-breaking discovery, ExoN activity was demonstrated biochemically for SARS-CoV [11] and – following its inactivation by reverse genetics – was indeed implicated in enhancing CoV replication fidelity [12]. Subsequently, the enzyme was the subject of further virological, biochemical, structural, and genetics studies. Evidence strongly supporting the 'proofreading exoribonuclease' hypothesis has now accumulated, in particular for SARS-CoV and murine hepatitis CoV (MHV) [13, 14], and will be summarized below. At the same time, quite different observations were made for multiple other CoVs, highlighting the need for a more extensive experimental characterization of the

importance and function of the unique ExoN domain, both within the CoV family and in other nidovirus subgroups.

ExoN acquisition by a nidoviral ancestor and the subsequent development of a beneficial interplay with the viral RNA RdRp [15, 16] are thought to have been key steps in relieving the constraints on genome size expansion in this virus lineage [17]. Strikingly, the replication of arteriviruses, the nidovirus family with the smallest genome (12-16 kb), does not depend on the presence of an ExoN domain in the viral replicase [10], suggesting they either diverged from other nidoviruses before ExoN acquisition or lost ExoN at a later stage of their evolutionary trajectory.

The amazing diversity of nidoviruses

The order *Nidovirales* currently comprises 88 formally recognized virus species of +RNA viruses, which are classified in 9 virus families across 7 different suborders [18][1]. These agents can infect a striking variety of vertebrate and invertebrate hosts, including mammals, birds, amphibians, fish, reptiles, arthropods, molluscs and helminths. Additional nidovirus genome sequences continue to be described, due to the extensive metagenomics-based virus discovery efforts of the past decade [9]. Their adequate classification will undoubtedly require the creation of additional nidovirus taxa. Unfortunately, the biological and (possible) pathogenic features of most novel nidoviruses remain uncharacterized thus far [19-21].

The groundwork for the nidovirus order was laid in the late 1980's when the first full-length genome sequences of corona-, arteri-, and toroviruses revealed striking similarities at the level of genome organization and expression. Moreover, the conservation of an array of replicase domains in these distantly related genomes pointed towards a common ancestry of the core of their replicative machinery, including the RNA-dependent RNA polymerase (RdRp) and helicase enzymes [22]. These findings were surprising at the time, in particular given the very different appearance and features of corona-, arteri-, and torovirus particles, and the large differences in genome size, which ranged from less than 13 kb for the arterivirus equine arteritis virus (EAV) to more than 31 kb for some CoVs, like MHV. The latter property placed the CoVs far apart from all other viral families characterized in the final decades of the 20th century [23]. This unique position also raised questions about the processivity and fidelity of the CoV RNA-synthesizing machinery, particularly in the light of the development of the emerging RNA virus quasispecies concept and the notion that RNA virus genome sizes are constrained by the high mutation rate of their RdRp (see above).

[1] ICTV website: https://talk.ictvonline.org/taxonomy/

The advent of metagenomics has taken our understanding of nidovirus host and genome diversity to the next level [19-21, 24], even though most of these new sequences remain to be analyzed in detail and many branches of the revised nidovirus order remain sparsely populated. In terms of RNA genome size, the known upper limit increased to more than 41 kb (see above) and at the same time the former gap between the ExoN-deficient arterivirus group and the large-genome nidoviruses that contain an ExoN signature sequence has largely disappeared. Clearly, genome size unlikely is the sole factor determining the requirement for an ExoN type of proofreading function, as other factors (in particular RdRp properties) may also prominently influence replication fidelity.

The rapid expansion of the nidovirus order has highlighted the strict conservation of an array of five 'core replicase' domains: (i) the main (or '3C-like') protease, (ii) the nidovirus RdRp-associated nucleotidyl transferase (NiRAN), (iii) the RdRp, (iv) a Zn-binding domain (ZBD) and (v) the superfamily 1 helicase domain (HEL1), with which the ZBD is always associated (Fig. 1A) [9, 25]. When present, the ExoN domain is found immediately downstream of these nidovirus-wide conserved domains, often residing in a bifunctional replicase cleavage product that also contains an N7-guanine methyltransferase (N7-MTase) activity [26, 27], as in the case of CoV nonstructural protein (nsp) 14. The size of the ExoN domain itself appears to be rather variable between different nidovirus lineages, roughly between 150 and 250 amino acid (aa) residues, depending on the presence or absence of two internal zinc finger domains [[17] and unpublished observations] (Fig.s 1B and 2A).

As mentioned above, for most of the novel metagenomics-derived nidoviruses we only know genome sequences, and their replication properties and enzymes have remained biologically uncharacterized thus far. This is clearly different for CoVs, which have a track record as an important group of (zoonotic) human and veterinary pathogens. With some exceptions [28], also the structure-function analysis of the nidoviral ExoN enzyme has been based on CoV-derived variants of the enzyme, on which we will focus our attention from this point forward.

Coronaviral RNAs and non-structural proteins

Like all nidoviruses, CoVs encode two very large replicase polyproteins, pp1a and pp1ab (Fig. 1A), of which the latter derives from a ribosomal frameshift occurring just upstream of the ORF1a termination codon. These primary translation products of roughly 4,000-4,500 (pp1a) and 6,700-7,200 (pp1ab) residues are processed by two or three internal proteases (residing in nsp3 and nsp5) [23, 29]. Most of the resulting 15 or 16 nsp cleavage products assemble into a ribonucleoprotein complex that produces different types of viral RNA transcripts. In the cytoplasm of the host cell, CoV infection induces the formation of unusual double-membrane

structures that are thought to support viral RNA synthesis [30, 31]. The synthesis of a nested set of subgenomic (sg) mRNAs, one of the original nidovirus hallmarks (L. *nidus* = nest), is a prominent CoV feature that drives the expression of the genes located downstream of ORF1b, encoding structural and accessory proteins (Fig. 1A). An additional complexity of CoV RNA synthesis is the fact that the sg mRNAs are produced from a set of subgenome-length templates, which are both 5' and 3' co-terminal with the full-length negative-stranded template used for genome replication. The mechanistic details of CoV RNA synthesis and its regulation have been summarized elsewhere [34-36].

Over the past 25 years, CoV replicase proteins have been characterized using a combination of bioinformatics, biochemistry, structural biology, and (reverse) genetics. By now, *in vitro* biochemical assays have been described for most (predicted) replicative enzyme functions. Increasingly supported by the availability of structural information, several key CoV enzymes were probed by site-directed mutagenesis, either using *in vitro* assays or by launching engineered mutant CoV genomes from cloned cDNA templates. The CoV replicase subunits nsp7 to nsp14 and nsp16 are most intimately associated with viral RNA synthesis, either as enzymatic entity or as important co-factor [for reviews, see [23, 37-41]]. Key players are the nsp12 and nsp13 subunits, which contain the RdRp and HEL domains, respectively. Each of these proteins also carries a unique N-terminal domain, NiRAN and ZBD, respectively, which both are nidovirus-specific markers whose functional importance remains to be studied in more detail [9, 25, 42, 43]. Several nsps (nsp10, nsp14, nsp16) have been assigned functions in CoV mRNA capping and cap modification [26, 27, 40, 44, 45], processes critical for both viral translation and innate immune evasion [46]. Several smaller subunits, which will be discussed below, appear to act as crucial co-factors of other nsps, and such nsp-nsp interactions are also assumed to be highly relevant for the proofreading activity of the nsp14-ExoN domain [15, 16, 47]. Clearly, our understanding of CoV replicase activities and the assembly of the viral RNA synthesizing machinery continues to develop, which may ultimately help to explain the evolutionary success of nidoviruses at large.

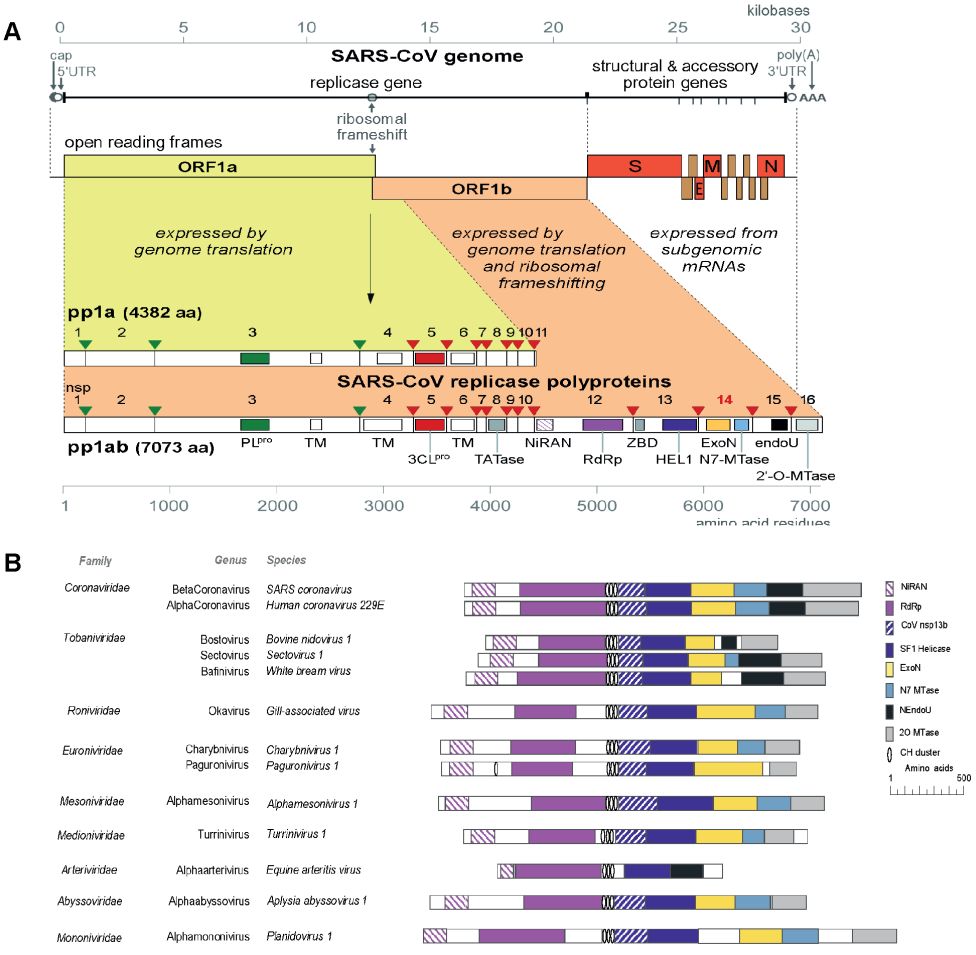

Fig. 1. (A) Outline of the CoV genome organization and expression strategy. Depicted are the SARS-CoV genome and its 14 open reading frames (ORFs), i.e., the replicase ORFs 1a and 1b, the four common CoV structural protein genes (S, E, M, and N) and the ORFs encoding "accessory proteins." The bottom half of the scheme summarizes the proteolytic processing and domain organization of the pp1a and pp1ab replicase polyproteins, the latter being produced by -1 ribosomal frameshifting. The nsp3 (PLpro, green) and nsp5 (3CLpro, red) proteases and their cognate cleavage sites are indicated in matching colors. The resulting 16 cleavage products (non-structural proteins, nsps) are indicated, as are the conserved replicase domains that are relevant for this review. See main text for references on nsp functions. Domain abbreviations and corresponding nsp numbers: PLpro, papain-like proteinase (nsp3); 3CLpro, 3C-like or main proteinase (nsp5); TM, transmembrane domain (nsp3, nsp4, and nsp6); NiRAN, nidovirus RdRp-associated nucleotidyl transferase (nsp12); RdRp, RNA-dependent RNA polymerase (nsp12); ZBD, zinc-binding domain (nsp13); HEL1, superfamily 1 helicase (nsp13); ExoN, 3'-to-5'exoribonuclease (nsp14); N7-MTase, N7-guanine methyl transferase (nsp14);

endoU, uridylate-specific endoribonuclease (nsp15); 2'-O-MTase, 2'-O-methyl transferase (nsp16); UTR, untranslated region. (B) Comparison of the predicted domain organization in the replicase polyprotein of selected members of the nine families currently classified within the order Nidovirales (ICTV release 2018b). Adapted from Bukhari et al., 2018, with permission. Domains were predicted using HHPred-search [32, 33]; for abbreviations see the legend to panel A. Genbank accession numbers of sequences used: SARS-coronavirus (AY274119.3); Human coronavirus 229E (AF304460.1); Bovine nidovirus 1 (KM589359.1); Sectovirus 1 (KX883637.1); White bream virus (DQ898157.1); Gill-associated virus (AF227196.1); Charybnivirus 1 (KX883628.1); Paguronivirus 1 (KX883627.1); Alphamesonivirus 1 (DQ458789.2); Turrinivirus 1 (KX883629.1); Equine arteritis virus (X53459.3); Aplysia abyssovirus (NC_040711.1); Planidovirus 1 (MH933735).

The coronavirus RdRp in the context of a multimeric enzyme complex

The C-terminal two-thirds of the CoV nsp12 subunit are occupied by a canonical RdRp domain containing the commonly encountered motifs A to F [39, 42, 43, 48]. Conserved aspartates in motif A and in motif C presumably are responsible for the coordination of two essential metal ions in the active site [15, 49, 50]. Most of our current knowledge of CoV RdRps is based on studies with SARS-CoV nsp12, which will be summarized below.

A structural prediction of the nsp12-RdRp domain was described as early as 2003 [51], but a crystal structure of the protein is still lacking. However, very recently, a cryo-EM-derived structure of SARS-CoV nps12, in complex with two copies of nsp8 and one copy of nsp7, was reported [43]. Like other +RNA viral RdRps, the CoV RdRp displays a characteristic "cupped right hand" organization, including thumb, palm and fingers subdomains [42, 43, 51, 52]. A so-called 'priming loop', a typical short β-strand that is considered to be a signature for primer-dependent RNA synthesis, is lacking.

Technical challenges in obtaining stable and active recombinant nsp12 have hampered the biochemical characterization of CoV RdRp activity. Only poor enzymatic activities were observed and initially both primer-dependent RNA synthesis and *de novo* initiation were reported [reviewed in [40, 43]]. However, in the presence of the small nsp7 and nsp8 subunits, the *in vitro* primer extension activity of nsp12 could be substantially increased and *de novo* initiation was observed on a 339-nt long template corresponding the 3'-terminal sequence of the SARS-CoV genome [53]. Recombinant SARS-CoV nsp7 and nsp8 previously had been shown to multimerize into a ring-shaped hexadecamer, which was proposed to act as a processivity factor for the nsp12-RdRp while copying the long CoV RNA genome [54]. Thus, CoV nsp12-RdRp activity was postulated to depend on the formation of a nsp7/nsp8/nsp12 tripartite complex, at least for some steps of RNA synthesis. The exact stoichiometry of this complex remains to be studied in more detail, particularly in the light of the recently published

cryo-EM structure of SARS-CoV nsp12, in which the protein was complexed with a single nsp7/nsp8 dimer plus an additional nsp8 monomer rather than an nsp7-nsp8 hexadecamer [43]. It should be noted that the *in vitro* RdRp activity of the latter complex remains to be demonstrated. Furthermore, for feline coronavirus (FCoV) nsp7 and nsp8, despite being structurally similar to their SARS-CoV equivalents, a higher-order complex quite different from the hexadecamer was described: a heterotrimer consisting of two copies of nsp7 and a single copy of nsp8 [55].

Early *in vitro* assays using recombinant SARS-CoV nsp8 revealed an RNA polymerase activity typically generating products of up to six nucleotides [56]. This activity was implicated in the priming of CoV RNA synthesis, particularly in light of the (predicted) absence of a priming loop in the nsp12-RdRp domain (see above). Thus, nsp8 was proposed to act as a primase that could synthesize small oligonucleotides to be extended by the nsp12-RdRp. However, when studying the activity of the nsp7/nsp8/nsp12 tripartite complex, no *de novo* initiation by nsp8 was detected when the nsp12-RdRp domain was inactivated by a motif C D760A substitution [15]. Most recently, an *in vitro* study employing nsp8 from human coronavirus (HCoV) 229E could not establish nsp8-associated primase or RdRp activities, but instead revealed a 3'-terminal adenylyl transferase activity that may serve to equip viral transcripts with their 3'-poly(A) tail [57]. Although, the importance of nsp8 as co-factor in RNA synthesis is undisputed, its interplay with nsp12 clearly remains to be investigated in more detail, in particular since the issue of nsp12 primer origin/usage seems to be wide open again.

Timeline of discovery and characterization of coronavirus ExoN

The bioinformatics-driven discovery of the nidoviral ExoN domain in 2003 was based on distant sequence similarities with cellular homologs belonging to the DEDD superfamily of exonucleases, such as the proofreading exonuclease domain of *E. coli* DNA polymerase I [10]. Subsequently, the predicted 3'-to-5' exoribonuclease activity was confirmed using *in vitro* assays with recombinant SARS-CoV nsp14 and synthetic RNA substrates [11]. By using reverse genetics, the same authors also demonstrated that ExoN activity is critical for viability of the *Alphacoronavirus* HCoV-229E, as inactivation of the enzyme's active site resulted in a severe defect in overall viral RNA synthesis and a failure to recover infectious viral progeny. Shortly thereafter, strikingly different findings were obtained for the corresponding ExoN-knockout mutants of two betacoronaviruses, MHV and SARS-CoV [12, 58], which are somewhat crippled, but viable in cell culture. In strong support of the original hypothesis that ExoN may act as a proofreading enzyme, ExoN inactivation was found to confer a 'mutator phenotype', as was evident from a 15- to 21-fold increase in mutation frequency – relative to the wild-type

(wt) control - during replication and passaging in cell culture. The ability of ExoN to excise 3'-terminal mismatched nucleotides from a double-stranded (ds) RNA substrate was demonstrated *in vitro* using SARS-CoV nsp14 [27]. This activity was strikingly enhanced by the addition of nsp10, suggesting the two subunits operate as a heterodimer in a mismatch repair mechanism that serves to promote the fidelity of CoV RNA synthesis. Follow-up studies from the Marseille laboratory also described the *in vitro* association of SARS-CoV nsp14 with the nsp7/nsp8/nsp12 tripartite complex [15] and demonstrated that ExoN can efficiently excise ribavirin 5'-monophosphate, possibly explaining why this broad-spectrum antiviral drug is poorly active against CoVs [10, 16].

In the meantime, it had become clear that the ExoN-containing nsp14 subunit of the CoV replicase, which is about 60 kDa in size, is a bifunctional protein. A genetic screening approach in a yeast system revealed that the C-terminal domain of nsp14 exhibits (N7-guanine)-methyltransferase (N7-MTase) activity [26]. Following the *in vitro* characterization of its activity, this enzyme was implicated in the N7-methylation of the (presumed) 5'-terminal cap structure of CoV mRNAs, a modification that is critical for mRNA recognition by the cellular translation machinery [27]. The bimodular ExoN/N7-MTase organization is conserved in most nidovirus families, but the N7-MTase domain is lacking in e.g. toroviruses, bafiniviruses [28] and several recently discovered nidoviruses (Fig. 1B) [8, 9, 59]. The latter findings raise new questions about the mRNA capping pathway(s) employed by these particular virus groups and nidoviruses at large.

Crystal structures of SARS-CoV nsp14 in complex with its nsp10 co-factor (PDB entries 5C8U and 5NFY) revealed several unique structural and functional features [16, 60]. Below we will discuss nsp14 structure and function in more detail, followed by a more extensive description of the reverse genetics data obtained with ExoN-knockout mutants of various CoVs and other functional considerations.

Coronavirus nsp14 harbours exoribonuclease and N7-methyltransferase activities

The CoV ExoN domain was originally identified on the basis of sequence similarities with distant cellular homologs [10] and classified into the superfamily of DEDD exonucleases, which contains the proofreading domains of many DNA polymerases as well as other eukaryotic and prokaryotic exonucleases [61]. These enzymes catalyse the excision of nucleoside monophosphates from nucleic acids in the 3'-to-5' direction using a mechanism that depends on two divalent metal ions and a reactive water molecule [62-64]. The name of the DEDD superfamily derives from its four conserved active site residues that are distributed over three canonical motifs (I, II, and III; Fig.s 2A and 2B) in the primary structure [65]. Originally, in SARS-

CoV nsp14, residues D90/E92 (motif I), D243 (motif II), and D273 (motif III) were identified as putative active site residues [10, 11]. Subsequently, the SARS-CoV nsp14 crystal structure revealed that ExoN in fact is a DEED enzyme as, instead of D243, E191 was identified as the acidic active site residue in motif II [60]. Interestingly, when aligning ExoN sequences from different nidovirus taxa, D243 in SARS-CoV nsp14 is fully conserved, whereas the equivalent of E191 alternates between E and D (Fig.s 2A and 2B). The structural studies [16, 60] also revealed the presence of a fifth catalytic residue (H268 in motif III), identifying ExoN as a member of the DEDDh/DEEDh subfamily [61, 66].

In contrast to nsp14's ExoN activity, which was inferred from bioinformatics analysis, the presence of an N7-MTase in the C-terminal domain of nsp14 was not predicted. This enzyme was discovered upon expression of TGEV and SARS-CoV nsp14 in the yeast *Saccharomyces cerevisiae*, which could rescue a mutant yeast strain lacking the native N7-MTase [26]. The N7-MTase activity was further corroborated using biochemical assays with purified recombinant SARS-CoV nsp14, which was found capable of adding a methyl group to non-methylated cap analogues or GTP substrates, in the presence of S-adenosyl methionine (SAM) as methyl donor [26, 67]. Alanine scanning mutagenesis and *in vitro* assays with nsp14 highlighted two clusters of residues that are key to the MTase activity [26, 68]. The importance of the first cluster, a canonical SAM-binding motif I (DxGxPxG/A; Fig. 3A and 3B) consisting of nsp14 residues 331-336, was confirmed by ^{3}H-labeled SAM cross-linking experiments [26]. The second cluster, encompassing residues 414 and 428, in the crystal structure forms a constricted pocket that holds the GTP moiety of the cap structure (GpppA) between two β-strands (β1 and β2) and helix 1 (Fig. 4C). In this manner, nsp14 positions the N7 position of the cap in close proximity of the methyl donor, thus facilitating transfer by an in-line mechanism [60]. Comparative sequence analysis of N7-MTase domains revealed that a number of residues crucial for substrate and ligand binding are conserved among homologous enzymes of different nidoviruses [9, 16, 60].

Biochemical analysis confirmed that the two enzymatic activities of nsp14 are functionally distinct [26] and physically independent, as also deduced from the structural studies summarized below [16, 60]. However, deletions within the ExoN domain, N-terminal nsp14 truncations of between 78 and 90 amino acids, and alanine substitutions in the N-terminal domain (R84A and W86A) all drastically attenuated or completely abolished the *in vitro* N7-MTase activity [26, 68]. Although such changes may affect overall protein structure and function, these results may also indicate that the two enzymatic domains of nsp14 are structurally interconnected, with N7-MTase activity depending on the integrity of the N-terminal ExoN domain. On the other hand, the ExoN domain is not directly involved in SAM

binding by the N7-MTase [26] nor does the N7-MTase activity depend on the nsp10-nsp14 interaction that strongly enhances ExoN activity [13].

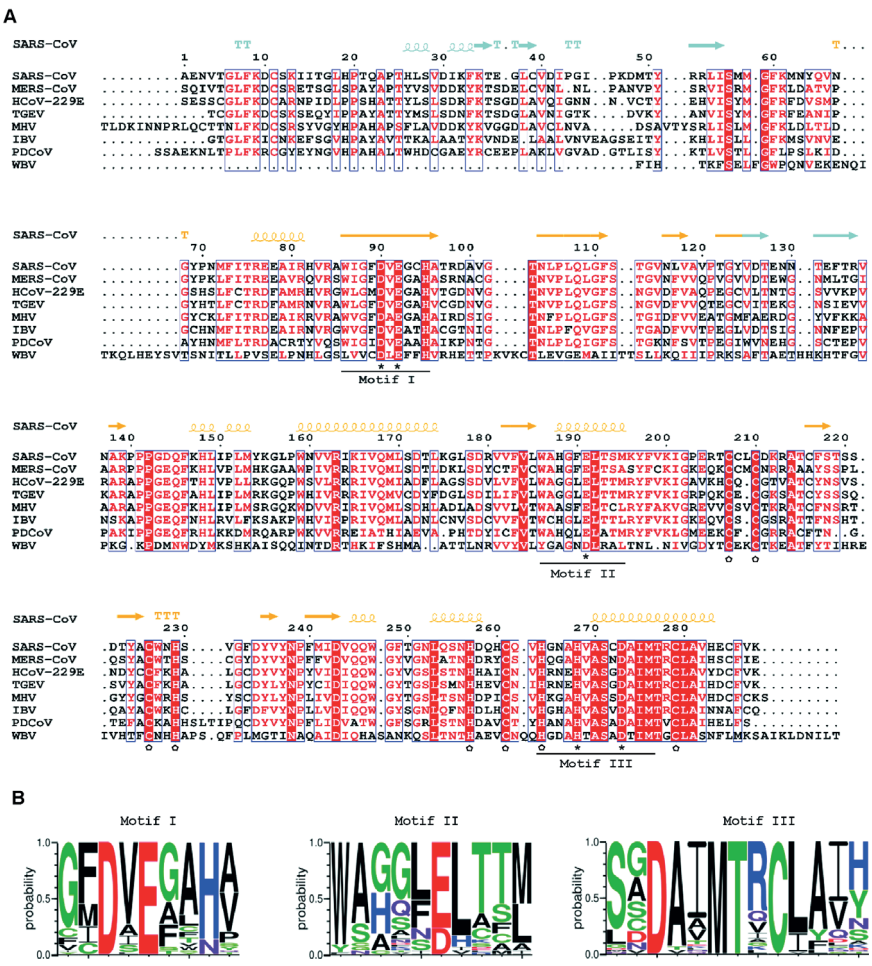

Fig. 2. (A) Amino acid sequence alignment of selected nidovirus ExoN domains, including those that have been characterized experimentally and are discussed in this review, which mainly derive from members of the CoV family: SARS-CoV (NC_004718); MERS-CoV (NC_019843); HCoV-229E (NC_002645); TGEV (P0C6Y5); MHV (NP_045298); IBV (NP_040829); porcine delta CoV (PDCoV; NC_016990), WBV (NC_008516). SARS-CoV nsp14 secondary structure (PDB: 5NFY) is indicated on top, coloured according to the following domain organization: nsp10-binding site (cyan), ExoN domain (orange), hinge region (purple), N7-MTase domain (blue). Fully conserved residues are in red font and boxed, whereas partially conserved residues are displayed in red font (above 70% conservation). Catalytic residues and residues involved in formation of zinc fingers are marked with asterisks and circles, respectively. (B) Web-logos highlighting the three core motifs of the ExoN domain and the family of exonucleases to which it belongs.

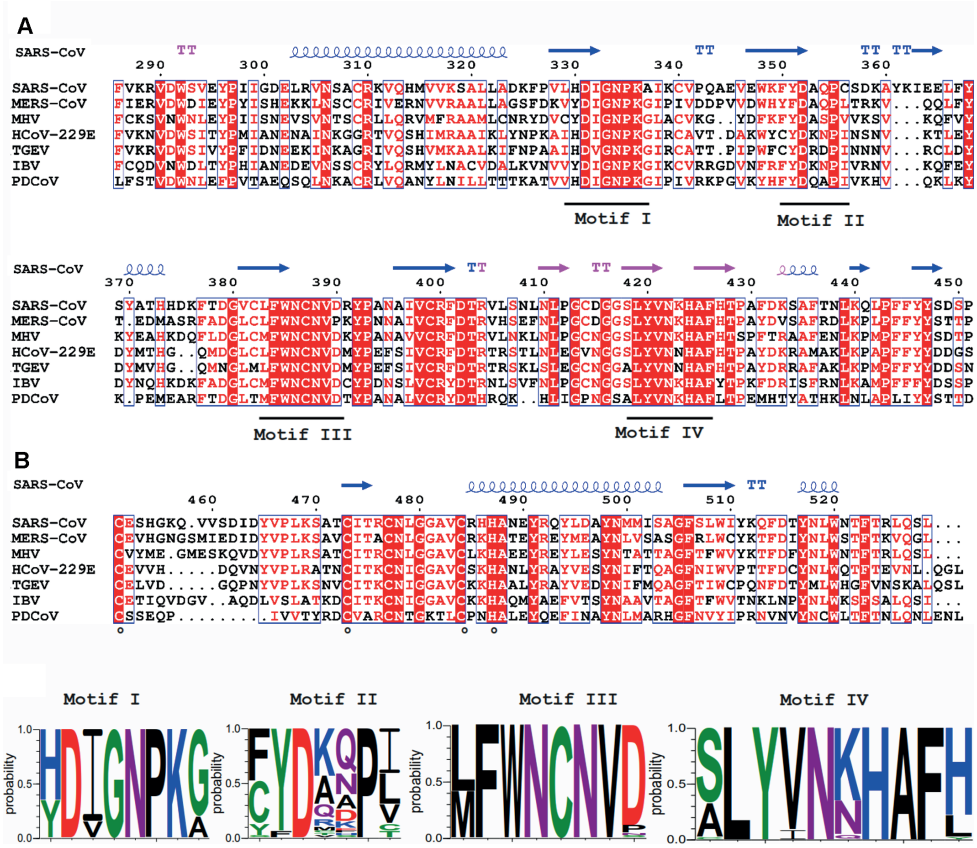

Fig. 3. (A) Amino acid sequence alignment of the N7-MTase domains from the coronaviruses listed in Figure 2. See the Figure 2 legend for viruses and accession numbers used. SARS-CoV nsp14 secondary structure (PDB: 5NFY) is indicated on top, and domain colours and sequence conservation are highlighted as explained in the Figure 2 legend. Residues involved in the formation of the ZF3 zinc finger are marked with circles. (B) Web-logos highlighting the four most-conserved motifs of the N7-MTase domain.

Structural biology of SARS-CoV nsp14

The crystal structure of SARS-CoV nsp14 confirmed a bimodular protein composed of ExoN and N7-MTase domains that are each accompanied by an N-terminal structural domain (Fig. 4A). The overall protein architecture is as follows: (i) a flexible N-terminal domain forming the nsp10 docking site, (ii) the ExoN domain, (iii) a flexible hinge region consisting of a loop and three strands, and (iv) the C-terminal N7-MTase domain [16, 60].

The CoV ExoN domain has an α/β fold reminiscent of other members of the DEDD exonuclease superfamily [69]. Its core is formed by a twisted central β-sheet composed of five β-strands

that are flanked by five α-helices [16, 60]. From this central domain, an inserted β-hairpin structure containing β5 and β6 protrudes to form with β1 a second anti-parallel β-sheet that binds to nsp10 (Fig. 4B). Nsp14 interacts with nsp10 figuratively similar to a "hand (nsp14) over fist (nsp10)" conformation [16]. The fingers of the hand are formed by the flexible N-terminal region of nsp14 (residues 1-50), β1 (residues 51-55), and an antiparallel β-strand protruding from the ExoN domain (residues 122–138), while the palm is composed of residues 55–69 (top) and residues 195–202 (side) (Fig. 4B). The interaction with nsp10 induces conformational changes in the N-terminal region of ExoN that modulate the distance between the catalytic residues in the back of the nsp14 palm and, consequently, impact ExoN activity [16].

The CoV ExoN structure shares the conserved general architecture of DEDD-type exonucleases, including other proofreading ExoN domains like that of the Klenow fragment of *E. coli* DNA polymerase I, the ε subunit of DNA polymerase III [60], and another viral exonuclease [70], currently being peer-reviewed. On the other hand, distinguishing features are the N-terminal nsp10 interaction domain, a β-hairpin structure containing β5 and β6 that also interacts with nsp10, and two zinc finger (ZF) motifs. The first zinc finger (ZF1) is placed between α4 and β10 and formed by residues Cys207, Cys210, Cys226, and His229. The second zinc finger (ZF2), comprising residues His257, Cys261, His264, and Cys279, is located between α5 and α6 (see Fig. 4C). The H268 and D273 active site residues are embedded within ZF2 (see Fig. 2A), which is conserved among all nidoviruses with the exception of PSCNV [9]. Site-directed mutagenesis studies suggested that ZF1 contributes to the structural stability of nsp14, since no soluble SARS-CoV nsp14 could be obtained upon ZF1 disruption. ZF2 is important for catalysis, as replacement of important residues abolished the enzymatic activity of recombinant ExoN [60].

The ExoN and N7-MTase domains of nsp14 are separated by a hinge region that is conserved across CoVs. The hinge may allow significant movement between the two enzymatic domains by allowing lateral and rotational movements of the C-terminal domain with respect to the N-terminal domain, which maybe important to coordinate nsp14's activities (Fig. 4C). The nsp14 N7-MTase domain does not exhibit the canonical Rossmann fold that is commonly found among RNA virus MTases or other RNA cap 0 MTases [71, 72] and does not belong to any of the five classes of SAM-dependent MTases [73], adding another dimension to the unique structural features of this bifunctional protein (Fig. 5) [16].

In general, the Rossmann fold follows a characteristic β-α-β architecture with seven parallel hydrogen-bonded β-strands composing the core of the β-sheet structure, with at least three α-helices on each side [16, 74]. The nsp14 N7-MTase comprises a total of twelve β-strands

and five α-helices, with the central β-sheet being composed of five β-helices instead of seven. Additionally, the N7-MTase domain ends with an α-helix, α10, a modification that stabilizes the local hydrophobic environment and is found in SAM-dependent MTases [75]. A ZF motif (ZF3) consisting of C452, C477, C484, and H487 is located between strand β21 and helix α9 and is important for the proper folding of this region (Fig. 4C and 5). The three ZF motifs are a specific structural signature of nsp14.

Biochemical support for ExoN-driven error correction

The first biochemical assays with purified SARS-CoV nsp14 demonstrated the capability to hydrolyze both double-stranded (ds) and single-stranded (ss) RNA substrates in the 3'-to-5' direction, with a preference for dsRNA substrates [11]. ExoN activity was not found to be RNA sequence-specific, but DNA substrates were not degraded. Ribonuclease activity depended on the presence of divalent metal ions, and was strongly reduced or lost upon substitution of the predicted catalytic residues in motifs I, II, or III with alanine [11]. Whereas basal ExoN activity does not require the presence of co-factors [11, 76], Bouvet *et al*. [13] demonstrated that SARS-CoV ExoN activity is enhanced >35-fold in the presence of nsp10, a small ORF1a-encoded subunit of the CoV replicase that also serves as a co-factor for nsp16's 2'-O-methyltransferase (2'O-MTase) activity [27]. Mutagenesis of nsp10 surface residues into alanine in many cases disrupted the interaction with nsp14, leading to a significant reduction of ExoN activity and the conclusion that nsp14 and nsp16 share a common interaction surface on nsp10 [13, 47]. The nsp10/nsp14 complex preferentially degrades dsRNA substrates suggesting that heterodimerization does not change ExoN's substrate specificity [13]. Furthermore, RNA substrates with a 3'-end duplex structure (like a stable hairpin) and fully base-paired RNA substrates were also efficiently hydrolyzed by the nsp10/nsp14 complex [13]. Importantly, in an assay intended to mimic RdRp incorporation errors, the SARS-CoV nsp10/nsp14 complex was able to excise 3'-terminal mismatched nucleotides from a dsRNA substrate [13]. A more elaborate analysis of ExoN substrate use and specificity suggested that catalysis is determined by the presence of mismatches rather than the nature of the misincorporated nucleotide [13, 16]. However, when the stretch of 3'-terminal mismatched nucleotides was increased beyond 2 nucleotides, a sharp decrease of excision activity was observed [13]. Comparable *in vitro* mismatch excision activity was reported recently for the ExoN domain of the bafinivirus white bream virus (WBV), using dsRNA substrates containing up to three mismatches [28]. These assays were performed using WBV's nsp14 equivalent alone, as no nsp10 homolog seems to be encoded by bafiniviruses. Thus far, this study

constitutes the only description of *in vitro* ExoN activity for a nidovirus that does not belong to the CoV family.

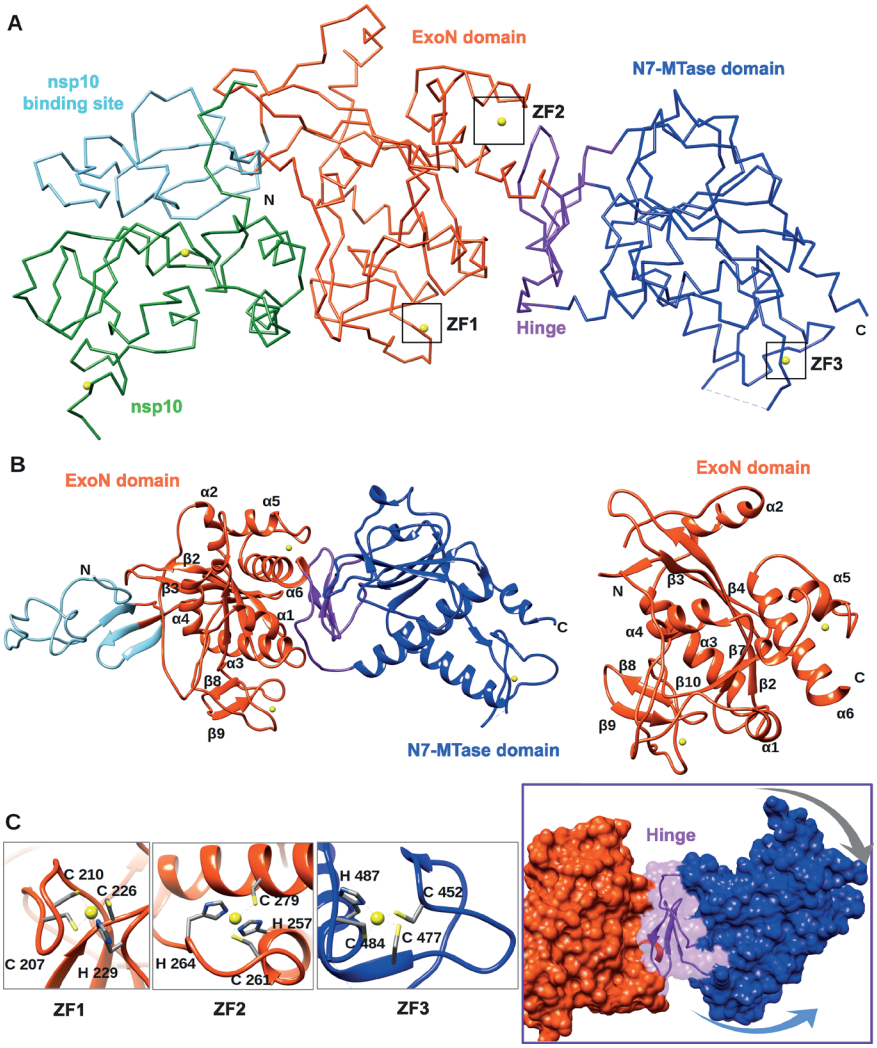

Fig. 4. Overall structure of the SARS-CoV nsp14–nsp10 complex (PDB: 5NFY). (A) Cartoon representation of the crystal structure of the nsp14–nsp10 heterodimer, with domain colours used as follows: nsp10, green; nsp10-binding site of nsp14, cyan; nsp14 ExoN domain, orange; hinge region, purple; nsp14 N7-MTase domain, blue. The unresolved nsp14 residues 454-464 are represented by a dashed line. Zinc ions are shown as yellow spheres. (B) Cartoon representation of SARS-CoV nsp14 (left) and its ExoN domain (right), highlighting the secondary structure elements referred to in the main text. (C) Close-ups of the three zinc fingers (ZF) of nsp14 and the hinge region that connects the ExoN and N7-MTase domains. Arrows indicate the positional flexibility of the N7-MTase domain, which is induced by the presence of the hinge region.

The above studies provided the first biochemical evidence that ExoN, likely in concert with the tripartite RdRp complex (nsp7/nsp8/nsp12 in CoVs), may function as a proofreading enzyme that preferentially targets 3'-terminal single mismatches. Indeed, SARS-CoV nsp14 and the nsp7/nsp8/nsp12 complex were able to associate with each other, while retaining their RNA synthesis, N7-MTase, and exoribonuclease activities [53]. Although, the structural basis of the interaction(s) between nsp14 and the nsp12-RdRp domain remains to be elucidated, *in vitro* studies revealed that both the ExoN and N7-MTase domains of nsp14 are involved [16]. Recent biochemical studies provided more insight into the interplay between the SARS-CoV nsp7/nsp8/nsp12 RdRp complex and the nsp10/14 heterodimer [16]. Using a primer-template substrate containing an A:A mismatch at the 3' end of the primer, extension of the primer was barely observed, suggesting that the SARS-CoV RdRp encounters a kinetic block to extend a substrate with a 3'-terminal mismatch [16]. Strikingly, addition of nsp10/nsp14 to this assay appeared to relieve these constraints and full-length polymerization products were observed, suggesting that ExoN had removed the A:A mismatch before polymerization was resumed. Sequencing of RNA products revealed that 90% had the corrected sequence [16]. Similarly, ribavirin 5'-monophosphate (a guanosine analogue) was efficiently excised from RNA substrates in the presence of nsp14 or nsp10/nsp14 [16].

Together with the mutator phenotype observed for ExoN-knockout mutants of SARS-CoV and MHV (see below), the above data strongly suggest that ExoN contributes to the fidelity of CoV RNA synthesis. It is striking, that in *in vitro* single-nucleotide incorporation assays the SARS-CoV RdRp complex (nsp7/nsp8/nsp12, without nsp14) displayed a lower fidelity than the RdRp of dengue virus, a flavivirus with a three-fold smaller genome [16]. Clearly, a direct *in vitro* comparison of the properties of (distantly related) viral RdRps is not straightforward. Moreover, our perception is 'fragmented' (at best…) when it comes to the biochemical evolution of RdRp and ExoN features following the postulated acquisition of the latter by an ancestral nidovirus [10, 17]. ExoN acquisition may indeed have facilitated genome expansion, but - to an unknown extent - it may also have relaxed the nucleotide selectivity of the RdRp, and therefore the fidelity of RNA synthesis, which would be in line with the biochemical observations outlined above [16]. This would also leave space for the possibility that may exist nidoviruses which combine the use of ExoN with an intrinsic RdRp fidelity that is substantially higher than that observed for present-day CoVs. In fact, also this scenario may have contributed to expand nidoviral genomes to the currently known upper limit (41.1 kb for PSCNV) [9] and (potentially) beyond. In this light, it would be highly interesting to perform similar *in vitro* assays to establish and compare the intrinsic RdRp fidelity of diverse nidoviruses, including those with the longest genomes and those naturally lacking an ExoN

domain [16]. Subsequently, nucleotide incorporation assays combining RdRps and their cognate ExoN may provide important insights into the biochemical synergy of the two enzymes, and may ultimately allow us to correlate intrinsic RdRp fidelity and ExoN activity across the broad spectrum of viruses included in the nidovirus order.

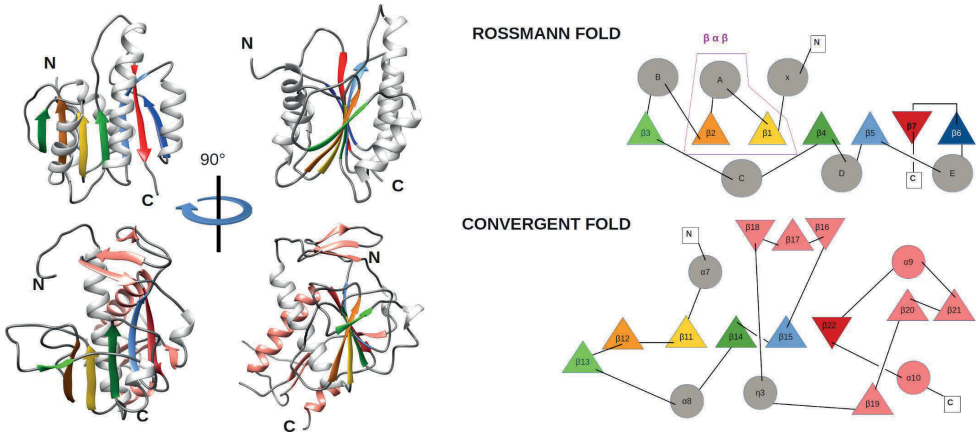

Fig. 5. (left) Comparison of MTase ribbon models of the canonical Rossmann fold (top) of the FtsJ MTase (PDB: 1EJ0) and the convergent fold of the SARS-CoV nsp14 N7-MTase domain (bottom). Two orientations related by a 90° rotation along the vertical axis are shown. Secondary structures are colored to highlight the topology: loop (grey), α-helix (white), and β-strands (green, orange, gold, green, light blue, red), extra α-helix and β-strand of nsp14 (salmon). (right) Corresponding topology diagrams of Rossman fold MTases and the nsp14 N7-MTase domain. β-strands (triangles) and α-helices (circles) follow the same color code as for the ribbon representation in panel A. The β-α-β structural motif, which defines the Rossmann fold, is boxed.

Characterization of coronavirus ExoN-knockout mutants

The study from the Ziebuhr laboratory that demonstrated SARS-CoV nsp14 *in vitro* exoribonuclease activity [11] also described the first engineered ExoN-knockout CoV mutants. However, for biosafety reasons, these experiments were performed using the *Alphacoronavirus* HCoV-229E rather than the *Betacoronavirus* SARS-CoV. The intracellular accumulation of HCoV-229E RNA was found to be severely reduced (by approximately 2 log) for several ExoN active site mutants in motifs I, II, and III. Moreover, relative molar ratios of sg mRNAs were altered and the production of alternative sg transcripts was suspected, based on an analysis of the low amounts of viral RNA produced in transfected cells. Most importantly, infectious virus progeny could not be recovered from the medium of cells transfected with full-length RNA carrying ExoN-inactivating mutations, and consequently ExoN activity was concluded to be critical for HCoV-229E replication [11].

If SARS-CoV rather than HCoV-229E had been the subject of this initial reverse genetics study, the conclusions would have been quite different. Subsequent work from the Denison and Baric laboratories showed that the replication of equivalent ExoN-knockout mutants of SARS-CoV and MHV was affected but certainly not abolished [12, 58]. This was the case when substituting conserved acidic residues of either motif I (D90/E92 in SARS-CoV; mutant ExoN1) or motif III (D273, mutant ExoN3) by alanine. For MHV, these mutations reduced overall viral RNA synthesis (by 75-90% for both genomic and sg RNA) and delayed replication (by several hours), whereas also a specific change in sg mRNA synthesis was observed (reduced mRNA2 production). In MHV, progeny titers of ExoN-knockout mutants were reduced up to 1 log, with plaque sizes of ExoN-knockout mutants also showing extreme heterogeneity [12]. For the corresponding SARS-CoV mutants, progeny titers were about 4-fold reduced without a clear overall change in replication kinetics [12], although intracellular RNA synthesis was not studied in detail. Upon serial passaging in cultured cells, sequence analysis using both conventional and next-generation techniques revealed that the genomes of ExoN-knockout MHV and SARS-CoV mutants accumulated up to 21-fold more mutations than their parental controls, thus providing direct experimental evidence for a connection between ExoN activity and CoV replication fidelity [12, 58].

To investigate this 'mutator phenotype' *in vivo*, mutant ExoN1 was engineered in a mouse-adapted (MA) SARS-CoV backbone [77]. During its *in vitro* characterization, this mutant's progeny titers were reduced by less than 1 log. Quantitative RT-PCR data indicated that the accumulation of wild-type and mutant genome initially was roughly equivalent (6 h p.i.), but that the mutant genome accumulated to about 10-fold lower levels later in infection (24 h p.i.), possibly due to the rapid accumulation of unfavourable mutations [77]. Similar to results obtained upon passaging in cell culture, the ExoN1-MA SARS-CoV mutant exhibited an 11.5-fold increased mutation frequency. The virulence of this mutant was attenuated, resulting in (strongly) reduced disease and expedited virus clearance [77]. Long-term persistent infection of SCID mice allowed a comparison of mutational loads after 30 days, revealing 9.6-fold more mutations across the genome for the progeny of ExoN-deficient MA SARS-CoV.

As expected, due to their reduced replication fidelity and/or impaired overall replication capacity, MHV and SARS-CoV ExoN mutants display increased sensitivity to mutagenic agents like the nucleoside analogue 5-fluorouracil (5-FU) [78]. Similarly, an MHV mutant in which the interaction of nsp14 with its nsp10 co-factor was predicted to be disturbed by two mutations (R80A/E82A in nsp10) was more sensitive to 5-FU than wt virus [79]. Although this finding could be taken as further support for the hypothesis that it is the nsp10/nsp14 complex that acts as a proofreading enzyme, the situation likely is more complex. Specifically, a single

alanine substitution at one of the nsp10 positions targeted for MHV proved to be lethal in SARS-CoV (mutant nsp10-H80A) [47]. Also other nsp10 mutations that disturb the interaction with nsp14 were lethal, and thus had a much stronger impact on SARS-CoV viability than the direct inactivation of ExoN's enzymatic activity [47]. Taking into account that the nsp10/nsp14 and nsp10/nsp16 interaction regions overlap [16], it can be hypothesized that some of the nsp10 mutations interfere with the activities of both complexes. Clearly, this raises important questions about the (multi)functionality of nsp10 and/or the nsp10-nsp14 complex in CoV replication.

Interestingly, and in spite of its reduced replication fidelity, reversion of the MHV-ExoN1 mutant was not reported thus far, even when it was serially passaged in cell culture 250 times [80]. However, over this long period of time, the passaged mutant virus exhibited an 8-fold higher mutation frequency and accumulated a variety of adaptive nonsynonymous mutations. These were spread across the genome and partially compensated for the replication defect and decreased mutagen sensitivity, possibly by improving RdRp fidelity or increasing 'mutational robustness' [80]. These compensatory mutations mapped to the nsp12-RdRp domain and to nsp14 itself, but also to subunits like nsp8, nsp9, and the nsp13 helicase domain. Full reversion of the ExoN1 mutations (DE□AA) would require a total of 4 nucleotide substitutions, but neither full nor partial reversion was observed, suggesting a narrow evolutionary pathway to reversion. It was proposed that replacement of only one of the active site residues suffices to minimize ExoN activity, as observed for the 3'-to-5' exonuclease of *E. coli* polymerase I [69], and that reversion at just one of the two motif I sites offers no selective advantage compared to the double mutant [80].

In view of the replication competence of MHV and SARS-CoV ExoN-knockout mutants summarized above, it is striking that equivalent mutants proved to be non-viable in at least three other CoVs: HCoV-229E [11], transmissible gastroenteritis virus (TGEV) [81], and – most recently – also MERS-CoV, according to an extensive mutagenesis study from our own laboratory. Using a replicon system for the alphacoronavirus TGEV, genome replication and sg mRNA synthesis were found to be only modestly reduced upon mutagenesis of ExoN active site residues [81]. Interestingly, a Cys-to-His change of the second Zn-coordinating residue of ZF1 (residue C210), severely affected sg mRNA synthesis while only mildly affecting genome replication. Upon introduction into the full-length TGEV genome, mutations equivalent to those in the SARS-CoV ExoN1 and ExoN3 mutants prevented the recovery of infectious progeny, with quantitative RT-PCR assays indicating a ~15-fold reduction in the accumulation of genomic RNA. Additionally, a second ZF1 mutation, His-to-Cys at the position of the fourth Zn-coordinating residue (H229), did not strongly affect TGEV RNA synthesis or progeny titers,

but was reported to trigger a weaker TGEV-induced antiviral response. This was attributed to a reduced accumulation of viral dsRNA, an important pathogen-associated molecular pattern (PAMP) that is recognized by innate immune sensors, which triggered a decrease of IFN-β mRNA synthesis and of IFN-induced immune factors in cell culture [81]. Unfortunately, no information is available on the enzymatic activity or replication fidelity of the two TGEV ExoN ZF1 mutants, which would be required to better understand the interesting phenotype of these mutants and their capability to modulate innate immune responses. The assumption that the viable ZF1 mutant (H229C) possesses increased ExoN activity, which could explain the reduced levels of dsRNA in infected cells, seems premature. Alternative explanations for this phenotype include changes in the efficiency or kinetics of RNA synthesis. Moreover, the reported reduction of viral double-stranded RNA accumulation by this mutant should be interpreted with caution, as this conclusion was based solely on the *in situ* immunodetection of dsRNA using a monoclonal antibody with a poorly defined specificity for CoV dsRNA replication intermediates. For example, it remains unknown how changes in the protein composition or subcellular localization of the RNA-synthesizing complex may affect the accessibility of dsRNA epitopes during such immunolabeling experiments.

The results recently obtained with ExoN-knockout mutants MERS-CoV are equally intriguing, particularly since MERS-CoV is a *Betacoronavirus*, like MHV and SARS-CoV. Using an elaborate set of ExoN active site mutants, carrying conservative or alanine substitutions, it was found that ExoN inactivation is lethal in MERS-CoV and that no sign of viral RNA synthesis can be discovered in cells transfected with these mutants' full-length RNA. Again, these observations suggest that the ExoN domain and/or nsp14 (also) play a more direct and basic role in CoV RNA synthesis than merely safeguarding the long-term fidelity of replication.

The remarkable phenotypic variation among ExoN-knockout mutants

As summarized above, depending on the CoV studied, the impact of ExoN inactivation on viral RNA synthesis ranges from a complete block (MERS-CoV) to various degrees of impairment, with residual RNA production supporting the generation of infectious progeny only in the case of MHV and SARS-CoV. For both these betacoronaviruses, in spite of their 'mutator phenotype', the long-term consequences of ExoN inactivation seem limited during propagation in cell culture. Viral RNA synthesis might indeed be expected to tolerate, at least to a certain extent, the inactivation of a proofreading activity that was postulated to not be directly required for RdRp activity, but to merely boost the overall quality of the replication process. Clearly, when replicating in the absence of a functional ExoN, deleterious mutations would first have to accumulate before viral fitness would begin to decrease. This does not

appear to be the case for a third *Betacoronavirus*, MERS-CoV, and for two alphacoronaviruses, HCoV-229E and TGEV, for which the immediate (full to strong) disruption of viral RNA synthesis was observed when ExoN-knockout mutants were launched by transfection of full-length RNA or DNA. In our opinion, technical variations are unlikely to explain these viability differences: with the exception of TGEV, ExoN knockout mutants were commonly launched by electroporation of *in vitro* produced full-length RNA into the cytosol of BHK-21 cells, thus providing an equal environment for the first, critical rounds of replication in a cell line that is known to be compromised in its innate immune response [82, 83]. During our studies with the non-viable MERS-CoV ExoN mutants, we attempted to amplify progeny virus released from transfected BHK-21 cells in both immune-competent and -incompetent cells (e.g. Huh7 and Vero cells, respectively) with an equally negative outcome. Thus, in addition to proofreading, ExoN somehow appears to play a more basic role in the functionality of the CoV RNA-synthesizing machinery, by virtue of its exoribonuclease activity, as a domain of the bifunctional nsp14 subunit, and/or as an interaction partner for other nsps in the viral RNA-synthesizing machinery.

Among the CoVs investigated thus far, MHV and SARS-CoV (in our experience) do stand out as the two viruses exhibiting the most robust RNA synthesis and overall replication in cultured cells. Possibly, the replication activity of ExoN-deficient mutants somehow needs to cross a certain 'threshold' to result in infectious progeny, and for ExoN-deficient mutants this is only achieved with the CoVs that replicate most efficiently. However, when considering the phenotypic differences of knockout mutants, in terms of virus viability and sensitivity to mutagenic agents in cell culture, it remains difficult to reconcile the reported 1- to 2-log reduction of progeny titers for ExoN-knockout MHV and SARS-CoV with the complete loss of infectious progeny reported for the ExoN-knockout mutants of various other CoVs. It is also relevant to consider the fact that low levels of residual enzymatic activity of ExoN active site mutants may go unnoticed in biochemical assays, but could still support a certain level of replication when launching the RNA of an ExoN-knockout CoV mutant. Despite the conservation of ExoN among CoVs and most other nidoviruses, the extent to which particular mutations affect enzymatic activity can only be assessed when studying these specific viral proteins in a biochemical assay [81, 84, 85].

Interactions with the host's innate immune system have been suggested to co-determine the phenotype of ExoN-knockout CoV mutants [81, 85, 86]. It has been proposed that CoV nsp14, by virtue of its ExoN activity, may counteract innate responses by degrading dsRNA replication intermediates in a similar manner as documented for the ExoN domain of the arenavirus nucleoprotein [87, 88]. As CoVs employ a range of innate immune evasion mechanisms [86],

it is difficult to study the importance of any single mechanism in a straightforward manner, as other innate immune antagonists will continue to operate in cells infected with mutants lacking one particular immune evasion function.

Case et al. showed that MHV ExoN(-) virus is sensitive to IFN-β, and that its replication is strongly attenuated in innate immune-competent bone marrow-derived macrophages (BMMs), an effect that was partially restored in interferon-alpha/beta receptor knockout (IFNAR-/-) BMMs [85]. However, upon infection with the MHV-ExoN 1 mutant, neither upregulation of interferon mRNA expression nor induction of the OAS/RNAseL or PKR pathway was observed, in contrast to what would be expected if nsp14 would indeed degrade a PAMP like viral dsRNA. The MHV ExoN1 mutant yielded progeny with a ~10-fold reduced specific infectivity and decreased relative fitness. This property was attributed to the lack of ExoN activity, but the mechanisms underlying the reduced fitness and altered IFN sensitivity remain to be investigated [85]. As summarized in the previous paragraph, TGEV ExoN active site mutants were non-viable (see also above), but an nsp14 mutant carrying a ZF1 mutation (H229C; close to the interaction region with nsp10) was reported to accumulate less dsRNA in infected cells and trigger a weaker antiviral response [81]. These results could be taken to suggest that ExoN may modulate innate immune responses, but TGEV nsp14 remains to be characterized biochemically and for now one can only speculate about the level of ExoN activity of this particular mutant.

Several cellular interferon-stimulated gene products have been implicated in the hypermutation of viral genomes, so it remains to be established how directly the properties of ExoN mutants are determined by a lack [85] or surmised increase of exoribonuclease activity [81]. An additional functional consideration is the fact that the bulk of CoV dsRNA replication intermediates were found to be confined to peculiar double-membrane vesicles, which are part of the CoV replication organelle that drives viral RNA synthesis in infected cells [31, 89]. This feature, which in itself has been proposed to be an innate immune evasion strategy, would potentially complicate access of nsp14 to viral dsRNA substrates.

Nsp14: An attractive target for antiviral drug design?

Currently, there are no FDA-approved antiviral drugs for the treatment of CoVs, which is mainly due to limited interest from the side of the pharmaceutical industry, despite the loss of human lives during the short-lived SARS outbreak and the continuing MERS epidemic. Moreover, antiviral hits identified so far often suffered from poor selectivity indexes. Drug development efforts were further restricted by the limitations of available animal models and potency failure in clinical trials [24]. Taking into account the combination of ExoN and N7-

MTase activities in a single protein, and its importance in viral replication, CoV nsp14 is an attractive target for antiviral drugs. Thus far, only two classes of compounds that (in)directly interfere with its activities have been analyzed in more detail: nucleoside analogues and methyltransferase inhibitors.

Nucleoside analogues can have different mechanisms of action. They may interfere with RNA synthesis directly (for instance by obligate chain termination) or may inhibit virus replication indirectly, for example by inducing lethal mutagenesis or perturbing intracellular nucleoside triphosphate pools. The ExoN proofreading function might counteract these compounds mode of action and, in order to circumvent this, a nucleoside would need to be incorporated more efficiently than it will be excised by ExoN, or should be resistant to ExoN-mediated removal [78, 90-92]. Recently, in spite of these potential complications, GS-5734 (Remdesivir, a monophosphoramidate prodrug of an adenosine analogue) was shown to be a potent inhibitor of the replication of human and zoonotic CoVs *in vivo* and *in vitro* [90, 92, 93]. Compared to the wt control, replication of the MHV ExoN1-knockout mutant was inhibited more efficiently by GS-5734, suggesting that the compound's activity is limited by ExoN's capability to excise and remove it after its incorporation into the RNA chain by the viral RdRp. The simultaneous targeting of RdRp and ExoN functionality with a combination of a nucleoside analogue and a specific exoribonuclease inhibitor may also be worth exploring. In the case of nucleoside analogs like ribavirin, such an approach may even restore antiviral efficacy against CoVs and other viruses equipped with a proofreading mechanism [16].

Regarding the inhibition of the nsp14 N7-MTase, only a few compounds have been identified that inhibit its activity *in vitro*: adenosylhomocysteine, aurintricarboxylic acid (ATA), and sinefugin [27, 94, 95]. Further work is needed to optimize these hits in order to study their activity *in vivo*, and investigate their specificity for this viral enzyme. Taking into account the unique fold of the N7-MTase enzyme compared to other MTases, this might facilitate the drug development of specific compounds targeting this domain [16, 60].

CONCLUSIONS AND FUTURE DIRECTIONS

The order *Nidovirales* constitutes a +RNA virus lineage displaying a unique combination of molecular biological features, including a genome size that ranges from 'somewhat above average' (arteriviruses, 12-16 kb) to the largest RNA virus genomes currently known (PSCNV, 41 kb). Upon its discovery, promoted by the relationship with other proofreading exonucleases, the ExoN domain was postulated to have played an important role in nidoviral evolution and genome expansion [10] by providing a proofreading activity that enhances the replication fidelity. Indeed, now that the nidovirus order has grown substantially over the past

decade, the conservation of ExoN across a wide range of distantly related nidoviruses with genome sizes above 18 kb testifies to the important role this enzyme must play. Consequently, this role was incorporated in an advanced theoretical model of nidoviral genome dynamics [9, 59], in which the ancestral expansion of ORF1b , which includes the ExoN domain, facilitated the subsequent growth of other parts of the genome. In parallel, experimental evidence has accumulated, mainly derived from studies with the well-studied betacoronaviruses SARS-CoV and MHV, leaving little doubt about the involvement of ExoN in fidelity control during genome replication [11-13, 16, 58, 77].

While the increasing genome size upper limit and the discovery of a proofreading mechanism constitute clear and exciting paradigm shifts in RNA virology, important questions regarding ExoN function and importance remain to be resolved. Among these, the wide phenotypic variation among the ExoN-knockout mutants of the different CoV species studied thus far (see above) is a remarkable issue. In this case, it appears to be particularly challenging to integrate the results from biochemistry, structural biology, (reverse) genetics, and the analysis of CoV-infected cells into a coherent model of ExoN function. It might also be instructive to reassess the increased mutation frequency and evolution of ExoN-knockout mutants using more advanced deep-sequencing methods that have been developed during recent years [96].

Although most of the ORF1b-encoded key replicative enzymes of CoVs (nsp12, nsp13, nsp14) and their co-factors (nsp7, nsp8, nsp10) now have been characterized *in vitro*, it is still quite unclear how these findings can be extrapolated to the viral enzyme complex in the infected cell [40, 97]. The impressive long-term passaging experiment with the MHV ExoN1 mutant [80] nicely illustrates the complexity and plasticity of the CoV replication machinery, documenting how a network of compensatory mutations in a variety of other nsps can – in the long run - help the virus to survive and circumvent an ExoN activity defect. Unfortunately, such studies are technically challenging or impossible for CoVs yielding non-viable ExoN-knockout mutants. In this context, it is necessary to expand the biochemical and structural characterization of CoV replicative enzymes, including ExoN, to other CoV species than SARS-CoV.

Further elucidation of the structure-function interplay between ExoN and other (viral and/or host) members of the CoV replication machinery will be key to understanding their role in viral RNA synthesis, immune evasion and pathogenesis. Such information will contribute to the design of new antiviral approaches, or the improvement of existing ones, including those relying on inducing 'lethal mutagenesis' [16]. Likewise, it will allow a better assessment of the applicability of ExoN inactivation as a broad strategy for designing live-attenuated vaccines against CoVs or other nidoviruses [77], which – in terms of vaccine production – clearly

depends on the viability of ExoN-knockout mutants. In this context, it would be highly interesting to explore the partial inactivation of ExoN in CoVs for which full inactivation was proven to be lethal. Now that metagenomics studies have informed us about the evolutionary success and remarkably broad host range of nidoviruses, it is important, more than ever before, to enhance our preparedness and design strategies to counter nidoviruses that are likely to emerge in human or animal host populations.

FUNDING

N.S.O. was supported by the Marie Skłodowska-Curie ETN European Training Network 'ANTIVIRALS' (EU Grant Agreement No. 642434). C.C.P and E.J.S. were supported by TOP-GO grant 700.10.352 from the Netherlands Organization for Scientific Research.

ACKNOWLEDGMENTS

We kindly acknowledge the ground-breaking contributions of Dr. Alexander Gorbalenya, to the nidovirus replicase field at large, and to the discovery and rationalization of the nidovirus ExoN domain in particular. We thank Dr. Ben Neuman for providing Fig. 1B.

CONFLICT OF INTEREST STATEMENT

The authors declare that the research was conducted in the absence of any commercial or financial relationships that could be construed as a potential conflict of interest.

AUTHOR CONTRIBUTIONS

Together with N.S.O., C.C.P. and E.J.S. (who contributed equally) conceived, wrote and edited this review. F.F., E.D., and B.C. revised and extended parts of the text, specifically in the areas of biochemistry and structural biology, and provided various other useful suggestions and contributions. Fig.s 2 to 5 were prepared by F.F. and Fig. 1A by E.J.S. and N.S.O. N.S.O. and E.J.S. prepared the final version of the manuscript, which was approved by all authors.

REFERENCES

1. Steinhauer, D.A., E. Domingo, and J.J. Holland, *Lack of evidence for proofreading mechanisms associated with an RNA virus polymerase.* Gene, 1992. **122**(2): p. 281-288.
2. Drake, J.W. and J.J. Holland, *Mutation rates among RNA viruses.* Proc Natl Acad Sci U S A, 1999. **96**(24): p. 13910-13913.
3. Eigen, M., *Error catastrophe and antiviral strategy.* Proc Natl Acad Sci U S A, 2002. **99**(21): p. 13374-13376.
4. Crotty, S., C.E. Cameron, and R. Andino, *RNA virus error catastrophe: direct molecular test by using ribavirin.* Proc Natl Acad Sci U S A, 2001. **98**(12): p. 6895-900.
5. Pfeiffer, J.K. and K. Kirkegaard, *Increased fidelity reduces poliovirus fitness and virulence under selective pressure in mice.* PLoS Pathog, 2005. **1**(2): p. e11.
6. Vignuzzi, M., et al., *Quasispecies diversity determines pathogenesis through cooperative interactions in a viral population.* Nature, 2006. **439**(7074): p. 344-8.
7. Manrubia, S.C., E. Domingo, and E. Lazaro, *Pathways to extinction: beyond the error threshold.* Philos Trans R Soc Lond B Biol Sci, 2010. **365**(1548): p. 1943-52.
8. Bukhari, K., et al., *Description and initial characterization of metatranscriptomic nidovirus-like genomes from the proposed new family Abyssoviridae, and from a sister group to the Coronavirinae, the proposed genus Alphaletovirus.* Virology, 2018. **524**: p. 160-171.
9. Saberi, A., et al., *A planarian nidovirus expands the limits of RNA genome size.* PLoS Pathog, 2018. **14**(11): p. e1007314.
10. Snijder, E.J., et al., *Unique and conserved features of genome and proteome of SARS-coronavirus, an early split-off from the coronavirus group 2 lineage.* J Mol Biol, 2003. **331**(5): p. 991-1004.
11. Minskaia, E., et al., *Discovery of an RNA virus 3'->5' exoribonuclease that is critically involved in coronavirus RNA synthesis.* Proc Natl Acad Sci U S A, 2006. **103**(13): p. 5108-13.
12. Eckerle, L.D., et al., *High fidelity of murine hepatitis virus replication is decreased in nsp14 exoribonuclease mutants.* J Virol, 2007. **81**(22): p. 12135-12144.
13. Bouvet, M., et al., *RNA 3'-end mismatch excision by the severe acute respiratory syndrome coronavirus nonstructural protein nsp10/nsp14 exoribonuclease complex.* Proc Natl Acad Sci U S A, 2012. **109**(24): p. 9372-9377.
14. Smith, E.C. and M.R. Denison, *Implications of altered replication fidelity on the evolution and pathogenesis of coronaviruses.* Curr Opin Virol, 2012. **2**(5): p. 519-24.
15. Subissi, L., et al., *SARS-CoV ORF1b-encoded nonstructural proteins 12-16: replicative enzymes as antiviral targets.* Antiviral Res, 2014. **101**: p. 122-30.
16. Ferron, F., et al., *Structural and molecular basis of mismatch correction and ribavirin excision from coronavirus RNA.* Proc Natl Acad Sci U S A, 2018. **115**(2): p. E162-E171.
17. Nga, P.T., et al., *Discovery of the first insect nidovirus, a missing evolutionary link in the emergence of the largest RNA virus genomes.* PLoS Pathog, 2011. **7**(9): p. e1002215.
18. Siddell, S.G., et al., *Additional changes to taxonomy ratified in a special vote by the International Committee on Taxonomy of Viruses (October 2018).* Arch Virol, 2019. **164**(3): p. 943-946.
19. Shi, M., et al., *Redefining the invertebrate RNA virosphere.* Nature, 2016. **540**(7634): p. 539-543.

20. Shi, M., et al., *Author Correction: The evolutionary history of vertebrate RNA viruses.* Nature, 2018. **561**(7722): p. E6.
21. Shi, M., et al., *The evolutionary history of vertebrate RNA viruses.* Nature, 2018. **556**(7700): p. 197-202.
22. den Boon, J.A., et al., *Equine arteritis virus is not a togavirus but belongs to the coronaviruslike superfamily.* J Virol, 1991. **65**(6): p. 2910-20.
23. Gorbalenya, A.E., et al., *Nidovirales: evolving the largest RNA virus genome.* Virus Res, 2006. **117**(1): p. 17-37.
24. Zumla, A., et al., *Coronaviruses - drug discovery and therapeutic options.* Nat Rev Drug Discov, 2016. **15**(5): p. 327-47.
25. Lehmann, K.C., et al., *Discovery of an essential nucleotidylating activity associated with a newly delineated conserved domain in the RNA polymerase-containing protein of all nidoviruses.* Nucleic Acids Res, 2015. **43**(17): p. 8416-34.
26. Chen, Y., et al., *Functional screen reveals SARS coronavirus nonstructural protein nsp14 as a novel cap N7 methyltransferase.* Proc Natl Acad Sci U S A, 2009. **106**(9): p. 3484-9.
27. Bouvet, M., et al., *In vitro reconstitution of SARS-coronavirus mRNA cap methylation.* PLoS Pathog, 2010. **6**(4): p. e1000863.
28. Durzynska, I., et al., *Characterization of a bafinivirus exoribonuclease activity.* J Gen Virol, 2018. **99**(9): p. 1253-1260.
29. Ziebuhr, J., E.J. Snijder, and A.E. Gorbalenya, *Virus-encoded proteinases and proteolytic processing in the Nidovirales.* J Gen Virol, 2000. **81**(Pt 4): p. 853-79.
30. Gosert, R., et al., *RNA replication of mouse hepatitis virus takes place at double-membrane vesicles.* J Virol, 2002. **76**(8): p. 3697-708.
31. Knoops, K., et al., *SARS-coronavirus replication is supported by a reticulovesicular network of modified endoplasmic reticulum.* PLoS Biol, 2008. **6**(9): p. e226.
32. Soding, J., *Protein homology detection by HMM-HMM comparison.* Bioinformatics, 2005. **21**(7): p. 951-60.
33. Zimmermann, L., et al., *A Completely Reimplemented MPI Bioinformatics Toolkit with a New HHpred Server at its Core.* J Mol Biol, 2018. **430**(15): p. 2237-2243.
34. Pasternak, A.O., W.J. Spaan, and E.J. Snijder, *Nidovirus transcription: how to make sense...?* J Gen Virol, 2006. **87**(Pt 6): p. 1403-21.
35. Sawicki, S.G., D.L. Sawicki, and S.G. Siddell, *A contemporary view of coronavirus transcription.* J Virol, 2007. **81**(1): p. 20-9.
36. Sola, I., et al., *Continuous and Discontinuous RNA Synthesis in Coronaviruses.* Annu Rev Virol, 2015. **2**(1): p. 265-88.
37. Decroly, E., et al., *Conventional and unconventional mechanisms for capping viral mRNA.* Nat Rev Microbiol, 2011. **10**(1): p. 51-65.
38. Neuman, B.W., et al., *Atlas of coronavirus replicase structure.* Virus Res, 2014. **194**: p. 49-66.
39. Sevajol, M., et al., *Insights into RNA synthesis, capping, and proofreading mechanisms of SARS-coronavirus.* Virus Res, 2014. **194**: p. 90-9.
40. Snijder, E.J., E. Decroly, and J. Ziebuhr, *The Nonstructural Proteins Directing Coronavirus RNA Synthesis and Processing.* Adv Virus Res, 2016. **96**: p. 59-126.
41. Denison, M.R., et al., *Coronaviruses: an RNA proofreading machine regulates replication fidelity and diversity.* RNA Biol, 2011. **8**(2): p. 270-9.

42. Posthuma, C.C., A.J.W. Te Velthuis, and E.J. Snijder, *Nidovirus RNA polymerases: Complex enzymes handling exceptional RNA genomes.* Virus Res, 2017. **234**: p. 58-73.
43. Kirchdoerfer, R.N. and A.B. Ward, *Structure of the SARS-CoV nsp12 polymerase bound to nsp7 and nsp8 co-factors.* Nat Commun, 2019. **10**(1): p. 2342.
44. Decroly, E., et al., *Crystal structure and functional analysis of the SARS-coronavirus RNA cap 2'-O-methyltransferase nsp10/nsp16 complex.* PLoS Pathog, 2011. **7**(5): p. e1002059.
45. Decroly, E., et al., *Coronavirus nonstructural protein 16 is a cap-0 binding enzyme possessing (nucleoside-2'O)-methyltransferase activity.* J Virol, 2008. **82**(16): p. 8071-84.
46. Zust, R., et al., *Ribose 2'-O-methylation provides a molecular signature for the distinction of self and non-self mRNA dependent on the RNA sensor Mda5.* Nat Immunol, 2011. **12**(2): p. 137-43.
47. Bouvet, M., et al., *Coronavirus Nsp10, a critical co-factor for activation of multiple replicative enzymes.* J Biol Chem, 2014. **289**(37): p. 25783-25796.
48. Gorbalenya, A.E., et al., *Coronavirus genome: prediction of putative functional domains in the non-structural polyprotein by comparative amino acid sequence analysis.* Nucleic Acids Res, 1989. **17**(12): p. 4847-61.
49. te Velthuis, A.J., et al., *The RNA polymerase activity of SARS-coronavirus nsp12 is primer dependent.* Nucleic Acids Res, 2010. **38**(1): p. 203-14.
50. Ahn, D.G., et al., *Biochemical characterization of a recombinant SARS coronavirus nsp12 RNA-dependent RNA polymerase capable of copying viral RNA templates.* Arch Virol, 2012. **157**(11): p. 2095-104.
51. Xu, X., et al., *Molecular model of SARS coronavirus polymerase: implications for biochemical functions and drug design.* Nucleic Acids Res, 2003. **31**(24): p. 7117-30.
52. Sexton, N.R., et al., *Homology-Based Identification of a Mutation in the Coronavirus RNA-Dependent RNA Polymerase That Confers Resistance to Multiple Mutagens.* J Virol, 2016. **90**(16): p. 7415-7428.
53. Subissi, L., et al., *One severe acute respiratory syndrome coronavirus protein complex integrates processive RNA polymerase and exonuclease activities.* Proc Natl Acad Sci U S A, 2014. **111**(37): p. E3900-E3909.
54. Zhai, Y., et al., *Insights into SARS-CoV transcription and replication from the structure of the nsp7-nsp8 hexadecamer.* Nat Struct Mol Biol, 2005. **12**(11): p. 980-6.
55. Xiao, Y., et al., *Nonstructural proteins 7 and 8 of feline coronavirus form a 2:1 heterotrimer that exhibits primer-independent RNA polymerase activity.* J Virol, 2012. **86**(8): p. 4444-54.
56. Imbert, I., et al., *A second, non-canonical RNA-dependent RNA polymerase in SARS coronavirus.* EMBO J, 2006. **25**(20): p. 4933-42.
57. Tvarogova, J., et al., *Identification and characterization of a human coronavirus 229E nonstructural protein 8-associated RNA 3'-terminal adenylyltransferase activity.* J Virol, 2019.
58. Eckerle, L.D., et al., *Infidelity of SARS-CoV Nsp14-exonuclease mutant virus replication is revealed by complete genome sequencing.* PLoS Pathog, 2010. **6**(5): p. e1000896.
59. Lauber, C., et al., *The footprint of genome architecture in the largest genome expansion in RNA viruses.* PLoS Pathog, 2013. **9**(7): p. e1003500.

60. Ma, Y., et al., *Structural basis and functional analysis of the SARS coronavirus nsp14-nsp10 complex.* Proc Natl Acad Sci U S A, 2015. **112**(30): p. 9436-9441.
61. Zuo, Y. and M.P. Deutscher, *Exoribonuclease superfamilies: structural analysis and phylogenetic distribution.* Nucleic Acids Res, 2001. **29**(5): p. 1017-1026.
62. Deutscher, M.P. and C.W. Marlor, *Purification and characterization of Escherichia coli RNase T.* J Biol Chem, 1985. **260**(11): p. 7067-7071.
63. Beese, L.S. and T.A. Steitz, *Structural basis for the 3'-5' exonuclease activity of Escherichia coli DNA polymerase I: a two metal ion mechanism.* EMBO J, 1991. **10**(1): p. 25-33.
64. Steitz, T.A. and J.A. Steitz, *A general two-metal-ion mechanism for catalytic RNA.* Proc Natl Acad Sci U S A, 1993. **90**(14): p. 6498-6502.
65. Bernad, A., et al., *A conserved 3'----5' exonuclease active site in prokaryotic and eukaryotic DNA polymerases.* Cell, 1989. **59**(1): p. 219-228.
66. Barnes, M.H., et al., *The 3'-5' exonuclease site of DNA polymerase III from gram-positive bacteria: definition of a novel motif structure.* Gene, 1995. **165**(1): p. 45-50.
67. Jin, X., et al., *Characterization of the guanine-N7 methyltransferase activity of coronavirus nsp14 on nucleotide GTP.* Virus Res, 2013. **176**(1-2): p. 45-52.
68. Chen, Y., et al., *Structure-function analysis of severe acute respiratory syndrome coronavirus RNA cap guanine-N7-methyltransferase.* J Virol, 2013. **87**(11): p. 6296-6305.
69. Derbyshire, V., N.D. Grindley, and C.M. Joyce, *The 3'-5' exonuclease of DNA polymerase I of Escherichia coli: contribution of each amino acid at the active site to the reaction.* EMBO J, 1991. **10**(1): p. 17-24.
70. Yekwa, E., et al., *Arenaviridae exoribonuclease presents genomic RNA edition capacity.* bioRxiv, 2019: p. 541698.
71. Byszewska, M., et al., *RNA methyltransferases involved in 5' cap biosynthesis.* RNA Biol, 2014. **11**(12): p. 1597-607.
72. Chouhan, B.P.S., et al., *Rossmann-Fold Methyltransferases: Taking a "beta-Turn" around Their Cofactor, S-Adenosylmethionine.* Biochemistry, 2019. **58**(3): p. 166-170.
73. Schubert, H.L., R.M. Blumenthal, and X. Cheng, *Many paths to methyltransfer: a chronicle of convergence.* Trends Biochem Sci, 2003. **28**(6): p. 329-35.
74. Rao, S.T. and M.G. Rossmann, *Comparison of super-secondary structures in proteins.* J Mol Biol, 1973. **76**(2): p. 241-56.
75. Martin, J.L. and F.M. McMillan, *SAM (dependent) I AM: the S-adenosylmethionine-dependent methyltransferase fold.* Curr Opin Struct Biol, 2002. **12**(6): p. 783-93.
76. Chen, P., et al., *Biochemical characterization of exoribonuclease encoded by SARS coronavirus.* J Biochem Mol Biol, 2007. **40**(5): p. 649-655.
77. Graham, R.L., et al., *A live, impaired-fidelity coronavirus vaccine protects in an aged, immunocompromised mouse model of lethal disease.* Nat Med, 2012. **18**(12): p. 1820-1826.
78. Smith, E.C., et al., *Coronaviruses lacking exoribonuclease activity are susceptible to lethal mutagenesis: evidence for proofreading and potential therapeutics.* PLoS Pathog, 2013. **9**(8): p. e1003565.
79. Smith, E.C., et al., *Mutations in coronavirus nonstructural protein 10 decrease virus replication fidelity.* J Virol, 2015. **89**(12): p. 6418-26.

80. Graepel, K.W., et al., *Proofreading-deficient coronaviruses adapt for increased fitness over long-term passage without reversion of exoribonuclease-inactivating mutations.* MBio, 2017. **8**(6): p. e01503-01517.
81. Becares, M., et al., *Mutagenesis of coronavirus nsp14 reveals its potential role in modulation of the innate immune response.* J Virol, 2016. **90**(11): p. 5399-5414.
82. Habjan, M., et al., *T7 RNA polymerase-dependent and -independent systems for cDNA-based rescue of Rift Valley fever virus.* J Gen Virol, 2008. **89**(Pt 9): p. 2157-2166.
83. Lam, V., K.A. Duca, and J. Yin, *Arrested spread of vesicular stomatitis virus infections in vitro depends on interferon-mediated antiviral activity.* Biotechnol Bioeng, 2005. **90**(7): p. 793-804.
84. Case, J.B., et al., *Mutagenesis of S-adenosyl-l-methionine-binding residues in coronavirus nsp14 N7-methyltransferase demonstrates differing requirements for genome translation and resistance to innate immunity.* J Virol, 2016. **90**(16): p. 7248-7256.
85. Case, J.B., et al., *Murine hepatitis virus nsp14 exoribonuclease activity is required for resistance to innate immunity.* J Virol, 2018. **92**(1): p. e01531-17.
86. Kindler, E. and V. Thiel, *To sense or not to sense viral RNA--essentials of coronavirus innate immune evasion.* Curr Opin Microbiol, 2014. **20**: p. 69-75.
87. Hastie, K.M., et al., *Structure of the Lassa virus nucleoprotein reveals a dsRNA-specific 3' to 5' exonuclease activity essential for immune suppression.* Proc Natl Acad Sci U S A, 2011. **108**(6): p. 2396-2401.
88. Russier, M., et al., *The exonuclease domain of Lassa virus nucleoprotein is involved in antigen-presenting-cell-mediated NK cell responses.* J Virol, 2014. **88**(23): p. 13811-13820.
89. Neuman, B.W., *How the Double Spherules of Infectious Bronchitis Virus Impact Our Understanding of RNA Virus Replicative Organelles.* mBio, 2013. **4**(6): p. e00987-13.
90. Warren, T.K., et al., *Therapeutic efficacy of the small molecule GS-5734 against Ebola virus in rhesus monkeys.* Nature, 2016. **531**(7594): p. 381-5.
91. Crotty, S., et al., *The broad-spectrum antiviral ribonucleoside ribavirin is an RNA virus mutagen.* Nat Med, 2000. **6**(12): p. 1375-9.
92. Agostini, M.L., et al., *Coronavirus Susceptibility to the Antiviral Remdesivir (GS-5734) Is Mediated by the Viral Polymerase and the Proofreading Exoribonuclease.* MBio, 2018. **9**(2).
93. Sheahan, T.P., et al., *Broad-spectrum antiviral GS-5734 inhibits both epidemic and zoonotic coronaviruses.* Sci Transl Med, 2017. **9**(396).
94. Sun, Y., et al., *Yeast-based assays for the high-throughput screening of inhibitors of coronavirus RNA cap guanine-N7-methyltransferase.* Antiviral Res, 2014. **104**: p. 156-64.
95. Aouadi, W., et al., *Toward the identification of viral cap-methyltransferase inhibitors by fluorescence screening assay.* Antiviral Res, 2017. **144**: p. 330-339.
96. Acevedo, A., L. Brodsky, and R. Andino, *Mutational and fitness landscapes of an RNA virus revealed through population sequencing.* Nature, 2014. **505**(7485): p. 686-90.
97. Ulferts, R., T.C. Mettenleiter, and J. Ziebuhr, *Characterization of Bafinivirus main protease autoprocessing activities.* J Virol, 2011. **85**(3): p. 1348-1359.

CHAPTER IV

The enzymatic activity of the nsp14 exoribonuclease is critical for replication of MERS-CoV and SARS-CoV-2

Natacha S. Ogando, Jessika C. Zevenhoven-Dobbe, Yvonne van der Meer,
Peter J. Bredenbeek, Clara C. Posthuma[§#] & Eric J. Snijder[§#]

Department of Medical Microbiology, Leiden University Medical Center, Leiden, The Netherlands
[#] Present address: Netherlands Commission on Genetic Modification, Bilthoven, The Netherlands

#authors contributed equally
Published in Journal of Virology
doi.org/10.1128/JVI.01246-20

ABSTRACT

Coronaviruses (CoVs) stand out for their large RNA genome and complex RNA-synthesizing machinery comprising 16 nonstructural proteins (nsps). The bifunctional nsp14 contains 3'-to-5' exoribonuclease (ExoN) and guanine-N7-methyltransferase (N7-MTase) domains. While the latter presumably supports mRNA capping, ExoN is thought to mediate proofreading during genome replication. In line with such a role, ExoN-knockout mutants of mouse hepatitis virus (MHV) and severe acute respiratory syndrome coronavirus (SARS-CoV) were previously reported to have crippled but viable hypermutation phenotypes. Remarkably, using reverse genetics, a large set of corresponding ExoN knockout mutations was now found to be lethal for another *Betacoronavirus*, Middle East respiratory syndrome coronavirus (MERS-CoV). For 13 mutants, viral progeny could not be recovered, unless – occasionally – reversion had first occurred. Only a single mutant was viable, likely because its E191D substitution is highly conservative. Remarkably, also a SARS-CoV-2 ExoN knockout mutant was found unable to replicate, resembling observations previously made for *Alphacoronavirus* and *Gammacoronavirus*, but starkly contrasting with the documented phenotype of ExoN knockout mutants of the closely related SARS-CoV. Subsequently, we established in vitro assays with purified recombinant MERS-CoV nsp14 to monitor its ExoN and N7-MTase activities. All ExoN knockout mutations that proved lethal in reverse genetics were found to severely decrease ExoN activity, while not affecting N7-MTase activity. Our study strongly suggests CoV nsp14 ExoN to have an additional function, which apparently is critical for primary viral RNA synthesis and thus differs from the proofreading function that – based on previous MHV and SARS-CoV studies – was proposed to boost longer-term replication fidelity.

IMPORTANCE

The bifunctional nsp14 subunit of the coronavirus replicase contains 3'-to-5' exoribonuclease (ExoN) and guanine-N7-methyltransferase domains. For the betacoronaviruses MHV and SARS-CoV, ExoN was reported to promote the fidelity of genome replication, presumably by mediating a form of proofreading. For these viruses, ExoN knockout mutants are viable while displaying an increased mutation frequency. Strikingly, we now established that the equivalent ExoN knockout mutants of two other betacoronaviruses, MERS-CoV and SARS-CoV-2, are non-viable, suggesting an additional and critical ExoN function in their replication. This is remarkable in light of the very limited genetic distance between SARS-CoV and SARS-CoV-2, which is highlighted, for example, by 95% amino acid sequence identity in their nsp14 sequences. For (recombinant) MERS-CoV nsp14, both its enzymatic activities were evaluated using newly developed in vitro assays that can be used to characterize these key replicative enzymes in more detail and explore their potential as target for antiviral drug development.

INTRODUCTION

RNA viruses commonly exhibit high mutation rates, a feature attributed to the relatively poor fidelity of their RNA-dependent RNA polymerase (RdRp) and the fact that nucleotide incorporation errors go uncorrected. This lack of proofreading contributes to the generation of 'quasispecies' populations, clouds of genome sequence variants that are subject to continuous natural selection [1-3]. On the one hand, their genetic heterogeneity allows RNA viruses to rapidly adapt to changing circumstances, in order to overcome environmental challenges such as host switching, antiviral drug treatment, or host immune responses [4, 5]. On the other hand, the accumulation of an excessive number of deleterious mutations can result in 'error catastrophe' and, consequently, in the extinction of a viral species [6-8]. In order to balance these opposing principles, RNA viruses are thought to operate close to their so-called 'error threshold', while balancing the interdependent parameters of replication fidelity, genome size, and genome complexity [9, 10]. This interplay is thought to have restricted the expansion of RNA virus genome sizes, which are below 15 kilobases (kb) for most RNA virus families [10-12].

The largest RNA virus genomes currently known are found in the order *Nidovirales,* which includes the *Coronaviridae* family and also the recently discovered planarian secretory cell nidovirus (PSCNV; [12, 13]), which has the largest RNA genome identified thus far (41.1 kb). One of the molecular mechanisms potentially driving the unprecedented expansion of nidovirus genomes was discovered about 17 years ago, during the in-depth bioinformatics analysis of the genome and proteome of the severe acute respiratory syndrome coronavirus (SARS-CoV). During this analysis, Alexander Gorbalenya and colleagues identified a putative 3'-to-5' exoribonuclease (ExoN) signature sequence in the N-terminal domain of nonstructural protein 14 (nsp14), a subunit of the large replicase polyprotein encoded by CoVs and related large-genome nidoviruses. Strikingly, this ExoN domain was found to be lacking in the replicases of nidoviruses with small(er) genomes (specifically, arteriviruses), and therefore it was proposed that the enzyme may provide a form of 'proofreading activity' that could have promoted the expansion of large nidoviral genomes to their current size [10-12, 14]. Comparative sequence analysis with cellular homologs classified the nidoviral/CoV ExoN domain as a member of the superfamily of DEDDh exonucleases, which also includes the proofreading domains of many DNA polymerases as well as other eukaryotic and prokaryotic exonucleases [15]. These enzymes catalyze the excision of nucleoside monophosphates from nucleic acids in the 3'-to-5' direction, using a mechanism that depends on two divalent metal ions and a reactive water molecule [16-18]. Five conserved active site residues arranged in three canonical motifs (I, II, and III; Fig. 1) orchestrate ExoN activity [14, 19-21]. Additionally,

the domain incorporates two zinc finger (ZF) motifs [10], ZF1 and ZF2 (Fig. 1), that were hypothesized to contribute to the structural stability and catalytic activity of ExoN, respectively [20].

The predicted 3'-to-5' exoribonuclease activity of the CoV ExoN domain was first confirmed *in vitro*, in biochemical assays using recombinant SARS-CoV nsp14 and different synthetic RNA substrates [19]. Originally, residues D90/E92 (motif I), D243 (motif II), and D273 (motif III) were identified as putative active site residues of SARS-CoV ExoN [14, 19]. However, the SARS-CoV nsp14 crystal structure revealed E191 rather than D243 to be the acidic active residue in motif II, demonstrating that ExoN is in fact a DEEDh enzyme [20]. By using reverse genetics for the *Alphacoronavirus* human coronavirus 229E (HCoV-229E), Minskaia *et al.* demonstrated that inactivation of the ExoN active site results in failure to recover infectious viral progeny [19]. Interestingly, a quite different phenotype was described for the corresponding ExoN-knockout mutants of two betacoronaviruses, mouse hepatitis virus (MHV) and SARS-CoV. While ExoN inactivation decreased replication fidelity in these viruses, conferring a 'mutator phenotype', the mutants were viable, both in cell culture [22, 23] and in animal models [24]. These findings suggested that ExoN may indeed be part of an error correction mechanism. Subsequently, the ability of ExoN to excise 3'-terminal mismatched nucleotides from a double-stranded (ds) RNA substrate was demonstrated *in vitro* using recombinant SARS-CoV nsp14 [25]. Furthermore, this activity was shown to be strongly enhanced (up to 35-fold) by the addition of nsp10, a small upstream subunit of the CoV replicase [26]. The two subunits were proposed to operate, together with the nsp12-RdRp, in repairing misincorporations that may be occur during CoV RNA synthesis [21, 27]. In cell culture, MHV and SARS-CoV mutants lacking ExoN activity exhibit increased sensitivity to mutagenic agents like 5-fluoracil (5-FU), compounds to which the wild-type virus is relatively resistant [28, 29]. Recently, ExoN activity was also implicated in CoV RNA recombination, as an MHV ExoN knockout mutant exhibited altered recombination patterns, possibly reflecting its involvement in other activities than error correction during CoV replication and subgenomic mRNA synthesis [30]. Outside the order *Nidovirales*, arenaviruses are the only other RNA viruses known to employ an ExoN domain, which is part of the arenavirus nucleoprotein and has been implicated in fidelity control [31] and/or immune evasion, the latter by possibly degrading viral dsRNA [32, 33]. Based on results obtained with TGEV and MHV ExoN knockout mutants, also the CoV ExoN activity was suggested to counteract innate responses [34, 35].

In the meantime, CoV nsp14 had been proven to be a bifunctional protein by the discovery of a guanine-N7-methyltransferase (N7-MTase) activity in its C-terminal domain [36] (Fig. 1). This enzymatic activity was further corroborated *in vitro,* using biochemical assays with purified

recombinant SARS-CoV nsp14. The enzyme was found capable of methylating cap analogues or GTP substrates, in the presence of S-adenosyl methionine (SAM) as methyl donor [36, 37]. The N7-MTase was postulated to be a key factor for equipping CoV mRNAs with a functional 5'-terminal cap structure, as guanine-N7-methylation is essential for cap recognition by the cellular translation machinery [25]. Although the characterization of the nsp14 N7-MTase active site and reaction mechanism was not completed, alanine scanning mutagenesis and *in vitro* assays with nsp14 highlighted several key residues (Fig. 1) [36, 38, 39]. Moreover, crystal structures of SARS-CoV nsp14 in complex with its nsp10 co-factor (PDB entries 5C8U and 5NFY) revealed several unique structural and functional features [20, 21]. These combined structural and biochemical studies confirmed that the two enzymatic domains of nsp14 are functionally distinct [36] and physically independent [20, 21]. Still, the two activities are structurally intertwined, as it seems that the N7-MTase activity depends on the integrity of the N-terminal ExoN domain, whereas the flexibility of the protein is modulated by a hinge region connecting the two domains [21].

Coronaviruses are abundantly present in mammalian reservoir species, including bats, and pose a continuous zoonotic threat [40-43]. To date, seven CoVs that can infect humans have been identified, and among these the severe acute respiratory syndrome coronavirus 2 (SARS-CoV-2) is currently causing an unprecedented pandemic outbreak. The previous zoonotic CoV to emerge, in 2012, was the Middle East respiratory syndrome coronavirus (MERS-CoV) [44]. Due to its transmission from dromedary camels and subsequent nosocomial transmission, MERS-CoV continues to circulate and cause serious human disease, primarily in the Arabian peninsula [45]. Occasional spread to other countries has also occurred, including an outbreak with 186 confirmed cases in South Korea in 2015 [46-48]. Like SARS-CoV, SARS-CoV-2, and MHV, MERS-CoV is classified as a member of the *Betacoronavirus* genus, although it belongs to a different lineage (subgenus) of that cluster [49, 50]. The current lack of approved therapeutics and vaccines to prevent or treat CoV infections, as well as the general threat posed by emerging CoVs, necessitates the further in-depth characterization of CoV replication and replicative enzymes. In this context, the quite different phenotypes described for ExoN knockout mutants of other CoVs (see above) prompted us to study the importance of this enzyme for MERS-CoV replication. To this end, using both reverse genetics and biochemical assays with recombinant nsp14, we engaged in an extensive site-directed mutagenesis study, targeting all active site motifs of the MERS-CoV ExoN domain. Strikingly, in contrast to what was observed for two other betacoronaviruses, MHV and SARS-CoV, our studies revealed that ExoN inactivation severely impacts MERS-CoV replication, resulting in failure to recover viable progeny. While completing our MERS-CoV nsp14 studies, given the developing pandemic, we

also evaluated the impact of ExoN inactivation (using a D90A/E92A ExoN motif I double mutant) on SARS-CoV-2 replication and viability. Given the close phylogenetic relationship between SARS-CoV and SARS-CoV-2, reflected for example in 95% nsp14 amino acid identity [51], we were highly surprised to find that – as for our MERS-CoV ExoN knockout mutants – it was not possible to rescue viable progeny for this SARS-CoV-2 mutant in which two key residues of the ExoN active site were mutated. Our biochemical evaluation of MERS-CoV nsp14 mutants suggested that this phenotype is not caused by inadvertent side-effects of ExoN inactivation on N7-MTase activity. Our combined data suggest that CoV ExoN and/or nsp14 play a more direct and fundamental role in CoV RNA synthesis than merely safeguarding the longer-term fidelity of replication, and can thus be considered a prominent target for the development of antiviral drugs.

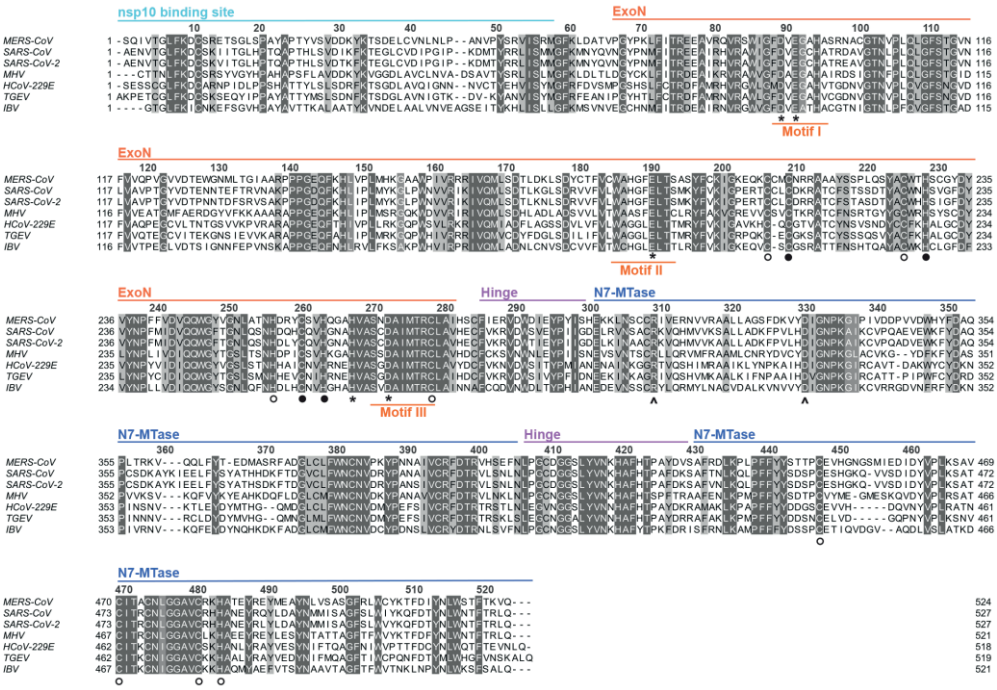

Fig. 1. Alignment of nsp14 amino acid sequences from selected coronaviruses. Sequences of the ExoN and N7-MTase domains in MERS-CoV (NC-019843); SARS-CoV (NC_004718); SARS-CoV-2 (NC_045512.2); MHV (NP_045298); HCoV-229E (NC_002645); TGEV (AJ271965); and IBV (NP_040829) were used for the analysis. The different domains indicated on the top are based on the SARS-CoV-nsp14 secondary structure (PDB 5NFY (21)). Fully conserved residues are boxed in dark grey with white letters (above 70% conservation), whereas partially conserved residues are displayed in lighter shades of grey. Catalytic residues and residues involved in formation of zinc fingers are marked with asterisks and circles, respectively. Full circles indicate zinc fingers targeted by

mutagenesis (Fig. 2A) while two black arrows identify the two N7-MTase domain residues mutated to generate the MTase negative control used in biochemical assays. The alignment was generated using Clustal Omega [52] and edited using Jalview version 2.11 [53].

RESULTS

ExoN inactivation is lethal for MERS-CoV

Previous studies into CoV ExoN function involved its biochemical characterization (based almost exclusively on the SARS-CoV version of the enzyme) and the phenotypic analysis of (predicted) ExoN knockout virus mutants, generated using reverse genetics approaches. The latter studies yielded replication-incompetent ExoN knockout mutants for the alphacoronaviruses HCoV-229E [19] and transmissible gastroenteritis virus (TGEV) [34]. However, the equivalent mutants of the betacoronaviruses SARS-CoV and MHV-A59 were somewhat crippled but clearly viable, while displaying a 15- to 20-fold increased mutation rate [22, 23]. An alignment of CoV nsp14 amino acid sequences is presented in Fig. 1, including SARS-CoV-2, which emerged in humans during the course of this project. It highlights the key motifs/residues of the two enzymatic domains of nsp14, as well as other structural elements, like the nsp10 binding site, the hinge region connecting the ExoN and N7-Mtase domains, and three previously identified nsp14 zinc finger domains [20, 21]. The alignment also illustrates the generally high degree of nsp14 sequence conservation across different CoV (sub)genera. In the present study, we targeted all five predicted active site residues of the MERS-CoV ExoN domain (D90, E92, E191, D273, and H268) by replacing them with alanine as well as more conservative substitutions (D to E or Q; E to D or Q). This yielded a total of 14 ExoN active site mutants (Fig. 2A), including the D90A/E92A motif-I double mutant (DM) that was frequently used as prototypic viable ExoN knockout mutant in MHV and SARS-CoV studies.

A BAC-based MERS-CoV reverse genetics system [54, 55], based on the sequence of the EMC/2012 isolate of MERS-CoV [56], served as the starting point to evaluate our ExoN mutants by transfection of full-length RNA that was obtained by *in vitro* transcription using T7 RNA polymerase. Transcripts were electroporated into BHK-21 cells, which lack the DPP4 receptor required for natural MERS-CoV infection [57, 58] but are commonly used to launch engineered CoV mutants because of their excellent survival of the electroporation procedure [19, 22, 23, 34, 54, 59]. As BHK-21 cells have a severely compromised innate immune response [60], they would seem an appropriate cell line to launch ExoN knockout mutants also in case the enzyme would be needed to counter innate immunity [34, 35]. To amplify any progeny virus released, transfected BHK-21 cells were mixed with either innate immune-deficient (Vero) or -competent (HuH7) cells, which both are naturally susceptible to MERS-CoV infection.

In stark contrast to what was previously described for MHV and SARS-CoV, mutagenesis of ExoN active site residues was found to render MERS-CoV non-viable. When cell cultures (BHK-21 mixed with Vero or HuH7 cells) were analyzed by immunofluorescence microscopy at 2 days post transfection (d p.t.), using antibodies recognizing dsRNA and nsp4, abundant signal and virus spread were always observed for wild-type MERS-CoV and the E191D mutant.

A

	nsp14 ExoN mutation	Number of transfections performed	Phenotype
DEEDh Motif	D90A	9	non-viable
	D90Q	5	non-viable
	D90E	8	non-viable
	E92A	7	non-viable
	E92D	4	non-viable
	E92Q	4	non-viable
	E191A	14	non-viable
	E191D	20	viable; mildly crippled
	E191Q	4	non-viable
	D273A	14	non-viable
	D273E	5	non-viable
	D273Q	3	non-viable
	H268A	8	non-viable
	D90A/ E92A (DM)	21	non-viable
ZF1	C210H	7	non-viable
	H229C	6	viable; severely crippled
ZF2	C261A	4	non-viable
	H264R	4	non-viable

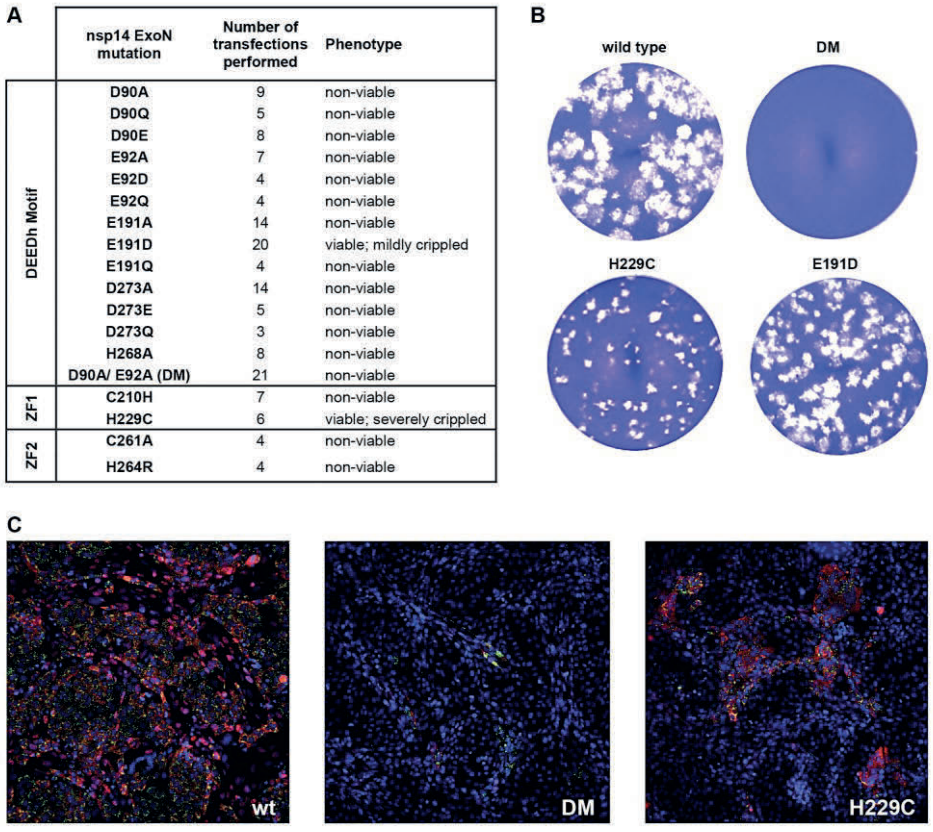

Fig. 2. MERS-CoV ExoN knockout mutants are non-viable. (A) Phenotype of MERS-CoV nsp14 ExoN mutants used in this study, scored at 2 d p.t. (B) Comparison of plaque phenotype of selected ExoN mutants in HuH7 cells. Plaque assays were performed using supernatants harvested from transfected cell cultures at 3 d p.t., which were diluted 10-4 for wt and mutant E191D, and used in undiluted form for the D90A/E92A ExoN knockout double mutant (DM) and the H229C ZF1 mutant. (C) Immunolabeling (2 d p.t.) of cell cultures consisting of a mixture of (non-susceptible) BHK-21 cells transfected with in vitro-made full-length MERS-CoV RNA and susceptible (DPP4-expressing) Vero cells used to amplify any infectious progeny released from the transfected BHK-21 cells. Images shown are for wt virus, the DM mutant, and the H229C mutant. Cells were labeled for dsRNA (green) and nsp4 (red). Bar is 100 µm

For the other 13 mutants tested, some labeling was generally observed in a low percentage (less than 2%) of the cells (Fig. 2C, middle panel), usually in the form of single positive cells or a few positive cells together. However, virus spreading across the dish was not observed regardless whether Vero or HUH7 cells were used for propagation of recombinant virus progeny, unless reversion had first occurred (see Discussion). In line with these observations, infectious progeny could not be detected when transfected cell culture supernatants harvested at 3 or 6 d p.t. were analyzed in plaque assays (Fig. 2 and data not shown). The single exception was the mutant carrying the conservative E191D replacement in ExoN motif II (Fig. 1), which was alive but somewhat crippled, as will be discussed in more detail below. These results were consistent across a large number of independent repeats (>10 for several of the mutants; Fig. 2A), performed with RNA transcribed from independently engineered (and fully sequenced) duplicate full-length cDNA clones. The non-viable phenotype of MERS-CoV ExoN mutants in both cell types suggests that innate immune responses did not influence the outcome of these experiments.

Co-expression of the viral nucleocapsid (N) protein has been reported to boost the transfection efficiency of full-length CoV RNA transcripts [61-63]. In an ultimate attempt to rescue progeny for our non-viable MERS-CoV mutants, an *in vitro* made mRNA expressing the MERS-CoV N protein gene mutant was co-transfected with nsp14 mutant or wild type (wt) full-length RNA. This modification indeed somewhat increased the BHK-21 transfection rate, as monitored by performing infectious center assays with recombinant wt MERS-CoV-transfected cells (data not shown). However, it did not result in the recovery of infectious progeny for any of six non-viable mutants tested (D90E, E191A, D273A, H268A, DM, C210H), unless (occasionally) reversion had first occurred, as confirmed by RT-PCR amplification and sequencing of the nsp14-coding region.

ExoN inactivation is also lethal for SARS-CoV-2

During the final stage of this study, given the ongoing pandemic, we evaluated whether ExoN inactivation also affects SARS-CoV-2 replication. This was not expected given the viable phenotype of SARS-CoV ExoN knockout mutants and the close relationship between that virus and SARS-CoV-2 [43, 50], which is for example reflected in nsp14 amino acid sequences being ~95% identical between the two viruses [51]. Four independently engineered and fully sequenced SARS-CoV-2 BAC clones were used to transcribe full-length RNA carrying the D90A/E92A double mutation in ExoN motif I, which has been used in many studies with MHV and SARS-CoV ExoN knockout mutants [23, 28, 29]. These transcripts were transfected into SARS-CoV N protein-expressing BHK-21 cells [61], in the presence or absence of a synthetic

mRNA expressing the SARS-CoV-2 N protein. Subsequently, the transfected cells were mixed (1:1) with Vero E6 cells to support propagation of any viable progeny virus. Wild-type SARS-CoV and its corresponding (viable) ExoN knockout mutant (D90A/E92A; DM) were taken along as positive controls in these experiments. Surprisingly, using culture supernatant harvested at 3 or 6 d p.t., viable progeny could not be recovered for the SARS-CoV-2 DM mutant in any of the four independent repeats (Fig. 3). In contrast, for SARS-CoV, already at 2 d p.t. both the wild-type and ExoN knockout mutant produced abundant progeny, although the plaque phenotype and titers (1.5- to 2-log difference) of the ExoN knockout mutant were clearly reduced compared to the parental virus (Fig. 3A). As for the corresponding MERS-CoV mutant, immunofluorescence microscopy revealed some signal for the SARS-CoV-2 DM mutant in a low percentage of the cells by 2 d p.t. (Fig. 3B), but virus spreading was not observed up to 6 d p.t. These results highlight that the impact of ExoN inactivation on general viability can be very different, even between two closely related CoVs.

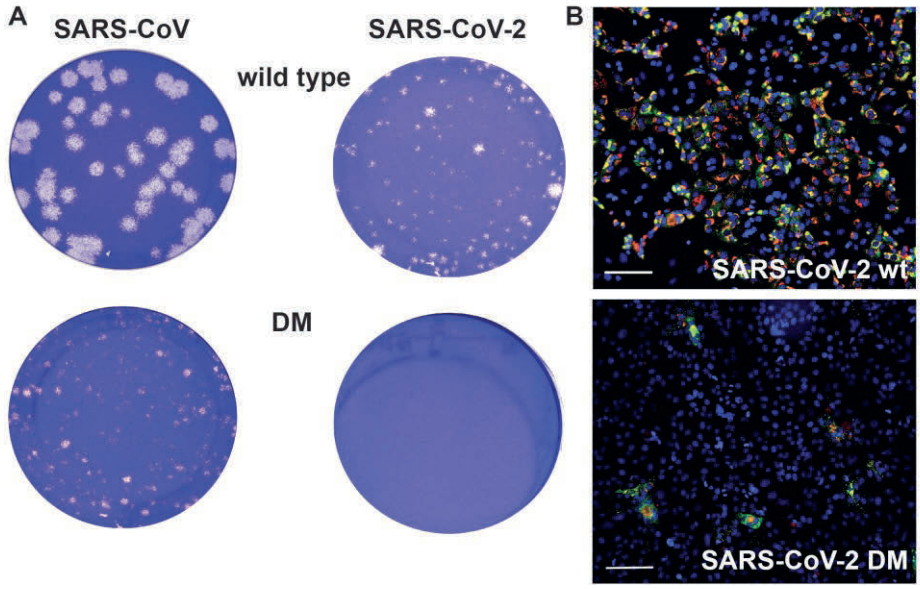

Fig. 3. SARS-CoV-2 ExoN knockout mutant is non-viable. (A) Plaque phenotype of wt SARS-CoV (left) and SARS-CoV-2 (right) and their corresponding ExoN motif-I knockout double mutants (DM, D90A/E92A) in Vero E6 cells. Plaque assays were performed using supernatants harvested from transfected cell cultures at 2 d p.t. for SARS-CoV and 3 d p.t for SARS-CoV-2. Samples were diluted 10-6 for SARS-CoV wt, 10-5 for SARS-CoV-2 wt and SARS-CoV DM, and 10-1 for the SARS-CoV-2 DM mutant. (B) Immunolabeling (2 d p.t.) as described in Fig. 2C, but now using Vero E6 cells for amplification of SARS-CoV-2 progeny released from BHK-21 cells transfected with wt (top) or DM (bottom) full-length RNA. Bar is 100 µm.

ExoN inactivation abrogates detectable MERS-CoV RNA synthesis

For a selection of MERS-CoV ExoN knockout mutants, intracellular RNA was isolated from transfected cell cultures at 2 d p.t. and analyzed by hybridization and RT-qPCR to more rigorously measure viral RNA synthesis (Fig. 4). In this analysis, a non-viable MERS-CoV mutant with an in-frame 100-aa deletion in the nsp12-RdRp domain was used as a negative control (NC) for viral RNA synthesis, in order to assess and correct for the detection of any residual full-length RNA transcript that might still be present at this timepoint after transfection. Upon direct in-gel hybridization analysis using a ^{32}P-labeled probe recognizing the 3' end of all viral mRNAs, the characteristic nested set of MERS-CoV transcripts could only be detected for the E191D mutant and the wt control (Fig. 4). Even after a 28-day exposure of the phosphor imager screen (data not shown), signal could not be detected for any of the other mutants.

The lack of detectable MERS-CoV-specific RNA synthesis was further confirmed using RT-PCR assays specifically detecting genomic RNA and subgenomic mRNA3. RNA accumulation was evaluated at 1 and 2 d p.t. for seven selected ExoN active site mutants (D90A, D90E, E191A, E191D, D273A, H268A, DM) using samples from two independent experiments both comprising duplicate transfections for each mutant. Again, MERS-CoV-specific genomic and subgenomic RNA synthesis was only detected for the E191D mutant and the wt virus control (data not shown). For all other mutants, the RT-PCR assays yielded Ct values in the range obtained for samples from mock-infected cells and the replication-deficient NC mutant. In conclusion, with the exception of E191D (see below), all our engineered ExoN active site mutations abrogated detectable viral RNA synthesis, suggesting that in the case of MERS-CoV – and likely also SARS-CoV-2 - the enzyme is indispensable for basic productive replication in cell culture.

Characterization of rMERS-CoV-nsp14-E191D replication kinetics and 5-FU sensitivity

Among our MERS-CoV ExoN active site mutants, only the E191D mutant yielded viable progeny (Fig. 2). This mutant appeared to be genetically stable as the substitution was preserved upon multiple consecutive passages in HuH7 or Vero cells (data not shown). Interestingly, the E191D mutation transforms the DEEDh catalytic motif into the DEDDh motif that is characteristic for members of the exonuclease family to which the CoV ExoN belongs [64]. In fact, when comparing ExoN sequences from different nidovirus taxa [14, 19], the equivalent of E191 alternates between E and D [65], in line with the observation that this mutation is tolerated in MERS-CoV ExoN.

To characterize the E191D mutant in more detail, its replication and fitness in cell culture were analyzed. Full-length genome sequencing of passage 2 of the E191D mutant virus revealed

that it had acquired two additional mutations when compared with the recombinant wt control: a synonymous mutation in the nsp2-coding region (U→C at nt position 2,315) and a non-synonymous mutation (C→A at nt position 6,541) specifying an A1235D substitution in the *Betacoronavirus*-specific marker (βSM) domain of nsp3, which has been predicted to be a non-enzymatic domain [66] and is absent in *Alphacoronavirus* and *Deltacoronavirus* genus [67, 68]. Thus, we assumed that any changes in viral replication were likely caused by the E191D mutation in nsp14 ExoN. The same virus stock was used to assess growth kinetics in HuH7 cells (Fig. 5B) and Vero cells (Fig. 5A), which were found to be quite similar for wt and mutant virus. Still, the E191D mutant was found to be somewhat crippled, yielding smaller plaque sizes and somewhat lower progeny titers in HuH7 cells (Fig. 5B-C and 2B), but not in Vero cells (Fig. 5A).

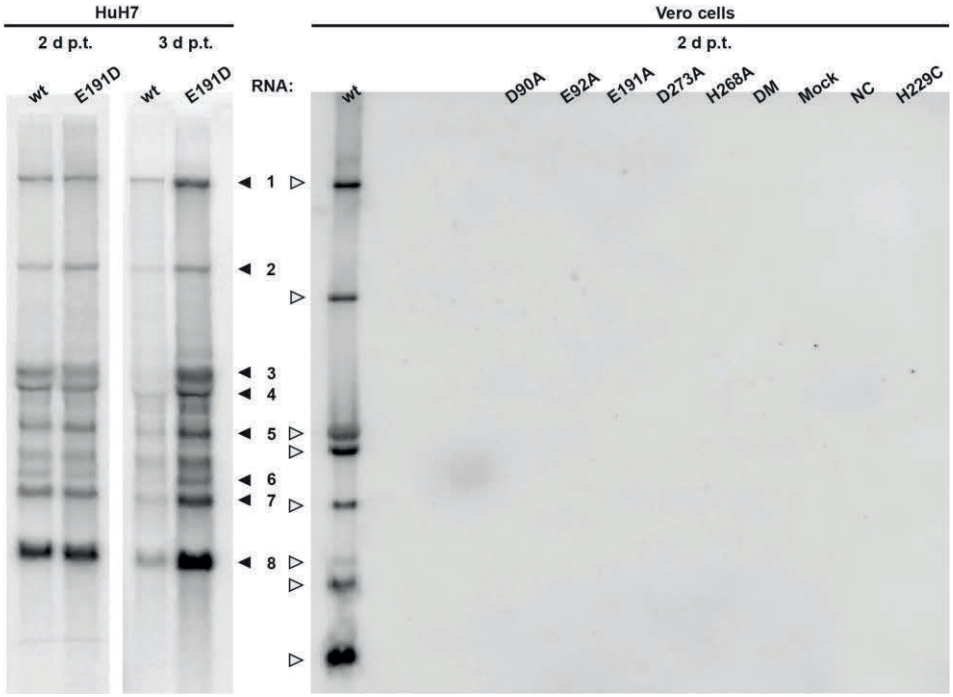

Fig. 4. Impact of ExoN inactivation on intracellular MERS-CoV RNA synthesis. In-gel hybridization analysis of intracellular RNA isolated after 2 or 3 d p.t. of transfected BHK-21 cells, which were subsequently mixed with HuH7 or Vero cells as indicated. Purified RNA was separated in an agarose gel and probed with a radiolabeled oligonucleotide probe recognizing the MERS-CoV genome and subgenomic mRNAs.

We next examined the sensitivity of E191D and wt virus to the mutagenic agent 5-FU, which intracellularly is converted into a nucleoside analogue that is incorporated into viral RNA [69, 70]. Previously, MHV and SARS-CoV ExoN knockout mutants were found to exhibit increased sensitivity to 5-FU treatment, in particular in multi-cycle experiments, which was attributed to a higher mutation frequency in the absence of ExoN-driven error correction [28]. We employed this same assay to assess the phenotype of the E191D mutant in more detail, by performing plaque assays in HuH7 cells in the presence of increasing 5-FU concentrations (Fig. 5C) and by growing mutant and wt virus in the presence of increasing 5-FU concentrations (Fig. 5D). No cytotoxicity was observed in HuH7 cells following treatment with up to 400 µM 5-FU (data not shown).

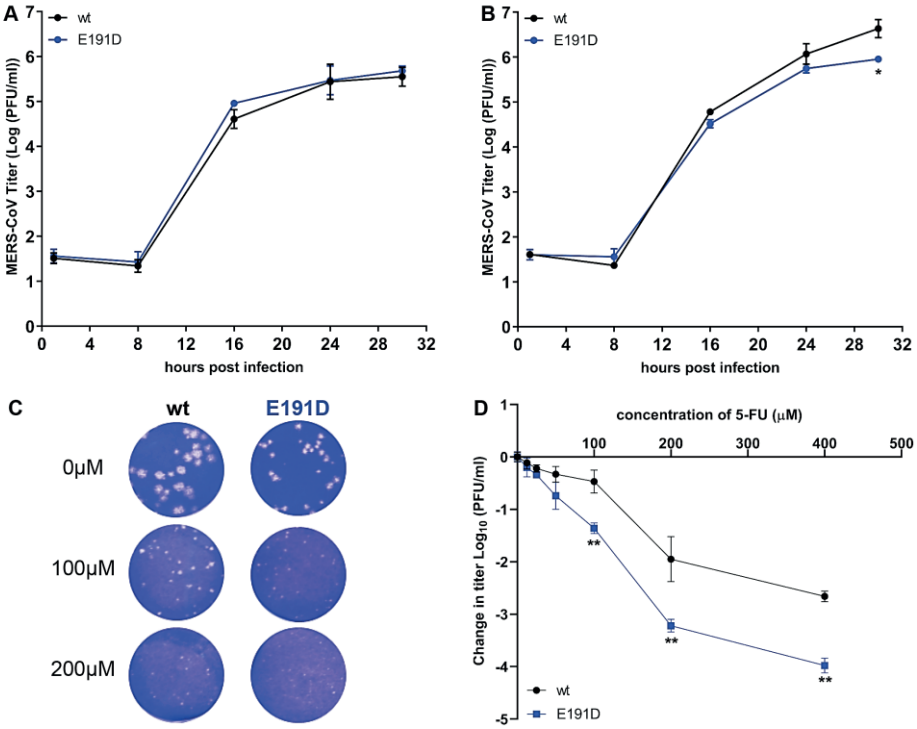

Fig. 5. Characterization of growth kinetics of rMERS-nsp14-E191D and its sensitivity to 5-FU treatment. (A) Vero cells or (B) HuH7 cells were infected at an m.o.i. of 3, supernatant was harvested at the indicated time points, and viral progeny titers were measured by plaque assay from two independent experiments using duplicates (n=4; mean ± sd is presented). (C) Plaque phenotype in HuH7 cells of rMERS-CoV nsp14-E191D and wt control in the absence or presence of the mutagenic agent 5-FU. (D) Dose response curve of wt and E191D mutant MERS-CoV in the presence of 5-FU concentrations up to 400µM (m.o.i. 0.1; n=4; mean ± sd is presented). Statistical significance of the difference with wt virus at each time point (A and B) or concentration (D) was assessed by paired t-test. *, $p<0.05$; ** $p<0.005$.

Plaque assays in HuH7 cells were performed for 3 days, using a standard inoculum of 30 p.f.u. and an increasing amount of 5-FU in the overlay. Similar dose-dependent reductions of plaque size were observed for E191D and wt virus, with E191D plaques being barely visible upon treatment with 200 µM 5-FU (Fig. 5C). In an alternative experiment, Huh7 cells were infected with an m.o.i. of 0.1 and treated with a different 5-FU dose for 30 h, after which progeny virus titers were determined by regular plaque assay. Again, both viruses exhibited a similar concentration-dependent decrease of replication (Fig. 5D), although the E191D mutant appeared to be somewhat more sensitive to the mutagenic agent, yielding ~1-log lower progeny titers than wt virus upon treatment with 5-FU concentrations between 100 and 400 µM.

Taken together, these experiments demonstrated that overall replication of mutant E191D is only mildly affected and that it is somewhat more sensitive to 5-FU treatment than wt MERS-CoV. This phenotype is consistent with the bioinformatics-based prediction that a mutant nsp14 carrying this substitution may retain ExoN activity, as will be demonstrated below.

ExoN zinc finger motifs are important for viral replication

Studies addressing the structural biology and biochemistry of SARS-CoV nsp14 suggested that the two ZF motifs within the ExoN domain contribute to either its structural stability (ZF1) or catalytic activity (ZF2) [20, 21]. Moreover, mutagenesis studies of the MHV and TGEV ZF1 domain supported their importance for viral replication in cell culture [34, 59]. To study the impact of similar mutations on MERS-CoV replication, the nsp14 ZF1 and ZF2 domains were targeted with two mutations each and their impact on virus viability was evaluated as described above. Two ZF1 residues (C210 and H229) were mutated from H to C or vice versa, which could theoretically preserve the zinc-coordinating properties [71, 72]. Two residues of the non-classical ZF2 motif were also substituted (C261A and H264R) to evaluate the same ZF2 mutations previously analyzed by Ma *et al.*, leading to disruption of ExoN activity *in vitro* [20].

The four ZF virus mutants were launched as described above, after which a low level of replication could be observed only for the H229C ZF1 mutant (Fig. 2C), for which the 2 d p.t. harvest yielded very small plaques (Fig. 2B) and 2- to 4-log reduced progeny titers, depending on the experiment and time point of harvesting (data not shown). For this mutant, RNA synthesis could not be detected by hybridization analysis (Fig. 4), but synthesis of genomic and subgenomic RNA (mRNA3) was detected by RT-PCR in intracellular RNA samples harvested at 2 d p.t. (data not shown). A 6 d p.t. harvest was used for full genome sequencing by NGS, which confirmed the presence of the engineered nsp14 mutation in addition to the

appearance of some minor genetic variants (point mutations representing less than 15% of the total population) in different regions of the genome, including the ORF1a domains encoding for nsp3, nsp6, nsp8, and nsp9. Taken together, our observations indicate that the H229C mutant is viable but severely crippled. In combination with the fact that the other ZF mutations (C210H in ZF1, and C261A and H264R in ZF2) abolished MERS-CoV replication, our study establishes the importance of both ExoN ZF motifs for MERS-CoV viability.

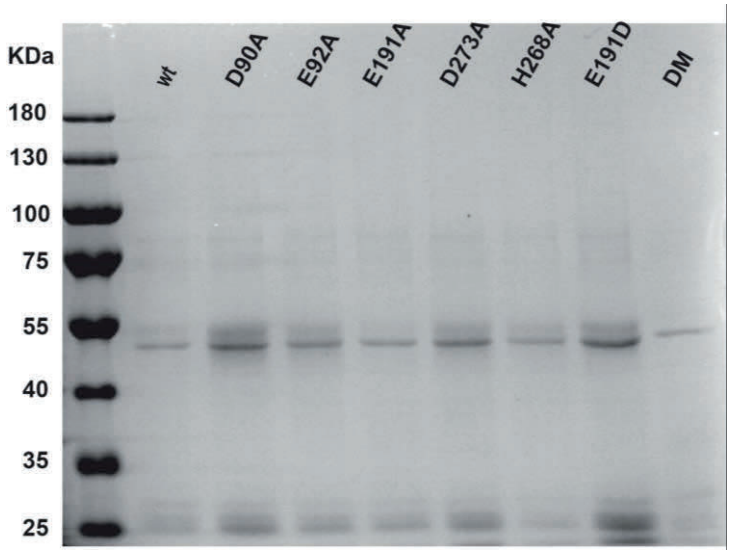

Fig. 6. Expression and purification of recombinant MERS-CoV nsp14. N-terminally His-tagged wt and mutant MERS-CoV nsp14 (~55 kDa) was expressed in E. coli, affinity purified, and analyzed in a 10% SDS-PAGE gel that was stained with Coomassie Blue. The molecular masses of the protein marker (Invitrogen) are given in kDa..

Development of a MERS-CoV ExoN activity assay using recombinant nsp14

In order to assess the impact of mutations on nsp14's enzymatic activities, we set out to purify recombinant MERS-CoV nsp14 and develop an *in vitro* ExoN assay. Thus far, such an assay had only been described for the equivalent SARS-CoV protein [19, 20, 26, 73]. Wild-type and mutant MERS-CoV nsp14 proteins carrying an N-terminal His-tag were expressed in *E. coli* Rosetta (DE3) pLysS. Proteins were purified by immobilized metal affinity chromatography (IMAC) followed by size exclusion chromatography. Upon SDS-PAGE, the purified MERS-CoV nsp14 was consistently detected as a doublet (with the lower band being most abundant), migrating at the expected molecular mass of ~55 kDa (Fig. 6). As a positive control, we purified SARS-CoV nsp14 [26] and used it during optimization of the enzymatic assays for MERS-CoV nsp14. The substrate used for ExoN activity assays was a 5'-^{32}P-labeled 22-nucleotide (nt) long

synthetic RNA, as previously used in similar assays with SARS-CoV nsp14 (referred to as oligonucleotide H4 in [26]). Nucleotides 5-22 of this substrate are predicted to form a hairpin with a stem consisting of seven G-C base pairs and a loop of 4 As [26], while the remaining 4 nucleotides form a 5'-terminal single-stranded tail.

Previously, the ExoN activity of SARS-CoV nsp14 was found to be dramatically stimulated by the addition of nsp10 as co-factor [26]. Consequently, we also expressed and purified MERS-CoV nsp10 and optimized the ExoN assay by testing different molar ratios between nsp14 and nsp10 (Fig. 7A, left-hand side), different nsp14 concentrations (Fig. 7B, left-hand side), and by different incubation times (Fig. 8, left-hand side). MERS-CoV nsp14 ExoN activity was found to be stimulated by nsp10 in a dose-dependent manner (Fig. 7A), while nsp10 did not exhibit any nuclease activity by itself (Fig. 7B, nsp10 lane). The full-length substrate is more completely degraded when a fourfold (or higher) excess of nsp10 over nsp14 was used compared to the effect of merely increasing the nsp14 concentration in the assay (Fig. 7B). Different substrate degradation patterns were observed when comparing nsp14 alone with the nsp14-nsp10 in complex, which likely derived from structural and functional differences between these two nsp14 conformations. Similar observations were previously reported for SARS-CoV nsp14 [20, 21, 26] and recently for SARS-CoV-2 nsp14 [74]. When using an excess of nsp14 over nsp10, an intermediate (or mixed) pattern of degradation products was obtained (Fig. 7B), including an elevated amount of products with a length of 21-17 and 11-6 nt. Introduction of the D90A/E92A motif-I double substitution resulted in a major reduction of ExoN activity, although a certain level of residual activity was observed, in particular when using large amounts of nsp14 (Fig. 7B, right-hand side) or a relatively high nsp10:nsp14 ratio (Fig. 7A, right-hand side). Similar observations were previously made for SARS-CoV nsp14 [20, 26].

Using a 4:1 ratio of nsp10 versus nsp14, MERS-CoV ExoN activity was analyzed in a time-course experiment (Fig. 8). Over time, the full-length substrate was progressively converted to a set of degradation products in the size range of 6-18 nt. We anticipated that the structure of the H4 RNA substrate would change from a duplexed to a single-stranded conformation, upon digestion of one side of the hairpin's stem by ExoN's nuclease activity. As the ExoN enzymes of other CoVs were reported to prefer dsRNA substrates [19, 73], the degradation of the substrate might be slowed down substantially after removal of the first couple of nucleotides from its 3' end [26]. This would explain the abundant generation of degradation products of 16 and 17 nt in length (Fig. 7-9) and suggest that the preference for dsRNA substrates is indeed shared by MERS-CoV ExoN.

Degradation of the RNA substrate could be observed within 5 min and the full-length substrate was essentially gone after 30 min. A similar reaction with the nsp14 DM mutant resulted in only a small amount of substrate degradation after 90 min (Fig. 8, leftmost lane). Taken together, our results convincingly demonstrate the *in vitro* 3'-to-5' exonuclease activity of purified MERS-CoV nsp14. As in the case of the SARS-CoV enzyme, nsp10 is a critical co-factor that can strikingly upregulate MERS-CoV ExoN activity *in vitro*.

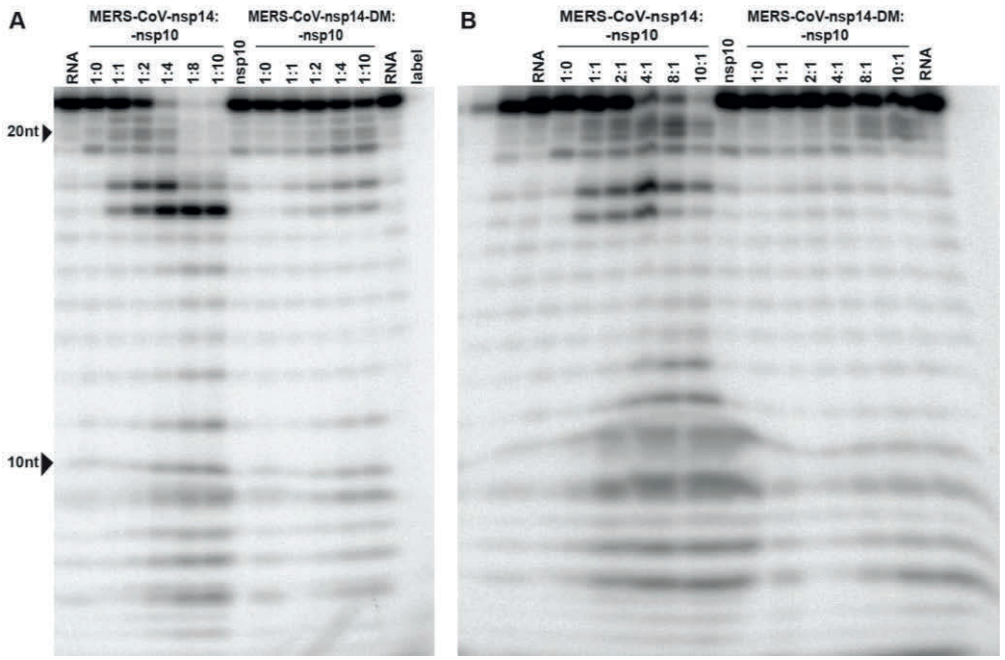

Fig. 7. Optimization of MERS-CoV nsp14 in vitro ExoN assay conditions. The substrate for the assay was a 22-nt long synthetic RNA (H4) that was 32P-labeled at its 5' terminus (*p-RNA). Cleavage products were separated by polyacrylamide gel electrophoresis and visualized by autoradiography. (A) Analysis of ExoN activity in the presence of an increasing amount of nsp10, using wt MERS-CoV-nsp14 (left) and the ExoN double knockout mutant (DM, D90A/E92A; right). The RNA substrate was hydrolyzed for 90 min at 37^{o}C using a fixed concentration of nsp14 (200 nM) and an increasing nsp10 concentration, ranging from 0 to 1600 nM. (B) Evaluation of the ExoN activity of an increasing concentration (200 to 2000 nM) of wt or DM nsp14 in the presence of a fixed amount of nsp10 (200 nM).

MERS-CoV nsp10 modulates nsp14 ExoN activity

In order to investigate differences that might explain the variable phenotype of CoV ExoN knockout virus mutants, we compared ExoN activities between SARS-CoV and MERS-CoV

nsp14, using the optimized *in vitro* assay described above. An incubation time of 90 min was used, unless indicated otherwise. The nsp14 and nsp10 preparations of both viruses were first tested individually in an assay containing the H4 RNA substrate and Mg^{+2} ions [26, 75, 76]. As expected, this revealed only traces of exonuclease activity for both nsp14 proteins alone (Fig. 9, lanes 4 and 6). When the two proteins were combined in the same reaction, a strong increase of ExoN activity was observed for both nsp14-nsp10 pairs, with the SARS-CoV pair appearing to be somewhat more active than the MERS-CoV pair (Fig. 9, lanes 2 and 9).

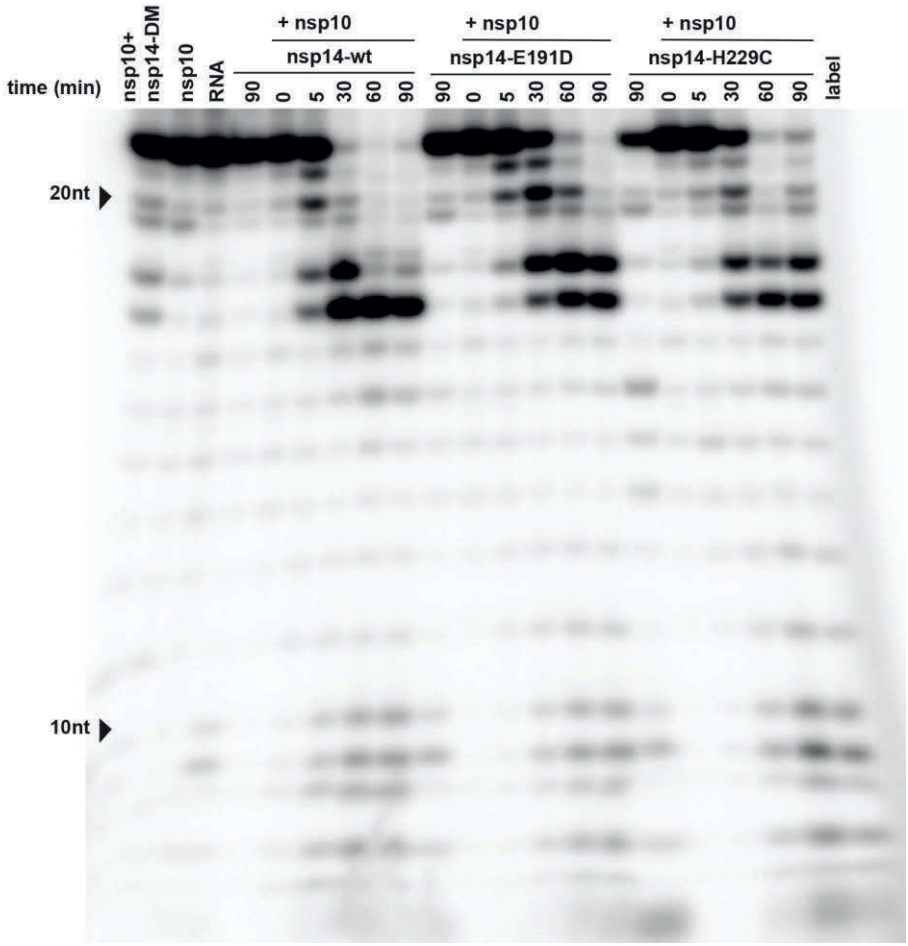

Fig. 8. Time course analysis of the in vitro ExoN activity of MERS-CoV nsp14. The ExoN activity of different recombinant nsp14 proteins (wt, D90A/E92A, E191D and H229C) was evaluated by incubating 200 nM of nsp14 and 800 nM of nsp10 for 0, 5, 30, 60 and 90 min at 37°C. As controls, individual proteins (800 nM) were incubated for 90 min. For technical details, see the legend to Fig. 7.

The exchange of the SARS-CoV and MERS-CoV nsp10 co-factors revealed that they can cross-activate the ExoN activity of nsp14 from the other virus, although some changes in the pattern of degradation products were observed (Fig. 9, Lanes 1-2 and lanes 8-9). However, the residual ExoN activity of the motif I double mutant (DM) apparently was not affected by the choice of nsp10 co-factor (Fig. 9, compare lanes 11 and 12). The observed subtle changes in degradation product patterns are another indication that nsp10 modulates nsp14 ExoN activity, presumably using interaction surfaces that are well-conserved across CoV genera [75, 76].

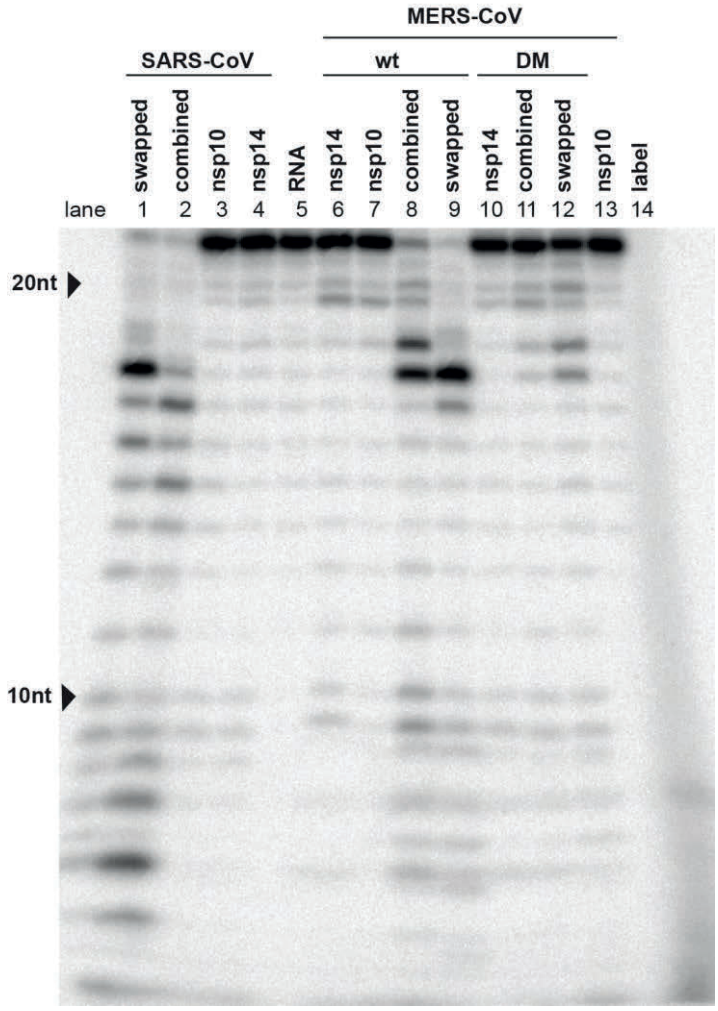

Fig. 9. Cross-activation of the in vitro activity of SARS-CoV and MERS-CoV nsp14 by heterologous nsp10. The nsp10 co-factor was exchanged in ExoN assays performed with MERS-CoV and SARS-CoV nsp14, using a 1:4 ratio between nsp14 and nsp10 and a 90-min incubation at 37^{o}C. For technical details, see the legend to Fig. 7..

ExoN activity of MERS-CoV active site and H229C mutants

Having established the optimal conditions for MERS-CoV ExoN *in vitro* activity, we evaluated the impact of a subset of the DEEDh active site mutations that were used during our reverse genetic analysis (Fig. 2A). For each mutant tested, two protein batches were purified and analyzed independently in duplicate using the same batch of MERS-CoV nsp10 for all assays. As can be seen in Fig. 10, replacement with Ala of each of the five active site residues resulted in a near-complete loss of ExoN activity, with the D90A, E92A, and H268A substitutions appearing to be slightly less detrimental than E191A and D273A. A clearly different result was again obtained with the E191D mutant, which displayed an activity level comparable to that of wt nsp14, corresponding with the properties of the corresponding virus mutant (Fig. 2, 4 and 5). Overall, the severe impact of active site mutations on ExoN activity was fully in line with the non-viable phenotypes observed for the same mutants when tested using reverse genetics (Fig. 2).

We also evaluated the impact of the H229C ZF1 mutation, which – despite its conservative nature - yielded a crippled mutant virus (Fig. 2), and of two N7-MTase mutations (to be discussed below). The N7-MTase mutants displayed wt nsp14-like ExoN activities (Fig. 10), suggesting that – as in SARS-CoV nsp14 - ExoN and N7-MTase activities are functionally separated [36]. Analyzing the substrate degradation pattern of the H229C mutant (Fig. 8) revealed that the enzyme was less efficient in its ability to degrade RNA when compared to wt nsp14. This can be seen, for example, when comparing the reaction products after 5-min assays in Fig. 8 and 10. A more detailed quantitative assessment of the activity level of nsp14 mutants is beyond the scope of this study. The H229C mutation clearly reduced ExoN activity *in vitro*, potentially by affecting the structure of the ExoN domain, as ZF1 is in close proximity of the nsp10 interaction surface [20]. However, a similar reduction of ExoN activity was observed for the E191D mutant (Fig. 8), which was much more viable than the H229C mutant in the context of our reverse genetics studies. This suggests that the H229C replacement may affect additional functions or interactions of the ExoN domain that are important for viral RNA synthesis and viability.

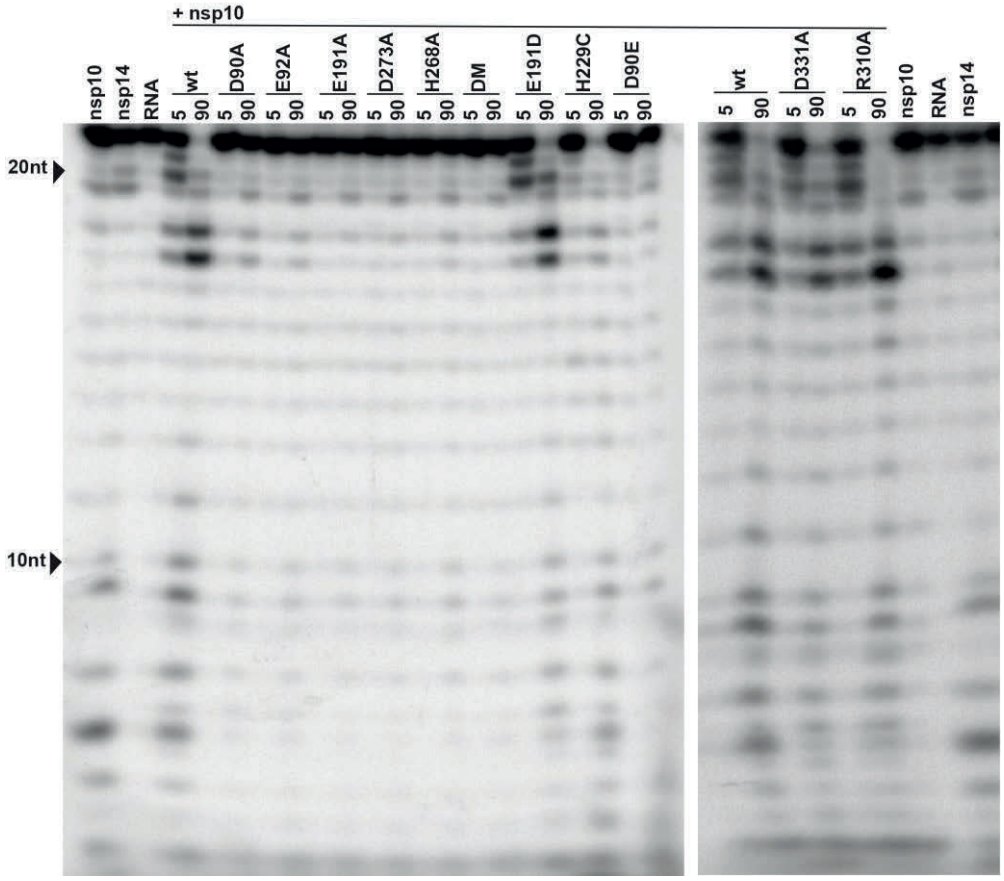

Fig. 10. In vitro ExoN activity of MERS-CoV nsp14 mutants. Residues from the DEDDh catalytic motif and ZF1 motif of the nsp14 ExoN domain and the nsp14 N7MTase domain were mutated as indicated. Assays were performed using a 1:4 ratio between nsp14 and nsp10 and a 90-min incubation at 37°C. For technical details, see the legend to Fig. 7.

ExoN mutations do not interfere with N7-MTase activity *in vitro*

The nsp14 N7-MTtase activity is deemed essential for formation of a functional RNA cap, enabling the translation of CoV mRNAs and protecting them from degradation. Consequently, at least in theory, ExoN mutations could also be detrimental for virus replication if they would somehow affect the crucial enzymatic activity of the other nsp14 domain. In order to evaluate this possibility, the same recombinant protein preparations used for the ExoN assays (Fig. 6) were evaluated in an N7-MTase biochemical assay using the synthetic cap analogues GpppA and m7GpppA (control) as substrates. Moreover, nsp14 mutants R310A and D331A were used as negative controls in view of their predicted involvement in the binding of the triphosphate

moiety of the RNA chain and the methyl donor (S-adenosylmethionine; SAM), respectively [20, 26, 36]. In this assay, nsp14 can methylate GpppA by transferring the [^{3}H]CH_3 moiety provided by [^{3}H]SAM. The resulting radio-labelled m7GpppA product can be quantified using a DEAE filter-binding assay, followed by liquid scintillation counting, and data normalization against the activity of wt control protein [25].

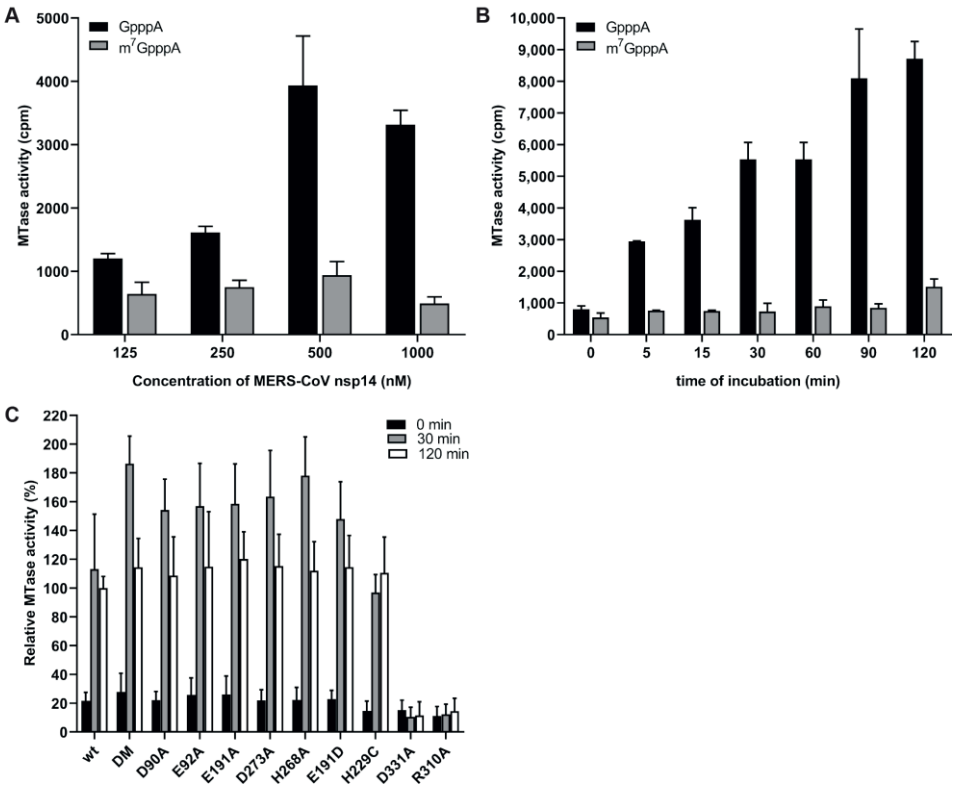

Fig. 11. In vitro N7-MTase activity of MERS-CoV nsp14 mutants. The N7-MTase activity of recombinant nsp14 was analyzed in vitro by filter binding assay using synthetic cap analogues as substrate. (A) Increasing concentrations of MERS-CoV nsp14 were incubated with GpppA and m7GpppA in the presence of [3H]SAM for 30 min. (B) The ability of nsp14 to methylate GpppA or m7GpppA was determined after reaction times between 0 and 120 min at 30°C. (C) The ability of nsp14 mutants to methylate GpppA was measured in four times in duplicate. Values were normalized to the wt control (n=8; mean ± sd are shown).

Recombinant MERS-CoV nsp14 was found to methylate GpppA, but not m7GpppA (Fig. 11A), which yielded a signal that was similar to the background signal in assays lacking nsp14 or substrate (data not shown). Methylation increased with time until reaching a plateau after

120 min (Fig. 11B). The N7-MTase activity of the various nsp14 mutants was compared with that of wt nsp14 after reaction times of 30 and 120 min (Fig. 11C). While the R310A and D331A control mutations fully inactivated the N7-MTase activity of MERS-CoV nsp14, none of the ExoN active site mutations tested was found to alter the enzyme's activity. These results again support the notion that ExoN and N7-MTase domains are functionally separated, as previously demonstrated for SARS-CoV-nsp14 [36]. We therefore conclude that the lethal impact of ExoN inactivation on MERS-CoV replication (Fig. 2A) cannot be attributed to inadvertent effects on the activity of the N7-MTase domain that is present in the same nsp14 replicase subunit.

DISCUSSION

In this study, we demonstrate that the impact of ExoN inactivation on virus viability and RNA synthesis distinguishes MERS-CoV and SARS-CoV-2 from two other betacoronaviruses, MHV and SARS-CoV. Whereas ExoN inactivation in the latter two viruses yields viable mutants that are only mildly crippled and exhibit a 'mutator phenotype' [22, 23, 29], both conservative and alanine substitutions of MERS-CoV ExoN catalytic residues abolished the recovery of infectious progeny (Fig. 2) and the detection of viral RNA synthesis (Fig. 4). The only exception was the conservative E191D mutant, which was found to exhibit near-wt ExoN activity (Fig. 7 and 10). Though limited in its scope, it is even more remarkable that our mutagenesis of SARS-CoV-2 yielded a very similar non-viable phenotype for an ExoN knockout mutant, in spite of the close relationship of this virus with SARS-CoV, for which ExoN knockout mutants are crippled but quite viable (Fig. 3). For most MERS-CoV ExoN knockout mutants and for the SARS-CoV-2 double mutant, immunofluorescence microscopy revealed some virus-specific signal in a few individual cells at 2 d p.t. (Fig. 2C and 3B), a time point at which wt viruses have already spread efficiently and infected all susceptible cells in the culture. The very limited labeling observed for mutant virus-transfected cultures is difficult to interpret and requires further analysis, but it suggests that viral RNA synthesis is not completely abrogated, at least not in all transfected cells, and likely explains that reversion occurred occasionally for several of the MERS-CoV single mutants late in the experiment.

Based on nsp14 conservation (Fig. 1) and the viable phenotype of SARS-CoV and MHV ExoN-knockout mutants, MERS-CoV and SARS-CoV-2 were expected to tolerate ExoN inactivation, in particular since the enzyme was proposed to improve the fidelity of CoV replication without being essential for RNA synthesis *per se* [10, 14, 21-23, 26, 29]. This notion is further supported by the fact that the CoV RdRp (nsp12) exhibits *in vitro* activity in the absence of nsp14 [27]. We therefore anticipated that an excess of deleterious mutations would first have to accumulate before becoming detrimental. Contrary to these expectations, an immediate lack

of viability was observed when MERS-CoV or SARS-CoV-2 ExoN knockout mutants were launched. It is noteworthy that similar observations were previously made for the corresponding ExoN knockout mutants of the alphacoronaviruses HCoV-229E [19] and TGEV [34], and the *Gammacoronavirus* avian infectious bronchitis virus (IBV) (E. Bickerton, S. Keep, and P. Britton, personal communication). Furthermore, in line with our observations, a recent report from the Denison laboratory - awaiting peer review – briefly mentions that also in their hands nsp14-ExoN catalytic mutants could not be rescued for both MERS-CoV and SARS-CoV-2 [30].

None of the ExoN mutations tested had a negative effect on the *in vitro* activity of the N7-MTase domain of nsp14, which is deemed essential for viral mRNA capping (Fig. 11). This is consistent with previous observations for SARS-CoV nsp14, in which the ExoN and N7-MTase activities were shown to be functionally distinct but structurally interconnected by a hinge region that confers flexibility [21, 36]. Given their unchanged N7-MTase activity, the non-viable phenotype of MERS-CoV ExoN active site mutants must be attributed to a negative effect on an additional and apparently critical function of the ExoN domain, which likely is directly involved in primary RNA synthesis rather than in (longer-term) fidelity control. At present we cannot explain, why SARS-CoV and MHV ExoN knockouts can apparently tolerate ExoN active site substitutions that are lethal to five other CoVs (including the closely related SARS--CoV-2). Within the *Betacoronavirus* group, in our experience, SARS-CoV and MHV display the most robust RNA synthesis and replication in cell culture when compared to MERS-CoV and SARS-CoV-2 [77-79], as also illustrated by the SARS-CoV and SARS-CoV-2 plaque phenotypes presented in Fig. 3. Possibly, the recovery of viable progeny depends on reaching a minimum level of RNA synthesis, which may somehow be achieved by only the most efficiently replicating CoVs. Admittedly, even bearing this possibility in mind, it remains difficult to reconcile the 1- to 2-log reduction of progeny titers observed for MHV and SARS-CoV ExoN-knockout mutants with the complete loss (> 6-log reduction) of infectious progeny observed for the ExoN-knockout mutants of the other CoVs.

In order to eliminate technicalities that might somehow prohibit the successful recovery of MERS-CoV ExoN knockout mutants and explain the phenotypic differences with other CoVs, we explored various details in the transfection protocol. This included the use of a DNA-launched system, similar to that used for TGEV [34], and the propagation of progeny virus in both innate immune-competent and -incompetent cells (Huh7 and Vero cells, respectively). However, this did not change the negative outcome of our transfection experiments, which were repeated more than 10 times for several of the non-viable mutants, always using wt and E191D MERS-CoV as positive controls that proved to be consistently viable. Next, we

performed experiments in which BHK-21 cells were co-transfected with a synthetic mRNA expressing the N protein, which has been reported to promote the recovery of recombinant CoVs [62, 63]. Indeed, judging from immunolabelings and early virus yields, such an effect could be observed, but it did not alter the outcome for the non-viable ExoN knockout mutants, and 3 d p.t. virus harvests continued to yield no plaques for both MERS-CoV and SARS-CoV-2. These combined observations strengthen our conclusion that – in addition to its proposed role as a proofreading enzyme – ExoN likely has an additional role in CoV RNA synthesis [65].

As reported for MHV and SARS-CoV ExoN mutants [23, 80], possible (late) reversion was observed for a few of our MERS-CoV ExoN active site mutants, specifically mutants E191A, D273E, D273A and in particular D90E, which had reverted by 6 d p.t. in four out of eight experiments. Together with the immunolabeling results presented in Fig.2C, this suggests that these mutants (and perhaps others as well) exhibit a low residual level of RNA synthesis that is the basis for these low-frequency reversion events. Furthermore, in follow-up studies with the crippled H229C ZF1 mutant, a possible pseudo-revertant carrying a second-site mutation (Q19R) in nsp8 was identified in three independently obtained progeny samples, providing genetic support for an interaction between nsp8 and nsp14, which may be relevant in the context of the association of nsp14 with the tripartite RdRp complex consisting of nsp7, nsp8, and nsp12 [21, 27, 81-83]. Future studies will address the properties of these nsp14 ExoN knockout mutants and their (pseudo) revertants in more detail.

In the only viable MERS-CoV ExoN active site mutant obtained, E191D, the catalytic motif was changed from DEEDh to the DEDDh that is characteristic of all members of the exonuclease family that ExoN belongs to [14, 15, 84]. The growth of the E191D virus mutant was comparable to that of wt virus (Fig. 4A-B). Biochemical assays revealed that the E191D-ExoN enzyme is able to hydrolyze a dsRNA substrate with an activity level approaching that of the wt protein (Fig. 8 and 10). Although the E191D mutant was somewhat more sensitive to the mutagenic agent 5-FU (Fig. 5C-D) [28, 80], its ExoN activity does not appear to be dramatically altered by this conservative substitution in the active site.

For this study, we developed an *in vitro* assay to evaluate MERS-CoV ExoN activity using a largely double-stranded RNA substrate (Fig. 7, 8, and 10). As previously observed for SARS-CoV nsp14 [26], MERS-CoV ExoN activity was strongly enhanced by the presence of nsp10 (Fig. 9), in line with the formation of an nsp10:nsp14 heterodimer as observed in biochemical and structural studies [20, 26, 85]. Slightly different patterns of degradation of the H4 substrate were observed when comparing the SARS-CoV and MERS-CoV ExoN enzymes *in vitro*. Likewise, the exchange of the nsp10 co-factor for the nsp10 subunit of the other virus, using the same substrate and the same nsp10:nsp14 ratio (1:4; Fig. 9), resulted in a somewhat

different pattern of substrate degradation, suggesting minor differences in the interaction of the nsp10:nsp14 complex with this particular RNA substrate. Previously, it was demonstrated that nsp10 is interchangeable between CoV subgenera in its role as co-factor for the nsp16 2'-O-methyltransferase, which was attributed to the high level of conservation of the nsp10-nsp16 interaction surface [86]. As nsp14 and nsp16 share a common interaction surface on nsp10 [21, 26, 75], we explored whether a similar co-factor exchange was possible in the context of nsp14's ExoN activity, which was indeed found to be the case (Fig. 9). Structurally, nsp14 interacts with nsp10 figuratively similar to a "hand (nsp14) over fist (nsp10)" conformation [21]. Upon formation of this complex, nsp10 induces conformational changes in the N-terminal region of ExoN that adjust the distance between the catalytic residues in the back of the nsp14 palm and, consequently, impact ExoN activity [21]. The exchange of the nsp10 co-factor between the two betacoronaviruses might affect this conformation and, consequently, modulate the ExoN activity of the nsp14:nsp10 complex.

Alanine substitutions of active site residues severely reduced but did not completely abrogate the *in vitro* activity of MERS-CoV ExoN (Fig. 8-10), as previously shown for certain SARS-CoV nsp14 mutants [20, 36] and recently also for SARS-CoV-2 ([74], not peer reviewed). Based on the two-ion-metal catalytic mechanism underlying the exonuclease activity of DEDDh family members [17, 64] and the SARS-CoV nsp14 structure, it was predicted that the various ExoN motifs contribute differently to the excision of nucleosides monophosphates [20, 21]. Mutation of ExoN catalytic residues can alter ion binding [31] or disturb the fragile chemical equilibrium, as shown for conservative mutations (corresponding to E191D and D273E) in the Klenow fragment, a member of the DEDDh exonuclease family, which reduced ExoN activity by >96% [87]. In general, all DEEDh mutations that yielded non-viable virus mutants exhibited similarly low levels of residual ExoN activity *in vitro* (Fig. 10), indicating that each of these residues is important for catalysis.

Our study suggests that, in addition to the active site residues, also other motifs in MERS-CoV ExoN are important for virus viability, specifically the two ZF motifs that were probed using two point mutations each (Fig. 2A). In previous ZF1 studies, a mutation equivalent to H229A caused solubility issues during expression of recombinant SARS-CoV nsp14 [20] and resulted in a partially active ExoN in the case of white bream virus, a tobanivirus that also belongs to the order *Nidovirales* [88]. It was suggested that ZF1 contributes to the structural stability of ExoN, as it is close to the surface that interacts with nsp10 [20]. Here, we demonstrate that the more conservative H229C replacement, which converts ZF1 from a non-classical CCCH type ZF motif into a classical CCCC type [71], was tolerated during recombinant protein expression and yielded an ExoN that is active *in vitro* (Fig. 8). This likely contributed to the fact

that the H229C virus mutant retained a low level of viability (Fig. 2 and data not shown). Nevertheless, its overall crippled phenotype and the non-viable phenotype of mutant C201H clearly highlighted the general importance of ZF1 for virus replication. In contrast, the corresponding TGEV mutant (ZF-C) was not strongly affected and could be stably maintained over several passages [34] The reverse genetics data suggest that ZF2, which is in close proximity to ExoN catalytic residues [20], is equally important, although technical complications with expression of the C261A and H264R nsp14 mutants prevented us to perform *in vitro* activity assays.

Like the ExoN domain of the arenavirus nucleoprotein [32, 33], the CoV ExoN was proposed to be involved in innate immune evasion [34, 35, 89], possibly by degrading viral ds RNA that in the case of CoVs is confined to characteristic double-membrane vesicles [90-92]. For TGEV, this suggestion was based on the reduced accumulation of dsRNA by the ZF-C mutant, which however remains to be characterized in more detail. In the absence of a TGEV ExoN activity assay, and in view of our data for the equivalent MERS-CoV ZF1 mutant, it seems premature to assume that the reduced levels of dsRNA in infected cells are caused by increased exonuclease activity of the ZF-C ExoN mutant [34].

In general, the properties of viable CoV ExoN mutants warrant further analysis. In future studies, the repertoire of residues probed by site-directed mutagenesis could be extended beyond active site and ZF motifs, which may help in particular to establish how directly reduced ExoN activity, primary viral RNA synthesis, and enhanced innate responses are interconnected. Regardless of its possible interactions with host cell pathways, nsp14 clearly is a key subunit of the multi-enzyme complex that drives CoV genome replication, subgenomic RNA synthesis, and RNA recombination. Understanding the structure-function interplay between ExoN and other (viral and/or host) components will be key to elucidating its role in CoV RNA synthesis and evolution [93, 94]. Taking into account the current SARS-CoV-2 pandemic, understanding the phenotypic differences between ExoN knockout mutants of different CoVs may contribute to the design of improved antiviral approaches, including those relying on 'lethal mutagenesis' or direct interference with viral RNA synthesis.

MATERIALS AND METHODS

Cell culture

Baby hamster kidney cells (BHK-21; ATCC CCL10), Vero E6, Vero (ATCC CCL81) and HuH7 cells were cultured as described previously [78, 95]. Vero and Vero E6 cells were kindly provided by the Department of Viroscience, Erasmus Medical Center, Rotterdam, the Netherlands, and HuH7 cells by Dr. Ralf Bartenschlager, Heidelberg University, Germany. For transfections, cells

were maintained in Eagle's minimal essential medium (EMEM; Lonza) with 8% fetal calf serum (FCS; Bodinco) supplemented with 100 IU/ml of penicillin and 100 µg/ml of streptomycin (Sigma), and 2 mM L-Glutamine (PAA Laboratories), and incubated at 37 °C with 5% CO2. Infection of Vero, Vero E6 and HuH7 cells was carried out in EMEM containing 2 % FCS. SARS-CoV and SARS-CoV-2 were grown in Vero E6 cells and MERS-CoV in Vero and HuH7 cells.

Reverse genetics

Mutations in the MERS-CoV nsp14-coding region were engineered in a bacterial artificial chromosome (BAC) vector [54, 55] containing a full-length cDNA copy of MERS-CoV strain EMC/2012 [44, 56], by two-step e*n passant* recombineering in *E. coli* [96]. For SARS-CoV and SARS-CoV-2, a BAC DNA vector containing a full-length cDNA copy of the SARS-CoV Frankfurt-1 sequence [97] or SARS-CoV-2 BetaCoV/Wuhan/IVDC-HB-01/2019 [61, 98] were used. When designing the primers, a translationally silent marker mutation was introduced near the site of mutagenesis in order to differentiate between the occurrence of reversion and (possible) contamination with parental virus. For each mutation, two mutant BACs were isolated independently, the nsp14-coding region was verified by sequencing, and both BACs were used for *in vitro* run-off transcription and virus launching.

Approximately 5 µg of BAC DNA was linearized with *Not*I and full-length RNA was obtained by *in vitro* transcription with T7 RNA polymerase followed by lithium chloride precipitation according to the manufacturer's protocol (mMessage-mMachine T7 Kit; Ambion). For some of the MERS-CoV and the SARS-CoV-2 transfections, synthetic mRNAs expressing the respective N proteins were generated as described previously [62, 63] and 10 µg was co-transfected with the corresponding full-length RNA. To this end, 5 µg of RNA was electroporated into $5x10^6$ BHK-21 cells (for MERS-CoV) or BHK-21 cells expressing SARS-CoV N protein (for SARS-CoV and SARS-CoV-2; [99]) using the Amaxa nucleofector 2b (program A-031) and Nucleofection T solution kit (Lonza). Transfected cells were mixed with HuH7 or Vero cells (for MERS-CoV) or Vero E6 cells (for SARS-CoV and SARS-CoV-2) in a 1:1 ratio and plated for harvesting supernatants, intracellular RNA isolation, and analysis by immunofluorescence microscopy. Immunolabelling was performed as described before [78], using antibodies recognizing double-stranded RNA (dsRNA; [100]) or SARS-CoV nsp4 [79, 101].

Cells were incubated at 37^{o}C up to a maximum of 6 days post transfection (d p.t.). Supernatants were collected when full cytopathic effect was observed, at 3 d p.t. or at the end of the experiment. Virus titers were determined by plaque assay in HuH7 and Vero cells [102]. In order to confirm the presence of engineered mutations in viral progeny, HuH7 and Vero cells were infected with supernatants harvested from transfected cells and intracellular

RNA was isolated at 18 h post infection as described above. cDNA was synthesized by reverse transcription using RevertedAid H minus reverse transcriptase (ThermoFischer Scientific) and random hexamer primers (Promega), in combination with a primer targeting the 3' end of the viral genome. The full-length genome or the nsp14-coding region were amplified by PCR using MyTaq DNA polymerase (Bioline) and after purification the PCR product was sequenced by Sanger sequencing. Genome sequencing by NGS was performed as described before [79]. All work with live (recombinant) class-3 CoVs was done in a biosafety level 3 laboratory at Leiden University Medical Center.

Analysis of viral RNA synthesis

Isolation of intracellular RNA was performed by lysing infected cell monolayers with TriPure isolation reagent (Roche Applied Science) according to the manufacturer's instructions. After purification, intracellular RNA samples were loaded onto a 1.5% agarose gel containing 2.2 M formaldehyde, which was run overnight at low voltage overnight in MOPS buffer (10 mM MOPS (sodium salt) (pH 7), 5 mM sodium acetate, 1 mM EDTA). Dried agarose gels were used for direct detection of viral mRNAs by hybridization with a ^{32}P-labeled oligonucleotide probe (5'-GCAAATCATCTAATTAGCCTAATC-3') that is complementary to the 3'-terminal sequence of MERS-CoV genome and all subgenomic mRNAs. After hybridization, RNA bands were visualized (using exposure times of up to 28 days) and quantified by phosphorimaging using a Typhoon-9410 variable mode scanner (GE Healthcare) and ImageQuant TL software (GE Healthcare).

PCR primers and Taqman probes targeting ORF1a (junction of nsp2-nsp3 coding region), the nucleocapsid (N) protein gene, or the leader-body TRS junction of subgenomic mRNA3 were designed and analyzed for multiplex quality using Beacon Designer™ Software (Premier Biosoft). Reverse transcription (RT) was performed using RevertedAid H minus reverse transcriptase (ThermoFischer Scientific) and a mix of specific reverse primers targeting ORF1a, ORF8, or subgenomic RNA 3 (primer sequences used available upon request). The mRNA derived from the cellular β-actin gene was used as a reference housekeeping gene. Tagged primers were used to differentiate between positive- and negative-stranded viral RNA. Samples were assayed by Taqman multiplex real-time PCR using TaqMan Universal Master Mix II and a CFX384 Touch™ Real Time PCR detection system (BioRad). A standard curve was obtained using an *in vitro* transcript derived from a synthetic plasmid that contained all PCR targets. cDNA was obtained as described above. Each RNA sample was analyzed in triplicate.

Plaque reduction assay

HuH7 cells seeded in 6-well clusters were infected with recombinant MERS-CoV at low m.o.i. (30 PFU/well) for 1 h at 37°C. Subsequently, the inoculum was replaced with 2 ml of a 1.2% suspension of Avicel (RC-581; FMC Biopolymer [103]) in DMEM (containing 2% FCS and antibiotics) and serial dilutions of 5-FU (F6627, Sigma-Aldrich) or Ribavirin (R9644, Sigma-Aldrich) ranging from 0 to 400 µM. Cells were incubated at 37°C for 72 h, fixed with 7.4% formaldehyde, and plaques were visualized using crystal violet staining.

To compare the effect of 5-FU treatment on the progeny titers of wt and nsp14-E191D rMERS-CoV, confluent monolayers of HuH7 were incubated for 30 min at 37^{o}C with solvent or a range of 5-FU concentrations. The drug was then removed and cells were infected at an m.o.i. of 0.1 during 1 h at 37^{o}C. After removal of the inoculum, EMEM containing 2% FCS and solvent or a matching concentration of 5-FU was added to the wells. Supernatants were collected after 30h and rMERS-CoV progeny titers were determined by plaque assay. All drug-treated samples were normalized to the untreated vehicle control, and values were expressed as fold change compared to untreated virus titers.

Expression and purification of recombinant CoV nsps

SARS-CoV nsp10 and nsp14 were produced as described before [25] and used as a positive control in all biochemical assays. MERS-CoV nsp10 was expressed using pET30a vector and purified as described in [86, 104]. All MERS-CoV nsp14 constructs were cloned into expression vector pDEST14 with an N-terminal His_6-tag using the Gateway system [25]. MERS-CoV nsp14 mutant expression plasmids were generated by Quikchange site-directed mutagenesis using Accuzyme DNA polymerase (Bioline) following the manufacturer's instructions. pDEST14 plasmids expressing MERS-CoV nsp14 were transformed into competent *E. coli* strain Rosetta (DE3) pLyS (Novagen) and cultured in Luria-Bertani (LB) broth supplemented with 100 µg/ ml of ampicillin and 30 µg/ ml of chloramphenicol. Protein expression was induced at an optical density (OD_{600nm}) of 0.8 by adding 50 µM of isopropyl-β-D-a-thiogalactopyranoside (IPTG; Bioline). After 24 h at 13^{o}C, induced cells were harvested and lysed in a buffer containing 50 mM Tris-HCl, pH 7.5, 150 mM NaCl, 5 mM β-mercaptoethanol, 5% glycerol, 1 mM PMSF, and 20 mM imidazole [105]. Next, the lysate was centrifuged at 12,000xg for 30 min, and the soluble fraction was column-purified by immobilized metal ion affinity chromatography using Nickel sepharose high performance beads (17526802, GE Healthcare). The eluate was fractionated by gel filtration on a Superdex-200 Increase 10/300GL column (GE Healthcare) in buffer containing 30 mM HEPES, pH 7,5, 300 mM NaCl, and 5% glycerol. In the end, proteins were concentrated using ultrafiltration devices with a molecular mass cut-off of 30 kDa

(Millipore), and protein concentrations were measured using spectrophotometry. All purified proteins were analyzed by SDS-PAGE followed by Coomassie blue staining as well as by Western blot using a mouse monoclonal antibody against the 6xHis-Tag (Novagen). Protein aliquots were stored at -80°C in 50% glycerol (v/v) and used for enzymatic assays.

Exonuclease activity assay

Synthetic RNA H4 [26] was radiolabeled at its 5' end using T4 polynucleotide kinase (Epicentre) and [γ-^{32}P]ATP (Perkin Elmer) [79]. Unless stated otherwise in figures or legends, reactions contained 200 nM of recombinant nsp14, 800 nM of nsp10, and 750 nM of radiolabeled substrate in 40 mM Tris-HCl pH 7.5 containing 5 mM of $MgCl_2$ and 1 mM of DTT. After incubation at 37°C for up to 90min, reactions were stopped by addition of an equal volume of loading buffer containing 96% formamide and 10mM EDTA. Samples were then loaded on 7M urea-containing 20% (wt/vol) polyacrylamide gels (acrylamide/bisacrylamide ratio 19:1) buffered with 0.5x Tris-borate-EDTA and run at high voltage (1600 V). Results were visualized by phosphorimaging as described above.

N7-methyltransferase activity assay

Methyltransferase assays were performed in 40 mM Tris-HCl, pH 8.0, 5 mM DTT, 2 µM of ^{7Me}GpppA or GpppA RNA cap analogue (New England Biolabs), 10 µM adenosyl-methionine (AdoMet, Thermofisher), 0.03 µCi/µl [^{3}H]AdoMet (PerkinElmer) [25]. In each reaction, MERS-CoV or SARS-CoV nsp14 was added to a final concentration of 500 or 250 nM, respectively. Reactions were incubated at 30°C for up to 120min, and were stopped by the addition of 10-fold volume of 100 µM ice-cold Adenosyl-Homocysteine (AdoHcy; ThermoFischer). Then, samples were spotted on a DEAE filter mat (PerkinElmer) pre-wet with Tris-HCl pH 8.0 buffer. Filter mats were washed twice with 10 mM ammonium formate (Sigma-Aldrich), pH 8.0, twice with MiliQ water, and once with absolute ethanol (Sigma-Aldrich). After air drying for 10 min, filter mats were cut and relevant pieces transferred to individual tubes. Betaplate scintillation fluid (PerkinElmer) was added and the amount or ^{3}H-label bound was measured in counts per minute (cpm) using a Wallac scintillation counter. For relative quantification, incorporation measurements for mutant proteins were normalized to values obtained with the wt control nsp14. Samples were measured in duplicate in each experiment.

ACKNOWLEDGMENTS

N.S.O. was supported by the Marie Skłodowska-Curie ETN European Training Network 'ANTIVIRALS' (EU Grant Agreement No. 642434). C.C.P and E.J.S. were supported in part by TOP-GO grant 700.10.352 from the Netherlands Organization for Scientific Research and by the SCORE project (EU Horizon 2020 research and innovation program, grant agreement 101003627). We thank Linda Boomaars for providing SARS- and MERS-CoV nsp10 and nsp14 expression constructs and Igor Sidorov for NGS assistance. We are indebted to Volker Thiel and colleagues (Institute of Virology and Immunology, Bern, Switzerland) for sharing their SARS-CoV-2 reverse genetics system and to Deyin Guo and colleagues (Wuhan University, China) for sharing their pET30-MERS-CoV-nsp10 expression vector. We are grateful to Etienne Decroly, Francois Ferron, and Bruno Canard (University of Aix-Marseille, France) for helpful discussions. We kindly acknowledge the sharing of unpublished information on IBV ExoN knockout mutants by Dr. Erica Bickerton and colleagues (Pirbright Institute, U.K.).

REFERENCES

1. Vignuzzi, M., et al., *Quasispecies diversity determines pathogenesis through cooperative interactions in a viral population.* Nature, 2006. **439**(7074): p. 344-348.
2. Eigen, M. and P. Schuster, *The hypercycle. A principle of natural self-organization. Part A: Emergence of the hypercycle.* Naturwissenschaften, 1977. **64**(11): p. 541-65.
3. Domingo, E., J. Sheldon, and C. Perales, *Viral quasispecies evolution.* Microbiol Mol Biol Rev, 2012. **76**(2): p. 159-216.
4. Sanjuan, R., *Mutational fitness effects in RNA and single-stranded DNA viruses: common patterns revealed by site-directed mutagenesis studies.* Philos Trans R Soc Lond B Biol Sci, 2010. **365**(1548): p. 1975-1982.
5. Sanjuan, R., et al., *Viral mutation rates.* J Virol, 2010. **84**(19): p. 9733-9748.
6. Steinhauer, D.A., E. Domingo, and J.J. Holland, *Lack of evidence for proofreading mechanisms associated with an RNA virus polymerase.* Gene, 1992. **122**(2): p. 281-288.
7. Drake, J.W. and J.J. Holland, *Mutation rates among RNA viruses.* Proc Natl Acad Sci U S A, 1999. **96**(24): p. 13910-13913.
8. Eigen, M., *Error catastrophe and antiviral strategy.* Proc Natl Acad Sci U S A, 2002. **99**(21): p. 13374-13376.
9. Eigen, M., *Selforganization of matter and the evolution of biological macromolecules.* Naturwissenschaften, 1971. **58**(10): p. 465-523.
10. Nga, P.T., et al., *Discovery of the first insect nidovirus, a missing evolutionary link in the emergence of the largest RNA virus genomes.* PLoS Pathog, 2011. **7**(9): p. e1002215.
11. Lauber, C., et al., *The footprint of genome architecture in the largest genome expansion in RNA viruses.* PLoS Pathog, 2013. **9**(7): p. e1003500.
12. Saberi, A., et al., *A planarian nidovirus expands the limits of RNA genome size.* PLoS Pathog, 2018. **14**(11): p. e1007314.
13. Bukhari, K., et al., *Description and initial characterization of metatranscriptomic nidovirus-like genomes from the proposed new family Abyssoviridae, and from a sister group to the Coronavirinae, the proposed genus Alphaletovirus.* Virology, 2018. **524**: p. 160-171.
14. Snijder, E.J., et al., *Unique and conserved features of genome and proteome of SARS-coronavirus, an early split-off from the coronavirus group 2 lineage.* J Mol Biol, 2003. **331**(5): p. 991-1004.
15. Zuo, Y. and M.P. Deutscher, *Exoribonuclease superfamilies: structural analysis and phylogenetic distribution.* Nucleic Acids Res, 2001. **29**(5): p. 1017-1026.
16. Deutscher, M.P. and C.W. Marlor, *Purification and characterization of Escherichia coli RNase T.* J Biol Chem, 1985. **260**(11): p. 7067-7071.
17. Beese, L.S. and T.A. Steitz, *Structural basis for the 3'-5' exonuclease activity of Escherichia coli DNA polymerase I: a two metal ion mechanism.* EMBO J, 1991. **10**(1): p. 25-33.
18. Steitz, T.A. and J.A. Steitz, *A general two-metal-ion mechanism for catalytic RNA.* Proc Natl Acad Sci U S A, 1993. **90**(14): p. 6498-6502.
19. Minskaia, E., et al., *Discovery of an RNA virus 3'->5' exoribonuclease that is critically involved in coronavirus RNA synthesis.* Proc Natl Acad Sci U S A, 2006. **103**(13): p. 5108-5113.
20. Ma, Y., et al., *Structural basis and functional analysis of the SARS coronavirus nsp14-nsp10 complex.* Proc Natl Acad Sci U S A, 2015. **112**(30): p. 9436-9441.

21. Ferron, F., et al., *Structural and molecular basis of mismatch correction and ribavirin excision from coronavirus RNA.* Proc Natl Acad Sci U S A, 2018. **115**(2): p. E162-E171.
22. Eckerle, L.D., et al., *High fidelity of murine hepatitis virus replication is decreased in nsp14 exoribonuclease mutants.* J Virol, 2007. **81**(22): p. 12135-12144.
23. Eckerle, L.D., et al., *Infidelity of SARS-CoV Nsp14-exonuclease mutant virus replication is revealed by complete genome sequencing.* PLoS Pathog, 2010. **6**(5): p. e1000896.
24. Graham, R.L., et al., *A live, impaired-fidelity coronavirus vaccine protects in an aged, immunocompromised mouse model of lethal disease.* Nat Med, 2012. **18**(12): p. 1820-1826.
25. Bouvet, M., et al., *In vitro reconstitution of SARS-coronavirus mRNA cap methylation.* PLoS Pathog, 2010. **6**(4): p. e1000863.
26. Bouvet, M., et al., *RNA 3'-end mismatch excision by the severe acute respiratory syndrome coronavirus nonstructural protein nsp10/nsp14 exoribonuclease complex.* Proc Natl Acad Sci U S A, 2012. **109**(24): p. 9372-9377.
27. Subissi, L., et al., *One severe acute respiratory syndrome coronavirus protein complex integrates processive RNA polymerase and exonuclease activities.* Proc Natl Acad Sci U S A, 2014. **111**(37): p. E3900-E3909.
28. Smith, E.C., et al., *Coronaviruses lacking exoribonuclease activity are susceptible to lethal mutagenesis: evidence for proofreading and potential therapeutics.* PLoS Pathog, 2013. **9**(8): p. e1003565.
29. Graepel, K.W., et al., *Proofreading-deficient coronaviruses adapt for increased fitness over long-term passage without reversion of exoribonuclease-inactivating mutations.* MBio, 2017. **8**(6): p. e01503-01517.
30. Gribble, J., et al., *The coronavirus proofreading exoribonuclease mediates extensive viral recombination.* bioRxiv, 2020: p. 2020.04.23.057786.
31. Yekwa, E., et al., *Arenaviridae exoribonuclease presents genomic RNA edition capacity.* bioRxiv, 2019: p. 541698.
32. Hastie, K.M., et al., *Structure of the Lassa virus nucleoprotein reveals a dsRNA-specific 3' to 5' exonuclease activity essential for immune suppression.* Proc Natl Acad Sci U S A, 2011. **108**(6): p. 2396-2401.
33. Russier, M., et al., *The exonuclease domain of Lassa virus nucleoprotein is involved in antigen-presenting-cell-mediated NK cell responses.* J Virol, 2014. **88**(23): p. 13811-13820.
34. Becares, M., et al., *Mutagenesis of coronavirus nsp14 reveals its potential role in modulation of the innate immune response.* J Virol, 2016. **90**(11): p. 5399-5414.
35. Case, J.B., et al., *Murine hepatitis virus nsp14 exoribonuclease activity is required for resistance to innate immunity.* J Virol, 2018. **92**(1): p. e01531-17.
36. Chen, Y., et al., *Functional screen reveals SARS coronavirus nonstructural protein nsp14 as a novel cap N7 methyltransferase.* Proc Natl Acad Sci U S A, 2009. **106**(9): p. 3484-3489.
37. Jin, X., et al., *Characterization of the guanine-N7 methyltransferase activity of coronavirus nsp14 on nucleotide GTP.* Virus Res, 2013. **176**(1-2): p. 45-52.
38. Chen, Y., et al., *Structure-function analysis of severe acute respiratory syndrome coronavirus RNA cap guanine-N7-methyltransferase.* J Virol, 2013. **87**(11): p. 6296-6305.

39. Case, J.B., et al., *Mutagenesis of S-adenosyl-l-methionine-binding residues in coronavirus nsp14 N7-methyltransferase demonstrates differing requirements for genome translation and resistance to innate immunity.* J Virol, 2016. **90**(16): p. 7248-7256.
40. Li, X., et al., *Bat origin of a new human coronavirus: there and back again.* Sci China Life Sci, 2020. **63**(3): p. 461-462.
41. Pyrc, K., B. Berkhout, and L. van der Hoek, *Identification of new human coronaviruses.* Expert Rev Anti Infect Ther, 2007. **5**(2): p. 245-253.
42. Munster, V.J., et al., *A novel coronavirus emerging in China - key questions for impact assessment.* N Engl J Med, 2020. **382**(8): p. 692-694.
43. Zhou, P., et al., *A pneumonia outbreak associated with a new coronavirus of probable bat origin.* Nature, 2020. **579**(7798): p. 270-273.
44. Zaki, A.M., et al., *Isolation of a novel coronavirus from a man with pneumonia in Saudi Arabia.* N Engl J Med, 2012. **367**(19): p. 1814-1820.
45. Cotten, M., et al., *Spread, circulation, and evolution of the Middle East respiratory syndrome coronavirus.* mBio, 2014. **5**(1): p. e01062-13.
46. Rabaan, A.A., et al., *Dynamics of scientific publications on the MERS-CoV outbreaks in Saudi Arabia.* J Infect Public Health, 2017. **10**(6): p. 702-710.
47. Farag, E., et al., *Drivers of MERS-CoV Emergence in Qatar.* Viruses, 2018. **11**(1): p. 22.
48. Al-Tawfiq, J.A. and Z.A. Memish, *Drivers of MERS-CoV transmission: what do we know?* Expert Rev Respir Med, 2016. **10**(3): p. 331-338.
49. Siddell, S.G., et al., *Additional changes to taxonomy ratified in a special vote by the International Committee on Taxonomy of Viruses (October 2018).* Arch Virol, 2019. **164**(3): p. 943-946.
50. Gorbalenya, A., et al., *The species Severe acute respiratory syndrome-related coronavirus: classifying 2019-nCoV and naming it SARS-CoV-2.* Nat Microbiol, 2020. **5**(4): p. 536-544.
51. Yoshimoto, F.K., *The Proteins of Severe Acute Respiratory Syndrome Coronavirus-2 (SARS CoV-2 or n-COV19), the Cause of COVID-19.* Protein J, 2020. **39**(3): p. 198-216.
52. Sievers, F., et al., *Fast, scalable generation of high-quality protein multiple sequence alignments using Clustal Omega.* Mol Syst Biol, 2011. **7**: p. 539.
53. Waterhouse, A.M., et al., *Jalview Version 2--a multiple sequence alignment editor and analysis workbench.* Bioinformatics, 2009. **25**(9): p. 1189-1191.
54. Almazan, F., et al., *Engineering a replication-competent, propagation-defective Middle East respiratory syndrome coronavirus as a vaccine candidate.* mBio, 2013. **4**(5): p. e00650-13.
55. Rabouw, H.H., et al., *Middle East respiratory coronavirus accessory protein 4a inhibits PKR-mediated antiviral stress responses.* PLoS Pathog, 2016. **12**(10): p. e1005982.
56. van Boheemen, S., et al., *Genomic characterization of a newly discovered coronavirus associated with acute respiratory distress syndrome in humans.* MBio, 2012. **3**(6): p. e00473-12.
57. Chan, J.F., et al., *Differential cell line susceptibility to the emerging novel human betacoronavirus 2c EMC/2012: implications for disease pathogenesis and clinical manifestation.* J Infect Dis, 2013. **207**(11): p. 1743-1752.
58. Raj, V.S., et al., *Dipeptidyl peptidase 4 is a functional receptor for the emerging human coronavirus-EMC.* Nature, 2013. **495**(7440): p. 251-254.

59. Eckerle, L.D., et al., *Effects of mutagenesis of murine hepatitis virus nsp1 and nsp14 on replication in culture.* Adv Exp Med Biol, 2006. **581**: p. 55-60.
60. Habjan, M., et al., *T7 RNA polymerase-dependent and -independent systems for cDNA-based rescue of Rift Valley fever virus.* J Gen Virol, 2008. **89**(Pt 9): p. 2157-2166.
61. Thao, T.T.N., et al., *Rapid reconstruction of SARS-CoV-2 using a synthetic genomics platform.* Nature, 2020.
62. Thiel, V., et al., *Multigene RNA vector based on coronavirus transcription.* J Virol, 2003. **77**(18): p. 9790-9798.
63. Scobey, T., et al., *Reverse genetics with a full-length infectious cDNA of the Middle East respiratory syndrome coronavirus.* Proc Natl Acad Sci U S A, 2013. **110**(40): p. 16157-16162.
64. Bernad, A., et al., *A conserved 3'----5' exonuclease active site in prokaryotic and eukaryotic DNA polymerases.* Cell, 1989. **59**(1): p. 219-228.
65. Ogando, N.S., et al., *The curious case of the nidovirus exoribonuclease: its role in RNA synthesis and replication fidelity.* Front Microbiol, 2019. **10**: p. 1813.
66. Neuman, B.W., et al., *Proteomics analysis unravels the functional repertoire of coronavirus nonstructural protein 3.* J Virol, 2008. **82**(11): p. 5279-5294.
67. Neuman, B.W., *Bioinformatics and functional analyses of coronavirus nonstructural proteins involved in the formation of replicative organelles.* Antiviral Res, 2016. **135**: p. 97-107.
68. Lei, J., Y. Kusov, and R. Hilgenfeld, *Nsp3 of coronaviruses: Structures and functions of a large multi-domain protein.* Antiviral Res, 2018. **149**: p. 58-74.
69. Noordhuis, P., et al., *5-Fluorouracil incorporation into RNA and DNA in relation to thymidylate synthase inhibition of human colorectal cancers.* Ann Oncol, 2004. **15**(7): p. 1025-1032.
70. Greenhalgh, D.A. and J.H. Parish, *Effect of 5-fluorouracil combination therapy on RNA processing in human colonic carcinoma cells.* Br J Cancer, 1990. **61**(3): p. 415-419.
71. Abbehausen, C., *Zinc finger domains as therapeutic targets for metal-based compounds - an update.* Metallomics, 2019. **11**(1): p. 15-28.
72. Imanishi, M., et al., *Zn(II) binding and DNA binding properties of ligand-substituted CXHH-type zinc finger proteins.* Biochemistry, 2012. **51**(16): p. 3342-3348.
73. Chen, P., et al., *Biochemical characterization of exoribonuclease encoded by SARS coronavirus.* J Biochem Mol Biol, 2007. **40**(5): p. 649-655.
74. Baddock, H.T., et al., *Characterisation of the SARS-CoV-2 ExoN (nsp14 ExoN-nsp10) complex: implications for its role in viral genome stability and inhibitor identification.* bioRxiv, 2020: p. 2020.08.13.248211.
75. Bouvet, M., et al., *Coronavirus Nsp10, a critical co-factor for activation of multiple replicative enzymes.* J Biol Chem, 2014. **289**(37): p. 25783-25796.
76. Rosas-Lemus, M., et al., *The crystal structure of nsp10-nsp16 heterodimer from SARS-CoV-2 in complex with S-adenosylmethionine.* bioRxiv, 2020: p. 2020.04.17.047498.
77. de Wilde, A.H., et al., *Alisporivir inhibits MERS- and SARS-coronavirus replication in cell culture, but not SARS-coronavirus infection in a mouse model.* Virus Res, 2017. **228**: p. 7-13.
78. de Wilde, A.H., et al., *MERS-coronavirus replication induces severe in vitro cytopathology and is strongly inhibited by cyclosporin A or interferon-alpha treatment.* J Gen Virol, 2013. **94**(Pt 8): p. 1749-60.

79. Ogando, N.S., et al., *SARS-coronavirus-2 replication in Vero E6 cells: replication kinetics, rapid adaptation and cytopathology.* J Gen Virol, 2020.
80. Graepel, K.W., et al., *Fitness barriers limit reversion of a proofreading-deficient coronavirus.* J Virol, 2019. **93**(20): p. e00711-19.
81. Kirchdoerfer, R.N. and A.B. Ward, *Structure of the SARS-CoV nsp12 polymerase bound to nsp7 and nsp8 co-factors.* Nat Commun, 2019. **10**(1): p. 2342.
82. Yin, W., et al., *Structural basis for inhibition of the RNA-dependent RNA polymerase from SARS-CoV-2 by remdesivir.* Science, 2020. **368**(6498): p. 1499-1504.
83. Hillen, H.S., et al., *Structure of replicating SARS-CoV-2 polymerase.* Nature, 2020. **584**(7819): p. 154-156.
84. Barnes, M.H., et al., *The 3'-5' exonuclease site of DNA polymerase III from gram-positive bacteria: definition of a novel motif structure.* Gene, 1995. **165**(1): p. 45-50.
85. Pan, J., et al., *Genome-wide analysis of protein-protein interactions and involvement of viral proteins in SARS-CoV replication.* PLoS One, 2008. **3**(10): p. e3299.
86. Wang, Y., et al., *Coronavirus nsp10/nsp16 methyltransferase can be targeted by nsp10-derived peptide in vitro and in vivo to reduce replication and pathogenesis.* J Virol, 2015. **89**(16): p. 8416-27.
87. Derbyshire, V., N.D. Grindley, and C.M. Joyce, *The 3'-5' exonuclease of DNA polymerase I of Escherichia coli: contribution of each amino acid at the active site to the reaction.* EMBO J, 1991. **10**(1): p. 17-24.
88. Durzynska, I., et al., *Characterization of a bafinivirus exoribonuclease activity.* J Gen Virol, 2018. **99**(9): p. 1253-1260.
89. Kindler, E. and V. Thiel, *To sense or not to sense viral RNA--essentials of coronavirus innate immune evasion.* Curr Opin Microbiol, 2014. **20**: p. 69-75.
90. Knoops, K., et al., *SARS-coronavirus replication is supported by a reticulovesicular network of modified endoplasmic reticulum.* PLoS Biol, 2008. **6**(9): p. e226.
91. Snijder, E.J., et al., *A unifying structural and functional model of the coronavirus replication organelle: Tracking down RNA synthesis.* PLoS Biol, 2020. **18**(6): p. e3000715.
92. Wolff, G., et al., *A molecular pore spans the double membrane of the coronavirus replication organelle.* Science, 2020.
93. Ulferts, R., T.C. Mettenleiter, and J. Ziebuhr, *Characterization of Bafinivirus main protease autoprocessing activities.* J Virol, 2011. **85**(3): p. 1348-1359.
94. Snijder, E.J., E. Decroly, and J. Ziebuhr, *The Nonstructural Proteins Directing Coronavirus RNA Synthesis and Processing.* Adv Virus Res, 2016. **96**: p. 59-126.
95. Nedialkova, D.D., A.E. Gorbalenya, and E.J. Snijder, *Arterivirus Nsp1 modulates the accumulation of minus-strand templates to control the relative abundance of viral mRNAs.* PLoS Pathog, 2010. **6**(2): p. e1000772.
96. Tischer, B.K., G.A. Smith, and N. Osterrieder, *En passant mutagenesis: a two step markerless red recombination system.* Methods Mol Biol, 2010. **634**: p. 421-430.
97. Pfefferle, S., et al., *Reverse genetic characterization of the natural genomic deletion in SARS-Coronavirus strain Frankfurt-1 open reading frame 7b reveals an attenuating function of the 7b protein in-vitro and in-vivo.* Virol J, 2009. **6**: p. 131.
98. Wu, F., et al., *A new coronavirus associated with human respiratory disease in China.* Nature, 2020. **579**(7798): p. 265-269.

99. Chang, G.H., et al., *Establishment of the eukaryotic cell lines for inducible control of SARS-CoV nucleocapsid gene expression.* Virol Sin, 2010. **25**(5): p. 361-368.
100. Weber, F., et al., *Double-stranded RNA is produced by positive-strand RNA viruses and DNA viruses but not in detectable amounts by negative-strand RNA viruses.* J Virol, 2006. **80**(10): p. 5059-5064.
101. van Hemert, M.J., et al., *SARS-coronavirus replication/transcription complexes are membrane-protected and need a host factor for activity in vitro.* PLoS Pathog, 2008. **4**(5): p. e1000054.
102. van den Worm, S.H., et al., *Reverse genetics of SARS-related coronavirus using vaccinia virus-based recombination.* PLoS One, 2012. **7**(3): p. e32857.
103. Matrosovich, M., et al., *New low-viscosity overlay medium for viral plaque assays.* Virol J, 2006. **3**: p. 63.
104. Chen, Y., et al., *Biochemical and structural insights into the mechanisms of SARS coronavirus RNA ribose 2'-O-methylation by nsp16/nsp10 protein complex.* PLoS Pathog, 2011. **7**(10): p. e1002294.
105. Aouadi, W., et al., *Toward the identification of viral cap-methyltransferase inhibitors by fluorescence screening assay.* Antiviral Res, 2017. **144**: p. 330-339.

CHAPTER V

Structure-function analysis of the nsp14 N7-guanine methyltransferase reveals an essential role in *Betacoronavirus* replication

Natacha S. Ogando[1#], Priscila El Kazzi[2#], Clara C. Posthuma[1*], Volker Thiel[3,4], Bruno Canard[2], François Ferron[2,3#], Etienne Decroly[2£#] & Eric J. Snijder[1#]

[1] Department of Medical Microbiology, Leiden University Medical Center, Leiden, The Netherlands, 2333ZA

[2] Architecture et Fonction des Macromolécules Biologiques, Centre National de la Recherche Scientifique, Aix-Marseille Université, Marseille, France, 13288

[3] European Virus Bioinformatics Center, Jena, Germany, 07743.

[4] Institute of Virology and Immunology (IVI), Bern, Switzerland,3350.

[5] Department of Infectious Diseases and Pathobiology, Vetsuisse Faculty, University of Bern, Bern, Switzerland, 3012.

[#] Present address: Netherlands Commission on Genetic Modification, Bilthoven, The Netherlands

[#]authors contributed equally

submitted to Proceedings of the National Academy of Sciencesβ

ABSTRACT

As coronaviruses (CoVs) replicate in the host cell cytoplasm, they rely on their own capping machinery to ensure the efficient translation of their mRNAs, protect them from degradation by cellular 5' exoribonucleases, and escape innate immune sensing. The CoV nonstructural protein 14 (nsp14) is a bi-functional replicase subunit harboring an N-terminal 3'-to-5' exoribonuclease (ExoN) domain and a C-terminal (N7-guanine)-methyltransferase (N7-MTase) domain that is assumed to be involved in viral mRNA capping. Here, we first revisited the crystal structure of severe acute respiratory syndrome (SARS)-CoV nsp14 to perform an *in silico* comparative analysis between different betacoronaviruses. In this study, we identified several residues likely to be involved in the formation of the catalytic pocket of N7MTase, which presents a fold that is distinct from the Rossmann fold observed in most known MTases. Next, for multiple *Betacoronavirus*, site-directed mutagenesis of selected residues was used to assess their importance for in vitro enzymatic activity and viral replication in cell culture. For SARS-CoV and Middle East respiratory syndrome-CoV, most of the engineered mutations abolished the N7-MTase function, while not affecting nsp14-ExoN activity. Upon reverse engineering of these mutations into *Betacoronavirus* genomes, we identified two substitutions (R310A and F426A in SARS-CoV) that abrogated viral progeny production and one mutation (H424A) that yielded a crippled phenotype across all betacoronaviruses tested. Our results identify the N7-MTase as a critical enzyme for *Betacoronavirus* replication and defined key residues of its catalytic pocket that can be targeted to design inhibitors with a potential pan-coronaviral activity spectrum.

SIGNIFICANCE STATEMENT

The ongoing SARS-CoV-2 pandemic emphasizes the urgent need to develop efficient broad-spectrum anti-CoV drugs. The structure-function characterization of conserved CoV replicative enzymes is key to identifying the most suitable drug targets. Using a multidisciplinary comparative approach and different *Betacoronavirus*, we characterized the key conserved residues of nsp14 (N7-guanine)-methyltransferase, a poorly defined subunit of the CoV mRNA-synthesizing machinery. Our study highlights the unique structural features of this enzyme and establishes its essential role in *Betacoronavirus* replicatiβon, while identifying two residues that are critical for the replication of all four betacoronaviruses tested, including SARS-CoV-2.

INTRODUCTION

At their 5' end, all eukaryotic mRNAs carry an N7-methylguanosine cap that ensures their translation by mediating mRNA recognition during the formation of the ribosomal pre-initiation complex. The co-transcriptional capping of cellular pre-mRNAs occurs in the nucleus and is also critical for pre-mRNA splicing and nuclear export (reviewed in [1-3]). The mRNA cap consists of an N7-methylated 5' guanosine moiety that is linked to the first nucleotide of the transcript by a 5'-5' triphosphate bridge [4]. Its synthesis requires (presumably) the consecutive involvement of triphosphatase, guanylyltransferase, and guanine-N7 methyltransferase activities to produce a cap-0 structure. The first 2 nucleotides of mammalian mRNAs are then methylated on the 2'OH position to yield a cap-1 structure that identifies the transcript as "self" and prevents activation of innate immune sensors (reviewed in [2, 5]. Furthermore, the cap structure promotes mRNA stability by providing protection from cellular 5' exoribonucleases.

Viruses rely on host ribosomes for their gene expression and have adopted different strategies to ensure translation of their own mRNAs. These include using the canonical nuclear capping pathway, so-called 'cap-snatching' mechanisms, and replacement of the cap by a ribosome-recruiting RNA structure (reviewed in [2, 6, 7]). Various cytosolically replicating virus families have evolved their own capping machinery. The latter applies to the coronavirus (CoV) family, which includes the severe acute respiratory syndrome coronavirus 2 (SARS-CoV-2), the causative agent of COVID-19 [8, 9], and a range of other CoVs infecting human or animal hosts [10, 11]. This century alone, the CoV family has given rise to three major zoonotic introductions: SARS-CoV-2, the Middle East respiratory syndrome-CoV (MERS-CoV) discovered in 2012, and SARS-CoV, emerging in South East Asia in 2002. All three belong to the genus *Betacoronavirus*, which is abundantly represented among CoVs circulating in bat species [12-15]. Despite their demonstrated potential to cross species barriers, prophylactic and therapeutic solutions for CoV infections to prevent or rapidly contain the current COVID-19 pandemic were not available.

The positive-sense CoV genome is unusually large (~30 kb) and its 5' proximal two-thirds encodes for two replicase polyproteins that are post-translationally cleaved into 16 nonstructural proteins (nsp) [16, 17]. The CoV replicative enzymes, including the nsp12 RNA-dependent RNA polymerase (RdRp), assemble into a protein complex that is embedded within virus-induced replication organelles [18-20] and directs the synthesis and capping of newly made viral genomes as well as subgenomic mRNAs that serve to express additional CoV genes. Capping is thought to involve the successive action of multiple CoV enzymes: (i) the nsp13 RNA triphosphatase removing the γ phosphate from the nascent 5'-triphosphorylated RNA

[21, 22]; (ii) an RNA guanylyltransferase (GTAse) producing a GpppN cap by transferring guanosine monophosphate (GMP) to the RNA's dephosphorylated 5' end, a role recently attributed to the nsp12 nucleotidyltransferase (NiRAN) domain, but remaining to be confirmed [23-25]; (iii) the nsp14 (N7-guanine)-methyltransferase (N7-MTase) methylating the N7 position of the cap while using S-adenosyl methionine (SAM) as methyl donor; (iv) the nsp16 ribose 2'-O-methyltransferase (2'-O-MTase) converting the cap-0 into a cap-1 structure ($^{7m}GpppN_{2'Om}$; [26, 27]) by performing additional methylation with the assistance of nsp10 as co-factor [26, 28, 29].

Over the past 15 years, the CoV capping machinery has mainly been analyzed *in vitro*, in particular for SARS-CoV, but its characterization in the context of the viral replication cycle has been lagging behind. This applies in particular to the CoV N7-MTase domain, expressed as part of the ~60-kDa nsp14, a bi-functional replicase subunit also containing an N-terminal 3'-to-5' exoribonuclease domain implicated in promoting the fidelity of CoV replication [30, 31]. Following the discovery of an N7-MTase activity associated with nsp14's C-terminal domain [27], the protein was found to methylate non-methylated cap analogues or guanosine triphosphate (GTP) substrates in the presence of SAM in biochemical assays [26, 32, 33]. While the association of nsp10 with nsp14 enhances its ExoN activity, the *in vitro* N7-MTase activity does not depend on any co-factor [26, 34]. Biochemical and structural characterization of the N7-MTase and ExoN domains demonstrated that the two domains are functionally distinct [35-38]. Nevertheless, truncations and alanine substitutions in the ExoN domain can severely affect SAM binding and N7-MTase activity [27, 33]. The notion that the two enzymatic domains are structurally intertwined was also supported by the SARS-CoV nsp14 crystal structure [35, 36] which was found to be composed of (i) a flexible N-terminal sub-domain forming the nsp10 binding site (aa 1-58), (ii) the 3'-to-5' exoribonuclease (ExoN) domain (aa 1-291), (iii) a flexible hinge region consisting of a loop that connects the N- and C-terminal domains, and three strands protruding from the C-terminal domain (aa 285-300 and aa 407-430), and (iv) the C-terminal N7-MTase domain (aa 292-527) ([35, 36]; Fig 1A).

Interestingly, the structural analysis of the SARS-CoV-nsp14 N7-MTase revealed a non-Rossmann fold [36], distinguishing this enzyme from commonly known cellular and viral methyltransferases [39, 40]. Despite the biochemical characterization of the CoV N7-MTase, the assessment of its importance for virus replication has remained limited to studies with a few point mutations introduced into nsp14 of murine hepatitis virus, a model ß-CoV [41-43]. These studies highlighted two motifs important for CoV replication: (i) the presumed SAM binding motif I (DxGxPxG/A, with x being any amino acid; Fig. 2C, motif III), first discovered by superimposition of a SARS-CoV nsp14 N7-MTase structure model with the crystal structures

of cellular N7-MTases [27]; (ii) nsp14 residues 420-428 that, based on the crystal structure, seem to form a constricted pocket holding the cap's GTP moiety [35]. Comparative analysis of N7-MTase domains revealed that a number of residues crucial for substrate and ligand binding are conserved among homologous enzymes in more distant CoV relatives [44].

Due to its conservation and unique structural features, the CoV N7-MTase constitutes an attractive target for antiviral drug development [45-47], to combat SARS-CoV-2 or future emerging CoV threats. Only a few compounds have been reported to inhibit nsp14 N7-MTase activity *in vitro* [26, 32, 45-47]. Evaluation of their antiviral activity revealed limited inhibition of CoV replication in cell culture, suggesting poor bio-availability and/or specificity [45, 48]. Structural, biochemical, and virological studies of CoV N7-MTase structure and function have not been integrated thus far. Here, we set out to define the catalytic pocket, characterize its involvement in enzymatic activity, and use these observations to probe the enzyme's importance for CoV replication. Using four different ß-CoVs (SARS-CoV, MERS-CoV, MHV, and SARS-CoV-2), we identified conserved features and residues supporting N7-MTase activity and viral replication, thus providing a solid framework for future efforts to design broad-spectrum inhibitors of this critical CoV enzyme.

RESULTS

Identification of key residues for RNA and SAM binding by the CoV N7-MTase.

The previously resolved SARS-CoV nsp14 structure [35, 36] revealed how the ExoN and N7-MTase domains are structurally interconnected, with possible functional implications (Fig. 1). Thus far, a structure of nsp14 in complex with 5'-capped RNA is lacking. Due to some structural peculiarities, it was unclear which conserved residues may be mechanistically involved in N7-methylation and how important these may be for overall CoV replication. Therefore, we first revisited the core structure of the CoV N7-MTase, to guide a subsequent biochemical and virological comparison across multiple *Betacoronavirus*.

In the SARS-CoV nsp14 structure [35], the ExoN core presents a fold characteristic of the DED/EDh family of exonucleases [31, 49, 50]. However, the N7-MTase domain does not exhibit the canonical 'Rossmann fold' that is common among RNA virus MTases, RNA cap-0 MTases at large [36], and all five classes of SAM-dependent MTases [51, 52]. A hinge region that is highly conserved across CoVs is present at the interface of nsp14's ExoN and N7-MTase domains (Fig. 2) and constitutes a unique structural feature of this bi-functional CoV protein. It not only connects the two domains, but also forms an extension that protrudes from the surface of the N7-MTase domain (Fig. 1B). Although, the overall structure suggests ExoN and N7-MTase to be separate domains, attempts to express and purify truncated forms of these

domains, with or without the hinge sub-domain, yielded insoluble recombinant proteins (data not shown). This might be related to the hydrophobic nature of the hinge, which is likely important for protein stability and folding. Several studies reported that the replacement of ExoN catalytic residues does not impair the N7-MTase activity, suggesting that the functional interplay between the two domains is limited [26, 27, 33, 38, 45, 53]. Whereas the hinge region allows lateral and rotational movement of the two nsp14 domains, one side of the hinge also constitutes the 'ceiling' of the N7-MTase active site (Fig. 1B).

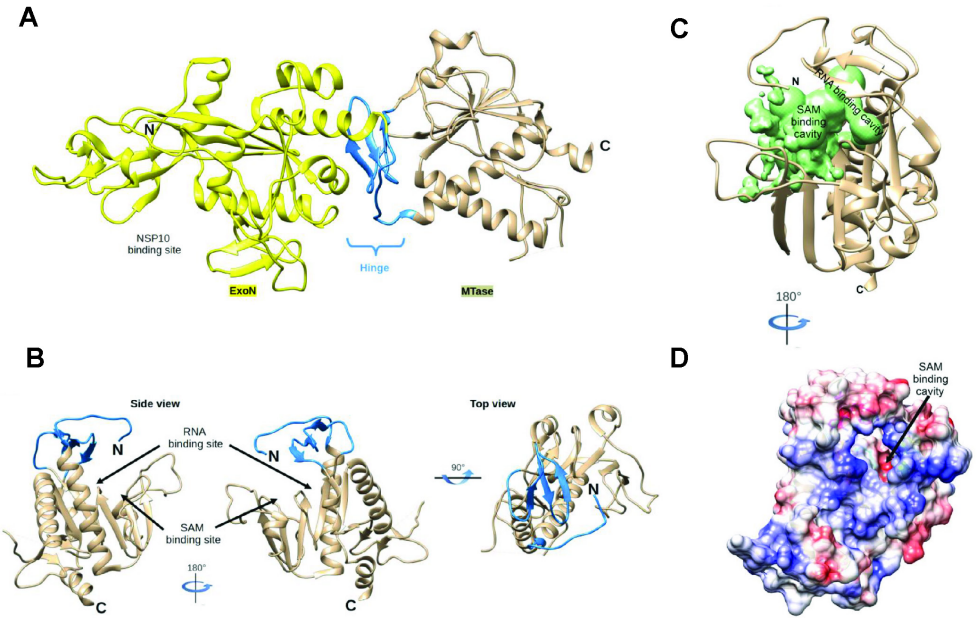

Fig. 1. Global architecture of coronavirus nsp14 (PDB 5NFY). (A) Architecture of SARS-CoV nsp14 showing the N-terminal ExoN domain (Yellow), inter-domain hinge (blue), C-terminal N7-MTase domain (brown). (B) Side and top view of the hinge region and N7-MTase domain. The three strands of the hinge (blue) protrude from the N7-MTase domain (brown). (C) Analysis of the volume of the N7-MTase active site, with the cavity highlighted in green. (D) Electrostatic surface representation of the CoV nsp14 hinge region and N7-MTase domain. Surface electrostatic potential calculated by Adaptive Poisson-Boltzmann Solver, from - 10 (red) to + 10 (blue) kT/e.

The structure of nsp14 in complex with SAM and GpppA (PDB: 5C8S and 5C8T; [35]) have defined the enzyme's cap-binding pocket. However, the crystal packing profoundly constrained the structural characterization of the N7-MTase domain and the overall low resolution left uncertainties regarding the positioning of the RNA ligand. Therefore, we performed a thorough structural analysis of the enzyme's cavity, supported by CoV-wide

nsp14 sequence comparisons, in order to define conserved N7-MTase residues that may be involved in enzymatic activity. Several aspects were taken into consideration while delimiting the SAM and RNA binding sites: the general geometry of the cavity, its electrostatic properties, and the conservation of specific amino acid residues. We used Surfnet software [54] to define the volume corresponding to the ligand-binding cavity (Fig. 1C). This volume is shaped as a dual bulb, with the larger pocket accommodating the capped RNA and the smaller one forming the SAM binding site. An electrostatic surface analysis shows positive charges lining the wall of the putative RNA-binding cavity (Fig. S1), which would be consistent with its function. Likewise, positive charges that might accommodate the carbocyclic part of the methyl donor were identified in the SAM binding pocket (Fig. 1D). Additionally, conserved hydrophobic residues (Motif I; Fig. 3B) were mapped to a deep hydrophobic cavity, supposedly accommodating the SAM base by a stacking interaction with F426. Finally, the integration of the structural models with CoV-wide N7-MTase sequence comparisons (Table S1) allowed the identification of conserved potential key residues within each cavity (blue regions in Fig. 2). Based on their conservation and positioning, six conserved motifs (I-VI) were identified, containing a series of specific charged or aromatic residues that have their side chain pointing toward the cavity (Fig. 3A and 3B). Their features suggested they can facilitate the methyl transfer from SAM onto the cap's guanine residue at the 5' end of RNA substrate, by stabilizing and/or correctly positioning the cap structure. The following potential key residues were identified (amino acid numbers matching those in SARS-CoV nsp14): Motif I, W292; Motif II, N306 and R310; Motif III, D331 and K336; Motif IV, D353; Motif V, N386; Motif VI, Y420, N422, H424, and F426 (Fig. 3A and 3B). To assess the possible impact of their replacement on nsp14 folding, we analyzed the predicted impact of single-site substitutions with alanine on the thermostability of nsp14 (Fig. 3C). Except for R310, all replacements yielded positive ΔΔG values, suggesting that these mutations may affect MTase stability (Fig. 3C). Noticeably, mutations in Motifs I and VI, which are spatially close as part of the hinge and most likely involved in the binding of capped-RNA, resulted in the largest ΔΔG gains. Similar observations were made when the impact of substitutions with other amino acids was evaluated for different betacoronaviruses (Table S2).

Identification of residues crucial for in vitro N7-MTase activity.

To experimentally verify the outcome of our structural analysis (Fig. 1 to 3), we probed the functional importance of selected residues through targeted mutagenesis and in vitro N7-MTase assays. Based on their conservation, charge, position, and potential role for RNA or SAM binding in the catalytic pocket (Fig. 3A and 3B), nine and seven residues in recombinant

SARS-CoV and MERS-CoV nsp14, respectively, were replaced with alanine. N-terminally His-tagged proteins were expressed in E. coli and purified using immobilized metal affinity chromatography (IMAC) followed by size exclusion chromatography (Fig. 4A and 4B).

We evaluated the N7-MTase activity of nsp14 mutants in an assay using a GpppACCCC capped RNA substrate and radiolabeled [3H]SAM. The transfer of the [3H]methyl group onto the RNA substrate was quantified using filter binding assays (Fig. 4C and 4D), as described previously [26, 34], and compared to the enzymatic activity of wild-type SARS-CoV or MERS-CoV nsp14. With the exception of N306A (30% residual activity) and H424A (40% remaining), all SARS-CoV mutations tested completely abrogated nsp14 N7-MTase activity (Fig. 4C). In the case of MERS-CoV nsp14, only mutant F422A retained partial N7-MTase activity (70%), while again all other mutations rendered the enzymatic activity undetectable (Fig. 4D). In terms of residual activity, differences were observed for some pairs of equivalent SARS-CoV and MERS-CoV mutants (e.g. the H and F in motif VI), but overall the results were fully in line with the outcome of our structural analysis. Thus, our data confirmed and extended a previous study [35] and showed that N7-MTase activity is affected by mutations that either inhibit SAM binding (W292A, D331A, G333A, K336A in SARS-CoV) or likely interfere with RNA chain stabilization (N306A, R310A, Y420A, F426A).

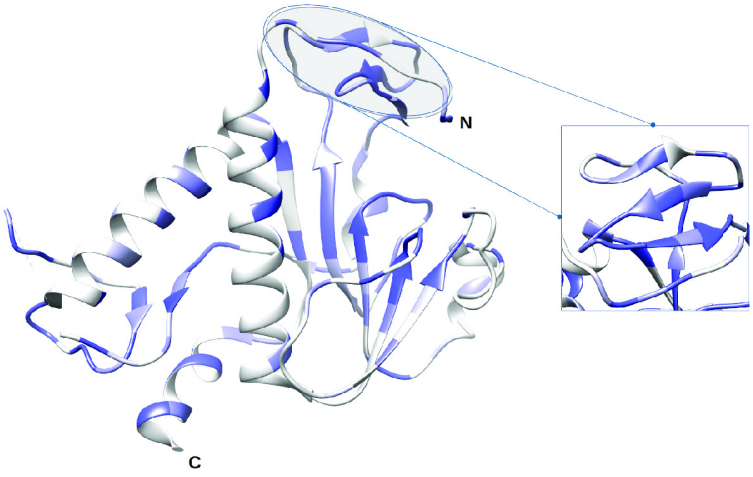

Fig. 2. Coronavirus-wide nsp14 N7-MTase conservation analysis. CoV nsp14 amino acid sequence conservation plotted on the structure (PDB 5NFY) of the SARS-CoV hinge region and N7-MTase domain (dark blue to white representing 100% to less than 50% sequence identity). A table of sequences used for comparison is presented in Table S1.

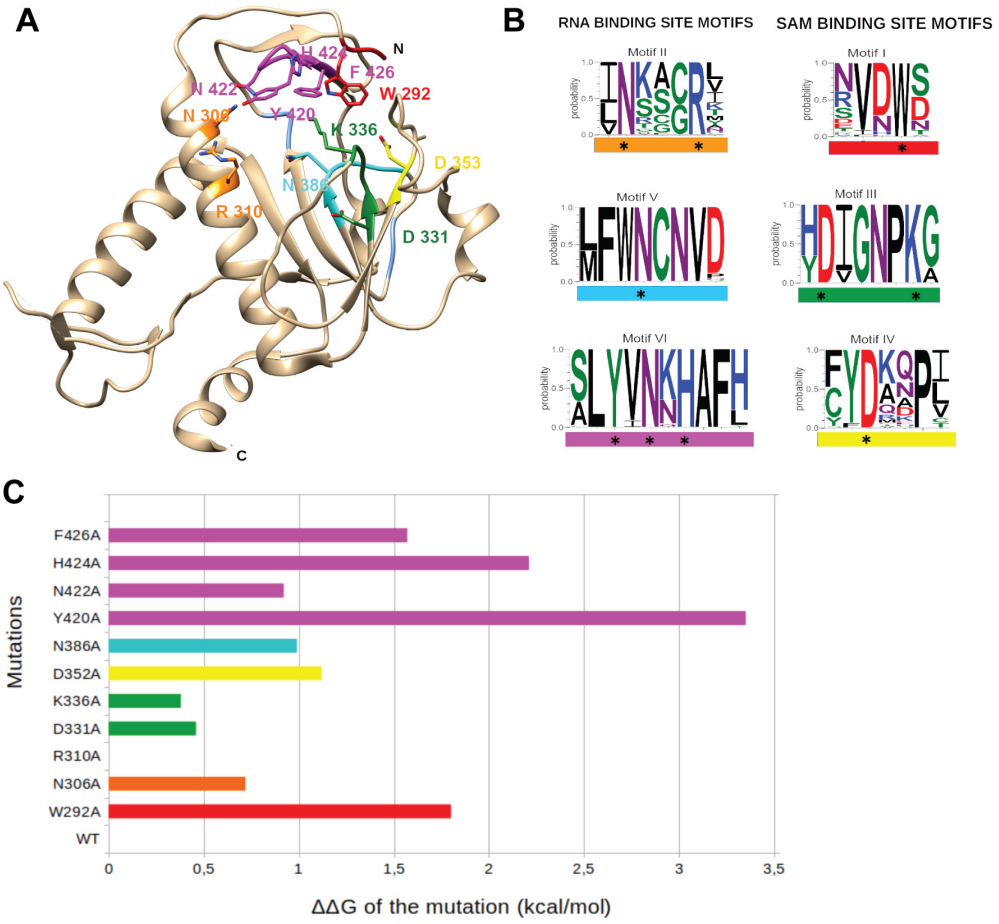

Fig. 3. Coronavirus-wide nsp14 N7-MTase sequence and structural analysis. (A) Close-up of identified conserved motifs/residues in the N7-MTase catalytic pocket. B) WebLogo representation of 6 conserved motifs (I-VI) identified in the catalytic pocket. Each motif is highlighted with a specific color (matching that in panel A) and categorized as a proposed SAM- or RNA-binding motif. Black stars highlight charged or aromatic residues most likely involved in ligand binding or catalytic activity. C) Projected impact on folding free energy by alanine substitutions of the identified core residues on the N7-MTase structure, as calculated by PoPMusic.

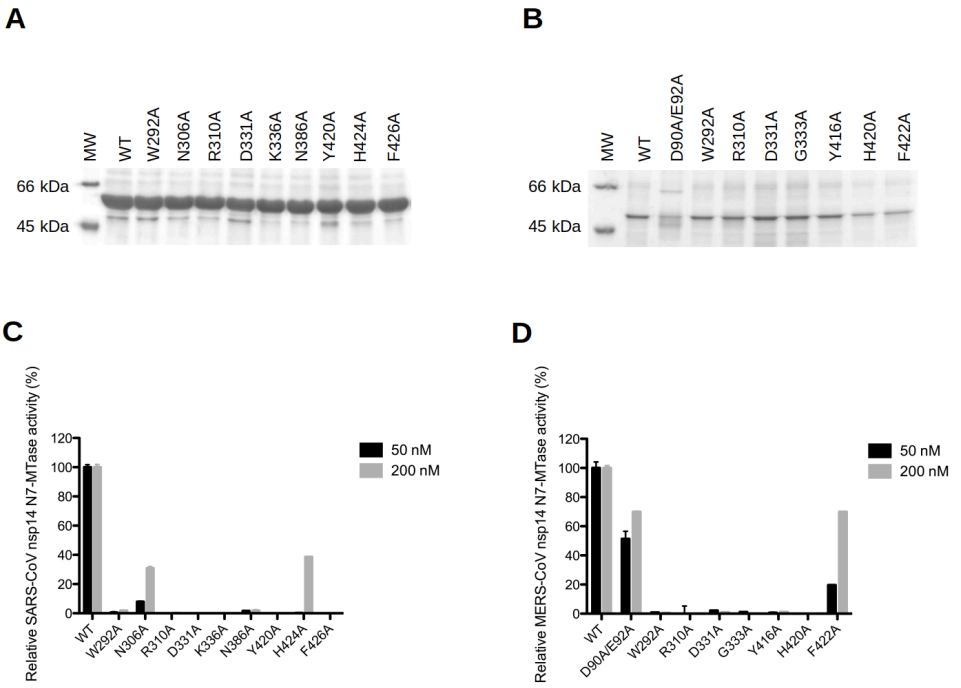

Fig. 4. Expression and *in vitro* N7-MTase activity of SARS-CoV and MERS-CoV nsp14 mutants. Recombinant SARS-CoV (A) and MERS-CoV (B) wild-type and mutant nsp14 proteins were expressed in *E. coli* and purified. Proteins were analyzed using 10% SDS-PAGE gels stained with Coomassie blue. The *in* vitro N7-MTase activity of SARS-CoV (C) and MERS-CoV (D) nsp14 mutants was determined using an assay with a GpppACCCC synthetic RNA substrate and radiolabeled SAM as methyl donor. Nsp14 concentrations (of 50 and 200 nM were used, as indicated. N7-MTase activities were compared to those of the respective wild-type nsp14 controls. For MERS-CoV, ExoN knockout mutant D90A/E92A was included as a control.

Revisiting the interplay between the N7-MTase and ExoN domains of nsp14.

Despite the notion that the ExoN and N7-MTase domains of CoV nsp14 may be functionally independent [27, 33, 35, 36], they are structurally interconnected by the hinge region (Fig. 1). Therefore, we evaluated the impact of all of our N7-MTase mutations on ExoN functionality, using an in vitro assay with 5'-radiolabeled RNA substrate H4 [34], a 22-nt RNA of which the largest part folds into a hairpin structure. Its degradation was monitored using denaturing polyacrylamide gel electrophoresis and autoradiography (Fig. 5). Nsp10 was added as a co-factor that importantly stimulates nsp14 ExoN activity [34, 35, 38], as again confirmed in the 'nsp14 only' control assay (Fig. 5). As expected, in time course experiments, we observed the progressive 3'-to-5' degradation of the RNA substrate by the wild-type nsp10-nsp14 pair of

both SARS-CoV (Fig. 5A) and MERS-CoV (Fig. 5B). In the same assay, most of our N7-MTase mutations barely affected ExoN activity (Fig. 5A and 5B), also supporting the notion that these mutant proteins had folded correctly. In contrast, the ExoN activity of SARS-CoV mutants Y420A, H424A, and F426A, and MERS-CoV mutants G333A and H420A was strongly reduced or abolished. In particular the negative impact of the MERS-CoV G333A mutation on ExoN activity was unexpected, as this mutation maps to the SAM binding domain of the N7-MTase (Motif III). Possibly this mutation destabilizes the recombinant protein. The remaining four mutations that affected ExoN activity all mapped to motif VI in the hinge region (Fig. 3A and 3B). Based on the structural analysis, we assume that these mutations affect either the overall nsp14 folding or – more likely - constrain the flexibility of the hinge subdomain with negative consequences for ExoN functionality [35, 36]. Conversely, a MERS-CoV ExoN knockout mutant (D90A/E92A), which was included as a control, was found to modestly impact N7-MTase activity (Fig. 4D). Taken together, our data suggest that, although the N7-MTase sequence is well conserved among *Betacoronavirus* [35, 38], the differences observed between SARS-CoV and MERS-CoV must be caused by a certain level of structural variability.

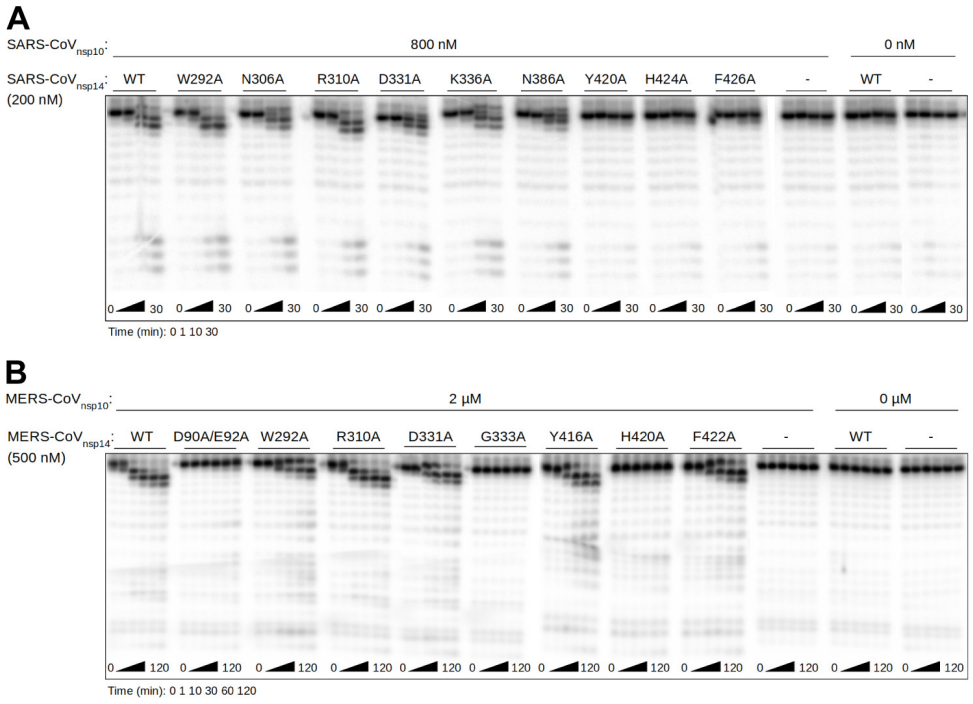

Fig. 5. *In vitro* Exoribonuclease activity of SARS-CoV and MERS-CoV N7-MTase mutants. The *in vitro* ExoN activity of SARS-CoV (A) and MERS-CoV (B) mutant nsp14 proteins (Fig. 3) was determined by monitoring the degradation of a 5' radiolabeled RNA substrate (see Methods). An nsp14

concentration of 200 or 500 nM was used (as indicated) and a fourfold molar excess of the corresponding nsp10 was added. A time course assay was performed using time points 0, 1, 10 and 30 min for SARS-CoV and 0, 1, 10, 30, 60, and 120 min for MERS-CoV nsp14. Reaction products were analyzed by denaturing gel electrophoresis and autoradiography

The nsp14 N7-MTase is critical for SARS-CoV viability.

As summarized above, most prior biochemical and structural studies of the CoV N7-MTase were performed using SARS-CoV nsp14, whereas mutagenesis in the context of virus replication (using reverse genetics) was restricted to MHV studies in which, for different reasons, the conserved D and G residues in motif III and the Y residue in motif VI were targeted [41, 43, 55]. To establish a connection between the biochemical and virological data on the N7-MTase, we first transferred ten single N7-MTase mutations to the SARS-CoV genome, using a bacterial artificial chromosome-based reverse genetics system. Each mutant was engineered in duplicate and launched by in vitro transcribing full-length RNA that was electroporated into BHK-21 cells. To propagate viral progeny, if released, transfected BHK-21 cells were mixed with Vero E6 cells and incubated up to 6 days. Each mutant was launched at least four times, using RNA from 2 independent clones in two independent experiments, and mutant phenotypes are summarized in Fig. 6A.

In line with the biochemical data, the non-viable phenotype of 6 of the mutants (Fig. 6B) provided clear support for the importance of key residues in N7-MTase motifs II (R310), III (D331 and G333), V (N386), and VI (Y420 and F426). As anticipated, mutations in the canonical SAM binding motif III (DxGxPxG/A) completely abrogated SARS-CoV replication (Fig. 6A), apparently confirming the critical role of D331, which was postulated to be a key residue for methylation upon the discovery of the CoV N7-MTase [27]. On the other hand, D331A was the only non-viable SARS-CoV mutant for which reversion to wild-type was occasionally observed, suggesting that a very low level of viral RNA synthesis remained possible in spite of this mutation (see also below). Remarkably, mutations N306A and K336A in motifs II and III, respectively, were found to yield viruses with plaque phenotypes and progeny titers similar to those of the wt control (Fig. 6), despite the major impact of these mutations on in vitro N7-MTase activity (Fig. 4A). Likewise, the viable but severely crippled (small-plaque) virus phenotypes of motif-I mutant W292A and motif VI-mutant H424A were surprising (Fig. 6B), although for the latter the biochemical assays did reveal some activity when performed with an increased enzyme concentration (Fig. 4C and [35]). For all four mutants, the presence of the original mutation in the viral progeny was confirmed by sequence analysis of the nsp14-coding region of the genome. For non-viable mutants, transfected cells were incubated and monitored for 6 days and absence of viral activity was also confirmed by immunofluorescence

microscopy with antibodies specific for double-stranded RNA and SARS-CoV nsp4 (data not shown).

In general, our data demonstrated the importance of the N7-MTase domain for SARS-CoV viability and confirmed the importance of most of the motifs/key residues identified using structural biology and biochemical approaches. Nevertheless, for several mutants the data from different types of assays were not readily aligned, which prompted us to expand the reverse genetics efforts to other ß-CoVs.

Phenotypic differences between *Betacoronavirus* N7-MTase mutants suggest complex structure-function relationships.

Even when targeting highly conserved viral functions, the introduction of equivalent mutations in closely related viruses can sometimes yield remarkably different mutant phenotypes. A recent example is the inactivation of the nsp14 ExoN, which is tolerated by MHV and SARS-CoV, but not by MERS-CoV and SARS-CoV-2, the latter virus having an nsp14 sequence that is 95% identical to that of SARS-CoV [38]. To expand our understanding of the impact of N7-MTase mutagenesis, we engineered, launched, and analyzed a set of MERS-CoV and MHV mutants, using technical procedures similar to those described above for SARS-CoV (see Methods). In this case, the production of viable progeny was facilitated by co-culturing transfected BHK-21 cells with host cells appropriate for the amplification of MHV (17clone1 cells) or MERS-CoV (Huh7 cells). Again, each mutant was launched at least four times (from duplicate clones) and results are summarized in Fig. 6.

The mutations tested for MERS-CoV and MHV had a large predicted impact in our folding free energy analysis (Fig. 3C) and/or yielded a non-viable or crippled phenotype in our SARS-CoV study (Fig. 6A). We evaluated whether these residues were equally critical for the replication of other *Betacoronavirus*. For clarity, in the text below we will refer to these mutants using SARS-CoV nsp14 amino acid numbering, but the correct (slightly different) MERS-CoV and MHV nsp14 amino acid numbers are used in Fig. 4, 5 and 6B.

In contrast to the SARS-CoV result, mutant W292A (motif I, SAM binding site) was not viable for both MERS-CoV and MHV. Strikingly, mutagenesis of D331 and G333 in motif III (SAM binding site) yielded the opposite outcome: both were not tolerated in SARS-CoV, but resulted in crippled or even wild type-like phenotypes for MERS-CoV and MHV, respectively (Fig. 6B). These results again suggested that CoV N7-MTase active site mutants can be (partially) viable, even in the absence of detectable enzymatic activity in vitro (Fig. 4D). Replacement of H424 in motif VI (RNA binding site) consistently crippled replication across SARS-CoV, MERS-CoV,

and MHV (Fig. 6B), while replacement of Y420A in the same motif was partially tolerated by MERS-CoV, but not by SARS-CoV and MHV.

Our ß-CoV comparison identified only two N7-MTase mutations that consistently abrogated the replication of all three viruses tested: R310A (motif II) and F426A (Motif VI), both mapping to the putative RNA binding site. This was surprising in the case of MERS-CoV, given the fact that this mutation (F422A in MERS-CoV) allowed substantial N7-MTase activity in the in vitro assay (Fig. 4D). When SARS-CoV-2 emerged during the course of this study, the R310A and F426A mutants were also engineered for this newly discovered virus and again found to fully abrogate virus replication (Fig. 6A).

A

N7-MTase Motif	nsp14 mutation	Mutant phenotype			
		SARS-CoV	MERS-CoV	MHV	SARS-CoV-2
I	W292A	viable; severely crippled	non-viable	non-viable	N.P.
II	N306A	viable; like wt	N.P.	N.P.	N.P.
	R310A	non-viable	non-viable	non-viable	non-viable
III	D331A	non-viable	viable; severely crippled	viable; like wt	N.P.
	G333A	non-viable	viable; severely crippled	non-viable	N.P.
	K336A	viable; mildly crippled	N.P	N.P	N.P.
V	N386A	non-viable	N.P	N.P	N.P.
VI	Y420A	non-viable	viable; severely crippled	non-viable	N.P.
	H424A	viable; severely crippled	viable; severely crippled	viable; mildly crippled	N.P.
	F426A	non-viable	non-viable	non-viable	non-viable

B

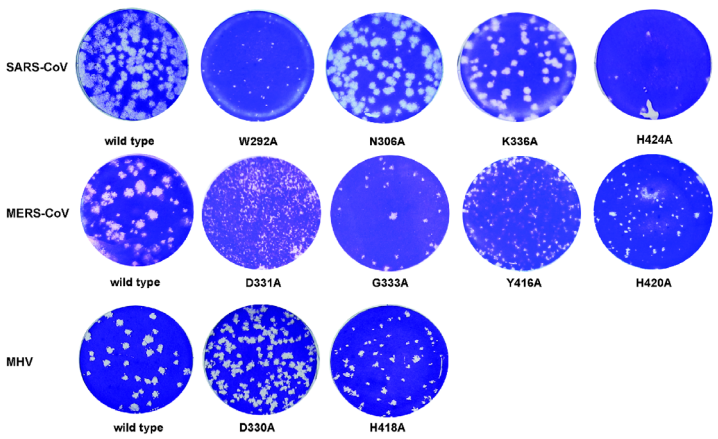

Fig. 6. Virological characterization of betacoronaviruses N7-MTase mutants. (A) Overview of the phenotype of CoV mutants that were evaluated by reverse engineering N7-MTase mutations into the genomes of SARS-CoV, MERS-CoV, MHV and SARS-CoV-2. The amino acid number indicated for each mutation refers to SARS-CoV nsp14. N.P., not performed. (B) Plaque phenotype of viable N7-MTase mutants. Plaque assays were performed using supernatants harvested from transfected cells at 3 (MERS-CoV and SARS-CoV) or 4 days (MHV) post transfection.

DISCUSSION

Most viral MTases belong to the Rossmann-fold family [52, 56], a ubiquitous higher-order structure among dinucleotide-binding enzymes [52, 57]. The CoV nsp14 N7-MTase was the first identified example of a non-Rossmann fold viral MTase [35, 36, 44], and the only one thus far for which some structural and functional information had been gathered. While some viral N7-MTase crystal structures have been resolved [35, 36, 58-60], their biochemical properties and signature sequences critical for RNA binding or enzymatic activity remain poorly defined compared to e.g. the 2'-O-MTases, an example of which is found in CoV nsp16 (reviewed in [6]).

Likewise, the biological role and relevance of the CoV N7-MTase have not been explored in much detail. In recent studies and reviews, often related to SARS-CoV-2, the enzyme is widely assumed to secure the translation of CoV subgenomic mRNAs and genome, which obviously is a critical step for any positive-stranded RNA virus. However, direct biochemical evidence showing that CoV mRNAs indeed carry an N7-methylated cap at their 5' end is still lacking. The presence of such a cap on CoV RNAs was first postulated following RNase T1 and T2 digestion studies with 32P-labeled MHV RNA, 40 years ago [61]. Additional support came from immunoprecipitation experiments using a cap-specific monoclonal antibody (recognizing both the rare nucleoside 2,2,7-trimethylguanosine and 7-methylguanosine (m7G) cap structures) that brought down the mRNAs of equine torovirus [62], a distant CoV relative for which – perhaps strikingly – an N7-MTase domain still remains to be identified [44]. The presence of enzymes required for capping in CoVs and many of their relatives [6, 17, 44, 63, 64] and the in vitro activity profile of recombinant CoV nsp14 [26, 27, 32, 33, 37, 38] lend additional credibility to CoV capping and cap methylation, but do not exclude the possibility that the CoV N7-MTase may target other substrates as well.

To enhance our overall understanding of nsp14 N7-MTase structure and function, also in the light of its emergence as an important drug target in the battle against SARS-CoV-2 [47, 65-67], we now revisited the SARS-CoV nsp14 X-ray structure to define the most likely residues involved in N7-MTase substrate binding and catalysis. Instead of a βαβ architecture (a seven-stranded β-sheet surrounded by 6 α-helices) and the canonical MTase motifs, the CoV N7-MTase incorporates 12 β-strands and 5 α-helices that form a five-stranded β-sheet core [36, 44]. The overall nsp14 structure reveals two domains interconnected by a hinge that may confer the flexibility needed to orchestrate the different functions of the protein during CoV replication [36]. Furthermore, the protein binds to nsp10, a critical co-factor for nsp14's ExoN activity [34, 68]. The conversion of a 5'-terminal GMP cap (GpppN) into a cap-0 structure (7mGpppN) involves multiple steps: stabilization of the RNA chain, SAM binding, methyl

transfer to the N7 position of the cap, release of the methylated RNA substrate, and SAH release. Our structural analysis identified several residues with their side chains pointing towards the catalytic pocket, which could be classified as likely RNA- or SAM-binding motifs (Fig. 3A). Taking into account the sequence conservation between MHV, SARS-CoV, SARS-CoV-2 and MERS-CoV (Fig. 2), we surmised these CoV N7-MTases to have an overall similar fold and structural organization. The impact of alanine substitutions of selected key residues in these motifs was then evaluated both in vitro, using recombinant nsp14, and in the context of the complete viral replication cycle, by engineering the corresponding virus mutants in different betacoronaviruses.

Although the biochemical and virological data presented in this study clearly provide support for the predictions from our structural analysis, the overall interpretation of the data set undeniably is much more complex than anticipated. Replacement of conserved SARS-CoV and MERS-CoV N7-MTase residues largely or completely abrogated enzymatic activity in vitro (Fig. 4C and 4D), supporting their identification as key residues for the enzyme's functionality. However, for several SARS-CoV and MERS-CoV mutations the data on enzymatic activity in vitro and virus mutant viability appeared to be at odds with each other (Fig. 4 and 6). One possible interpretation is that (very) low levels of N7-MTase activity may still suffice to support viral replication in cell culture models. Alternatively, the in vitro N7-MTase assays may have suffered from technical complications such as suboptimal or incorrect (mutant) protein folding in contrast to nsp14 expressed in the context of the virus and its different partner proteins. Mutations mapping to motif VI (hinge region), and for MERS-CoV also to motif III (G333A), yielded inconsistent results when comparing prior in vitro studies [26, 27, 32-35], which might be attributed (in part) to different in vitro assay conditions.

Such technical explanations, however, do not apply when introducing equivalent substitutions in different ß-CoVs and evaluating them in the context of the viral replication cycle. Also here apparent inconsistencies were observed in terms of the variable impact of certain mutations on the overall replication of virus mutants. The results obtained with mutations in motif III (the presumed SAM binding motif DxGxPxG/A) were a striking example: the viral phenotype for the D-to-A mutant (D331A in SARS-CoV, D330A in MHV) ranged from non-viable for SARS-CoV to wild type-like for MHV (Fig. 6). SARS-CoV residue D331 was first identified as important for N7-MTase activity by the superimposition of nsp14 with cellular N7-MTase structures [27]. However, a previous MHV study [43] had already documented that a D330A substitution did not affect MHV replication, and pointed to G332 as a more important residue in motif III, which was confirmed in this study (Fig. 6). These results are consistent with the SARS-CoV nsp14 crystal structure showing that residue G333 in the DxG motif (G332 in MHV) is in direct

contact with the SAM methyl donor [35], although apparently its replacement is not sufficient to render all ß-CoVs non-viable.

The only other N7-MTase position probed by reverse genetics so far was the conserved tyrosine in motif VI (Fig. 3B; Y414 in MHV). This residue attracted attention by the intriguing serendipitous finding that its replacement with histidine did not affect replication of MHV strain A59 in cell culture, but strongly reduced replication and virulence in mice [41]. Also, an Y414A substitution was tolerated in MHV-A59 [55], but in our study Y414A prevented the recovery of infectious progeny for MHV strain JHM, which exhibits less robust RNA synthesis and overall replication than MHV-A59. The results for the corresponding SARS-CoV (non-viable) and MERS-CoV (crippled) mutants were also variable, adding to the complexity of the overall picture.

A substantial set of N7-MTase mutations was monitored for 'side effects' at the level of ExoN activity (Fig. 5), although for SARS-CoV and MHV these would unlikely explain a lack of viability as ExoN knock-out mutants for both these viruses are only mildly crippled [42, 55, 69]. Strikingly, for MERS-CoV, which does not tolerate ExoN inactivation [38], two of the N7-MTase mutations (G333A in motif III and H420A in motif VI) abolished detectable ExoN activity in vitro (Fig. 5B), but still allowed a certain level of virus replication (small-plaque phenotype), an observation that clearly warrants further investigation. In more general terms, the ExoN biochemical assay (Fig. 5) suggested that the functional separation between the two enzyme domains may be less strict than previously concluded, as also recently hypothesized following an in silico analysis [70]. Alternatively, structural variation may explain the discrepancies observed. The impact of SARS-CoV N7-MTase motif-VI mutations on ExoN activity was major, highlighting the peculiar structural organization of nsp14, in which part of the N7-MTase substrate-binding cavity maps to the hinge that connects the N7-MTase and ExoN domains (Fig. 1). For other N7-MTase motifs probed, the functional separation from ExoN was confirmed, as also deduced from previous studies [27, 33, 35, 38].

In our ß-CoV reverse genetics studies, a consistent phenotype was observed only for N7-MTase mutants R310A (motif II, non-viable), H424A (motif VI, crippled), and F426A (motif VI, non-viable). SARS-CoV residue R310 was previously reported to play a role in SAM binding [33], whereas F426 was proposed to entrench and stabilize the guanosine's purine moiety in proximity of SAM [35]. Our analysis (Fig. 3B) redefined both residues as part of putative RNA binding site motifs II and VI, respectively, and they were found to be essential for in vitro N7-MTase activity in both SARS-CoV and MERS-CoV. Our results highlight the importance of nsp14 N7-MTase for CoV replication, but the variable impact of the replacement of several conserved residues suggests a substantial degree of conformational or functional flexibility in

the enzyme's active site. Other factors, such as interactions of nsp14 with other replicase subunits, may also contribute to the observed phenotypic differences between equivalent N7-MTase mutants of different ß-CoVs. Likewise, the translation of in vitro N7-MTase activity to virus viability is not straightforward and suggests complex structure-function relationships for the structurally unique CoV N7-MTase. Given both its essential role in CoV replication and its emerging status as a target for antiviral drug development efforts, it will be important to further expand the integrated biochemical and virological analysis to support the rational design of broad-spectrum inhibitors of the CoV N7-MTase.

MATERIALS AND METHODS

Bioinformatics analysis.

Forty-seven CoV nsp14 sequences were retrieved (a complete list is provided in Supplementary Table 1) and aligned using MAFFT [71]. Delineation of motif I to Vi was done manually using Seaview and WebLogo [72, 73]. Structure analysis (PDB: 5NFY; [36]), volume estimation, cavity determination and sequence conservation was plotted onto the structure using UCSF Chimera [74]. Electrostatic surface calculations were done using APBS [75]. Predicting the structural impact of mutations was done using the PoPMuSiC server (http://dezyme.com/en/software) [76]. This program introduces single-site mutations into a protein's structure and estimates the change in ΔΔGs values of such mutations. In the next step, all possible single-site mutations (4731 mutations) were sorted by their ΔΔGs, but only those in the conserved motifs in the vicinity of the catalytic pocket were used for further studies. PopMuSic predictions were cross-validated with SNAP2 to assess the impact of single amino acid substitutions on protein function [77].

Recombinant protein expression and purification.

Recombinant SARS- and MERS-CoV nsp10 and nsp14 were expressed in E. coli and purified as described previously [26], MERS-CoV-nsp14 [38, 46] and MERS-nsp10 [29, 78]. Vectors for mutant nsp14 expression were generated by QuikChange site-directed mutagenesis using Accuzyme DNA polymerase (Bioline) and verified by sequence analysis. For each recombinant protein used, two batches were produced and tested in enzymatic assays.

In vitro nsp14 N7-MTase activity assay.

Reaction mixtures contained 50 or 200 nM of SARS-CoV or MERS-CoV recombinant nsp14, 7 nM GpppACCCC synthetic RNA substrate, 40 mM Tris-HCl (pH 8.0), 10 mM DTT, 5 mM $MgCl_2$, 1.9 µM SAM, 0.1 µM 3H-SAM (Perkin Elmer). After a 30-min incubation at 30°C, the assay was

stopped by addition of a 10-fold volume of ice-cold 100 µM S-adenosyl-homocysteine (SAH; Thermo Fisher). Samples were spotted on DEAE filter mats (PerkinElmer) and washed twice with 10 mM ammonium formate (Sigma-Aldrich) (pH 8.0), twice with MilliQ water, and once with absolute ethanol (Sigma-Aldrich) (Bouvet, Debarnot et al. 2010), and MTase activity was quantified using a Wallac scintillation counter. To determine relative enzyme activities, the incorporation measurements for mutant proteins were normalized to values obtained with wild-type nsp14. Samples were measured in duplicate in each experiment.

In vitro nsp14 ExoN assay.

Synthetic RNA substrate H4 (Bouvet, Imbert et al. 2012) was radiolabeled at its 5' end using T4 polynucleotide kinase (Epicentre) and [γ-32P]ATP (Perkin Elmer) and used as substrate in ExoN activity assays. To this end, recombinant SARS-CoV or MERS-CoV nsp14 and nsp10 proteins were mixed in a 1:4 concentration ratio of nsp14:nsp10 as indicated in Fig. 5 and added to 750 nM radiolabeled substrate in their respective reaction buffer (40 mM Tris-HCl (pH 8), 1 mM MgCl2, 5 mM DTT for SARS-CoV; 40 mM Tris-HCl (pH 7.5), 5 mM MgCl2 and 1 mM DTT for MERS-CoV). Assays were performed at 37°C and stopped by addition of an equal volume of loading buffer containing 96% formamide and 10 mM EDTA. Samples were analyzed on 7 M urea-containing 14% (wt/vol) polyacrylamide gels (acrylamide/bisacrylamide ratio, 19:1) buffered with 0.5xTris-taurine-EDTA and run at high voltage (1,600 V). Results were visualized by phosphorimaging using a Typhoon-9410 variable-mode scanner (GE Healthcare).

Cell culture.

Baby hamster kidney cells (BHK-21; ATCC CCL10), Vero E6 (ATCC; CCL-81), HuH7 cells and mouse 17 Cl1 cells were grown as described previously [19, 38, 79, 80]. In order to amplify viral progeny and titrate recombinant CoVs by plaque assay, Vero E6 cells were used for SARS-CoV and SARS-CoV-2, HuH7 cells for MERS-CoV, and 17Cl1 cells for MHV. Cells were cultured in Eagle's minimal essential medium (EMEM; Lonza) with 8% fetal calf serum (FCS; Bodinco) supplemented with 100 IU/ml of penicillin and 100 µg/ml of streptomycin (Sigma) and 2 mM L-Glutamine (PAA Laboratories). After infection, complete EMEM medium containing 2% FCS was used.

Viruses and reverse genetics.

Mutations in the nsp14-coding region were engineered by two-step en passant recombineering in E. coli [81] using a bacterial artificial chromosome (BAC) vector with a full-

length cDNA copy of a ß-CoV genome. Virus isolates used were MERS-CoV strain EMC/2012 [82, 83]), SARS-CoV Frankfurt-1 [84], MHV-JHM-IA [85]}, and SARS-CoV-2 BetaCoV/Wuhan/IVDC-HB-01/2019 [86]. When designing mutations, an additional translationally silent marker mutations was introduced near the site of mutagenesis, in order to analyze possible reversion and rule out potential contaminations with parental virus. For each mutant, two independent BAC clones were obtained, verified by sequencing of the nsp14-coding region, and used for in vitro transcription (mMessage-mMachine T7 Kit; Ambion) and virus launching. Transfections with full-length RNA transcripts were performed as described before (Ogando, Zevenhoven-Dobbe et al. 2020). Briefly, 5 µg RNA was electroporated into BHK-21 cells using an Amaxa nucleofector 2b (program A-031) and Nucleofection T solution kit (Lonza). Transfected BHK-21 cells were mixed in a 1:1 ratio with cells susceptible to CoV infection: Vero E6 cells (for SARS-CoV and SARS-CoV-2), HuH7 cells for MERS-CoV, or 17Cl1 cells (for MHV). Cell culture supernatants were collected when full cytopathic effect was observed, or at 6 days post transfection and progeny virus titers were determined by plaque assay (van den Worm, Eriksson et al. 2012). Viral replication was also monitored by immunofluorescence microscopy using antibodies recognizing double-stranded RNA (dsRNA; [87]) and non-structural or structural CoV proteins [38, 80, 88]. To confirm the presence of the original mutations in viral progeny, supernatant from transfected cells was used to infect fresh cells, after which intracellular RNA was isolated with TriPure isolation reagent (Roche Applied Science). Next, the nsp14-coding region was amplified using standard RT-PCR methods and the purified amplicon was sequenced by Sanger sequencing. All work with live (recombinant) class-3 CoVs was done in a biosafety level 3 laboratory at Leiden University Medical Center.

ACKNOWLEDGMENTS

N.S.O. was supported by the Marie Skłodowska-Curie ETN European Training Network ‘ANTIVIRALS’ (EU Grant Agreement No. 642434). P.E.K. was the recipient of a scholarship from the Fundation “Méditerranée Infection”. This work was supported by the Fondation pour la Recherche Médicale (Aide aux Équipes) and the SCORE project (EU Horizon 2020 research and innovation program, grant agreement 101003627). We thank LUMC colleagues Tessa Nelemans, Brenda Bontes and Jessika Zevenhoven-Dobbe for excellent technical support.

SUPPLEMENTARY MATERIAL

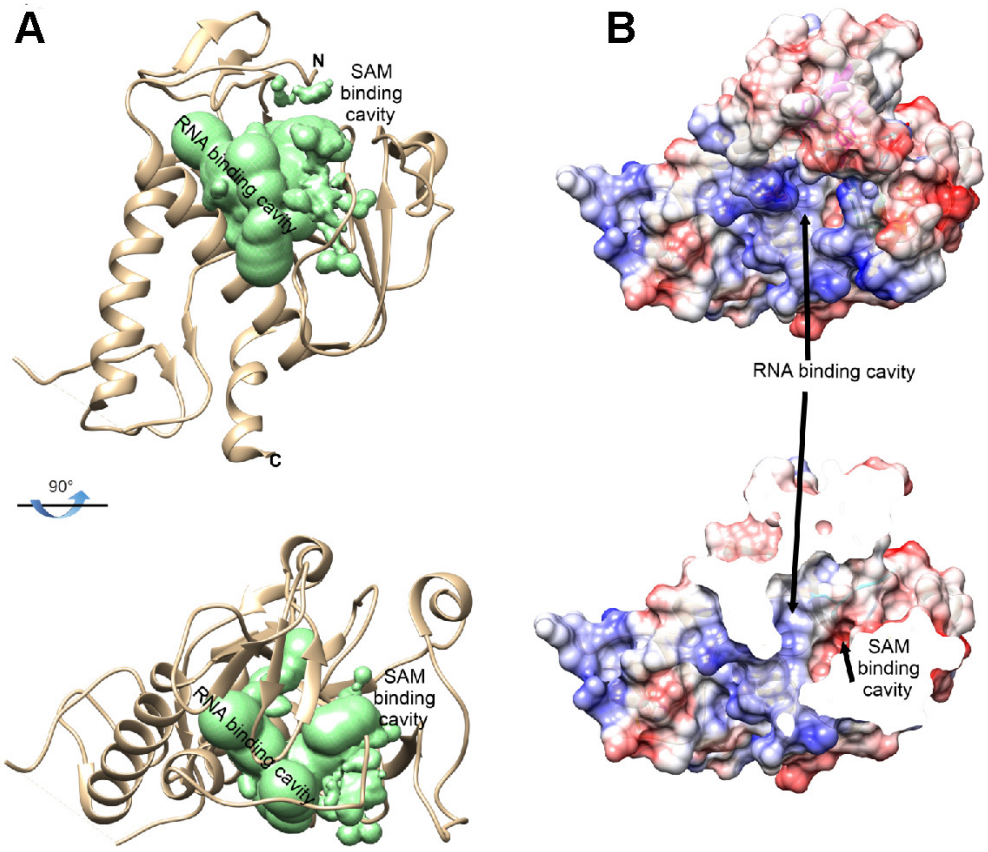

Fig. S1. Catalytic site of CoV nsp14 Hinge and N7-MTase domain structure analysis. A) Determination of the volume of the catalytic site (green bubble placing the mold of the cavity B) Electrostatic surface representation of CoV nsp14 Hinge and N7-MTase domain structure. Surface electrostatic potential calculated by APBS from - 10 (red) to + 10 (blue) kT/e.

Table S1- List of CoV genomes and accession numbers used to extract nsp14 sequences for structural studies

Virus	Acession number
Alphacoronavirus BtMs-AlphaCoV/GS 2013	A0A0U1WHG4
Avian infectious bronchitis virus (IBV)	P0C6Y2
Bat coronavirus 1A	YP_001718603.1
Bat coronavirus BM48-31	E0XIZ2
Bat coronavirus CDPHE15/USA/200 6	YP_008439224.1
Bat coronavirus HKU4	P0C6W3
Bat coronavirus HKU5	P0C6W4
Bat coronavirus HKU9	P0C6W5
Bat Hp- betacoronavirus	A0A088DIE1
Beluga whale coronavirus SW1	YP_001876435.1
Betacoronavirus Erinaceus	U5KNA9
Betacoronavirus HKU24	A0A0A7UXR0
Bovine coronavirus	P0C6W8
BtMr-AlphaCoV/ SAX2011	A0A0U1UZC3
BtNv-AlphaCoV/SC2013	YP_009201729.1
BtRf-AlphaCoV/HuB2013	YP_009199789.1
Camel *Alphacoronavirus*	ALA50136.1
Common moorhen coronavirus HKU21	H9BR34
Feline infectious peritonitis virus	AGZ84515.1
Ferret coronavirus	YP_009256195.1
Human coronavirus 229E (HCoV-229E)	P0C6X1
Human coronavirus HKU1 (HCoV-HKU1)	P0C6X2
Human coronavirus NL63 (HCoV-NL63)	P0C6X5
Lucheng Rn rat coronavirus	YP_009336483.1
Magpie-robin coronavirus HKU18	H9BR07
Middle East respiratory syndrome-related coronavirus	K9N7C7
Miniopterus bat coronavirus HKU8	YP_001718610.1
Mink coronavirus strain WD1127	YP_009019180
Munia coronavirus HKU13-3514	YP_002308505.1
Murine coronavirus (strain A59) (MHV- A59)	P0C6X9
Night heron coronavirus HKU19	H9BR16
Porcine *Deltacoronavirus*	A0A140ESF0
Porcine epidemic diarrhea virus	NP_839967
Rabbit coronavirus HKU14	H9AA60
Rat coronavirus Parker	YP_009924380.1
Rhinolophus bat coronavirus HKU2	A8JNZ0
Rousettus bat coronavirus	A0A1B3Q5W8
Rousettus bat coronavirus HKU10	AFU92103
Scotophilus bat coronavirus 512	YP_001351683
Severe acute respiratory syndrome coronavirus (SARS-CoV)	P0C6X7
Severe acute respiratory syndrome coronavirus-2 (SARS-CoV-2)	P0DTD1

Table S1.1- List of CoV genomes and accession numbers used to extract nsp14 sequences for structural studies

Virus	Acession number
Sparrow coronavirus HKU17	H9BQZ9
Swine acute diarrhea syndrome related coronavirus BtRf2	AVM80482.1
Thrush coronavirus HKU12	B6VDX7
Turkey coronavirus	YP_001941187
White-eye coronavirus HKU16	YP_005352837.1
Wigeon coronavirus HKU20	H9BR24

Table S2: Functional effects of mutations on nsp14 SARS-CoV, MERS-CoV, MHV predicted with SNAP2

	SARS-CoV	MERS-CoV	MHV	SARS-CoV	MERS-CoV	MHV	SARS-CoV	MERS-CoV	MHV	SARS-CoV	MERS-CoV	MHV
aa change	**W292**	**W292**	**W291**	**N306**	**N306**	**N305**	**R310**	**R310**	**R309**	**D331**	**D331**	**D330**
A	72	66	78	51	26 *	54	66	30 *	63	75	67	78
R	82	81	88	75	32 *	82				91	80	90
N	80	63	86				71	41	71	77	78	83
D	88	72	91	67	58	78	85	74	84			
C	59	62	69	48	22 *	58	65	18 *	63	73	65	76
Q	76	74	84	48	35 *	65	60	32 *	61	81	79	84
E	82	72	87	73	63	82	81	61	78	70	73	74
G	82	82	87	53	41	64	81	31 *	79	79	84	88
H	78	62	86	50	36 *	63	59	29 *	60	87	84	89
I	72	69	79	71	35 *	77	73	35 *	71	88	85	89
L	73	75	82	72	35 *	79	73	21 *	70	90	81	91
K	85	84	90	63	59	80	41	20 *	45	91	91	92
M	66	71	78	63	34 *	73	66	29 *	65	87	84	89
F	45	55	63	74	52	80	81	52	78	89	80	90
P	83	89	94	77	64	83	86	70	85	91	91	93
S	78	77	78	41	22 *	58	70	32 *	68	74	74	80
T	78	80	86	49	24 *	64	69	32 *	66	79	77	83
W				81	70	86	87	66	85	92	88	93
Y	29 *	50	52	70	54	77	79	53	77	90	83	91
V	71	60	78	67	26 *	76	74	38 *	72	87	83	88

All data are predicted above 70 % expected accuracy except for * above 53 % - Positive value indicates a destabilising effect - Negative value indicates a neutral effect

Table S2.1: Functional effects of mutations on nsp14 SARS-CoV, MERS-CoV, MHV predicted with SNAP2

	SARS-CoV	MERS-CoV	MHV	SARS-CoV	MERS-CoV	MHV	SARS-CoV	MERS-CoV	MHV	SARS-CoV	MERS-CoV	MHV
aa change	**K336**	**K336**	**K335**	**D352**	**D352**	**D349**	**N386**	**N382**	**N380**	**Y420**	**Y416**	**Y414**
A	31 *	20 *	39 *	34 *	63	73	60	45	56	71	66	74
R	-17 *	-20 *	-1 *	45	85	87	78	73	77	89	85	91
N	28 *	26 *	44	22 *	73	69				86	71	88
D	69	63	76				62	56	63	90	73	92
C	22 *	7 *	-16 *	27 *	57	69	60	15	57	61	54	64
Q	16 *	6 *	29 *	43	74	73	47	52	64	82	77	86
E	52	45	60	26 *	67	53	75	70	74	87	82	89
G	52	41	60	49	77	78	51	55	49	87	81	88
H	7 *	-6 *	19 *	21 *	74	80	63	51	63	59	70	78
I	-15 *	-70	-40 *	59	78	86	77	53	76	69	62	70
L	22 *	8 *	33 *	61	80	88	80	49	78	74	70	74
K				48	87	88	76	71	76	90	86	91
M	10 *	-39 *	18 *	55	78	84	74	52	73	78	72	79
F	52	41	55	23 *	71	87	81	67	80	42	47	40
P	62	30 *	69	72	89	89	71	76	82	88	91	94
S	22 *	13 *	36 *	29 *	65	65	44	31	42	85	69	86
T	26 *	13 *	39 *	34 *	69	69	51	30 *	33 *	86	79	88
W	67	56	67	66	81	90	87	78 *	86	68	71	71
Y	48	35 *	51	32 *	76	86	79	38 *	78			
V	22 *	8 *	32 *	53	76	83	75	41	75	68	49	70

All data are predicted above 70 % expected accuracy except for * above 53 % - Positive value indicates a destabilising effect - Negative value indicates a neutral effect

Table S2.2: Functional effects of mutations on nsp14 SARS-CoV, MERS-CoV, MHV predicted with SNAP2

	SARS-CoV	MERS-CoV	MHV	SARS-CoV	MERS-CoV	MHV	SARS-CoV	MERS-CoV	MHV
aa change	**N422**	**N418**	**N416**	**H424**	**H420**	**H418**	**F426**	**F422**	**F420**
A	66	33 *	69	63	62	64	56	59	67
R	81	72	84	74	26 *	35 *	83	81	85
N				63	70	65	82	79	83
D	64	65	79	84	86 *	85	89	88	90
C	61	41	66	64	20	64	48 *	39 *	50
Q	64	4 *	70	65	69	67	78	72	80
E	80	71	83	79	81	80	84	72	85
G	64	20 *	64	75	66	76	81	79	83
H	60	49	67				59	76	79
I	79	71	83	76	69	76	58 *	10 *	60
L	81	72	85	76	41	75	63	50	59
K	79	69	81	81	81	82	85	82	87
M	76	63	80	72	65	72	60	49	47
F	69	74	85	64	75	76			
P	84	76	87	90	90	90	89	87	91
S	52	-3 *	59	70	71	72	79	75	80
T	59	42	65	64	72	76	78	60	80
W	88	81	90	81	82	82	69	69	67
Y	79	71	83	65	70	67	49	49	49
V	78	65	81	71	54	72	62 *	37 *	65

All data are predicted above 70 % expected accuracy except for * above 53 % - Positive value indicates a destabilising effect - Negative value indicates a neutral effect.

REFERENCES

1. Ghosh, A. and C.D. Lima, *Enzymology of RNA cap synthesis.* Wiley Interdiscip Rev RNA, 2010. **1**(1): p. 152-72.
2. Ramanathan, A., G.B. Robb, and S.H. Chan, *mRNA capping: biological functions and applications.* Nucleic Acids Res, 2016. **44**(16): p. 7511-26.
3. Ferron, F., et al., *The viral RNA capping machinery as a target for antiviral drugs.* Antiviral Res, 2012. **96**(1): p. 21-31.
4. Shatkin, A.J., *Capping of eucaryotic mRNAs.* Cell, 1976. **9**(4 PT 2): p. 645-53.
5. Kindler, E. and V. Thiel, *To sense or not to sense viral RNA--essentials of coronavirus innate immune evasion.* Curr Opin Microbiol, 2014. **20**: p. 69-75.
6. Decroly, E., et al., *Conventional and unconventional mechanisms for capping viral mRNA.* Nat Rev Microbiol, 2011. **10**(1): p. 51-65.
7. Koonin, E.V. and B. Moss, *Viruses know more than one way to don a cap.* Proc Natl Acad Sci U S A, 2010. **107**(8): p. 3283-4.
8. Zhou, P., et al., *A pneumonia outbreak associated with a new coronavirus of probable bat origin.* Nature, 2020. **579**(7798): p. 270-273.
9. Gorbalenya, A., et al., *The species Severe acute respiratory syndrome-related coronavirus: classifying 2019-nCoV and naming it SARS-CoV-2.* Nat Microbiol, 2020. **5**(4): p. 536-544.
10. van der Hoek, L., *Human coronaviruses: what do they cause?* Antivir Ther, 2007. **12**(4 Pt B): p. 651-8.
11. Wang, Y., M. Grunewald, and S. Perlman, *Coronaviruses: An Updated Overview of Their Replication and Pathogenesis.* Methods Mol Biol, 2020. **2203**: p. 1-29.
12. Ge, X.Y., et al., *Isolation and characterization of a bat SARS-like coronavirus that uses the ACE2 receptor.* Nature, 2013. **503**(7477): p. 535-8.
13. Menachery, V.D., et al., *A SARS-like cluster of circulating bat coronaviruses shows potential for human emergence.* Nat Med, 2015. **21**(12): p. 1508-13.
14. Hu, B., et al., *Discovery of a rich gene pool of bat SARS-related coronaviruses provides new insights into the origin of SARS coronavirus.* PLoS Pathog, 2017. **13**(11): p. e1006698.
15. Cui, J., F. Li, and Z.L. Shi, *Origin and evolution of pathogenic coronaviruses.* Nat Rev Microbiol, 2019. **17**(3): p. 181-192.
16. Snijder, E.J., et al., *Unique and conserved features of genome and proteome of SARS-coronavirus, an early split-off from the coronavirus group 2 lineage.* J Mol Biol, 2003. **331**(5): p. 991-1004.
17. Snijder, E.J., E. Decroly, and J. Ziebuhr, *The Nonstructural Proteins Directing Coronavirus RNA Synthesis and Processing.* Adv Virus Res, 2016. **96**: p. 59-126.
18. Knoops, K., et al., *SARS-coronavirus replication is supported by a reticulovesicular network of modified endoplasmic reticulum.* PLoS Biol, 2008. **6**(9): p. e226.
19. Snijder, E.J., et al., *A unifying structural and functional model of the coronavirus replication organelle: Tracking down RNA synthesis.* PLoS Biol, 2020. **18**(6): p. e3000715.
20. Klein, S., et al., *SARS-CoV-2 structure and replication characterized by in situ cryo-electron tomography.* Nat Commun, 2020. **11**(1): p. 5885.
21. Seybert, A., et al., *The human coronavirus 229E superfamily 1 helicase has RNA and DNA duplex-unwinding activities with 5'-to-3' polarity.* RNA, 2000. **6**(7): p. 1056-68.

22. Ivanov, K.A. and J. Ziebuhr, *Human coronavirus 229E nonstructural protein 13: characterization of duplex-unwinding, nucleoside triphosphatase, and RNA 5'-triphosphatase activities.* J Virol, 2004. **78**(14): p. 7833-8.
23. Lehmann, K.C., et al., *Discovery of an essential nucleotidylating activity associated with a newly delineated conserved domain in the RNA polymerase-containing protein of all nidoviruses.* Nucleic Acids Res, 2015. **43**(17): p. 8416-34.
24. Yan, L., et al., *Cryo-EM Structure of an Extended SARS-CoV-2 Replication and Transcription Complex Reveals an Intermediate State in Cap Synthesis.* Cell, 2020.
25. Shannon, A., et al., *Protein-primed RNA synthesis in SARS-CoVs and structural basis for inhibition by AT-527.* bioRxiv, 2021: p. 2021.03.23.436564.
26. Bouvet, M., et al., *In vitro reconstitution of SARS-coronavirus mRNA cap methylation.* PLoS Pathog, 2010. **6**(4): p. e1000863.
27. Chen, Y., et al., *Functional screen reveals SARS coronavirus nonstructural protein nsp14 as a novel cap N7 methyltransferase.* Proc Natl Acad Sci U S A, 2009. **106**(9): p. 3484-3489.
28. Decroly, E., et al., *Coronavirus nonstructural protein 16 is a cap-0 binding enzyme possessing (nucleoside-2'O)-methyltransferase activity.* J Virol, 2008. **82**(16): p. 8071-84.
29. Chen, Y., et al., *Biochemical and structural insights into the mechanisms of SARS coronavirus RNA ribose 2'-O-methylation by nsp16/nsp10 protein complex.* PLoS Pathog, 2011. **7**(10): p. e1002294.
30. Denison, M.R., et al., *Coronaviruses: an RNA proofreading machine regulates replication fidelity and diversity.* RNA Biol, 2011. **8**(2): p. 270-9.
31. Ogando, N.S., et al., *The curious case of the nidovirus exoribonuclease: its role in RNA synthesis and replication fidelity.* Front Microbiol, 2019. **10**: p. 1813.
32. Jin, X., et al., *Characterization of the guanine-N7 methyltransferase activity of coronavirus nsp14 on nucleotide GTP.* Virus Res, 2013. **176**(1-2): p. 45-52.
33. Chen, Y., et al., *Structure-function analysis of severe acute respiratory syndrome coronavirus RNA cap guanine-N7-methyltransferase.* J Virol, 2013. **87**(11): p. 6296-6305.
34. Bouvet, M., et al., *RNA 3'-end mismatch excision by the severe acute respiratory syndrome coronavirus nonstructural protein nsp10/nsp14 exoribonuclease complex.* Proc Natl Acad Sci U S A, 2012. **109**(24): p. 9372-9377.
35. Ma, Y., et al., *Structural basis and functional analysis of the SARS coronavirus nsp14-nsp10 complex.* Proc Natl Acad Sci U S A, 2015. **112**(30): p. 9436-9441.
36. Ferron, F., et al., *Structural and molecular basis of mismatch correction and ribavirin excision from coronavirus RNA.* Proc Natl Acad Sci U S A, 2018. **115**(2): p. E162-E171.
37. Saramago, M., et al., *New targets for drug design: Importance of nsp14/nsp10 complex formation for the 3'-5' exoribonucleolytic activity on SARS-CoV-2.* bioRxiv, 2021: p. 2021.01.07.425745.
38. Ogando, N.S., et al., *The enzymatic activity of the nsp14 exoribonuclease is critical for replication of MERS-CoV and SARS-CoV-2.* J Virol, 2020.
39. Xie, L. and P.E. Bourne, *Detecting evolutionary relationships across existing fold space, using sequence order-independent profile-profile alignments.* Proc Natl Acad Sci U S A, 2008. **105**(14): p. 5441-6.

40. Gana, R., et al., *Structural and functional studies of S-adenosyl-L-methionine binding proteins: a ligand-centric approach.* BMC Struct Biol, 2013. **13**: p. 6.
41. Sperry, S.M., et al., *Single-amino-acid substitutions in open reading frame (ORF) 1b-nsp14 and ORF 2a proteins of the coronavirus mouse hepatitis virus are attenuating in mice.* J Virol, 2005. **79**(6): p. 3391-400.
42. Eckerle, L.D., et al., *High fidelity of murine hepatitis virus replication is decreased in nsp14 exoribonuclease mutants.* J Virol, 2007. **81**(22): p. 12135-12144.
43. Case, J.B., et al., *Mutagenesis of S-adenosyl-l-methionine-binding residues in coronavirus nsp14 N7-methyltransferase demonstrates differing requirements for genome translation and resistance to innate immunity.* J Virol, 2016. **90**(16): p. 7248-7256.
44. Ferron, F., et al., *A N7-guanine RNA cap methyltransferase signature-sequence as a genetic marker of large genome, non-mammalian Tobaniviridae.* NAR Genom Bioinform, 2020. **2**(1): p. lqz022.
45. Sun, Y., et al., *Yeast-based assays for the high-throughput screening of inhibitors of coronavirus RNA cap guanine-N7-methyltransferase.* Antiviral Res, 2014. **104**: p. 156-64.
46. Aouadi, W., et al., *Toward the identification of viral cap-methyltransferase inhibitors by fluorescence screening assay.* Antiviral Res, 2017. **144**: p. 330-339.
47. Ahmed-Belkacem, R., et al., *Synthesis of adenine dinucleosides SAM analogs as specific inhibitors of SARS-CoV nsp14 RNA cap guanine-N7-methyltransferase.* Eur J Med Chem, 2020. **201**: p. 112557.
48. He, R., et al., *Potent and selective inhibition of SARS coronavirus replication by aurintricarboxylic acid.* Biochem Biophys Res Commun, 2004. **320**(4): p. 1199-203.
49. Barnes, M.H., et al., *The 3'-5' exonuclease site of DNA polymerase III from gram-positive bacteria: definition of a novel motif structure.* Gene, 1995. **165**(1): p. 45-50.
50. Zuo, Y. and M.P. Deutscher, *Exoribonuclease superfamilies: structural analysis and phylogenetic distribution.* Nucleic Acids Res, 2001. **29**(5): p. 1017-1026.
51. Byszewska, M., et al., *RNA methyltransferases involved in 5' cap biosynthesis.* RNA Biol, 2014. **11**(12): p. 1597-607.
52. Chouhan, B.P.S., et al., *Rossmann-Fold Methyltransferases: Taking a "beta-Turn" around Their Cofactor, S-Adenosylmethionine.* Biochemistry, 2019. **58**(3): p. 166-170.
53. Saramago, M., et al., *New targets for drug design: Importance of nsp14/nsp10 complex formation for the 3'-5' exoribonucleolytic activity on SARS-CoV-2.* FEBS J, 2021.
54. Laskowski, R.A., *SURFNET: a program for visualizing molecular surfaces, cavities, and intermolecular interactions.* J Mol Graph, 1995. **13**(5): p. 323-30, 307-8.
55. Eckerle, L.D., et al., *Effects of mutagenesis of murine hepatitis virus nsp1 and nsp14 on replication in culture.* Adv Exp Med Biol, 2006. **581**: p. 55-60.
56. Medvedev, K.E., L.N. Kinch, and N.V. Grishin, *Functional and evolutionary analysis of viral proteins containing a Rossmann-like fold.* Protein Sci, 2018. **27**(8): p. 1450-1463.
57. Rao, S.T. and M.G. Rossmann, *Comparison of super-secondary structures in proteins.* J Mol Biol, 1973. **76**(2): p. 241-56.
58. Sutton, G., et al., *Bluetongue virus VP4 is an RNA-capping assembly line.* Nat Struct Mol Biol, 2007. **14**(5): p. 449-51.
59. Tao, Y., et al., *RNA synthesis in a cage--structural studies of reovirus polymerase lambda3.* Cell, 2002. **111**(5): p. 733-45.

60. Egloff, M.P., et al., *An RNA cap (nucleoside-2'-O-)-methyltransferase in the flavivirus RNA polymerase NS5: crystal structure and functional characterization.* EMBO J, 2002. **21**(11): p. 2757-68.
61. Lai, M.M. and S.A. Stohlman, *Comparative analysis of RNA genomes of mouse hepatitis viruses.* J Virol, 1981. **38**(2): p. 661-70.
62. van Vliet, A.L., et al., *Discontinuous and non-discontinuous subgenomic RNA transcription in a nidovirus.* EMBO J, 2002. **21**(23): p. 6571-80.
63. Seybert, A., et al., *A complex zinc finger controls the enzymatic activities of nidovirus helicases.* J Virol, 2005. **79**(2): p. 696-704.
64. Saberi, A., et al., *A planarian nidovirus expands the limits of RNA genome size.* PLoS Pathog, 2018. **14**(11): p. e1007314.
65. Pearson, L.A., et al., *Development of a High-Throughput Screening Assay to Identify Inhibitors of the SARS-CoV-2 Guanine-N7-Methyltransferase Using RapidFire Mass Spectrometry.* SLAS Discov, 2021: p. 24725552211000652.
66. Devkota, K., et al., *Probing the SAM Binding Site of SARS-CoV-2 nsp14 in vitro Using SAM Competitive Inhibitors Guides Developing Selective bi-substrate Inhibitors.* bioRxiv, 2021: p. 2021.02.19.424337.
67. Basu, S., et al., *Identification of SARS-CoV-2 Antiviral Compounds by Screening for Small Molecule Inhibitors of the nsp14 RNA Cap Methyltransferase.* bioRxiv, 2021: p. 2021.04.07.438810.
68. Bouvet, M., et al., *Coronavirus Nsp10, a critical co-factor for activation of multiple replicative enzymes.* J Biol Chem, 2014. **289**(37): p. 25783-25796.
69. Smith, E.C., et al., *Coronaviruses lacking exoribonuclease activity are susceptible to lethal mutagenesis: evidence for proofreading and potential therapeutics.* PLoS Pathog, 2013. **9**(8): p. e1003565.
70. Moeller, N.H., et al., *Structure and dynamics of SARS-CoV-2 proofreading exoribonuclease ExoN.* bioRxiv, 2021: p. 2021.04.02.438274.
71. Nakamura, T., et al., *Parallelization of MAFFT for large-scale multiple sequence alignments.* Bioinformatics, 2018. **34**(14): p. 2490-2492.
72. Gouy, M., S. Guindon, and O. Gascuel, *SeaView version 4: A multiplatform graphical user interface for sequence alignment and phylogenetic tree building.* Mol Biol Evol, 2010. **27**(2): p. 221-4.
73. Crooks, G.E., et al., *WebLogo: a sequence logo generator.* Genome Res, 2004. **14**(6): p. 1188-90.
74. Pettersen, E.F., et al., *UCSF Chimera--a visualization system for exploratory research and analysis.* J Comput Chem, 2004. **25**(13): p. 1605-12.
75. Jurrus, E., et al., *Improvements to the APBS biomolecular solvation software suite.* Protein Sci, 2018. **27**(1): p. 112-128.
76. Dehouck, Y., et al., *PoPMuSiC 2.1: a web server for the estimation of protein stability changes upon mutation and sequence optimality.* BMC Bioinformatics, 2011. **12**: p. 151.
77. Hecht, M., Y. Bromberg, and B. Rost, *Better prediction of functional effects for sequence variants.* BMC Genomics, 2015. **16 Suppl 8**: p. S1.
78. Wang, Y., et al., *Coronavirus nsp10/nsp16 methyltransferase can be targeted by nsp10-derived peptide in vitro and in vivo to reduce replication and pathogenesis.* J Virol, 2015. **89**(16): p. 8416-27.

79. Nedialkova, D.D., A.E. Gorbalenya, and E.J. Snijder, *Arterivirus Nsp1 modulates the accumulation of minus-strand templates to control the relative abundance of viral mRNAs.* PLoS Pathog, 2010. **6**(2): p. e1000772.
80. de Wilde, A.H., et al., *MERS-coronavirus replication induces severe in vitro cytopathology and is strongly inhibited by cyclosporin A or interferon-alpha treatment.* J Gen Virol, 2013. **94**(Pt 8): p. 1749-60.
81. Tischer, B.K., G.A. Smith, and N. Osterrieder, *En passant mutagenesis: a two step markerless red recombination system.* Methods Mol Biol, 2010. **634**: p. 421-430.
82. Almazan, F., et al., *Engineering a replication-competent, propagation-defective Middle East respiratory syndrome coronavirus as a vaccine candidate.* mBio, 2013. **4**(5): p. e00650-13.
83. Rabouw, H.H., et al., *Middle East respiratory coronavirus accessory protein 4a inhibits PKR-mediated antiviral stress responses.* PLoS Pathog, 2016. **12**(10): p. e1005982.
84. Pfefferle, S., et al., *Reverse genetic characterization of the natural genomic deletion in SARS-Coronavirus strain Frankfurt-1 open reading frame 7b reveals an attenuating function of the 7b protein in-vitro and in-vivo.* Virol J, 2009. **6**: p. 131.
85. Fehr, A.R., et al., *The nsp3 macrodomain promotes virulence in mice with coronavirus-induced encephalitis.* J Virol, 2015. **89**(3): p. 1523-36.
86. Thao, T.T.N., et al., *Rapid reconstruction of SARS-CoV-2 using a synthetic genomics platform.* Nature, 2020.
87. Weber, F., et al., *Double-stranded RNA is produced by positive-strand RNA viruses and DNA viruses but not in detectable amounts by negative-strand RNA viruses.* J Virol, 2006. **80**(10): p. 5059-5064.
88. van Hemert, M.J., et al., *SARS-coronavirus replication/transcription complexes are membrane-protected and need a host factor for activity in vitro.* PLoS Pathog, 2008. **4**(5): p. e1000054.

CHAPTER VI

6',6'-Difluoro-aristeromycin is a potent inhibitor of MERS-coronavirus replication

Natacha S. Ogando[1], Jessika C. Zevenhoven-Dobbe[1], Dnyandev B. Jarhad[2], Sushil Kumar Tripathi[2], Hyuk Woo Lee[3], Lak Shin Jeong[2], Eric J. Snijder[1], Clara C. Posthuma[1*]

[1] Molecular Virology Laboratory, Department of Medical Microbiology, Leiden University Medical Center, Leiden, The Netherlands

[2] Research Institute of Pharmaceutical Sciences, College of Pharmacy, Seoul National University, Seoul 08826, Korea

[3] Future Medicine Company Ltd, Seongnam, Gyeonggi-do 13449, Korea

* Present address: Netherlands Commission on Genetic Modification, Bilthoven, The Netherlands

Submitted to Microbiology Spectrum

ABSTRACT

The severe acute respiratory syndrome coronavirus 2 (SARS-CoV-2) pandemic has highlighted the lack of treatments to combat infections with human or (potentially) zoonotic CoVs. Thus, it is critical to develop antiviral compounds that either directly target CoV functions or modulate host functions involved in viral replication. Here, we demonstrate that low-micromolar concentrations of 6',6'-difluoro-aristeromycin (DFA), an adenosine nucleoside analogue, strongly inhibit the replication of Middle East respiratory syndrome coronavirus (MERS-CoV) in a cell-based infection assay. DFA was designed to target S-adenosylhomocysteine (SAH) hydrolase and, consequently, may affect intracellular levels of the methyl donor S-adenosylmethionine, which is used by two CoV methyltransferases involved in the capping of the 5'-end of the viral mRNAs. Passaging of wild-type MERS-CoV in the presence of DFA selected a mutant with a ~100-fold decreased DFA sensitivity. This drug-resistant population carried various amino acid substitutions in different viral nonstructural proteins (nsp), including mutations in the nsp12 and nsp13, the latter containing a nucleoside triphosphate hydrolase activity that has been implicated in CoV capping. Based on our results, we hypothesize that DFA directly or indirectly affects viral cap methylation, either by inhibiting the viral enzymes involved or by binding to SAH hydrolase. We also evaluated the antiviral activity of DFA against other *Betacoronavirus*, but found it to have limited impact on their replication, while being quite cytotoxic to the Calu-3 cells used for this comparison. Nevertheless, our results justify the further characterization of DFA derivatives as an inhibitor of MERS-CoV replication.

INTRODUCTION

Previously, the emergence of severe acute respiratory syndrome coronavirus (SARS-CoV; in 2003 in China) and Middle East respiratory syndrome coronavirus (MERS-CoV; in 2012 in Saudi Arabia) highlighted the potential pandemic threat posed by this type of zoonotic pathogens and the need to develop rapid response options to contain them [1-4]. Due to the severity of the diseases caused by SARS-CoV and MERS-CoV, and their potential for zoonotic transmission and global spread, both these agents received a priority status from the World Health Organization and other government agencies for the development of prophylactic and therapeutic treatment strategies [5, 6]. The current SARS-CoV-2 pandemic [7, 8] and its burden on public health worldwide further emphasize the critical nature of the quest for anti-CoV drugs with high clinical efficacy. Thus far, only remdesivir was approved for emergency treatment of COVID-19 patients in the United States of America, Europe, and Japan. Many drug classes currently are under evaluation as inhibitors of CoV replication, including both compounds directly targeting viral functions, like viral proteases and the RNA polymerase, and host factor-targeting inhibitors (reviewed in [9-12].

Coronaviruses are positive-stranded RNA (+RNA) viruses with a single genomic RNA of approximately 30 kb that is replicated in the cytoplasm of infected cells. Following entry, the 5'-capped viral genome is recognized and translated by host ribosomes to yield the replicase polyproteins pp1a and pp1ab [13]. Subsequently, these large precursors are processed into 16 individual nonstructural proteins (nsp 1 to 16), which are released following polyprotein cleavage by two or three internal proteases. Together, the nsps form a multi-enzyme complex that ensures the replication of the viral genome and the transcription of a set of subgenomic mRNAs (reviewed in [14, 15]). The enzymatic core of this complex is formed by the nsp12 RNA-dependent RNA polymerase (RdRp) that synthesizes RNA with the help of the auxiliary factors nsp7 and nsp8 [16, 17], the nsp13 helicase that unwinds RNA duplexes [18-20], and several other RNA-processing enzymes residing in nsp12-nsp16 (reviewed in [15, 21, 22]). These also include a 3'-to-5' exoribonuclease (nsp14-ExoN) that is thought to increase replication fidelity by correcting mismatches sustained during RNA synthesis (reviewed in [23-26]). The viral structural and accessory proteins, encoded by smaller open reading frames located in the 3'-proximal part of the genome, are expressed from a set of 5'-capped and 3'-polyadenylated subgenomic mRNAs (reviewed in [15, 22]). Apart from ensuring mRNA recognition during formation of the ribosomal preinitiation complex, the 5'-terminal cap structure protects the viral mRNAs from degradation by cellular ribonucleases and prevents detection by the host's intracellular pathogen recognition receptors, which would trigger innate immune responses (reviewed in [27]).

The CoV capping mechanism is thought to consist of four sequential reactions: (i) an RNA triphosphatase activity residing in nsp13 removes the γ-phosphate group from the 5'-triphosphorylated RNA [28, 29]; (ii) a guanosine monophosphate (GMP) is transferred to the 5'-diphosphate terminus by a yet to be confirmed guanylyltransferase (GTase)[30], which was recently proposed to reside in the N-terminal nucleotidyl transferase (NiRAN) domain of nsp12 [31]; (iii) the nsp14 methyltransferase (MTase) methylates the cap's 5'-terminal guanine at the N7-position, producing the so-called cap-0 structure, ^{7me}GpppN [32]; (iv) finally, a cap-1 structure is formed when nsp16, in complex with its nsp10 co-factor, methylates the ribose 2'-O-position of the first transcribed nucleotide of each viral RNA, converting ^{7me}GpppN into ^{7me}GpppN$_{2'me}$ [33]. Biochemical studies demonstrated that N7-methylation of the cap is a pre-requisite for its subsequent 2'-O-methylation by nsp16/nsp10 [34-36]. Given the central position of the RNA-synthesizing and capping machinery in the CoV replication cycle, each single component constitutes a potential target for direct-acting antiviral drug development.

As in cellular methylation reactions, S-adenosyl-L-methionine (SAM) is the most common methyl donor used by viral MTases, such as those present in CoV nsp14 and nsp16 [37, 38]. Thus, the identification of compounds that can interfere with viral mRNA capping, by either directly targeting viral MTases or indirectly affecting the concentrations of essential cellular metabolites, constitutes a viable strategy to develop broad-spectrum CoV inhibitors. S-Adenosyl-homocysteine (SAH) is released upon the transfer of the methyl group of SAM to a nucleic acid substrate by a SAM-dependent MTase. Consequently, accumulation of SAH can interfere with SAM-dependent MTase function due to product inhibition [39]. Inhibitors targeting S-Adenosyl-homocysteine (SAH) hydrolase have been reported as potential broad-spectrum antiviral drugs in different studies [40-42]. This hydrolase catalyzes the reversible conversion of SAH into adenosine and L-homocysteine, which both are then further metabolized for use in different cellular pathways [43, 44].

Recently, using cell-based assays for MERS-CoV, SARS-CoV, chikungunya and Zika virus replication, we described the inhibitory potential of a set of adenosine and selenoadenosine analogues [41]. These compounds were derived from aristeromycin, a well-known carbocyclic nucleoside compound that inhibits SAH hydrolase and exhibits anti-viral, anti-cancer and anti-toxoplasma activities (reviewed in [45]). These aristeromycin derivatives are nucleoside analogues designed to directly target viral RdRp activity and/or indirectly target the methylation of viral RNA by inhibiting the host SAH hydrolase [41]. From this library, we identified 6',6'-difluoro-aristeromycin (DFA) as the aristeromycin derivative that inhibited MERS-CoV replication most efficiently in cell-based assays [41]. In different cell lines, DFA inhibited MERS-CoV replication at low micromolar concentrations and could potently reduce

the progeny titers produced by MERS-CoV. Evaluation of the potential of DFA as a broad-spectrum antiviral compound revealed limited inhibition of the replication of different *Betacoronavirus* at non-cytotoxic concentrations. This suggests that DFA-based derivatives need to be developed to improve the antiviral activity of this compound class and reduce the cytotoxic side- effects.

RESULTS

DFA inhibits MERS-CoV replication at low-micromolar concentrations in different cell lines

DFA was part of a library of more than 80 adenosine and selenoadenosine analogues that was previously evaluated for its antiviral activity against MERS-CoV, SARS-CoV and mouse hepatitis virus (MHV) using cell-based cytopathic effect (CPE) reduction assays. From this analysis, DFA was identified as the most potent inhibitor of MERS-CoV and SARS-CoV replication, with EC_{50} values (half-maximum effective concentration) of 0.2 µM and 0.5 µM, respectively. The compound was found to be more effective in reducing the progeny titers of MERS-CoV than those of SARS-CoV, yielding reductions of more than 3 log_{10} and 1 log_{10}, respectively, when treating Vero cells with 1.2 µM of DFA [41]. We now evaluated the antiviral activity of DFA against MERS-CoV in more detail using two independent cell-based assays: a CPE-reduction assay and a dose response assay, using previously described protocols [46, 47].

Different cell lines of human (Huh7 and MRC-5) and non-human origin (Vero) were treated with increasing concentrations of DFA and infected with MERS-CoV at a low multiplicity of infection (MOI) of 0.01. Remdesivir (RDV) and chloroquine (CHO) were included as positive controls for inhibition of viral replication. The mean EC_{50} values in Vero cells for these control compounds, RDV and CHO, were 0.4 µM and 25 µM, respectively, similar to what was described previously [48, 49]. Using CPE reduction assays, EC_{50} values in the low-micromolar range were measured for DFA in each of the three cell lines: 0.2 µM in Vero cells, 5.2 µM in Huh7 cells, and 2.3 µM in MRC-5 cells (Fig. 1A-C). In cytotoxicity control studies, the corresponding CC_{50} values (the compound concentration resulting in 50% cytotoxicity) were calculated to be 3.6 µM in Vero, 64 µM in Huh7, and >100 µM in MRC-5 cells (Fig 1A-C). Differences between cell lines in sensitivity (cytotoxicity) to DFA treatment, as observed here, may reflect variation in SAH hydrolase expression (a target of DFA) or uptake and metabolization of the compound.

In order to analyze the inhibitory effect of DFA on MERS-CoV progeny production in more detail, a multiple-cycle dose response assay was performed. Cells were again infected at MOI 0.01, which was followed by treatment with an increasing dose of DFA, ranging from 0.05 to 50 µM. Infected cell culture supernatants were harvested at 48 h post infection (h p.i). and

viral progeny titers were determined by plaque assay in Vero cells. A dose-dependent reduction of viral progeny was observed, with a 4 to 5 log_{10} decrease following treatment with >1.2 µM of DFA in Vero cells, >2.4 µM in Huh7, and >12.5 µM in MRC-5, respectively (Fig. 1D-F). Similar or lower EC_{50} values than in the CPE reduction assay were calculated from these studies: 0.2 µM in Vero cells, ~0.8 µM in Huh7 cells, and 1.4 µM in MRC-5 cells. These results indicated that DFA exhibits a similar antiviral activity across multiple cell lines resulting in a consistent ~3.5 to 4-log_{10} reduction of MERS-CoV progeny titers.

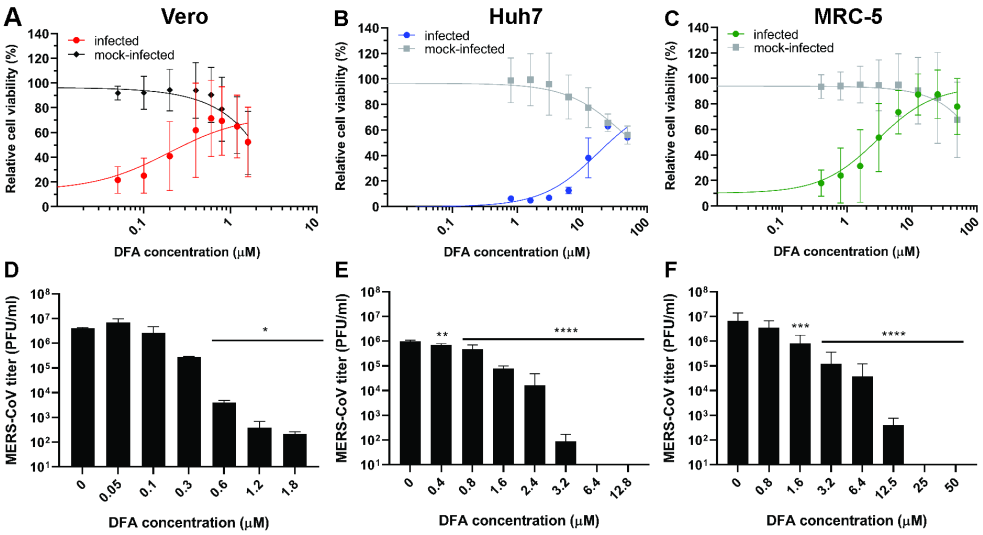

Fig. 1. DFA inhibits MERS-CoV replication in different cell lines. Vero (A and D), Huh7 (B and E) and MRC-5 (C and F) were treated with a two-fold dilution series of DFA in the low-micromolar range and infected with MERS-CoV. Inhibitory effect was evaluated by a CPE-reduction assay (A-C) or dose response assay (D-F). For the CPE-reduction assay, cell viability was assayed using the CellTiter 96 Aqueous One Solution cell proliferation assay (MTS assay) 3 d p.i.. The graphs show the results of at least two independent experiments (mean ± sd are shown). A non-linear regression analysis was applied. In the dose response assay, cell supernatants were collected after 2 d.p.i and viral progeny was titrated by plaque assay on Vero cells. Error bars represent standard deviation. Statistical significance was determined by one-way ANOVA. *, p<0.1; **, p<0.01; ***, p<0.001; ****, p<0.0001.

Having established the strong inhibition of MERS-CoV replication by DFA, we also tested its monophosphoramidate pro-drug (pDFA; Fig. 2A) in a CPE-reduction assay. This compound was synthesized in order to circumvent the rate-limiting first phosphorylation step that presumably restricts the efficient metabolization of nucleoside analogues like DFA following their uptake by the cell (reviewed in [50]). Unfortunately, in this case the pro-drug was less

active than DFA itself, independent of the cell line used (Fig. 2B). Although the chemical and structural modifications of the prodrug decreased its cytotoxicity, the calculated EC_{50} values, 9 µM in Vero cells and 36 µM in MRC-5 cells, were more than 10 times higher than the ones measured for DFA (Fig. 1). Therefore, pDFA was not included in subsequent experiments.

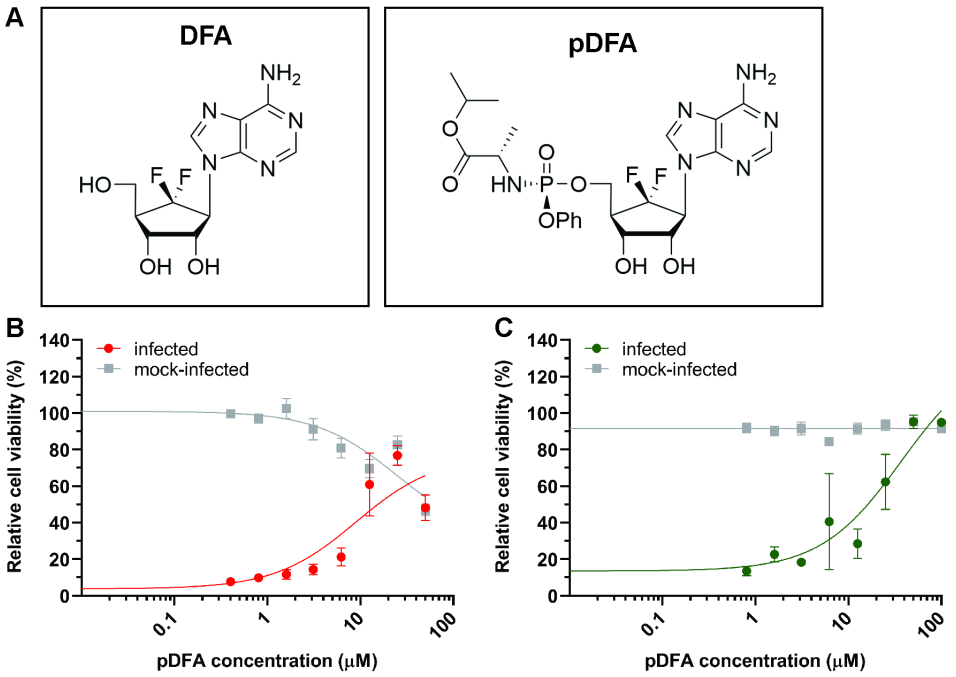

Fig. 2. DFA prodrug inhibits MERS-CoV replication. (A) DFA and pDFA schematic structure. pDFA antiviral activity was evaluated by a CPE-reduction assay. (B) Vero or (C) MRC-5 cells were treated with two-fold serial dilution of pDFA and infected with MERS-CoV. After 3 d p.i., cell viability was measured using the CellTiter 96 Aqueous One Solution cell proliferation assay (MTS assay). The graphs show the results of two independent experiments (mean ± sd are shown). A non-linear regression analysis was applied.

DFA inhibits the early stage of MERS-CoV replication

To characterize the mechanism of action of DFA in more detail, a time-of-addition assay was performed to determine which stage of the viral replication cycle was inhibited by the compound. For this purpose, Vero or MRC-5 cells were infected with MERS-CoV at high MOI (3 PFU/cell) and treated with DFA at different time points pre and post infection at a concentration equaling 4 times the EC_{50}. We observed inhibition of replication when the compound was administered before infection and at time points up to 4 h p.i. in Vero (Fig. 3A) and 8 h p.i. in MRC-5 (Fig. 3B). In Vero cells, a 2 log_{10} reduction of progeny virus titers was

observed when the compound was administered between 24 h before infection and 1 h p.i. In MRC-5 cells, DFA treatment led to a larger decrease of viral progeny production, >3 log_{10}, when treatment was started up to 4 h p.i. At the DFA dosage used, no cytotoxicity was detected in either cell line (data not shown). Replication kinetics of MERS-CoV is similar in Vero and MRC-5 cells [51, 52]. Thus, the different levels of progeny titer reduction observed between the two cell lines may be explained by variation in uptake or metabolic conversion of the compound [53]. In any case, these results demonstrated that DFA inhibits an early stage of MERS-CoV replication.

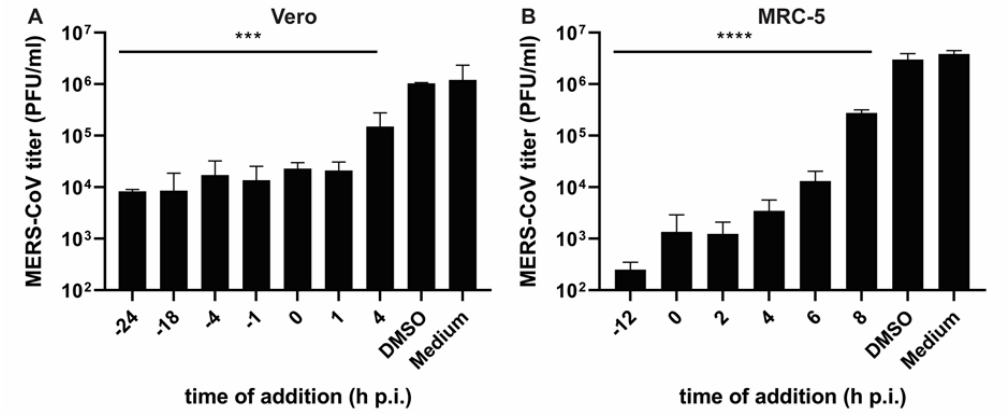

Fig. 3. DFA inhibits early steps of MERS-CoV replication. Vero (A) and MRC-5 (B) cells were treated with 0.6 and 12.5 µM, respectively, at the indicated time points pre- and post-infection. Viral progeny in supernatant harvested at 16 h p.i. was determined by plaque assay in Vero cells. The data represent the results from duplicates of 2 independent experiments. Error bars represent standard deviations. Statistical significance was determined by one-way ANOVA.; *, p<0.1; **, p<0.01; ***, p<0.001; ****, p<0.0001.

Selection of MERS-CoV mutants with 100-fold increased DFA resistance

In order to explore the mode of action of DFA, we selected for compound-resistant MERS-CoV mutants. For this purpose, wild-type MERS-CoV (wtP0) was serially passaged 10 times in MRC-5 cells in the presence of increasing DFA concentrations (from 2.5 µM up to 45 µM). In each passage, two controls were taken along: untreated cells infected with wt virus to monitor for cell culture adaptations (referred to as 'untreated wt'), and mock-infected cells treated with the corresponding concentration of DFA to assess compound cytotoxicity. Development of CPE was monitored microscopically, and plaque phenotype and viral progeny production were evaluated by plaque assay after each passage. From passage 8 (P8) onwards, two of the three independently generated lineages showed no increased CPE compared to uninfected, DFA-

treated control cells, meaning that these virus populations could not replicate in the presence of DFA concentrations above 35 µM, which were used in these later passages. When P8 virus from lineages 1 or 2 was tested in a CPE-reduction assay, no increased DFA resistance was noticed compared to an untreated wt virus control (data not shown). In contrast, lineage 3 (L3) virus did show clear signs of developing DFA resistance. After 10 passages, infection of cells with L3P10 virus in the presence of 45 µM DFA led to full CPE, which developed equally fast as for the untreated wt control. When L3P10 virus was tested in a dose response assay, only a small (<0.5 $\log_{10}$) effect of DFA treatment on viral progeny production was observed in the presence of up to 100 µM of DFA (Fig. 4A). When compared to untreated wt (wtP10) or parental virus (wtP0), L3P10 virus displayed a more than 100-fold increased drug resistance, with an EC_{50} value >100 µM against 0.8 µM for wtP10 and 0.4 µM for wtP0.

In order to assess if the increased DFA resistance of L3P10 affected its replication kinetics in comparison to the wt control, multi-cycle infections of MRC-5 cells were performed. The two viruses showed similar growth kinetics (Fig. 4B) with peak titers of 6.1×10^6 PFU/ml (wt) and 7.5×10^6 PFU/ml (L3P10) at 48 h p.i. Taken together, the replication kinetics and strongly increased DFA resistance suggested that, during serial passaging in the presence of DFA, the L3P10 virus population had acquired mutations that account for a strongly increased resistance to the compound.

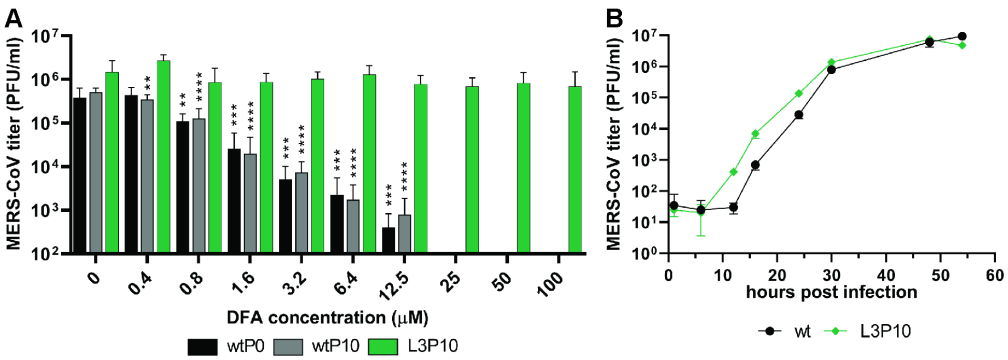

Fig. 4. Resistant MERS-CoV mutants selected by passaging in the presence of DFA. Replication in MRC-5 cells of a DFA-resistant virus population (L3P10) in the presence of increasing concentrations of DFA, compared to the parental virus (wtP0) and untreated wt virus (wtP10). Cells were infected with MOI 0.01 and virus progeny in supernatant harvested at 48 h p.i. The data represent the results from four replicates obtained in 2 independent experiments. (B) Characterization of growth kinetics of selected resistant mutant (L3P10). MRC-5 cells were infected with MOI 0.01 and supernatants were harvested at indicated time points from triplicate wells. Viral progeny titers were determined by plaque assay in Vero cells (mean ± sd is presented). Statistical significance was determined by one-way ANOVA. *, p<0.1; **, p<0.01; ***, p<0.001; ****, p<0.0001.

Mutations in the L3P10 virus population implicate DFA in the inhibition of viral capping

In order to identify mutations that contribute to DFA resistance, we sequenced the wtP10 and L3P10 virus population by Illumina next-generation sequencing. Subsequently, sequencing reads were mapped to the reference sequence of MERS-CoV strain EMC/2012 (NC_019843.3; [3]). Sequence variants constituting less than 10% of the total population of viral reads were excluded from further analysis. The short read length (150 nucleotides) did not allow us to determine which mutations were combined in the same genome. A total of 14 mutations was identified: five synonymous and nine non-synonymous mutations distributed across genes encoding nine different viral proteins. Translationally silent mutations were considered unlikely to be relevant for the phenotypic profile of L3P10 and disregarded for further analysis. As shown in Table 1, the majority of the identified non-synonymous mutations were present in only part of the viral population (in 37% to 55% of the total reads), suggesting a complex pattern of virus evolution with DFA resistance possibly relying on (different) combinations of mutations. Only L3P10 mutations leading to amino acid substitutions in the viral replicase (nsp1 to nsp16) were considered to possibly be associated with DFA resistance, as accessory proteins like that encoded by ORF5 are not essential for viral replication in cell culture ([54] and reviewed in [55]). The CoV spike protein is involved in receptor recognition and viral entry [56] and therefore an unlikely target for inhibition by nucleoside analogues. A G12033 to A mutation in the nsp7-coding region and a C21068 to T mutation in the nsp16-coding region resulting in a D73N and L156F substitution, respectively, were also identified in untreated wtP10 and therefore concluded to result from cell culture adaptation. The remaining mutations that should be considered mapped to nsps 1, 3, 12 and 13 (Table 1).

As DFA is a nucleoside analog and was designed as a dual-target inhibitor of RdRps and (indirectly) MTases [41], we were particularly interested in mutations identified in viral enzymes involved in RNA synthesis and capping. Therefore, we considered three nonsynonymous substitutions most likely to contribute to the observed DFA-resistance of the L3P10 virus population: Y218F in the nsp12-NiRAN domain, and R22K and R161H in the nsp13 ZBD-helicase subunit (Table 1). Recently, the nsp12 NiRAN domain was proposed to function as the capping GTase [31] while nsp13 is thought to be involved in the CoV capping mechanism (see Introduction; reviewed in [30]). Therefore, we hypothesize that DFA treatment affects the MERS-CoV capping mechanism and - consequently – overall virus replication, although we cannot exclude the possibility that there are multiple ways to acquire resistance to DFA.

Table 1- Summary of non-synonymous mutations identified in MERS-CoV L3P10 by NGS

Coding region	nt change	aa change	Domain	Presence in L3P10 (NGS)
nsp1	G795C	D172H	CTD	55%
nsp3	C6777T	R1314C	PLnc	37%
nsp7	G12033A*	D73N		>99%
nsp12	A14061T	Y218F	NiRAN	48%
nsp13	G16272A	R22K	ZBD	49%
	G16689A	R161H	1B	40%
nsp16	C21068T*	L156F	2'-O-MTase	>99%
spike	T24085_24086*ins*ACTCAACAGGTG	P876_*V877insTQQV*		37%
ORF5	G26927_26928T	Not in frame		48%

nt, nucleotide; aa, amino acid; CTD, C-terminal domain; PLnc, papain-like noncanonical domain; NiRAN, Nidovirus RdRp associated nucleotidyl transferase domain; ZBD, Zinc binding domain; 1B, 1B domain of helicase; * also present in wtP10 control

Evaluation of DFA potential as a pan-coronaviral inhibitor

Taking into account the lack of antivirals against SARS-CoV-2 and the capacity of DFA to inhibit both SARS-CoV and MERS-CoV replication, we decided to explore the potential of DFA as a broad-spectrum antiviral. To this end, Calu-3 cells, a human lung cell line that supports MERS-CoV, SARS-CoV and SARS-CoV-2 replication [57, 58], were treated with increasing concentrations of DFA and infected with each of these viruses in a dose response assay. By using the same cell line for each of these CoVs, differences in DFA up-take or metabolic conversion to its triphosphate form were eliminated. The results showed a dose-dependent decrease in the production of viral progeny for MERS-CoV (Fig. 5A) and SARS-CoV-2 (Fig. 5C) that follows the cytotoxicity of the compound. At a DFA concentration of 3.2 µM, only a small reduction of MERS-CoV and SARS-CoV-2 progeny was observed, 0.5 to 1$\log_{10}$. Surprisingly, the antiviral activity of DFA against MERS-CoV in Calu-3 cells was severely reduced when compared to results obtained in other cell lines, including another human lung cell line MRC-5 (Fig. 1D-F). In the case of SARS-CoV infection, a minor inhibitory effect was observed at concentrations that appeared to be somewhat cytotoxic (Fig. 5B and 5D), contrary to what was demonstrated in Vero E6 cells ([41] and Table 2). Unfortunately, in Calu-3 cells cytotoxicity was detected at low compound concentrations (>6.2 µM) and the inhibitory

effects observed could thus be associated with an overall decrease in relative cell viability. This indicates that the design of improved DFA derivatives is needed to decrease cytotoxicity and improve inhibitory potency.

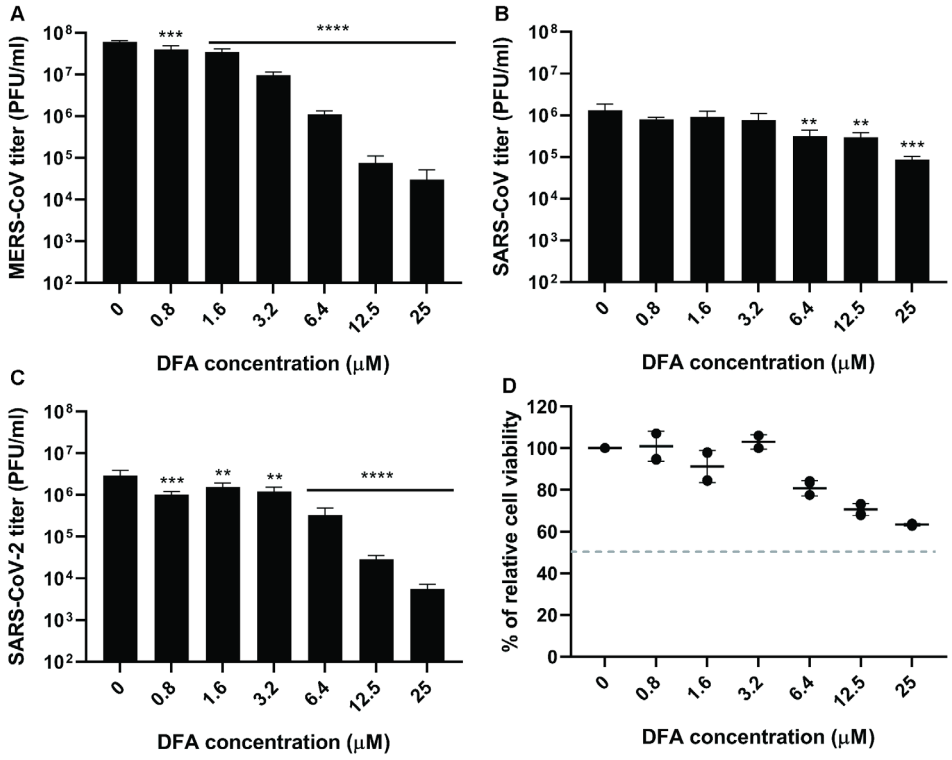

Fig. 5. DFA antiviral activity is reduced in Calu-3 cells. Calu-3 cells were infected with MERS-CoV (A), SARS-CoV (B) and SARS-CoV-2 (C) in the presence of various concentrations of DFA. An MOI of 1 was used, based on titrations of virus stocks on Vero cells. Progeny virus titers in supernatants harvested at 24 h p.i. were determined by plaque assay in Vero cells. (D) Cytotoxicity of DFA was measured in mock-infected cells, and was determined at 24 h p.i. in a CPE-reduction assay by use of the CellTiter 96 Aqueous One Solution cell proliferation assay (MTS assay). The data represent triplicates of 2 independent experiments and error bars show standard deviations. Statistical significance was determined by one-way ANOVA. No*, no significance; *, p<0.1; **, p<0.01; ***, p<0.001; ****, p<0.0001.

Table 2 – The antiviral effect of DFA on the replication of different β-CoVs.

Virus	Cell line	EC_{50} (µM)	CC_{50} (µM)	SI
MERS-CoV	Vero	0.2	>3.2	>16
	HuH7	0.6	>50	>80
	MRC-5	0.8	>50	>60
	Calu-3	~2	>25	>12
SARS-CoV	Vero E6*	0.5	>5	>10
	Calu-3	~5	>25	>5
SARS-CoV-2	Calu-3	~2	>25	>12

EC_{50}s values were calculated based on results obtained in dose response assay, while CC_{50}s values were determined in a cell viability assay as described in materials and methods. SI, selectivity index was calculated by comparing CC_{50} with EC_{50} values. *as described in [41]

DISCUSSION

This study describes that treatment with low-micromolar concentrations of DFA exhibit a strong antiviral effect on MERS-CoV replication in cell culture-based infection models (Fig. 1). Time-of-addition assays indicated that DFA reduced MERS-CoV progeny production when cells were treated prior to, at the time of, or within 4 h after infection (Fig. 3), suggesting that DFA interferes with the early stage of replication. Propagation of MERS-CoV in the presence of DFA led to the selection of a virus population with strongly enhanced resistance to this compound (Fig. 4). Subsequent sequence analysis revealed a potentially complex pattern of resistance evolution, exhibiting multiple mutations that are present in only part of the virus population, including several that map to enzymes involved in viral RNA synthesis and mRNA capping (Table 1).

DFA was originally designed to target the host SAH hydrolase directly and was demonstrated to inhibit this enzyme *in vitro* with an IC_{50} (50% inhibitory concentration) of 1.06 µM [41]. The compound is a carbocyclic adenosine analogue based on the parental inhibitor aristeromycin [59, 60], which was further modified by incorporation of a difluorine group at the 6' (top) position of its sugar ring ([41] and Fig. 2A). This modification improved the binding affinity of the compound for human SAH hydrolase and, consequently, the inhibition of its enzymatic activity.

Previous studies demonstrated that treatment of cells with high-affinity SAH hydrolase inhibitors, such as neplanocin A and aristeromycin, increases the intracellular SAH concentration, preventing the metabolic conversion of SAH to adenosine and L-homocysteine (reviewed in [61]). Therefore, SAH hydrolase inhibitors reduce or deplete the intracellular

pools of homocysteine and adenosine, the latter being produced exclusively by SAH hydrolysis. As the SAM methyl donor is formed via homocysteine trans-sulfuration or the adenosine kinase pathway, SAH hydrolase regulates the intracellular SAM levels and consequently the cell's SAM-dependent methylation reactions. Moreover, SAH accumulation can also reduce the activity of SAM-dependent methyltransferases by feed-back inhibition, as SAH can bind to their active site with higher affinity than SAM itself [39].

A correlation between the antiviral effect of adenosine analogues and their ability to interfere with viral capping has been demonstrated in previous studies with chikungunya virus, dengue virus, West Nile virus and vaccinia virus [62-65]. Both CoV methyltransferases use SAM as a methyl donor for their enzymatic activity [36, 66, 67]. Thus, SAH hydrolase inhibition and reduced SAM concentrations may impact, if not block, their activity. Previous studies with 5'-β-fluoroadenosine and derivatives of aristeromycin demonstrated that inhibition of SAH hydrolase affects viral replication by reducing RNA methylation (reviewed in [61]). Moreover, neplanocin A, another SAH hydrolase inhibitor, was proved to bind to methionine and prevent SAM production. Consequently, this leads to a block of 2'-O-methylation up to 60% (reviewed in [68]). Biochemical analysis of the MERS-CoV nsp16/nsp10 complex showed the capacity of this enzyme complex to bind SAH with greater affinity than SAM [34] , whereas superimposition of the SARS-CoV nsp16/nsp10 in complex with SAH demonstrated that the same binding site is used by both substrates [69]. In addition, increased SAH concentrations reduced the 2'-O-methylation of N7-methylated substrates [34, 67]. In a similar manner, inhibition of the CoV capping pathway is a likely mode of action (MoA) of DFA, although the genotypic profile of the L3P10 virus population does not exclude the possibility that DFA may inhibit CoV replication using multiple mechanisms. As the identified mutations have not been characterized in structural or biochemical studies, one can only speculate about their potential role in viral replication and DFA resistance. However, it is striking that, with the exception of nsp1-D172H and nsp3-R1314C, they all map to replicase subunits that have been implicated in viral capping: nsp12 (Y218F) and nsp13 (R22K and R161H). The capping GTase role of the nsp12-NiRAN domain was (only recently) proposed following structural and biochemical studies [31], and is still a matter of debate [70, 71]. Based on the SARS-CoV-2 nsp12 structure, the identified Tyr to Phe change (Y218F in MERS-CoV) is located in the proposed interaction interface with nsp9, next to two residues of nsp12 (D218 and R116 in SARS-CoV-2) that form close contacts with the β-phosphate of the GDP, according to the recently acquired cryo-EM structure of a mini-RTC (nsp7/nsp8/nsp9/nsp12/nsp13 complex) [31]. The nsp13 mutations R22K and R161H represent (semi)conservative replacements of residues in the N-terminal Cys/His-rich zinc-binding domain (ZBD) and domain 1B of the

helicase, respectively, according to the MERS-CoV nsp13 crystal structure (pdb 5WWP; [72]). These regions are known to be important for nsp13's interactions with other RTC components and for protein flexibility [72, 73]. In addition, helicase domain 1B constitutes the RNA-binding channel.

An additional passage of L3P10 in the presence of 45 µM of DFA (yielding L3P11) yielded a population with a similar genetic profile albeit with an additional disruptive single-nucleotide insertion in ORF4. A similar stable presence of multiple (potential) resistance mutations in part of the population has been observed for viruses treated with other mutagenic agents too [74-76]. Further phenotypical and mechanistic studies will be needed to better understand the mode of action of DFA. Additionally, cloning of L3P10 viruses by plaque picking could help to define the combination(s) of mutations that are the basis for DFA resistance, by evaluating their frequency of occurrence and associated replication and plaque phenotype. Unfortunately, time restrictions prevented us from extending our studies to understand which mutations identified in the L3P10 population may contribute to DFA resistance.

As a nucleoside analogue, DFA was considered to be a potential RdRp inhibitor. This would require uptake by the cell's nucleoside transporters, and subsequent phosphorylation into a triphosphorylated product that could be incorporated into the RNA chain during viral RNA synthesis (reviewed on [50]). In order to improve absorption of the compound by the cells and metabolism into its active form, a prodrug of DFA was synthesized and its antiviral activity was evaluated. In theory, the monophosphoramidate mask would promote the second phosphorylation to occur once the compound enters the cytoplasm by circumventing the rate-limiting step of the first phosphorylation. However, when compared to DFA, the EC_{50} of the prodrug was more than 10 times higher (Fig. 2), in contrast to results obtained with prodrugs of other nucleoside analogues [49, 77]. In previous work, structure-activity studies and tests of several purine and pyrimidine analogues of DFA suggested that DFA is most likely not targeting the RdRp [41, 64, 78]. This notion is also supported by the fact that the genotypic profile obtained for L3P10 did not reveal mutations in the RdRp domain of nsp12.

Currently, there is a lack of antiviral drugs with proven efficacy against human CoV infections, including the MERS-CoV that is endemic in the Middle East, the current pandemic SARS-CoV-2 and potential future zoonotic CoV. This highlights the importance to investigate new drug targets and identify antiviral compounds with potential broad-spectrum activity against CoVs. Previous reports demonstrated that SAH hydrolase inhibitors are active against different DNA viruses (in particular poxviruses), double-stranded RNA viruses (reoviruses), (–)RNA viruses (bunya-, arena-, rhabdo-, filo-, ortho- and paramyxoviruses) and (+)RNA viruses like alpha- and flaviviruses [63, 64, 79-83]. This type of compounds, that mainly targets cellular proteins,

usually exhibits a broader antiviral spectrum, but has a higher likelihood of being toxic. The cell-dependent antiviral activity of DFA against MERS-CoV emphasizes the importance of comparing different cell lines when testing compounds that can target cellular factors. In this study, we demonstrate that DFA can inhibit the replication of MERS-CoV, but that the design and development of DFA-based derivatives will be required to reduce cytotoxic side effects. Combining our results in this study with our previous report [41], showing that DFA can inhibit chikungunya and Zika virus, DFA appears to be an interesting compound for further development as a broad-spectrum antiviral agent.

MATERIALS AND METHODS

Cell culture and viruses

Vero cells were a kind gift from the Department of Viroscience, Erasmus Medical Center, Rotterdam, the Netherlands, and Huh7 cells were provided by Dr. Ralf Bartenschlager, Heidelberg University, Germany. Vero, Vero E6 and Huh7 were cultured as described before [51, 84, 85]. MRC-5 cells (ATCC CCL-171) were maintained in Eagle's minimum essential medium (EMEM; Lonza) supplemented with non-essential amino acids (PAA), 8% fetal calf serum (FCS; Bodinco), 100 units/ml penicillin (Lonza), 100 units/ml streptomycin (Lonza) and 2 mM L-glutamine (PAA). Calu-3 cells (ATCC HTB-55) were cultured in EMEM medium complemented with 10% FCS, penicillin/streptomycin, 2 mM L-glutamine, non-essential amino acids and sodium pyruvate (Life technologies). All cells were incubated at 37°C with 5% CO_2. Infections were carried out in EMEM containing 25 mM HEPES (Lonza), 2% FCS, penicillin/streptomycin and L-glutamine (nominated from now on as EMEM-2%FCS). MERS-CoV (strain EMC/2012; [3, 4]), SARS-CoV (Frankfurt-1 strain,[86]) and SARS-CoV-2/Leiden-0002 (GenBank accession nr. MT510999; [87]) were used for infections with wild type virus. CoV infections were performed inside biosafety cabinets in a certified biosafety level 3 (BSL3) facilities at Leiden University Medical Center.

Compounds

6',6'-Difluoro-aristeromycin (DFA) and its adenine phosphoramidate pro-drug (pDFA) were designed and synthesized, designated as 2c and 3a, respectively, as described in a previous report [41]. Different batches of powder were dissolved in DMSO to a final concentration of 20 mM and single use aliquots were stored at 4°C. Remdesivir (RDV; HY-104077) was purchased from MedChemexpress and chloroquine (C6628) from Sigma. Both compounds were dissolved in adequate solvents (DMSO or PBS, respectively) and single use aliquots were stored at -20°C.

Cytopathic effect (CPE) reduction assay

Cells were seeded in 96-well flat bottom plates in 100 µl at a density of 10000 cells/well of Huh7, 15000 cells/well of MRC-5 or 20000 cells/well of Vero cells. After overnight culture at 37°C, cells were pre-incubated for 30 min with 50 µl of two-fold serial dilutions of compounds prepared in EMEM-2%FCS. Subsequently, half of the wells were infected with MERS-CoV at low MOI in a total volume of 150 µl of medium with increasing concentrations between 0.05 to 100 uM of compound, to evaluate the inhibitory effect of compound. The other half of the wells were "mock"-infected with medium to monitor the (potential) cytotoxicity of the compound. Plates were incubated for three days (or as mentioned) at 37°C, after which cell viability was measured using the colorimetric CellTiter 96® Aqueous Non-Radioactive Cell Proliferation kit (Promega). The absorption at 495 nm was measured using a monochromatic filter in a multimode plate reader (Envision; Perkin Elmer). Data were normalized to the "mock"-infected control, after which EC_{50} and CC_{50} values were calculated using non-linear regression with Graph-Pad Prism V8.0. Each experiment was performed at least in quadruplicate and repeated at least twice.

Dose response assay

To evaluate the effect of compound treatment on viral progeny titers, confluent monolayers of Vero, Huh7 or MRC-5 were seeded in 24-well plates. Cells were incubated for 30 min at 37^{o}C with solvent or a range of DFA concentrations (from 0.1 to 100 uM). Then, cells were infected with MERS-CoV at an MOI of 0.01 for 1 h. After infection, cells were washed three times with PBS and 1 ml of medium with compound at corresponding concentration was added. Supernatants were collected at 48 h p.i. and viral progeny titers were determined by plaque assay in Vero cells as described before [88].

In 96-well clusters, Calu-3 cells were seeded at a density of 3 x 10^4 cells per well in 100 µl culture medium. Two days later, cells were pre-incubated for 30 min with 2-fold serial dilutions of compound, starting at a concentration of 25 µM. Subsequently, cells were infected with MERS-CoV, SARS-CoV or SARS-CoV-2 (MOI of 1 based on titer determined on Vero cells) in the presence of compound for 1 h. Next, cells were washed three times with PBS and 100 µl of compound solution in EMEM-2%FCS was added. Supernatants were collected at 24 h p.i. and progeny virus titers were determined by plaque assay.

Time of addition assay

Confluent monolayers of MRC-5 or Vero cells were seeded in 12-well plates in 1 ml/well of the appropriate medium (see above), and were grown overnight at 37^{o}C. Treatment of cells

(before, during or after infection) was performed using 0.6 µM (for Vero) and 12.5 µM (for MRC-5) of compound solution freshly prepared in EMEM-2%FCS medium. Cells were infected with MERS-CoV inoculum (MOI of 5) for 1h and washed three times with PBS. Subsequently, EMEM-2%FCS medium was added to the cells and supplemented with compound solution in 2-h intervals to a final concentration as mentioned above. Supernatants were collected 16 h p.i. and viral titers were determined by plaque assay.

Resistance culturing and next-generation sequencing (NGS)

Recombinant wt MERS-CoV strain EMC/2012(rMERS-CoV) was passaged in triplicate in presence of increasing concentrations of DFA ranging from 3.2 µM to 45 µM. Infections were performed at an MOI of 0.05 in every passage in MRC-5 monolayers. In parallel, rMERS-CoV wt was passaged in the same conditions in the absence of compound, to identify possible mutations associated with cell culture adaptation. Additionally, a "mock"-infected well treated with the same concentration of compound in each passage was evaluated for cytotoxicity by light microcopy. Supernatants were harvested when 80% to full CPE was observed (usually at 3 d p.i.). Three lineages were generated by serial passaging, but only lineage 3 was used for next-generation sequencing. To this end, RNA was isolated from 200 µl of virus-containing cell culture supernatants using TriPure isolation reagent (Roche Applied Science) and purified according to manufacturer's instructions. The RNA concentration was measured using a Qubit fluorometer and RNA High Sensitivity kit (Thermo Fisher Scientific). NGS sample preparation and analysis were performed as described previously [89]. After filtration and trimming of data, the remaining reads were mapped to the MERS-CoV GenBank reference sequence (NC_019843;[3]). Changes (mutation, deletions and insertions) were considered relevant when constituting more than 10% of the total population of viral reads (Table 1)[4]. Raw NGS data sets for wtP10 and L3P10 samples analysed in this study were deposited in NCBI Bioproject and are available under the following link: http://www.ncbi.nlm.nih.gov/bioproject/730836. Only MERS-CoV-specific reads were included in these data files.

ACKNOWLEDGMENTS

N.S.O. was supported by the Marie Skłodowska-Curie ETN European Training Network 'ANTIVIRALS' (EU Grant Agreement No. 642434). We thank Adriaan de Wilde and Martijn van Hemert for their support and for helpful discussions.

REFERENCES

1. Ksiazek, T.G., et al., *A novel coronavirus associated with severe acute respiratory syndrome.* N Engl J Med, 2003. **348**(20): p. 1953-66.
2. Peiris, J.S., et al., *Coronavirus as a possible cause of severe acute respiratory syndrome.* Lancet, 2003. **361**(9366): p. 1319-25.
3. Zaki, A.M., et al., *Isolation of a novel coronavirus from a man with pneumonia in Saudi Arabia.* N Engl J Med, 2012. **367**(19): p. 1814-1820.
4. van Boheemen, S., et al., *Genomic characterization of a newly discovered coronavirus associated with acute respiratory distress syndrome in humans.* MBio, 2012. **3**(6): p. e00473-12.
5. Brende, B., et al., *CEPI-a new global R&D organisation for epidemic preparedness and response.* Lancet, 2017. **389**(10066): p. 233-235.
6. Mehand, M.S., et al., *The WHO R&D Blueprint: 2018 review of emerging infectious diseases requiring urgent research and development efforts.* Antiviral Res, 2018. **159**: p. 63-67.
7. Zhou, P., et al., *A pneumonia outbreak associated with a new coronavirus of probable bat origin.* Nature, 2020. **579**(7798): p. 270-273.
8. Munster, V.J., et al., *A novel coronavirus emerging in China - key questions for impact assessment.* N Engl J Med, 2020. **382**(8): p. 692-694.
9. Zumla, A., et al., *Coronaviruses - drug discovery and therapeutic options.* Nat Rev Drug Discov, 2016. **15**(5): p. 327-47.
10. Garcia-Serradilla, M., C. Risco, and B. Pacheco, *Drug repurposing for new, efficient, broad spectrum antivirals.* Virus Res, 2019. **264**: p. 22-31.
11. Dittmar, M., et al., *Drug repurposing screens reveal FDA approved drugs active against SARS-Cov-2.* Cell Rep, 2020: p. 108959.
12. Valle, C., et al., *Drugs against SARS-CoV-2: What do we know about their mode of action?* Rev Med Virol, 2020. **30**(6): p. 1-10.
13. Snijder, E.J., et al., *Unique and conserved features of genome and proteome of SARS-coronavirus, an early split-off from the coronavirus group 2 lineage.* J Mol Biol, 2003. **331**(5): p. 991-1004.
14. Fehr, A.R. and S. Perlman, *Coronaviruses: an overview of their replication and pathogenesis.* Methods Mol Biol, 2015. **1282**: p. 1-23.
15. V'Kovski, P., et al., *Coronavirus biology and replication: implications for SARS-CoV-2.* Nat Rev Microbiol, 2020.
16. Subissi, L., et al., *One severe acute respiratory syndrome coronavirus protein complex integrates processive RNA polymerase and exonuclease activities.* Proc Natl Acad Sci U S A, 2014. **111**(37): p. E3900-E3909.
17. Kirchdoerfer, R.N. and A.B. Ward, *Structure of the SARS-CoV nsp12 polymerase bound to nsp7 and nsp8 co-factors.* Nat Commun, 2019. **10**(1): p. 2342.
18. Seybert, A., et al., *The human coronavirus 229E superfamily 1 helicase has RNA and DNA duplex-unwinding activities with 5'-to-3' polarity.* RNA, 2000. **6**(7): p. 1056-68.
19. Adedeji, A.O., et al., *Severe acute respiratory syndrome coronavirus replication inhibitor that interferes with the nucleic acid unwinding of the viral helicase.* Antimicrob Agents Chemother, 2012. **56**(9): p. 4718-28.
20. Chen, J., et al., *Structural Basis for Helicase-Polymerase Coupling in the SARS-CoV-2 Replication-Transcription Complex.* Cell, 2020. **182**(6): p. 1560-1573 e13.

21. Posthuma, C.C., A.J.W. Te Velthuis, and E.J. Snijder, *Nidovirus RNA polymerases: Complex enzymes handling exceptional RNA genomes.* Virus Res, 2017. **234**: p. 58-73.
22. Snijder, E.J., E. Decroly, and J. Ziebuhr, *The Nonstructural Proteins Directing Coronavirus RNA Synthesis and Processing.* Adv Virus Res, 2016. **96**: p. 59-126.
23. Ulferts, R. and J. Ziebuhr, *Nidovirus ribonucleases: Structures and functions in viral replication.* RNA Biol, 2011. **8**(2): p. 295-304.
24. Denison, M.R., et al., *Coronaviruses: an RNA proofreading machine regulates replication fidelity and diversity.* RNA Biol, 2011. **8**(2): p. 270-9.
25. Ogando, N.S., et al., *The curious case of the nidovirus exoribonuclease: its role in RNA synthesis and replication fidelity.* Front Microbiol, 2019. **10**: p. 1813.
26. Robson, F., et al., *Coronavirus RNA Proofreading: Molecular Basis and Therapeutic Targeting.* Mol Cell, 2020. **79**(5): p. 710-727.
27. Kindler, E. and V. Thiel, *To sense or not to sense viral RNA--essentials of coronavirus innate immune evasion.* Curr Opin Microbiol, 2014. **20**: p. 69-75.
28. Ivanov, K.A., et al., *Multiple enzymatic activities associated with severe acute respiratory syndrome coronavirus helicase.* J Virol, 2004. **78**(11): p. 5619-32.
29. Ivanov, K.A. and J. Ziebuhr, *Human coronavirus 229E nonstructural protein 13: characterization of duplex-unwinding, nucleoside triphosphatase, and RNA 5'-triphosphatase activities.* J Virol, 2004. **78**(14): p. 7833-8.
30. Decroly, E., et al., *Conventional and unconventional mechanisms for capping viral mRNA.* Nat Rev Microbiol, 2011. **10**(1): p. 51-65.
31. Yan, L., et al., *Cryo-EM Structure of an Extended SARS-CoV-2 Replication and Transcription Complex Reveals an Intermediate State in Cap Synthesis.* Cell, 2021. **184**(1): p. 184-193 e10.
32. Chen, Y., et al., *Functional screen reveals SARS coronavirus nonstructural protein nsp14 as a novel cap N7 methyltransferase.* Proc Natl Acad Sci U S A, 2009. **106**(9): p. 3484-3489.
33. Decroly, E., et al., *Coronavirus nonstructural protein 16 is a cap-0 binding enzyme possessing (nucleoside-2'O)-methyltransferase activity.* J Virol, 2008. **82**(16): p. 8071-84.
34. Aouadi, W., et al., *Binding of the Methyl Donor S-Adenosyl-l-Methionine to Middle East Respiratory Syndrome Coronavirus 2'-O-Methyltransferase nsp16 Promotes Recruitment of the Allosteric Activator nsp10.* J Virol, 2017. **91**(5).
35. Bouvet, M., et al., *Coronavirus Nsp10, a critical co-factor for activation of multiple replicative enzymes.* J Biol Chem, 2014. **289**(37): p. 25783-25796.
36. Bouvet, M., et al., *In vitro reconstitution of SARS-coronavirus mRNA cap methylation.* PLoS Pathog, 2010. **6**(4): p. e1000863.
37. Lu, S.C., *S-Adenosylmethionine.* Int J Biochem Cell Biol, 2000. **32**(4): p. 391-5.
38. Struck, A.W., et al., *S-adenosyl-methionine-dependent methyltransferases: highly versatile enzymes in biocatalysis, biosynthesis and other biotechnological applications.* Chembiochem, 2012. **13**(18): p. 2642-55.
39. Kloor, D. and H. Osswald, *S-Adenosylhomocysteine hydrolase as a target for intracellular adenosine action.* Trends Pharmacol Sci, 2004. **25**(6): p. 294-7.
40. De Clercq, E., *Strategies in the design of antiviral drugs.* Nat Rev Drug Discov, 2002. **1**(1): p. 13-25.

41. Yoon, J.S., et al., *Design, Synthesis, and Anti-RNA Virus Activity of 6'-Fluorinated-Aristeromycin Analogues.* J Med Chem, 2019.
42. Chen, Q., et al., *5'-Nor-3-Deaza-1',6'-Isoneplanocin, the Synthesis and Antiviral Study.* Molecules, 2020. **25**(17).
43. Cantoni, G.L., *Biological methylation: selected aspects.* Annu Rev Biochem, 1975. **44**: p. 435-51.
44. Palmer, J.L. and R.H. Abeles, *The mechanism of action of S-adenosylhomocysteinase.* J Biol Chem, 1979. **254**(4): p. 1217-26.
45. Rawal, R.K., J. Bariwal, and V. Singh, *Chemistry and Bioactivities of Aristeromycins: An Overview.* Curr Top Med Chem, 2016. **16**(28): p. 3258-3273.
46. de Wilde, A.H., et al., *MERS-coronavirus replication induces severe in vitro cytopathology and is strongly inhibited by cyclosporin A or interferon-alpha treatment.* J Gen Virol, 2013. **94**(Pt 8): p. 1749-60.
47. de Wilde, A.H., et al., *Alisporivir inhibits MERS- and SARS-coronavirus replication in cell culture, but not SARS-coronavirus infection in a mouse model.* Virus Res, 2017. **228**: p. 7-13.
48. de Wilde, A.H., et al., *Screening of an FDA-approved compound library identifies four small-molecule inhibitors of Middle East respiratory syndrome coronavirus replication in cell culture.* Antimicrob Agents Chemother, 2014. **58**(8): p. 4875-84.
49. Agostini, M.L., et al., *Coronavirus Susceptibility to the Antiviral Remdesivir (GS-5734) Is Mediated by the Viral Polymerase and the Proofreading Exoribonuclease.* MBio, 2018. **9**(2).
50. Jordheim, L.P., et al., *Advances in the development of nucleoside and nucleotide analogues for cancer and viral diseases.* Nat Rev Drug Discov, 2013. **12**(6): p. 447-64.
51. de Wilde, A.H., et al., *MERS-coronavirus replication induces severe in vitro cytopathology and is strongly inhibited by cyclosporin A or interferon-alpha treatment.* J Gen Virol, 2013. **94**(Pt 8): p. 1749-1760.
52. Knaap, R.C.M., et al., *The deubiquitinating activity of Middle East respiratory syndrome coronavirus papain-like protease delays the innate immune response and enhances virulence in a mouse model.* bioRxiv, 2019: p. 751578.
53. El-Awady, R., et al., *The Role of Eukaryotic and Prokaryotic ABC Transporter Family in Failure of Chemotherapy.* Front Pharmacol, 2016. **7**: p. 535.
54. Menachery, V.D., et al., *MERS-CoV Accessory ORFs Play Key Role for Infection and Pathogenesis.* mBio, 2017. **8**(4).
55. Liu, D.X., et al., *Accessory proteins of SARS-CoV and other coronaviruses.* Antiviral Res, 2014. **109**: p. 97-109.
56. Mou, H., et al., *The receptor binding domain of the new Middle East respiratory syndrome coronavirus maps to a 231-residue region in the spike protein that efficiently elicits neutralizing antibodies.* J Virol, 2013. **87**(16): p. 9379-83.
57. Hoffmann, M., et al., *Chloroquine does not inhibit infection of human lung cells with SARS-CoV-2.* Nature, 2020. **585**(7826): p. 588-590.
58. Lau, S.K., et al., *Delayed induction of proinflammatory cytokines and suppression of innate antiviral response by the novel Middle East respiratory syndrome coronavirus: implications for pathogenesis and treatment.* J Gen Virol, 2013. **94**(Pt 12): p. 2679-90.
59. Kusaka, T., et al., *Streptomyces citricolor nov. sp. and a new antibiotic, aristeromycin.* J Antibiot (Tokyo), 1968. **21**(4): p. 255-63.

60. Wolfe, M.S., et al., *4'-modified analogues of aristeromycin and neplanocin A: synthesis and inhibitory activity toward S-adenosyl-L-homocysteine hydrolase.* J Med Chem, 1992. **35**(10): p. 1782-91.
61. WANG, J.R., R. K.; CHU, C. K., *Recent Advances in Carbocyclic Nucleosides: Synthesis and Biological Activity.* Med. Chem. Nucleic Acids, 2011: p. 1-100.
62. Hasobe, M., J.G. McKee, and R.T. Borchardt, *Relationship between intracellular concentration of S-adenosylhomocysteine and inhibition of vaccinia virus replication and inhibition of murine L-929 cell growth.* Antimicrob Agents Chemother, 1989. **33**(6): p. 828-34.
63. Ransohoff, R.M., et al., *Priming of influenza mRNA transcription is inhibited in CHO cells treated with the methylation inhibitor, neplanocin A.* Antiviral Res, 1987. **7**(6): p. 317-27.
64. Kovacikova, K., et al., *6'-beta-Fluoro-Homoaristeromycin and 6'-Fluoro-Homoneplanocin A Are Potent Inhibitors of Chikungunya Virus Replication through Their Direct Effect on Viral Nonstructural Protein 1.* Antimicrob Agents Chemother, 2020. **64**(4).
65. Chen, H., et al., *S-adenosyl-homocysteine is a weakly bound inhibitor for a flaviviral methyltransferase.* PLoS One, 2013. **8**(10): p. e76900.
66. Jin, X., et al., *Characterization of the guanine-N7 methyltransferase activity of coronavirus nsp14 on nucleotide GTP.* Virus Res, 2013. **176**(1-2): p. 45-52.
67. Aouadi, W., et al., *Toward the identification of viral cap-methyltransferase inhibitors by fluorescence screening assay.* Antiviral Res, 2017. **144**: p. 330-339.
68. Chiang, P.K., *Biological effects of inhibitors of S-adenosylhomocysteine hydrolase.* Pharmacol Ther, 1998. **77**(2): p. 115-34.
69. Decroly, E., et al., *Crystal structure and functional analysis of the SARS-coronavirus RNA cap 2'-O-methyltransferase nsp10/nsp16 complex.* PLoS Pathog, 2011. **7**(5): p. e1002059.
70. Shannon, A., et al., *Protein-primed RNA synthesis in SARS-CoVs and structural basis for inhibition by AT-527.* bioRxiv, 2021: p. 2021.03.23.436564.
71. Slanina, H., et al., *Coronavirus replication-transcription complex: Vital and selective NMPylation of a conserved site in nsp9 by the NiRAN-RdRp subunit.* Proc Natl Acad Sci U S A, 2021. **118**(6).
72. Hao, W., et al., *Crystal structure of Middle East respiratory syndrome coronavirus helicase.* PLoS Pathog, 2017. **13**(6): p. e1006474.
73. Yan, L., et al., *Architecture of a SARS-CoV-2 mini replication and transcription complex.* Nat Commun, 2020. **11**(1): p. 5874.
74. Urakova, N., et al., *beta-d-N (4)-Hydroxycytidine Is a Potent Anti-alphavirus Compound That Induces a High Level of Mutations in the Viral Genome.* J Virol, 2018. **92**(3).
75. Agostini, M.L., et al., *Small-Molecule Antiviral beta-d-N (4)-Hydroxycytidine Inhibits a Proofreading-Intact Coronavirus with a High Genetic Barrier to Resistance.* J Virol, 2019. **93**(24).
76. Shannon, A., et al., *Rapid incorporation of Favipiravir by the fast and permissive viral RNA polymerase complex results in SARS-CoV-2 lethal mutagenesis.* Nat Commun, 2020. **11**(1): p. 4682.

77. Meier, C. and J. Balzarini, *Application of the cycloSal-prodrug approach for improving the biological potential of phosphorylated biomolecules.* Antiviral Res, 2006. **71**(2-3): p. 282-92.
78. Shin, Y.S., et al., *Identification of 6'-beta-fluoro-homoaristeromycin as a potent inhibitor of chikungunya virus replication.* Eur J Med Chem, 2020. **187**: p. 111956.
79. De Clercq, E., *Carbocyclic adenosine analogues as S-adenosylhomocysteine hydrolase inhibitors and antiviral agents: recent advances.* Nucleosides Nucleotides, 1998. **17**(1-3): p. 625-34.
80. Bray, M., J. Driscoll, and J.W. Huggins, *Treatment of lethal Ebola virus infection in mice with a single dose of an S-adenosyl-L-homocysteine hydrolase inhibitor.* Antiviral Res, 2000. **45**(2): p. 135-47.
81. Huggins, J., Z.X. Zhang, and M. Bray, *Antiviral drug therapy of filovirus infections: S-adenosylhomocysteine hydrolase inhibitors inhibit Ebola virus in vitro and in a lethal mouse model.* J Infect Dis, 1999. **179 Suppl 1**: p. S240-7.
82. De Fazio, G., et al., *Antiviral activity of S-adenosylhomocysteine hydrolase inhibitors against plant viruses.* Antiviral Res, 1990. **13**(5): p. 219-26.
83. De Clercq, E., et al., *Broad-spectrum antiviral activities of neplanocin A, 3-deazaneplanocin A, and their 5'-nor derivatives.* Antimicrob Agents Chemother, 1989. **33**(8): p. 1291-7.
84. Ogando, N.S., et al., *The enzymatic activity of the nsp14 exoribonuclease is critical for replication of MERS-CoV and SARS-CoV-2.* J Virol, 2020.
85. Nedialkova, D.D., A.E. Gorbalenya, and E.J. Snijder, *Arterivirus Nsp1 modulates the accumulation of minus-strand templates to control the relative abundance of viral mRNAs.* PLoS Pathog, 2010. **6**(2): p. e1000772.
86. Pfefferle, S., et al., *Reverse genetic characterization of the natural genomic deletion in SARS-Coronavirus strain Frankfurt-1 open reading frame 7b reveals an attenuating function of the 7b protein in-vitro and in-vivo.* Virol J, 2009. **6**: p. 131.
87. Salgado-Benvindo, C., et al., *Suramin Inhibits SARS-CoV-2 Infection in Cell Culture by Interfering with Early Steps of the Replication Cycle.* Antimicrob Agents Chemother, 2020. **64**(8).
88. van den Worm, S.H., et al., *Reverse genetics of SARS-related coronavirus using vaccinia virus-based recombination.* PLoS One, 2012. **7**(3): p. e32857.
89. Ogando, N.S., et al., *SARS-coronavirus-2 replication in Vero E6 cells: replication kinetics, rapid adaptation and cytopathology.* J Gen Virol, 2020.

CHAPTER VII

The cyclophilin-dependent calcineurin inhibitor voclosporin inhibits SARS-CoV-2 replication in cell culture

Natacha S. Ogando[1], Erik Metscher [2], Dirk Jan A.R. Moes[2,4], Eline J. Arends[3], Ali Tas[1], Jennifer Cross[5], Eric J. Snijder[1], Y.K. Onno Teng[3,4], Aiko P.J. de Vries[3,4], Martijn J. van Hemert[1]

[1]Department of Medical Microbiology, Leiden University Medical Center, Leiden, The Netherlands
[2] Department of Clinical Pharmacy and Toxicology, Leiden University Medical Center, Leiden, The Netherlands
[3] Department of Nephrology, Leiden University Medical Center, Leiden, The Netherlands
[4] Leiden Transplant Center, Leiden University Medical Center, Leiden, The Netherlands
[5] Aurinia Pharmaceuticals Inc., Victoria Canada

Submitted to Kidney international

ABSTRACT

Kidney transplant recipients (KTRs) are at increased risk for a more severe course of COVID-19, due to their comorbidity and maintenance immunosuppression. Consensus protocols recommend lowering immunosuppression in KTRs with severe acute respiratory syndrome coronavirus 2 (SARS-CoV-2) infection, but the optimal combination remains unclear. Calcineurin inhibitors (CNIs) are cornerstone immunosuppressants in KTRs and some have been reported to possess antiviral activity against RNA viruses, including coronaviruses. We evaluated the effect of the CNIs tacrolimus, cyclosporine A , and voclosporin (VCS), as well as other immunosuppressants, on SARS-CoV-2 replication in cell-based assays. Loss of compound due to plastic binding and interference of excipients in pharmaceutical formulations (false-positive results) complicated the determination of EC50 values in our antiviral assays. We could circumvent some of these issues by using exclusively glass labware. VCS reduced viral progeny yields in human Calu-3 cells at low micromolar concentrations and did so more effectively than cyclosporin A and tacrolimus. Although, we cannot recommend a particular immunosuppressive regimen in KTRs with COVID-19, our data suggest a potential benefit of cyclophilin-dependent CNIs, in particular VCS, which warrants further clinical evaluation in SARS-CoV-2-infected KTRs.

TRANSLATION STATEMENT

As the efficacy of the vaccines is uncertain in immunocompromised hosts like KTRs and effective (antiviral) treatment options icient therapies are limited, finding alternative solutions is crucial to protect these patients. In this study, CNIs demonstrated more potent inhibitory effect of SARS-CoV-2 replication (in cell culture) than other classes of immunosuppressive agents. Strikingly, VCS displayed antiviral activity at 8-fold lower concentrations lower than TAC. Of note, the concentrations of VCS that reduced SARS-CoV-2 viral load can be correlated with tolerable doses in humans that are attainable in KTRs. Therefore, VCS becomes an attractive CNI and it is currently under investigation for COVID-19 infected KTRs.

INTRODUCTION

Between December 2019 and January 2021, severe acute respiratory syndrome coronavirus-2 (SARS-CoV-2), the causative agent of coronavirus disease-2019 (COVID-19), has resulted in over 90 million infections globally. A more severe course of COVID-19 has been correlated to comorbidities commonly present in solid organ transplant recipients[1-3]. Moreover, initial reports showed that the latter are among those at increased risk of COVID-19 related death[4].

Finding the balance between preventing rejection and controlling infections is the conundrum when prescribing immunosuppressive regimens for transplant recipients[5]. The current standard for immunosuppressive therapy in most transplant centers consists of a calcineurin inhibitor (CNI), either tacrolimus (TAC) or cyclosporin A (CsA), an antimetabolite agent such as mycophenolate (MPA/MPS) and most often, maintenance steroids. An mTOR inhibitor such as everolimus (EVL) may be prescribed alternatively to MPA[6]. The precise impact of immunosuppression on the course of COVID-19 is poorly understood. Early in the disease, (over)immunosuppression might prevent a proper antiviral response, whereas later some immunosuppression might protect against pathological immune overactivation, resulting in less severe disease. Consequently, consensus protocols recommend to reduce but not completely cede immunosuppression in SARS-CoV-2 infected KTR's, depending on the risk of rejection and disease severity[7, 8].

Previous reports suggest that CNIs and mTOR inhibitors like EVL in addition to MPA have antiviral activity against human coronaviruses such as SARS-CoV and Middle East respiratory syndrome (MERS-) CoV [9]. TAC (which targets FKBP12) was reported to inhibit CoV replication in cell culture at non-cytotoxic concentrations[10], and was recently proposed as a potential inhibitor of SARS-CoV-2 replication by computational analysis[11].

Next to its immunosuppressive effects[12-17], CsA was reported to inhibit replication of different RNA viruses in cell culture, including influenza virus[18], human immunodeficiency virus-1[19], hepatitis C virus[20], flaviviruses[14], and human and zoonotic CoVs[17, 21-24]. Several non-immunosuppressive CsA derivatives, like alisporivir (Debio-025), also inhibit the replication of CoVs in cell culture[12, 22, 25], including SARS-CoV-2[26, 27]. Collectively, these studies established the broad-spectrum antiviral activity of CsA and derivatives in cell-based infection models. Since cyclophilins (Cyps) were also implicated in CoV replication, CsA has been recommended for KTRs during the COVID-19 pandemic as an alternative to other regimens to prevent rejection[28]. Although Cyp inhibitors can affect CoV replication, the exact role of these host proteins in CoV replication remains elusive[29].

Voclosporin (VCS) is a novel CNI which has been studied in psoriasis, renal organ transplantation, and was recently FDA-approved for treatment of active lupus nephritis in combination with background immunosuppressive therapy[30-32]. Structurally similar to CsA, VCS incorporates a methyl group at the amino acid residue position 1, which enhances its binding to calcineurin, and confers better metabolic stability[33, 34]. (Pre)clinical observations suggest that VCS is more potent and less toxic at therapeutic levels than other immunosuppressants in its class[31, 33-36]. Moreover, VCS was shown to inhibit norovirus replication in a CypA-dependent manner and more effectively than CsA [16]. Therefore, VCS is an interesting candidate to evaluate for inhibitory activity on SARS-CoV-2 replication.
In this study we compared the effect of three calcineurin inhibitors (TAC, CSA, VCS) and other immunosuppressants commonly used in KTR's on SARS-CoV-2 replication using cell-based assays.

RESULTS

Inhibition of SARS-CoV-2 replication in Calu-3 cells by VCS, CsA and TAC

To evaluate the effect of VCS, CsA and TAC on SARS-CoV-2 replication, viral load reduction assays were performed using human lung epithelial cells (Calu-3). VCS is highly lipophilic and binds to plastic, which could compromise its bioavailability in standard cell-based assays using plastic labware. Therefore, we compared the effect of the compound in standard assays using plastics and custom assays using glass tubes, containers and pipettes. RDV was included as a positive control for inhibition of SARS-CoV-2 replication.
Cells were treated with different concentrations of compound before, during and after SARS-CoV-2 (Fig. 1A and 1B) or mock infection (Fig. 1C and 1D). Calu-3 cells in glass remained viable and supported SARS-CoV-2 replication, as titers of 1.7 x 10^6 PFU/ml were measured in the medium at 24 h p.i. (Fig. 1A). Treatment of infected cells with 10 µM of RDV inhibited viral replication resulting in infectious progeny titers just above the limit of detection of the plaque assay (data not shown). Treatment of cells with 3.2 µM VCS caused a more than 1.5 log reduction in SARS-CoV-2 infectious progeny titers, while an ~0.5 log reduction was observed when the same concentration of CsA or TAC was used (Fig. 1A). However, treatment with 3.2 µM VCS or CsA also caused cytotoxic effects, as cell viability dropped to ~75% (Fig. 1C). Therefore, it cannot be excluded that part of the observed antiviral effect is due to pleiotropic effects (toxicity).
In experiments using plastic materials, a dose-dependent reduction in infectious progeny titers was observed when cells were treated with VCS, leading to a more than 1 log reduction at 6.4 µM (Fig. 1B). CsA treatment led to a similar reduction at 25 µM, but at 6.4 µM inhibited

less than VCS. However, at concentrations of 12.5 µM or above CsA displayed significant cytotoxicity while VCS did not (Fig. 1D). TAC did not display much cytotoxicity, but a concentration of 25 µM was required to reduce the infectious virus progeny titer by more than 1 log. VCS had a stronger effect in experiments performed with glass instead of plastic labware, likely due to loss of the compound by binding to plastic. We therefore measured the concentration of free VCS after incubating various solutions in glass containers either with or without cells. No significant loss of compound from solution was observed after a 24h incubation at 37°C in glass without cells (Table 1). When VCS solutions with concentrations from 0.2 to 3.2 µM were incubated in glass bottles with Calu-3 cells, a ~75% reduction of the VCS concentration was measured, suggesting the compound was bound or taken up by cells. We also measured the VCS concentration in the medium of (infected) cells after 24h treatment with 25 µM VCS in experiments performed with standard plastic labware, which turned out to be as low as 0.68 µM. Even considering a 75% reduction due to cellular binding or uptake, it implies that 90% of VCS was lost due to plastic binding. The similar reduction in virus titers by 3.2 and 25 µM of VCS in glass and plastic, respectively, corroborated that when using plastic, the bioavailable amount of VCS is likely ~10% of what was added initially.

Table 1- VCS concentration in samples from experiments using only glass labware, measured by LC-MS/MS

	Concentration of VCS in supplied solution											
	3.2 µM		**3.2 µM**		**1.6 µM**		**0.8 µM**		**0.4 µM**		**0.2 µM**	
	Without cells		**With cells**									
Incubation time	**Conc. in µM**	**% remaining**	**Conc. in µM**	**% remaining**	**Conc. in µM**	**% remaining**	**Conc. in µM**	**% remaining**	**Conc. in µM**	**% remaining**	**Conc. in µM**	**% remaining**
0 h	2.91		2.91		1.77		0.99		0.45		0.33	
24 h	2.79	**96**	0.82	**28**	0.35	**20**	0.15	**15**	0.10	**22**	<0.07*	**ND**

*below detection limit of LC/MS-MS Note: The percentages indicate the ratio of the measured (true) concentration at 24 h and the concentration of the prepared solution administrated to the cells (at 0 h incubation time).

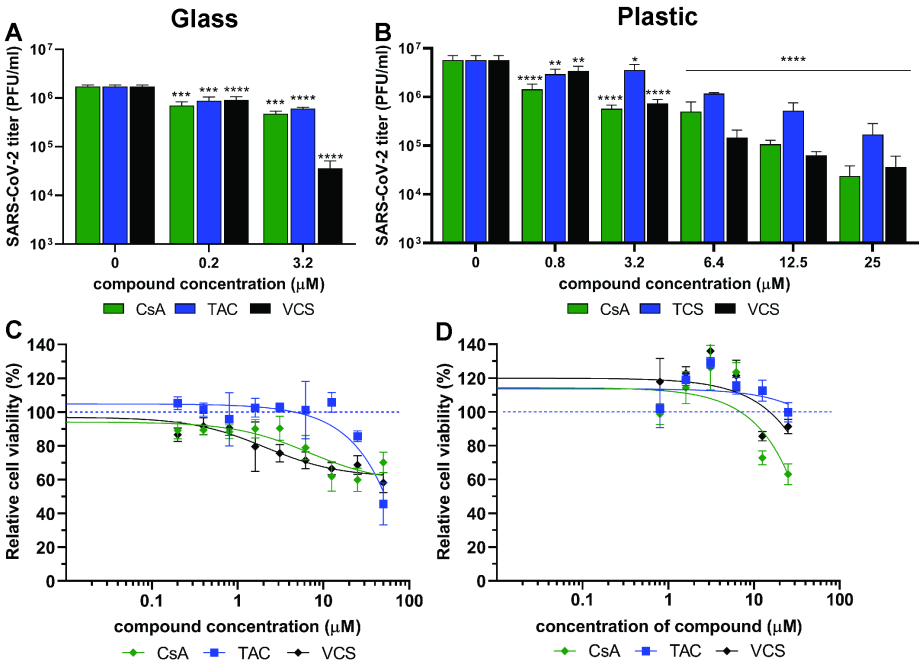

Fig. 1. Impact of CsA, TAC and VCS treatment on the production of infectious SARS-CoV-2 progeny by human Calu-3 cells. Experiments were performed using either glass (A and C) or plastic labware (B and D). Cells were infected with SARS-CoV-2 in the presence of different concentrations of VCS, CsA and TAC using stock solutions prepared from pure powders dissolved in DMSO. The viral load in the medium of infected cells was determined by plaque assay on Vero E6 cells using supernatant harvested at 24 h p.i. Viability of uninfected Calu-3 cells treated with the same range of compound concentrations was measured in parallel by a colorimetric viability assay (C; n=12; D; n=3). Mean values ± SD are shown and statistical significance of the difference between each concentration and solvent control was assessed by one-way ANOVA. *, *p<0.1*; **, *p<0.01*; ***, *p<0.001*; ****, *p<0.0001*.

Inhibition of SARS-CoV-2 replication in cell culture by various immunosuppressive drugs

In order to avoid problems with solubility and plastic binding (as described above) and to compare the antiviral effect of different immunosuppressive drugs commonly used in KTRs, we performed SARS-CoV-2 CPE reduction assays with the pharmaceutical formulations (including excipients, co-solvents and other components) of VCS, CsA, TAC, EVL, and MMF. In parallel, drug cytotoxicity was assessed in non-infected cells. For VCS we confirmed by LC-MS/MS that the intended concentrations were achieved when dissolving stock solutions at 6.4 µM (data not shown).

The CNIs VCS, CsA, and TAC inhibited virus-induced cell death with EC_{50} values in the sub- to low micromolar range (Fig. 2A, 2B, 2C). EVL (Fig. 2D) did not show an inhibitory effect at tested

concentrations. The prodrug MMF (Fig. 2E) was included in our comparison, but was not expected to inhibit virus replication, as it is likely not metabolized into its active form MPA[37] in our assay [38, 39]. Thus, we attributed the apparent antiviral effect of MMF mainly to excipients present in the drug formulation (see below).

The EC_{50} values of VCS, CsA and TAC were 0.22 ± 0.01 µM, 4.3 ± 0.6 µM and 10 ± 1 µM, respectively. Apart from VCS, none of the compounds showed cytotoxicity, and therefore their CC_{50} values were higher than 100 µM. Although VCS displayed higher cytotoxicity, with a CC_{50} of ~4 µM, its EC_{50} was also 18-45 times lower compared to the other compounds tested.

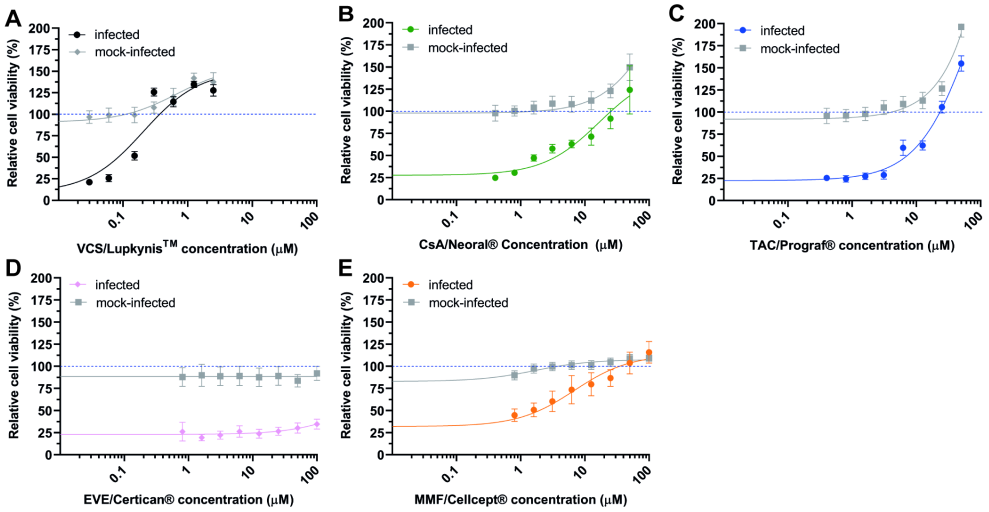

Fig. 2. Effect of immunosuppressive drugs on SARS-CoV-2 replication. Inhibition of SARS-CoV-2 replication (colored symbols and curves) in Vero E6 cells by various drugs were determined by CPE-reduction assay. For each drug, two-fold serial dilutions of the pharmaceutical formulations were tested. (A) VCS, (B) cyclosporine A/ Neoral, (C) TAC/ Prograf, (D) EVL/ Afinitor and (E) MMF/ Cellcept. After preincubation with compound, cells were infected with SARS-CoV-2 and kept in medium containing the drug for 3 days, after which cell viability was measured with a colorimetric assay. Cytotoxicity of the drugs was evaluated in parallel using mock-infected, compound-treated cells (solid grey line). Data points represent the mean ± SD of two independent experiments. The CC50 and EC50 were determined by non-linear regression analysis and the regression curves are plotted in the graphs (solid lines).

An excipient in the pharmaceutical formulation of VCS inhibits SARS-CoV-2 replication in CPE reduction assays

To investigate whether one or more excipients contributed to the low EC_{50} (Fig. 2A) of the pharmaceutical formulation of VCS, CPE reduction assays were performed to assess the

antiviral effect of the content of VCS capsules and placebo capsules. Surprisingly, both the VCS formulation (Fig. 3A) and the placebo (Fig. 3B) inhibited SARS-CoV-2 replication in a similar dose-dependent manner. The absence of VCS in placebo capsules was confirmed by LC-MS/MS analysis (not shown). Therefore, one or more excipients in the drug formulation appear to have an antiviral effect in this experimental setup (further evaluation in supporting information).

To avoid interference by excipients in our antiviral assays we performed CPE reduction assays with DMSO solutions prepared from high purity powders of the various immunosuppressive drugs. In the case of Neoral (CsA microemulsion), CsA powder, the most commonly used CsA derivative in KTR treatment, was evaluated. VCS solutions prepared from pure powder did not confer the same level of protection to SARS-CoV-2 infected-cells (Fig. 4A) as solutions made from the pharmaceutical formulation (Fig. 3A). However, the VCS solution from pure powder also caused less cytotoxicity. The same issue was observed with CsA and MPA (Fig. 4B and 4D), suggesting that also in cell-based assays these drugs need excipients to ensure solubility/bioavailability for optimal activity. Interestingly, TAC solutions prepared from pure powder inhibited SARS-CoV-2 with similar efficacy as the drug formulations, i.e., with an EC_{50} of ~15 µM (compare Fig. 2C and 4C), suggesting that the pharmaceutical formulation of TAC does not contain excipients with antiviral effects.

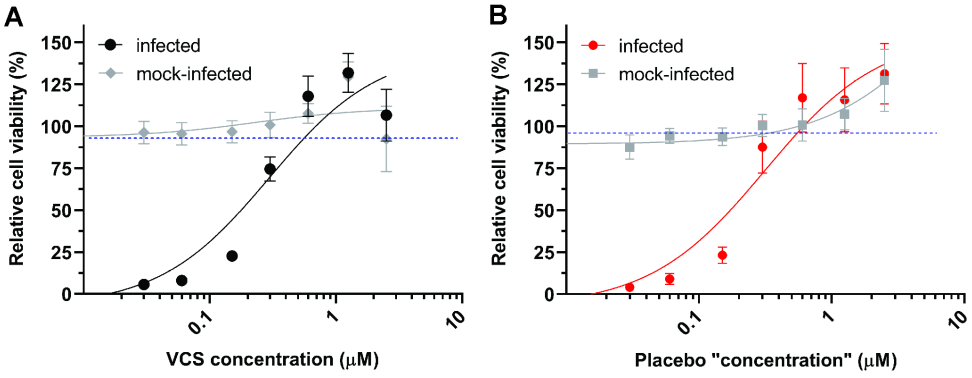

Fig. 3. Comparison of the antiviral effect of VCS and placebo pharmaceutical formulations. The inhibition of SARS-CoV-2 replication in Vero E6 cells treated with the content of VCS pharmaceutical formulation (A) or placebo (B) was determined by CPE reduction assays as described in the legend of Fig. 2.

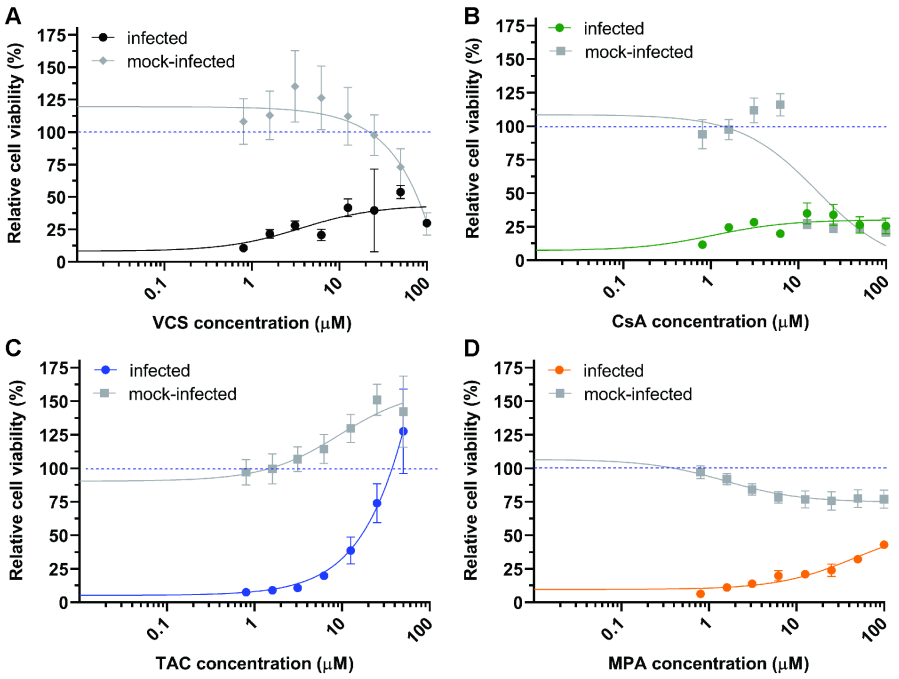

Fig. 4. Inhibition of SARS-CoV-2 replication by immunosuppressive compounds in CPE-reduction assays with stocks prepared from pure compound powders. (A) VCS, (B) CsA, (C) TAC, and (D) MPA. For details, see the legend to Fig. 2.

DISCUSSION

KTR's are at increased risk for developing a severe course of COVID-19 owing to older age, comorbidities or their immunocompromised state[4, 40, 41]. The attributable effect of immunosuppression for a more severe course of COVID-19 as well as the most optimal treatment in KTRs is yet unclear[5, 9]. Different clinical observations suggested that immunosuppression did not impose an increased risk for severe COVID-19 disease or mortality[42-45]. However, increased death rates have been observed for immunocompromised COVID-19 patients[4, 46, 47]. As the efficacy of approved vaccines is yet uncertain in KTRs, gaining more insight is crucial.

In general, COVID-19 displays a triphasic course: starting with mild flu-like symptoms, followed by a second phase of viral replication and pneumonia, which in a small percentage of cases is followed by a third phase of life-threatening disease, e.g., due to a cytokine storm[48]. Antiviral drug treatment is expected to be most effective during earliest stages of

disease, while immunosuppressants (e.g. steroids, tocilizumab) may be considered a therapeutic option in later stages of disease to reduce inflammation.

An immunosuppressive regimen might ideally prevent rejection, possess antiviral properties and reduce (over)inflammation, whilst still mounting an effective antiviral response to prevent a severe disease course simultaneously. Consensus recommendations advocated to lower but not completely halt immunosuppression and some advocated steroids with CNI's based on theoretical (in vitro) advantages[49]. There is scant clinical data. Interestingly, one large single-center observational study found a clear survival benefit for patients when put on CsA compared to other experimental (off-panel) anti-inflammatory therapy for COVID-19[50] Various studies, also by our group, previously demonstrated that CNIs like CsA and TAC inhibit replication of a variety of (human) CoVs such SARS- and MERS-CoV[10, 17, 21, 51, 52]. As these *Betacoronavirus* are closely related to SARS-CoV-2 [9, 53, 54], these drugs were hypothesized to inhibit SARS-CoV-2 replication as well. In this study, we evaluated the antiviral effect of CNIs with a focus on VCS, a novel CNI with a modified amino acid–1 group on the CsA structure, which increases its affinity for calcineurin[33, 34, 55]. A potential advantage of VCS over CsA is its lower nephrotoxicity[56]. Our study demonstrates that VCS inhibits SARS-CoV-2 infection in cell culture with an EC_{50} in the sub-micromolar range, at lower concentrations than CsA or TAC. We evaluated the effect of these different CNIs on SARS-CoV-2 replication by viral load reduction assays in Calu-3 cells, a human lung epithelial cell line that was shown to be permissive to SARS-CoV-2[57, 58]. Our findings are in line with those reported in a non-peer reviewed manuscript that reported CsA inhibited SARS-CoV-2 replication in HuH7.5 and Calu-3 cells, but not in Vero cells[59]. In contrast to our finding that TAC inhibits SARS-CoV-2 replication in Vero E6 cells with an EC_{50} of ~15 μM, Dittmar et al found no activity for TAC in any of these cell lines[59], which might be due to the use of different Vero cell subclones.

While testing the pharmaceutical formulations of different immunosuppressive drugs commonly used in KTRs, we discovered that the excipients in these preparations have antiviral effects in our cell-based assays which prevented the determination of true EC_{50} values of active ingredients. Unexpectedly, this was not due to virucidal effects of surfactants that can damage the viral envelope[60-62], but rather through an effect on infected cells that could not be elucidated further in this study. Testing of highly pure powders of the various immunosuppressive compounds to circumvent the interference caused by excipients in our antiviral assays, led to much higher EC_{50} values for VCS, CsA and TAC, demonstrating that excipients that improve solubility and bioavailability of the active compound in pharmaceutical formulations also affect results in cell-based assays. VCS is known to bind to plastic, and since in general mainly plastic labware is used, we determined the available free

VCS concentrations in the medium at the beginning and end of experiments using a validated LC-MS/MS method. This revealed that VCS binding to plastic caused a>80% loss of the compound from solution. Consequently, the use of stock solutions prepared from pure VCS powder using plastic labware leads to a serious underestimation of the compound's efficacy in antiviral assays. VCS is a highly lipophilic compound, and interactions between plastic surfaces and hydrophobic drugs[63] that have a negative effect on bioavailability have been described before[64, 65]. Our attempts to prevent VCS binding to plastic by treating labware with various coatings were unsuccessful as none led to a more than ~10% recovery of the initial VCS concentration.

Since we were unable to use the oral formulation of VCS and were not able to overcome the plastic binding and loss of compound when using preparations of pure VCS, we performed experiments using glass labware only. These conditions supported growth of human Calu-3 cells and SARS-CoV-2 replication, while measurement of VCS concentrations demonstrated that there was hardly any loss of the compound. Using this setup, demonstrated that VCS reduced the production of SARS-CoV-2 infectious progeny in a dose-dependent manner in infected Calu-3 cells, and more effectively than CsA and TAC.

In summary, in this study we demonstrate that cyclophilin-dependent CNIs inhibit SARS-CoV-2 replication in cell culture more potently than other classes of immunosuppressants, like EVL and MPA. VCS inhibited SARS-CoV-2 replication at 8-fold lower concentrations than TAC. Of note, TAC concentrations that are required to inhibit SARS-CoV-2 replication likely correlate with intolerable or toxic concentrations in humans (EC_{50} of 0.2 µM equals 160 ng/ml for TAC), without taking into account that the free fraction in traffic is around one tenth of the total concentration. For CsA and VCS 0.2 µM corresponds to a concentration of 241 and 243 ng/ml respectively. Notably, VCS is also known to distribute into organs such as the lungs in higher concentrations than in blood, and higher concentrations are found in red blood cells. Consequently, higher concentrations in specific organs or cells might enable some inhibition of the virus. In conclusion, VCS has become an attractive alternative CNI for therapy that might also inhibit SARS-CoV-2 replication at concentrations that are safe in humans. Since VCS is thought to have comparable efficacy to TAC for prevention of rejection in KTRs, VCS might be an interesting option in COVID-19 patients. Based solely on the experimental data presented in this study, we do not advocate the use of VCS merely for its potential antiviral properties. However, our data suggest a potential benefit of cyclophilin-dependent CNIs, in particular VCS, among immunosuppressants commonly used in transplant medicine. This warrants further clinical evaluation and VCS is currently under investigation in SARS-CoV-2-infected KTRs [EudraCT 2020-001467-82].

MATERIALS AND METHODS

Virus and cell lines

SARS-CoV-2/Leiden-0002 (GenBank MT510999) was isolated from a nasopharyngeal sample at LUMC in March 2020. Infections were performed with a virus stock that had been passaged twice in Vero E6 cells. Vero E6 cells and Calu-3 2B4 cells [66], referred to as Calu-3 cells in this manuscript, were cultured as described previously[67]. Infections were performed in Eagle's minimal essential medium (EMEM; Lonza) with 25 mM HEPES (Lonza), 2% FCS, 2 mM L-glutamine, and antibiotics (EMEM-2% FCS). All experiments with infectious SARS-CoV-2 were performed in a biosafety level 3 facility at the LUMC.

Immunosuppressive compounds

Voclosporin (Lupkynis™), cyclosporine A (Neoral®, Novartis), tacrolimus (Prograf®, Astellas), mycophenolate mofetil (CellCept®, Roche) or everolimus (Certican®, Novartis) stock solutions were prepared by dissolving the pharmaceutical formulation of these drugs in dimethyl sulfoxide (DMSO, Sigma-Aldrich). Placebo capsules and pure VCS powder were supplied by Aurinia Pharmaceuticals Inc., Inc. Tacrolimus (PHR1809), cyclosporin A (30024) and mycophenolic acid (M5255) were purchased from Sigma-Aldrich. Remdesivir (RDV; HY-104077) was acquired from MedChemExpress and was used as a control in all experiments. All compounds were dissolved in DMSO and single use aliquots were stored at -20°C.

Measurement of cyclosporin A, tacrolimus and voclosporin concentrations by validated LC-MS / MS

Quantification of CsA and TAC was performed by LC-MS/MS as previously described [68] by diluting samples in methanol and subsequently in blank whole blood. A Thermo Quantiva UPLC-MS/MS system (Ultimate 3000 series UHPLC system, coupled to a TSQ Quantiva triple stage quadrupole mass spectrometer) was used with an Acquity UPLC BEH C18 1.7 µm; 2.1 x 50 mm column coupled to a VanGuard BEH C18 1.7 µm precolumn for chromatographic seperation. Online solid phase extraction was performed using a Xbridge 10 µm 30 x 2.1 mm column. Before analysis, samples were diluted in methanol and subsequently whole blood to fall within the calibration line of 0-15-600 µg/L of VCS. Human whole blood was added to 10- or 20-µl samples to a final volume of 200 µl and 200 µl of 0.1 M zinc-sulphate and 500 uL of internal standard solution (32 ug/L of VCS D_4 in acetonitrile) were added. Samples were then vortexed at 2000 rpm for 5 min and centrifuged at 13000 rpm for 5 min and 20 µl was injected into the LC-MS/MS system. The method was validated according to the EMA bioanalytical method validation guideline[69].

Cytopathic effect (CPE) reduction assay

CPE reduction assays in Vero E6 cells were performed as previously described [26]. Briefly, Vero E6 cells in 96-well plates were pre-incubated with 2-fold serial compound dilutions for 30 min. Subsequently, cells were either mock-infected (to assess cytotoxicity of compounds) or infected with 300 plaque-forming units (PFU) of SARS-CoV-2 per well (multiplicity of infection (MOI) of 0.015) in a total volume of 150 µl of medium with compound. Plates were incubated for three days at 37°C, after, which cell viability was determined using the colorimetric CellTiter 96® Aqueous Non-Radioactive Cell Proliferation kit (Promega). The absorption at 495 nm was measured with an EnVision Multilabel Plate Reader (PerkinElmer) and the EC_{50} (50% effective concentration, required to inhibit virus-induced cell death by 50%), and CC_{50} (50% cytotoxic concentration, reduces the viability of uninfected cells to 50% of control), were determined using non-linear regression with GraphPad Prism v8.0. For each compound, at least two independent experiments (each in quadruplicate) were performed.

Viral yield reduction assays

Calu-3 cells were seeded in 96-well plates (3×10^4 cells per well) in 100 µl of culture medium. The next day, cells were pre-incubated for 60 min with 2-fold serial dilutions of CsA, TAC or VCS, starting at 25 µM concentration and RDV starting at 10 µM. Subsequently, cells were infected with SARS-CoV-2 (MOI of 1, based on titer determined on Vero E6 cells) in 50 µl of medium with compound. After a 1h incubation at 37°C, cells were washed three times with PBS and 100 µl of medium with compound was added. The medium was harvested from the wells at 24-hours post-infection (h p.i.). Analysis of viral progeny released from the infected Calu-3 cells was performed by plaque assay on Vero E6 cells as described[67]. VCS concentrations were measured by validated LC-MS/MS after adding 9 volumes of methanol to the harvested medium. , . A cytotoxicity assay with mock infected cells, treated in the same way, was performed in parallel, as described for the CPE reduction assay.

Viral yield reduction assays in glass bottles

Borosilicate glass reagent bottles (50-ml) were treated with glacial acetic acid to remove possible detergent residues, followed by washing twice with absolute ethanol. The bottles dried and UV-sterilized prior to use. Three times concentrated compound solutions were prepared in EMEM-2% FCS using sterile glass culture tubes, a glass 50-µl syringe (Hamilton) and glass Pasteur pipettes. One ml of each compound dilution was transferred to three different reagent bottles (triplicates). Confluent monolayers of Calu-3 cells grown in culture flasks were infected with SARS-CoV-2/Leiden-002 at an MOI of 1. After incubation for 1h at

37°C, cells were washed three times with warm PBS, trypsinized and resuspended in EMEM-2% FCS. Two ml of this cell suspension (~10^6 cells) was added to each reagent bottle that already contained 1 ml of a 3x concentrated compound solution in medium. After incubation for 24h at 37°C, the medium was collected and the infectious virus titer was determined by plaque assay on Vero E6 cells. VCS concentrations in the medium were determined by LC-MS/MS as described above.

Determination of compound cytotoxicity in glass culture tubes

Calu-3 cells were trypsinized and 1.5 x 105 cells in 1 ml of EMEM-2% FCS were divided over glass culture tubes.. Two-fold dilutions of VCS, TAC and CsA starting at 150 µM concentration (3x final concentration) were prepared in EMEM-2% FCS medium using glass labware, and 0.5 ml was added to corresponding tubes with cells (three tubes per concentration). After a 24h incubation, cell viability was determined as described above.

SUPPORTING INFORMATION

Potential virucidal activity by an excipient of pharmaceutical formulations

Since the excipients include surfactants that could destroy the viral envelope, we tested whether the contents of the placebo capsules had a virucidal effect. To determine the virucidal potential of compounds or formulations, SARS-CoV-2 virions ($5x10^4$ PFU) were incubated for 2 h at 37°C with one of the following solutions: medium, a VCS solution prepared from pure powder, the dissolved content of VCS capsules, placebo capsules or Tween solutions (present in the capsules). The effect of these treatments on SARS-CoV-2 infectivity was determined by plaque assay on Vero E6 cells (Fig. S1). Phosphate-buffered saline (PBS) was used as a negative control and 50% ethanol as a positive control for virucidal activity. The (remaining) infectious virus titer was determined by plaque assay on Vero E6 cells as described[67]. A control treatment with 50% ethanol reduced the amount of infectious SARS-CoV-2 to below the limit of detection (<100 PFU/ml), while none of the other treatments significantly affected the remaining infectivity of the virus. Therefore, we concluded that the drug product excipients had no virucidal effect, but through an uncharacterized mechanism interfered with the readout of our CPE reduction assays. This made it impossible to determine the true EC_{50} values of these compounds when they were tested in their pharmaceutical formulations.

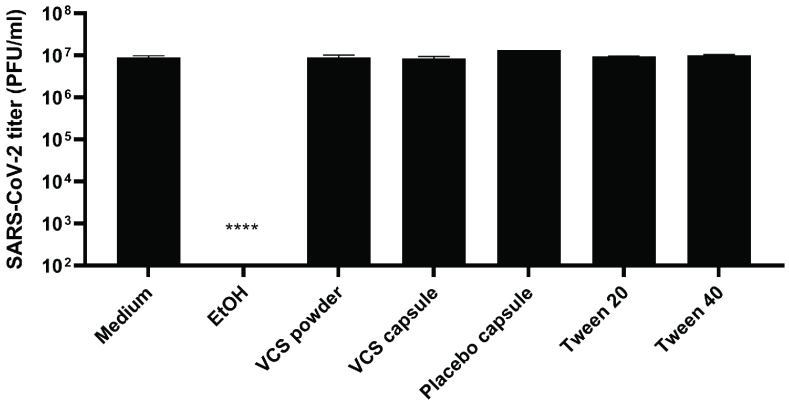

Fig. S1. Virucidal activity of VCS powder (3.2 µM), the drug formulation of VCS (3.2 µM), and content of placebo formulations (corresponding to 3.2 µM VCS), and 50% ethanol by incubation with a SARS-CoV-2 virus stock for 2 h, followed by quantification of the remaining amount of infectious virus titer by plaque assay. Statistical significance was determined by one-way ANOVA. *, p<0.1; **, p<0.01; ***, p<0.001; ****, p<0.0001.

Effect of Coating of plastic materials

The excipients in the pharmaceutical formulation of VCS appear to be critical for its bioavailability (to prevent plastic binding) but their (non-specific) antiviral effect also interferes with the determination of the true EC50 of VCS. To enable the use of VCS solutions prepared from pure powder in antiviral assays, we attempted to prevent VCS binding to plastic by coating all plastic labware used with 3 different coating agents that were described in literature: 100 mg/ml bovine serum albumin in PBS (BSA; Sigma) [70], 1% polyethylene glycol 3350 in MilliQ water (PEG-3350; Sigma)[71, 72] and 0.2% polysorbate 40 in MilliQ water (Tween40; Fluka) [73]. In addition, we saturated the plastic materials with VCS by treating them with a 500 mM VCS solution in DMSO (Sigma). Labware, including all tubes, tips and culture plastics, was filled with blocking solution and incubated for 2 h at room temperature with rocking to homogenously coat the surfaces. After rinsing twice with MilliQ water, the items were left to dry at room temperature until further use in experiments. Solutions of 0.2 and 2 µM of VCS were prepared in EMEM-2% FCS and 100 µl of each VCS solution was incubated in coated 96-well plates. After a 2 h incubation at 37°C the remaining VCS concentration was measured by validated LC-MS/MS. None of the coating treatments were able to reduce the nonspecific binding to plastic and loss of VCS (Table S1), as only 5 to 7% of the original concentration was recovered after a 2 h incubation. Even at t=0 only ~27% of the original stock concentration could be recovered due to VCS loss in pipette tips and tubes during the preparation of dilutions. Saturation of binding sites on plastic by treatment with 500 mM of VCS prevented loss of VCS from solution, but led to non-controlled VCS leaching from the plastic. This resulted in unpredictable concentrations that were higher than those in the input solution, e.g., we measured a VCS concentration of >15 µM when a 2 µM solution was incubated in a VCS saturated plastic plate. Since none of the coating treatments prevented nonspecific binding to plastic, the problem was circumvented by using glassware instead of plastics (Table 1). We also determined whether TAC and CsA bind to plastic using the same method as for VCS. Binding to plastic was minimal for TAC (24% loss) and for CsA we observed that after a 2 h incubation the CsA concentration was still 62% of the initial concentration (Table S2)

Table 2- VCS concentration in samples incubated in plastic labware with different coatings, measured by LC-MS/MS

	Type of coating applied									
	Uncoated		500 mM VCS		100 mg/ml BSA solution		1% PEG-3350 solution		0.2% Tween-40 solution	
Incubation time	Conc. (µM)	% remaining	Conc. (µM)	% remaining	Conc. (µM)	% remaining	Conc. (µM)	% remaining	Conc. (µM)	% remaining
0 h	0.56 ±0.25	**28**	17.21 ±2.36	**861**	0.55 ±0.21	**27**	0.51 ±0.16	**26**	0.56± 0.35	**28**
2 h	0.13 ±0.07	**7**	2.73 ±1.00	**137**	0.10 ±0.04	**5**	0.09 ±0.02	**4**	0.09 ±0.04	**4**

Conc. means concentration. Note: The percentages indicate the remaining concentration relative to the concentration of the original 2 µM of VCS stock solution.

Table 3- Concentration of TAC and CsA in samples incubated in plastic labware, measured by LC-MS/MS

	TAC		CsA	
Incubation time	Conc. µM	% remaining	Conc. µM	% remaining
0 h	0.85		0.76	
2 h	0.65	**76**	0.47	**62**

Note: The percentages indicate the remaining concentration relative to the concentration of the original compound stock solution (0.8 µM).

DISCLOSURE STATEMENT

The authors of this manuscript have conflicts of interest to disclose. This is investigator-initiated research. J.L.C. is an employee of Aurinia Pharmaceuticals Inc. O.T. received a grant without restrictions from Aurinia Pharmaceuticals Inc. to support part of this project and is an investigator of Aurinia clinical trials. Aurinia Pharmaceuticals Inc. had no role in the decision (what and when) to publish. There are no other conflicts of interest to disclose.

DATA AVAILABILITY STATEMENT

The data that support the findings of this study are available from the corresponding author upon reasonable request.

AUTHORSHIP:

NO Designed experiments, performed experiments, analyzed data and wrote the paper.
EM performed LC/MS-MS measurements and analyzed data.
EJA Performed background/literature research and contributed to writing the paper.
DJM Performed experiments, analyzed data and contributed to writing the paper.
AT Performed experiments.
JLC Provided essential reagents and data and contributed to writing the paper.
EJS Provided essential materials, analyzed the data and wrote the paper.
YKOT Designed the study and wrote the paper.
APJdV Designed the study and wrote the paper.
MJvH Designed and supervised the study, analyzed data and wrote the paper.

ACKNOWLEDGMENTS

N.S.O., E.J.S. and M.J.v.H. were supported by the #wakeuptocorona crowdfunding initiative of Leiden University Fund (LUF) and LUMC Bontius Foundation.

REFERENCES

1. Zhou, F., et al., *Clinical course and risk factors for mortality of adult inpatients with COVID-19 in Wuhan, China: a retrospective cohort study.* Lancet, 2020. **395**(10229): p. 1054-1062.
2. Huang, C., et al., *Clinical features of patients infected with 2019 novel coronavirus in Wuhan, China.* Lancet, 2020. **395**(10223): p. 497-506.
3. Guan, W.J., et al., *Comorbidity and its impact on 1590 patients with COVID-19 in China: a nationwide analysis.* Eur Respir J, 2020. **55**(5).
4. Williamson, E.J., et al., *Factors associated with COVID-19-related death using OpenSAFELY.* Nature, 2020. **584**(7821): p. 430-436.
5. Poulsen, N.N., et al., *Cyclosporine and COVID-19: Risk or favorable?* Am J Transplant, 2020.
6. Pascual, J., et al., *Everolimus with Reduced Calcineurin Inhibitor Exposure in Renal Transplantation.* J Am Soc Nephrol, 2018. **29**(7): p. 1979-1991.
7. Maggiore, U., et al., *How should I manage immunosuppression in a kidney transplant patient with COVID-19? An ERA-EDTA DESCARTES expert opinion.* Nephrol Dial Transplant, 2020. **35**(6): p. 899-904.
8. Fishman, J.A., *The Immunocompromised Transplant Recipient and SARS-CoV-2 Infection.* J Am Soc Nephrol, 2020. **31**(6): p. 1147-1149.
9. Schoot, T.S., et al., *Immunosuppressive Drugs and COVID-19: A Review.* Front Pharmacol, 2020. **11**: p. 1333.
10. Carbajo-Lozoya, J., et al., *Replication of human coronaviruses SARS-CoV, HCoV-NL63 and HCoV-229E is inhibited by the drug FK506.* Virus Res, 2012. **165**(1): p. 112-7.
11. Gordon, D.E., et al., *A SARS-CoV-2 protein interaction map reveals targets for drug repurposing.* Nature, 2020. **583**(7816): p. 459-468.
12. Ma-Lauer, Y., et al., *Influences of cyclosporin A and non-immunosuppressive derivatives on cellular cyclophilins and viral nucleocapsid protein during human coronavirus 229E replication.* Antiviral Res, 2020. **173**: p. 104620.
13. Ishii, N., et al., *Diverse effects of cyclosporine on hepatitis C virus strain replication.* J Virol, 2006. **80**(9): p. 4510-20.
14. Qing, M., et al., *Cyclosporine inhibits flavivirus replication through blocking the interaction between host cyclophilins and viral NS5 protein.* Antimicrob Agents Chemother, 2009. **53**(8): p. 3226-35.
15. Braaten, D., et al., *Cyclosporine A-resistant human immunodeficiency virus type 1 mutants demonstrate that Gag encodes the functional target of cyclophilin A.* J Virol, 1996. **70**(8): p. 5170-6.
16. Dang, W., et al., *Inhibition of Calcineurin or IMP Dehydrogenase Exerts Moderate to Potent Antiviral Activity against Norovirus Replication.* Antimicrob Agents Chemother, 2017. **61**(11).
17. de Wilde, A.H., et al., *Cyclosporin A inhibits the replication of diverse coronaviruses.* J Gen Virol, 2011. **92**(Pt 11): p. 2542-2548.
18. Ma, C., et al., *Discovery of cyclosporine A and its analogs as broad-spectrum anti-influenza drugs with a high in vitro genetic barrier of drug resistance.* Antiviral Res, 2016. **133**: p. 62-72.
19. Franke, E.K., H.E. Yuan, and J. Luban, *Specific incorporation of cyclophilin A into HIV-1 virions.* Nature, 1994. **372**(6504): p. 359-62.

20. Nakagawa, M., et al., *Specific inhibition of hepatitis C virus replication by cyclosporin A.* Biochem Biophys Res Commun, 2004. **313**(1): p. 42-7.
21. de Wilde, A.H., et al., *MERS-coronavirus replication induces severe in vitro cytopathology and is strongly inhibited by cyclosporin A or interferon-alpha treatment.* J Gen Virol, 2013. **94**(Pt 8): p. 1749-1760.
22. Carbajo-Lozoya, J., et al., *Human coronavirus NL63 replication is cyclophilin A-dependent and inhibited by non-immunosuppressive cyclosporine A-derivatives including Alisporivir.* Virus Res, 2014. **184**: p. 44-53.
23. von Brunn, A., et al., *Genetic deficiency and polymorphisms of cyclophilin A reveal its essential role for Human Coronavirus 229E replication.* Curr Opin Virol, 2015. **14**: p. 56-61.
24. Favreau, D.J., et al., *Human coronavirus-induced neuronal programmed cell death is cyclophilin d dependent and potentially caspase dispensable.* J Virol, 2012. **86**(1): p. 81-93.
25. de Wilde, A.H., et al., *Alisporivir inhibits MERS- and SARS-coronavirus replication in cell culture, but not SARS-coronavirus infection in a mouse model.* Virus Res, 2017. **228**: p. 7-13.
26. Ogando, N.S., et al., *SARS-coronavirus-2 replication in Vero E6 cells: replication kinetics, rapid adaptation and cytopathology.* J Gen Virol, 2020.
27. Softic, L., et al., *Inhibition of SARS-CoV-2 Infection by the Cyclophilin Inhibitor Alisporivir (Debio 025).* Antimicrob Agents Chemother, 2020. **64**(7).
28. Kronbichler, A., et al., *COVID-19: implications for immunosuppression in kidney disease and transplantation.* Nat Rev Nephrol, 2020. **16**(7): p. 365-367.
29. de Wilde, A.H., et al., *Cyclophilins and cyclophilin inhibitors in nidovirus replication.* Virology, 2018. **522**: p. 46-55.
30. Papp, K., et al., *Efficacy of ISA247 in plaque psoriasis: a randomised, multicentre, double-blind, placebo-controlled phase III study.* Lancet, 2008. **371**(9621): p. 1337-42.
31. Busque, S., et al., *The PROMISE study: a phase 2b multicenter study of voclosporin (ISA247) versus tacrolimus in de novo kidney transplantation.* Am J Transplant, 2011. **11**(12): p. 2675-84.
32. Rovin, B.H., et al., *A randomized, controlled double-blind study comparing the efficacy and safety of dose-ranging voclosporin with placebo in achieving remission in patients with active lupus nephritis.* Kidney Int, 2019. **95**(1): p. 219-231.
33. Birsan, T., et al., *The novel calcineurin inhibitor ISA247: a more potent immunosuppressant than cyclosporine in vitro.* Transpl Int, 2005. **17**(12): p. 767-71.
34. Kuglstatter, A., et al., *Structural basis for the cyclophilin A binding affinity and immunosuppressive potency of E-ISA247 (voclosporin).* Acta Crystallogr D Biol Crystallogr, 2011. **67**(Pt 2): p. 119-23.
35. Stalder, M., et al., *In vivo evaluation of the novel calcineurin inhibitor ISATX247 in non-human primates.* J Heart Lung Transplant, 2003. **22**(12): p. 1343-52.
36. Gregory, C.R., et al., *Compared with cyclosporine, ISATX247 significantly prolongs renal-allograft survival in a nonhuman primate model.* Transplantation, 2004. **78**(5): p. 681-5.
37. Ransom, J.T., *Mechanism of action of mycophenolate mofetil.* Ther Drug Monit, 1995. **17**(6): p. 681-4.

38. Ritter, M.L. and L. Pirofski, *Mycophenolate mofetil: effects on cellular immune subsets, infectious complications, and antimicrobial activity.* Transpl Infect Dis, 2009. **11**(4): p. 290-7.
39. Neyts, J., G. Andrei, and E. De Clercq, *The novel immunosuppressive agent mycophenolate mofetil markedly potentiates the antiherpesvirus activities of acyclovir, ganciclovir, and penciclovir in vitro and in vivo.* Antimicrob Agents Chemother, 1998. **42**(2): p. 216-22.
40. Coates, P.T., et al., *Early experience with COVID-19 in kidney transplantation.* Kidney Int, 2020. **97**(6): p. 1074-1075.
41. Husain, S.A., et al., *Early Outcomes of Outpatient Management of Kidney Transplant Recipients with Coronavirus Disease 2019.* Clin J Am Soc Nephrol, 2020. **15**(8): p. 1174-1178.
42. Li, F., J. Cai, and N. Dong, *First cases of COVID-19 in heart transplantation from China.* J Heart Lung Transplant, 2020. **39**(5): p. 496-497.
43. Zhang, H., et al., *Identification of Kidney Transplant Recipients with Coronavirus Disease 2019.* Eur Urol, 2020. **77**(6): p. 742-747.
44. Guillen, E., et al., *Case report of COVID-19 in a kidney transplant recipient: Does immunosuppression alter the clinical presentation?* Am J Transplant, 2020. **20**(7): p. 1875-1878.
45. Montagud-Marrahi, E., et al., *Preliminary data on outcomes of SARS-CoV-2 infection in a Spanish single center cohort of kidney recipients.* Am J Transplant, 2020. **20**(10): p. 2958-2959.
46. Deng, G., et al., *Clinical determinants for fatality of 44,672 patients with COVID-19.* Crit Care, 2020. **24**(1): p. 179.
47. Docherty, A.B., et al., *Features of 20 133 UK patients in hospital with covid-19 using the ISARIC WHO Clinical Characterisation Protocol: prospective observational cohort study.* BMJ, 2020. **369**: p. m1985.
48. Siddiqi, H.K. and M.R. Mehra, *COVID-19 illness in native and immunosuppressed states: A clinical-therapeutic staging proposal.* J Heart Lung Transplant, 2020. **39**(5): p. 405-407.
49. Willicombe, M., D. Thomas, and S. McAdoo, *COVID-19 and Calcineurin Inhibitors: Should They Get Left Out in the Storm?* J Am Soc Nephrol, 2020. **31**(6): p. 1145-1146.
50. Guisado-Vasco, P., et al., *Clinical characteristics and outcomes among hospitalized adults with severe COVID-19 admitted to a tertiary medical center and receiving antiviral, antimalarials, glucocorticoids, or immunomodulation with tocilizumab or cyclosporine: A retrospective observational study (COQUIMA cohort).* EClinicalMedicine, 2020. **28**: p. 100591.
51. Pfefferle, S., et al., *The SARS-coronavirus-host interactome: identification of cyclophilins as target for pan-coronavirus inhibitors.* PLoS Pathog, 2011. **7**(10): p. e1002331.
52. Sauerhering, L., et al., *Cyclophilin Inhibitors Restrict Middle East Respiratory Syndrome Coronavirus Via Interferon lambda In Vitro And In Mice.* Eur Respir J, 2020.
53. Wang, Y., et al., *A retrospective cohort study of methylprednisolone therapy in severe patients with COVID-19 pneumonia.* Signal Transduct Target Ther, 2020. **5**(1): p. 57.
54. Yin, Y. and R.G. Wunderink, *MERS, SARS and other coronaviruses as causes of pneumonia.* Respirology, 2018. **23**(2): p. 130-137.

55. Schultz, C., *Voclosporin as a treatment for noninfectious uveitis.* Ophthalmol Eye Dis, 2013. **5**: p. 5-10.
56. Li, Y., et al., *Pharmacokinetic Disposition Difference Between Cyclosporine and Voclosporin Drives Their Distinct Efficacy and Safety Profiles in Clinical Studies.* Clin Pharmacol, 2020. **12**: p. 83-96.
57. Hoffmann, M., et al., *The novel coronavirus 2019 (2019-nCoV) uses the SARS-coronavirus receptor ACE2 and the cellular protease TMPRSS2 for entry into target cells.* bioRxiv, 2020.
58. Hoffmann, M., et al., *Chloroquine does not inhibit infection of human lung cells with SARS-CoV-2.* Nature, 2020. **585**(7826): p. 588-590.
59. Dittmar, M., et al., *Drug repurposing screens reveal FDA approved drugs active against SARS-Cov-2.* bioRxiv, 2020: p. 2020.06.19.161042.
60. Kampf, G., *Efficacy of ethanol against viruses in hand disinfection.* J Hosp Infect, 2018. **98**(4): p. 331-338.
61. Kratzel, A., et al., *Inactivation of Severe Acute Respiratory Syndrome Coronavirus 2 by WHO-Recommended Hand Rub Formulations and Alcohols.* Emerg Infect Dis, 2020. **26**(7): p. 1592-1595.
62. Galabov, A.S., *Virucidal agents in the eve of manorapid synergy.* GMS Krankenhhyg Interdiszip, 2007. **2**(1): p. Doc18.
63. Fukazawa, T., Y. Yamazaki, and Y. Miyamoto, *Reduction of non-specific adsorption of drugs to plastic containers used in bioassays or analyses.* J Pharmacol Toxicol Methods, 2010. **61**(3): p. 329-33.
64. Lipinski, C.A., *Drug-like properties and the causes of poor solubility and poor permeability.* J Pharmacol Toxicol Methods, 2000. **44**(1): p. 235-49.
65. Palmgren, J.J., et al., *Drug adsorption to plastic containers and retention of drugs in cultured cells under in vitro conditions.* Eur J Pharm Biopharm, 2006. **64**(3): p. 369-78.
66. Tseng, C.T., et al., *Apical entry and release of severe acute respiratory syndrome-associated coronavirus in polarized Calu-3 lung epithelial cells.* J Virol, 2005. **79**(15): p. 9470-9.
67. Salgado-Benvindo, C., et al., *Suramin Inhibits SARS-CoV-2 Infection in Cell Culture by Interfering with Early Steps of the Replication Cycle.* Antimicrob Agents Chemother, 2020. **64**(8).
68. Zwart, T.C., et al., *Therapeutic drug monitoring of tacrolimus and mycophenolic acid in outpatient renal transplant recipients using a volumetric dried blood spot sampling device.* Br J Clin Pharmacol, 2018. **84**(12): p. 2889-2902.
69. Agency, E.M., *EMEA/CHMP/EWP/192217/2009 - Guideline on bioanalytical method validation*. 2011: United Kingdom.
70. Zanetti-Domingues, L.C., et al., *A systematic investigation of differential effects of cell culture substrates on the extent of artifacts in single-molecule tracking.* PLoS One, 2012. **7**(9): p. e45655.
71. Kenan, D.J., et al., *Peptide-PEG amphiphiles as cytophobic coatings for mammalian and bacterial cells.* Chem Biol, 2006. **13**(7): p. 695-700.
72. Schmitt, S.K., et al., *Polyethylene Glycol Coatings on Plastic Substrates for Chemically Defined Stem Cell Culture.* Adv Healthc Mater, 2015. **4**(10): p. 1555-64.

73. Senturk Parreidt, T., et al., *Effect of Presence and Concentration of Plasticizers, Vegetable Oils, and Surfactants on the Properties of Sodium-Alginate-Based Edible Coatings.* Int J Mol Sci, 2018. **19**(3).

CHAPTER VIII

General Discussion

PREFACE

Before the ongoing COVID-19 pandemic, researchers studying CoVs encompassed a small community, of whom the majority had been working in this field for decades [1]. This reality has changed since early 2020, when SARS-CoV-2 emerged and COVID-19 was declared a public health emergency of international concern by WHO. Many research groups specialized in different fields, including structural biology, chemistry and immunology, shifted their focus to CoVs and have been contributing their expertise to the accelerated development of our knowledge about these viruses, and more specifically SARS-CoV-2. These efforts translated into a *boom* of publications, more than 1000 per week, accepted for publication by journals or pre-printed in scientific databases [2]. Therefore, it is difficult to keep up with and summarize all the new discoveries in the CoV field, and any effort made to do so today (in May 2021) may be outdated or incomplete in a few months from now.

Coronavirus infection in humans can be asymptomatic, result in common cold symptoms, or cause mild to severe pneumonia. The development of severe symptoms is mostly associated with other comorbidities and infection with zoonotic CoVs. Over the past two decades, three zoonotic and (highly) pathogenic CoVs emerged: SARS-CoV in 2002, MERS-CoV in 2012 (more likely earlier) and SARS-CoV-2 in 2019. The mortality, societal impact and economic costs of the latter zoonotic CoV exploded and these unprecedented consequences emphasize the immeasurable value of solutions to prevent transmission of these viruses and treat those infected.

Before 2020, there were no registered drugs that could inhibit pathogenic CoV replication or treat associated diseases. Over the past year, some therapeutics for emergency treatment of COVID-19 patients and at least four COVID-19 vaccines were approved. However, these resources are not (immediately) available or suitable to be administered to everyone. Together with the (potential) problems caused by continuous virus evolution, this means that it is essential to continue the identification and development of antiviral drugs and vaccine research. The main objective of the studies described in this thesis was to characterize CoV drug targets and search for broad-spectrum CoV inhibitors. For this purpose, two strategies were used: (i) studying CoV replication to characterize potential targets for new compounds and (ii) performing phenotypic screening of previously developed compounds. Cell-based screenings were performed (as described in **chapter II**) using different classes of compounds including immunosuppressive and non-immunosuppressive derivatives of cyclosporin A, hits from FDA-approved drug libraries and molecules synthesized by collaborators such as fleximers (nucleoside analogues [3]) and SAH hydrolase inhibitors [4]. Subsequently, some

compounds that reduced the virus-induced cytopathic effect without being cytotoxic were characterized further in mechanistic studies, genotyping of drug-resistant mutants, followed by confirmation using reverse genetics. **Chapters VI** characterizes a new small-molecule inhibitor, DFA, with antiviral activity against MERS-CoV, while **chapter VII** describes the potential beneficial use of Voclosporin, a recently marketed compound to treat active lupus nephritis, which may also reduce SARS-CoV-2 viral loads. The latter is currently being evaluated in a clinical trial for the treatment of COVID-19 in kidney transplant recipients (KTRs), who are already receiving immunosuppressive treatment. The development of antiviral therapies requires understanding of coronavirus replication and its interplay with host cells. In **chapters III to V**, the in-depth characterization of nsp14, one of the replication and transcription complex (RTC) components, provides evidence for its importance for virus viability and fitness, while establishing that nsp14 might be a good target for drug design. In this Discussion (**chapter VIII**), new findings important to understand CoV molecular biology are highlighted. In addition, developments in antiviral research are summarized, describing potential targets for drug design and exploring the road to the future development of effective inhibitors of CoV replication.

ANTIVIRAL RESEARCH

As long as humankind exists, infectious diseases have caused suffering and claimed millions of lives. Over the past 50 years, the number of newly emerging infectious diseases appears to have increased and they are also spreading more quickly. Based on our records of outbreaks and epidemics, a large number of these events have been caused by RNA viruses infecting the respiratory tract, like influenza virus, Nipah and Hendra virus, hantavirus and various CoVs [5]. Lower respiratory tract infections are among the ten leading causes of death globally, according to the last WHO report [6]. Despite the burden of these viral diseases, our armamentarium of antivirals remains limited to about 90 drugs approved for the treatment of human infections caused by only 10 viral pathogens including influenza virus, HCV, RSV and HIV [7]. None of these drugs was specifically designed/developed to target CoVs. However, upon the emergence of SARS-CoV, MERS-CoV and SARS-CoV-2, some of these existing antivirals were tested [8, 9], which led to the discovery of compounds with broad-spectrum activity potential, like protease inhibitors and nucleoside analogues.

At first, in an epidemic/pandemic emergency situation, when there is no approved treatment available, the search for drugs is centered on the re-purposing of compounds that were originally licensed for use against other (viral) infections or to treat other diseases. Drugs that were withdrawn or abandoned, due to sub-optimal efficacy against their primary indication,

can potentially be repurposed as well. The advantage of using this strategy is the availability of knowledge regarding the safety, pharmacokinetics, potential side-effects, optimal formulation and dosage of a drug. This information (supposedly) accelerates the process of drug approval that is time-consuming and costly. To date (May 2021), more than 2400 clinical trials have been initiated since the emergence of SARS-CoV-2, to test single compounds or drug combinations for the treatment of COVID-19 patients [10]. These trials include antibodies and several classes of small molecules, such as existing antivirals, natural molecules, antiparasitic and antibacterial drugs, and immunomodulators that inhibit CoV replication in infected cells and, for some, also in small-animal models.

Learning by trial and error: the importance of appropriate models

At the start of the pandemic (March 2020), one of the first compounds proposed for the treatment of COVID-19 was hydroxychloroquine, a less toxic derivative of chloroquine. This drug was first synthesized in 1946 and has been used as an antimalarial therapy. The broad-spectrum antiviral activity of these drugs against different CoVs (including MERS-CoV, SARS-CoV and HcoV-229E) and other RNA viruses *in vitro* [11-14] raised interest to immediately investigate its inhibitory effect in SARS-CoV-2 infected cells [15, 16], as also presented in **chapter II**. Based on the promising *in vitro* data, many clinical trials with hydroxychloroquine were started and the FDA even temporarily recommended its use in COVID-19 patients in March 2020. However, not much later both FDA and WHO advised against its use based on the risk of developing dangerous side-effects and the meta-analysis of randomized controlled trials that demonstrated a lack of efficacy to reduce progress of infection, morbidity and hospital admissions [17]. The presumed mode of action of these drugs relies on the increase of endosomal pH by the capturing of protons (reviewed in [18]). As one of the entry pathways used by CoVs is endocytosis, it was hypothesized that these drugs would prevent the fusion of viral and cellular membranes and thus the release of the viral genome into the cytoplasm. The inhibitory effect of chloroquine and hydroxychloroquine that was originally demonstrated in cell-based assays using Vero cells (monkey kidney cells) could however not be reproduced when human lung cells or more complex cell cultures like organoids were used [19, 20]. The main reason for this discrepancy is that the SARS-CoV-2 Spike (S) protein, which mediates viral entry, can be activated by different proteases that are differentially expressed in different cell lines. In some cell lines, like Vero cells, viral entry is activated by the endosomal-pH-dependent cysteine protease cathepsin L, while in lung cell lines, which present low expression of cathepsin, cell entry is dependent on other pH-independent proteases, like TMPRSS2 [21, 22]. Thus, in the latter cells, entry occurs by a different pathway, fusion at the cell surface, that is

not blocked by hydroxychloroquine. When tested in SARS-CoV-2 infection experiments using hamsters and non-human primate models, hydroxychloroquine provided no therapeutic benefit [20]. In general, no differences in clinical manifestations or viral load were observed between untreated and treated animals, even in a prophylactic set-up in which animals were treated at least 24 h before infection [23-25]. Randomized clinical trial results correlated with the pre-clinical studies, demonstrating that there was no difference between placebo- or hydroxychloroquine-treated COVID-19 patients [18].

The story of (hydroxy)chloroquine emphasizes that the use of appropriate cell-culture or animal models that properly mimic the *in vivo* conditions can be critical to investigate the inhibitory activity of compounds before following them up in clinical trials. Cell lines expressing the appropriate virus receptor (susceptible) and supporting complete viral replication (permissive) need to be used. When developing cell-based screening assays, the choice of cell line is primarily based on the degree of cytopathic effect caused by viral infection. Compared to MERS-CoV, unfortunately, not many cell lines support SARS-CoV and SARS-CoV-2 replication, unless facilitated by the artificial expression of co-factors such as TMPRSS2 [21, 26, 27]. Ideally, HAE cultures developed from nasal, tracheal or bronchial primary cells [28-30], lung organoids [31] or lung-on-a-chip [32] should be used to study CoVs, as these may more closely reflect the events occurring during infection in humans. However, the use of this type of tools comes with a high financial burden and technical challenges.

Timing and regime of antiviral treatment

The SARS-CoV-2 replication is often already declining by the time that symptoms develop and antiviral drug are then administered too late to have impact. Accordingly, coronavirus inhibitors targeting essential stages of viral replication would only be expected to decrease the severity of disease if they are administered early enough to reduce the viral load and spread within the body. Severe disease manifestations, such as acute respiratory distress syndrome, appear to be primarily driven by host-mediated inflammatory responses rather than ongoing viral replication [33].

One antiviral drug approved for emergency use against SARS-CoV-2 is remdesivir, an adenosine analogue with broad-spectrum activity against CoVs and some other groups of RNA viruses. Studies with MERS-CoV and SARS-CoV revealed the high efficacy of this compound in reducing viral loads in cell culture-based infection models and showed both its prophylactic and therapeutic efficacy in different animal models [34-36]. In some clinical trials for COVID-19, remdesivir treatment was reported to shorten the time to recovery in hospitalized adults [37, 38]. However, a large WHO clinical trial demonstrated that remdesivir treatment did not

reduce the duration of hospitalization or need for ventilation [17]. Moreover, remdesivir showed only modest clinical efficacy and no impact on the survival of COVID-19 patients, although this outcome may have been influenced by the timing of the start of treatment. So far, remdesivir has mostly been administered by intravenous infusion to hospitalized patients, (presumably) at a time point that the viral load has already decreased. If patients progress from the viral replication phase to the stage of elevated inflammatory response (cytokine storm), remdesivir cannot be beneficial as it is not an immunomodulatory agent. A combination therapy that tackles both viral replication and the inflammatory response could be ideal for the treatment of COVID-19 patients. Dual therapies using remdesivir and corticosteroids (like dexamethasome) and cytokine inhibitors (like tocilizumab EXO-CD24) are currently under evaluation in clinical trials.

To be administered as early as possible, remdesivir should become available in a different formulation than the one requiring intravenous injection, allowing its use during the asymptomatic phase immediately after diagnosis, or even prophylactically. According to remdesivir manufacturer Gilead, the development of an oral formulation is in progress. Two other nucleotide prodrugs, AT-527 and EIDD-2801 (Table 1), both available in pills, showed broad-spectrum activity against different CoVs in cell-based assays [39-41]. In addition, EIDD-2801 was demonstrated to have a potent antiviral effect against SARS-CoV-2 in mouse models when administered by oral gavage before intranasal infection [42]. This shows that the compound can be metabolized and is distributed to the lungs of the animals. This promising result suggests that an oral formulation at least in this case allows sufficient bioavailability. As an alternative, taking into consideration that SARS-CoV-2 replicates well in the nose, intranasal formulations could be developed.

Some new things in the loop

The lack of resources for anti-CoV drug discovery before 2019 was related with the low incidence of SARS and MERS in the human population. Treatment options that demonstrated potent *in vitro* and *in vivo* antiviral activity against SARS-CoV, MERS-CoV or other CoVs were not prioritized for clinical development [9]. Also the lack of reliable animal models to prove antiviral activity efficacy stalled further evaluation of prospective compounds. For example, rhesus macaques were validated as a valuable model for MERS-CoV infection only in 2016 [43], when autopsies of MERS patients confirmed the pathology described during experiments with this non-primate model performed 3 years earlier [44, 45]. Overall, drug development efforts needed to start almost from scratch when SARS-CoV-2 emerged.

One of the main limitations of studying zoonotic CoVs is the requirement for biosafety laboratories of containment level category 3, which restricts the access to trained people and increases the costs of research. In order to circumvent this problem, non-live virus solutions like pseudoviruses, chimeric particles expressing envelop proteins from CoVs on the surface of a benevolent carrier virus, can be used for screening of entry inhibitors and evaluation of neutralizing antibodies [46-49]. Moreover, this tool has been applied to understand the mechanisms of viral entry, for example the role of the furin cleavage site (**chapter II**), and monitor current vaccine efficacy [46, 50].

All along the path of drug development, two main requirements need to be met: drugs should demonstrate a high degree of safety and strong inhibition of viral replication. The identification and study of compounds targeting viral components (direct-acting antivirals) or compounds targeting host factors, which may indirectly inhibit viral replication, have been widely explored using different (new) strategies. Technological advances like genome- and proteome-wide approaches have created opportunities to map virus-host interactions and explore their relevance for virus replication and pathogenesis [51-53]. These interactomes have highlighted pro-viral factors that can potentially be explored as a target for broad-spectrum inhibitors across different CoVs. Examples are the interaction of the ORF9b protein of SARS-CoV and SARS-CoV-2 with Tom 70, a mitochondrial import receptor [51, 54], and the effect on CoV replication of the knockdown or knockout of Sigma1 receptor [51], which has also been implicated in HCV and Sendai virus replication [55, 56]. However, high cytotoxicity is often related with the use of host factor-targeting inhibitors as they are more likely to also have deleterious effects on the host cell. To mitigate this risk, more specific and potent inhibitors need to be used at lower concentrations and/or should be used for shorter periods of time.

The fact that protein structures can now be obtained much more easily by cryo-electron microscopy (Cryo-EM) and can be used in advanced computational approaches [57] enhances the design of drugs with higher potential specificity for their target and helps to understand the interactions between inhibitor and target. Interestingly, different databases have been created to promote sharing of scientific information on developed molecules and structures of potential targets, which reflect the adaptation of research to the new technology and big data sharing: the international crowdsourced initiative COVID moonshot and the platform covid19dataportal are two good examples. The small number of drugs that currently meet the criteria for approval for COVID-19 treatment by health authorities underlines the large need for robust preclinical drug discovery programs. This involves not only the design and

development of new compounds (instead of repurposing), but also dissecting the mode of action of available compounds in clinical and pre-clinical studies.

THE CORONAVIRUS REPLICATION AND TRANSCRIPTION COMPLEX

The success rate of drug design will be importantly improved by understanding the molecular biology of CoVs in more detail. Since the writing of **chapter III**, the knowledge on the CoV RTC has greatly expanded. In particular the acquisition of cryo-EM-derived protein structures and the expanded NGS possibilities, including long-read sequencing, contributed to a better understanding of how the subunits forming the CoV RTC orchestrate RNA synthesis. The following paragraphs describe the latest mechanistic insights, their implications for virus fitness and how some nucleoside analogues target the RTC.

The art of copying large RNA genomes

The replication and transcription of all positive-stranded RNA viruses occur in the cytoplasm of the infected cell. Coronaviruses encode two large replicase polyproteins, pp1a and pp1ab, that are processed into mature nsps by viral proteases that are embedded within the ORF1a-encoded part of the polyproteins [58, 59]. Most of these subunits assemble into a ribonucleoprotein complex (replication and transcription complex, RTC) that produces different types of viral transcripts. Viral trans-membrane proteins modify cellular membranes and create a micro-environment ('replication organelle') for viral RNA synthesis with which the RTC is associated (reviewed in [60]). The CoV RTC includes a range of nsps that play different roles during RNA synthesis, such as the RdRp, helicase, exoribonuclease, methyltransferases and corresponding auxiliary co-factors. The functions of most of the CoV replicase subunits have been discovered and characterized using a combination of bioinformatics, biochemistry, structural biology and (reverse) genetics (reviewed in [61-63]). For a long time, a notable knowledge gap was the lack of a structure of the nsp12-RdRp the central player of the RTC. Technical challenges in obtaining stable and active nsp12 proteins/complexes prevented the acquisition of crystal structures and complicated the biochemical characterization of the CoV RTC. In 2003, a prediction of the structure of nsp12-RdRp was published [64], but only in 2019, Kirchdoerfer and Ward solved the structure of the SARS-CoV nsp12, bound to its essential nsp7 and nsp8 co-factors, using cryo-EM [65]. Since then, several additional structures of nsp12-nsp7-nsp8_2, complexed with RNA and/or nucleoside analogues or with other RTC subunits such as nsp9 and nsp13, have been reported [66-73]. These structures will be important tools during the further elucidation of the

molecular mechanisms underlying specific steps of viral replication, the design of new antivirals targeting the RTC and the characterization of their (potential) MoA.

The CoV nsp12 possesses at least two functional domains: the Nidovirus RdRp associated nucleotidyl transferase domain (NiRAN) located in the N-terminal part of nsp12 and the RdRp domain. The latter is organized in motifs A to G distributed across three subdomains, the so-called finger, palm and thumb of the RdRp structure [64, 74, 75]. These seven conserved motifs are involved in: template binding (motif G), nucleotide selection and binding, and catalysis at the active site, which is composed of motif A and C and supported by motifs B and D. The initiation mechanism (priming) of CoV RNA synthesis remains to be elucidated and both primer-dependent and *de novo* (primer-independent) mechanisms have been proposed. If *de novo*-initiation is used, an RdRp commonly employs specific structural elements to guide and position the initiating NTPs for catalysis, as for example demonstrated for HCV [76]. Some biochemical support for such a mechanism was obtained using SARS-CoV proteins [77, 78]. In contrast, if a primer-dependent mechanism is used, another factor than the RdRp is needed to deliver a primer. So far, based on biochemical assays, nsp8, nsp12-NiRAN and nsp9 have been proposed to play a role in priming, which therefore is a matter of ongoing studies and debate. Initially, the viral nsp8 subunit was reported to be capable of synthesizing short oligonucleotide primers that could be used by the nsp12-RdRp [77, 79, 80]. In arteriviruses, the NiRAN domain was shown to perform NMP-ylation, covalently bind nucleoside monophosphates (NMP) to itself (self-NMP-ylation), or to other viral proteins while releasing pyrophosphate [75]. Additionally, a preference for UMP and GMP was observed [75, 81]. More recently, its counterpart in CoV nsp12 was shown to mediate the transfer of NMPs (nucleotidyltransferase) to nsp9 [75, 81]. One of the proposed possible roles of UMP-nsp9 is the priming of RNA synthesis starting at the polyadenylated 3' end of the viral RNA. This initiation mechanism would bear resemblance to that used by picornaviruses, in which the uridilylated viral protein VPg serves to prime viral RNA synthesis [82]. This model is also supported by bioinformatic analyses revealing structural similarities between CoV nsp12-RdRp and picornavirus polymerases, suggesting involvement of their common G motif in primer-dependent initiation of RNA synthesis [64, 83, 84]. Recently, nsp8 was identified as an alternative substrate for UMPylation by nsp12-NiRAN [85]. In the same study, both *de novo* and primer-dependent mechanisms for initiation of minus strand RNA synthesis were proposed to be used by the nsp12-nsp7-nsp8$_2$ complex, although the functional significance of having alternative initiation mechanisms remains to be elucidated [85].

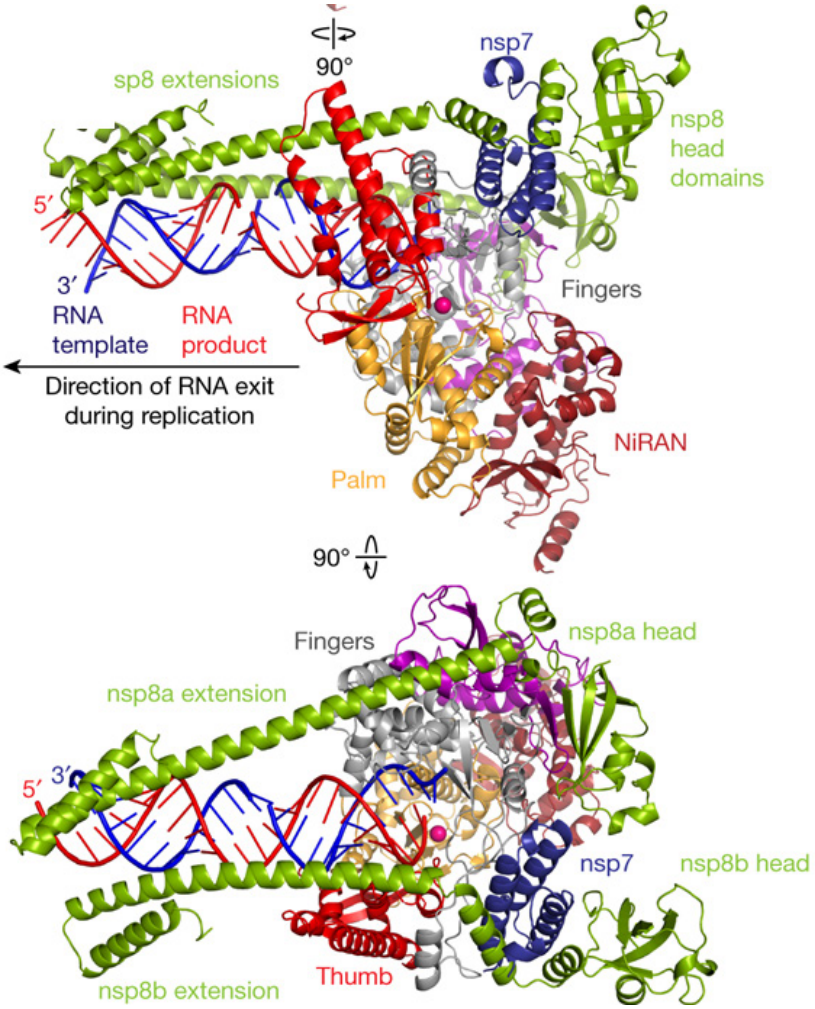

Fig. 1- Ribbon structure of nsp12-nsp8$_2$-nsp7 complex of SARS-CoV-2. RNA template in blue and RNA product in red. The nsp12 NiRAN and RdRp (fingers, palm and thumb) domains are depicted. Two positively charged 'sliding poles' extend from the RdRp and are formed by one nsp8 subunit in complex with nsp7 and one single nsp8 subunit. Interactions between positive-charged nsp8 residues and the emerging dsRNA during replication are thought to prevent premature dissociation of the replication machinery from its template. The sphere on top of the RdRp palm subdomain represents a metal ion in the active site of the RdRp. Re-used with permission from [69]

Minus strand RNA synthesis must start at the precise terminus of the RNA template or by priming at the genome-poly(A) tail junction, to ensure that the genetic information is copied completely [85]. Synthesis of new RNA proceeds by using +RNA strand as a template to produce a complementary full-length genome or sub-genome -RNA strand (as described in **chapter I**). In turn, these -RNAs strand then serve as a template for the synthesis of +RNA

strand molecules of both types (genome or sub-genome RNA). The newly synthesized full length +RNA can serve as template for further genomic -RNA, as mRNAs for viral protein production or as genomic RNA for packaging into viral progeny, while sub-genome length +RNA strands are used as a transcript for structural and accessory protein synthesis (reviewed in [63, 86]). The ssRNA template is expected to thread its way up to the active site, where incorporation of matching NTPs into the nascent strand occurs, fed through a separate tunnel [65]. At the RdRp active site, incoming NTPs base pair with the RNA template strand, while the 2' and 3' hydroxyl groups form hydrogen bonds with the polymerase [65]. During elongation, a helical double-stranded (ds) RNA product is formed consisting of the RNA template bound to the newly synthesized RNA strand, as depicted in Fig. 1 [66, 69].

The acquisition of a mini-RTC structure by expression of recombinant proteins and assembly of a nsp12-nsp7-nsp8_2-nsp13 complex allowed to better define the interactions between these replicase subunits (Fig. 2A). Nsp13 is the helicase, capable of unwinding RNA in a 5'-to-3' direction [87, 88] and presumably able to clear RNA secondary structures (or RNA-binding proteins), resulting in a single-stranded template that can be used for RNA synthesis. The nsp12-nsp7-nsp8_2-nsp13 complex displayed an increased *in vitro* helicase velocity compared with nsp13 alone [72]. The majority of complexes obtained *in vitro* were formed by two subunits of nsp13, each interacting with the N-terminal region of a nsp8 subunit. The nsp12-nsp7-nsp8_2-nsp13_2 complex showed better resolution and stability than the one formed with only a single nsp13 subunit [72, 73], which suggests that this six multi-part complex is most likely to prevail. The fact that the nsp12-RdRp and nsp13-helicase would translocate in opposite directions, 3'-to-5' and 5'-to-3', respectively, during RNA chain elongation presents a conundrum [73]. In order to explain how the two enzymes may work together, it was proposed that the polymerase may be pushed backwards on the template strand, a mechanism called backtracking. This mechanism has been well-characterized, mainly in DNA-dependent RNA polymerases (DdRp [89]), and has been observed for other viral RdRps [90, 91]. During backtracking, the RdRp would be temporarily inactive (i.e., not performing NTP incorporation) and the template RNA would be held by the helicase, while the product RNA (ssRNA) would be extruding from the RdRp through a secondary channel (Fig. 2B), resembling the one in DdRps that can accommodate single-stranded nucleic acids [73]. This mechanism was demonstrated to help rescue of stalled elongation complexes and removal of misincorporated nucleotides in bacterial and eukaryotic multi-part RNA polymerase complexes (reviewed in [92]). As well, in bacteria, backtracking can be induced by helicases [93], suggesting that the hypothesized backtracking process for nsp12-nsp7-nsp8_2-nsp13 is widespread among different RNA polymerase complexes. In the case of CoVs, a backtracking

mechanism could facilitate the process of template switching during synthesis of sgRNA [94], and/or it could make the 3'-end of the nascent strand accessible for proofreading [73, 95].

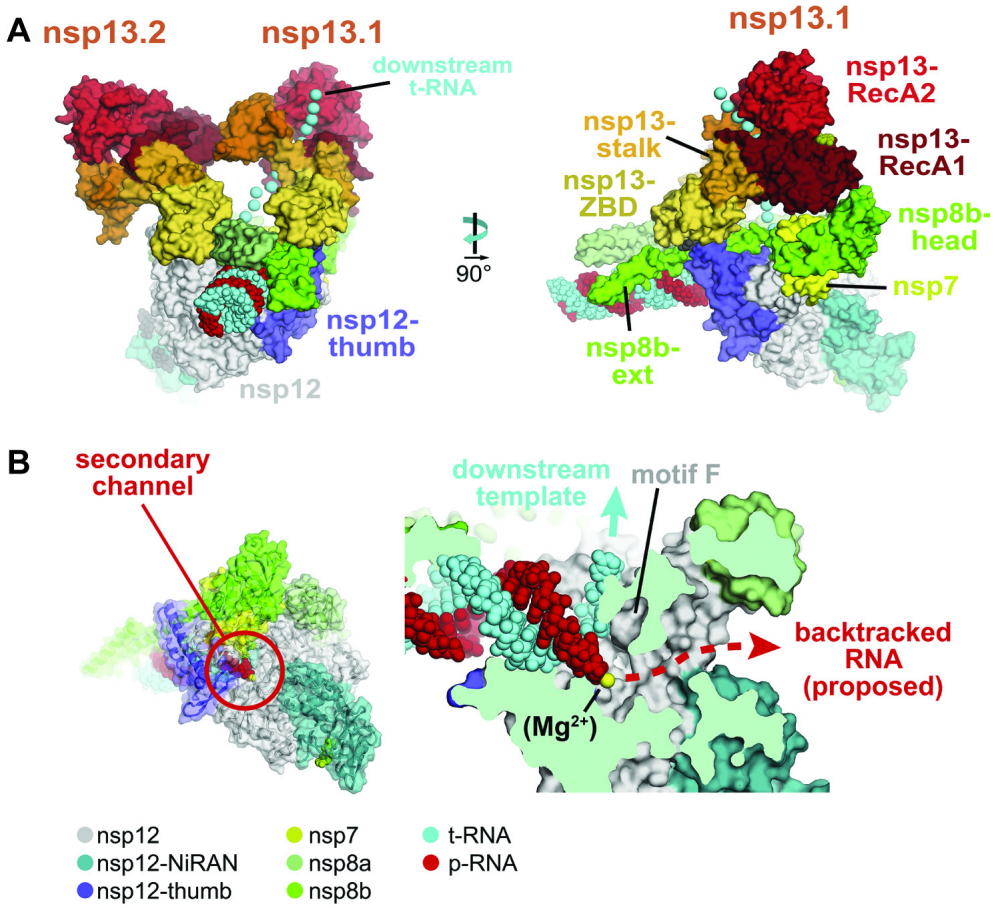

Figure 2- (A)Schematic illustration of the structure of a SARS-CoV-2 mini-RTC composed of nsp7, nsp8, nsp12 and nsp13 subunits. Two copies of nsp13 (nsp13.1 and nsp13.2) form a complex with nsp8 (extension of nsp8b) and nsp12 (thumb). The nsp13-helicase unwinds downstream dsRNA. (B) Localization of the secondary channel in the RdRp structure. The color coding in panel A and B are consistent.

During RNA synthesis, the CoV RdRp can erroneously incorporate mismatching NTPs, which are thought to be detected and excised by a 'proofreading' mechanism in which the central player is the nsp14 exoribonuclease (ExoN) [96], as described in more detail in **chapters III** and **IV**. In this manner, nsp14-ExoN is thought to decrease the CoV mutation rate. For maximal ExoN activity, nsp14 needs to form a complex with nsp10, which results in a conformational change that positions the ExoN catalytic residues closer together and enhances the enzymatic

activity [97]. The nsp10/nsp14 complex is thought to interact with the nsp12-nsp8$_2$-nsp7-nsp13 multimer in order to access a mismatched nucleotide and excise it from the 3' end of the nascent strand using its 3'-to-5' exonuclease activity [77, 96, 97]. Based on biochemical assays, this ExoN activity can use both ssRNA or RNA duplexes as a substrate [97, 98], although the latter is too large to fit in the RdRp secondary channel (Fig. 2B). Correction of dsRNA mismatches was only demonstrated *in vitro* by performing biochemical assays using nsp12-nsp7-nsp8 mixed with nsp10/nsp14 [96]. Supposedly, in this mechanism, nsp10/nsp14 complex would operate near the exit channel of the RdRp on the synthesized dsRNA (composed of the RNA template and RNA product). In this manner, the sequential recognition of mismatches, their excision and the incorporation of the correct NTP should be possible in a coordinated fashion. However, the structural analysis of the mini RTC (Fig. 2A; nsp12-nsp7-nsp8$_2$-nsp13($_2$)) revealed that the RdRp active site is too narrow to accommodate the nsp10/nsp14 complex [73], which suggests that error correction upon backtracking would be more feasible. Based on these structural considerations, the proposed mechanism is that nsp10/nsp14 binds at the mouth of the RdRp secondary channel (Fig. 2B), where it would encounter the 3' end of the nascent RNA strand. Then, the nsp10/nsp14 would have to hydrolyze this RNA, starting at its 3' end, until the mis-incorporated nucleobase is removed. This would require a tight coordination between all RTC subunits (nsp13, nsp12-nsp7-nsp8$_2$, nsp10/nsp14), like a delicate dance with back and forward steps, in order to guarantee the synthesis of a continuous and correct RNA strand. According to this model, the helicase would have a role in promoting the replication fidelity by directing the RNA towards the nsp14-ExoN active site. To date, an nsp10/nsp14 structure has been obtained only for SARS-CoV [96, 99] whereas a structure for the nsp14-ExoN domain in complex with nsp10 was recently reported for SARS-CoV-2 [100]. Due to stability and solubility issues, a structure of nsp12-nsp7-nsp8$_2$ or nsp12-nsp7-nsp8$_2$-nsp13 in complex with nsp10/nsp14 has not been acquired thus far, leaving the question unanswered whether the assembly of this multi-protein complex is possible and which motif or domain of nsp12 would interact with the nsp14.

The fact that some nucleoside/nucleotide analogues are capable of stalling RNA elongation whereas others fail due to the ExoN proofreading function [101], emphasizes how critical it is to better understand the CoV RNA replication/transcription mechanism. Future studies will be needed to clarify how the nsp10/nsp14 complex interacts with the RTC and how post-transcriptional modifications involving these and other replicase subunits are performed. Still, most of the hypotheses described above remain to be investigated by enzymatic assays and extrapolated to the context of the RTC in the living CoV-infected cell.

Messing up the code: Nucleoside/ nucleotide analogues

To date, one of the most extensively explored classes of antiviral drugs are nucleoside analogues, synthetic derivatives of natural purines and pyrimidines in which the sugar moiety and/or the heterocyclic ring is altered. These compounds can be formulated as nucleoside precursors, prodrugs or nucleotides (mono-, di- or triphosphorylated). Once administered, with the exception of NTPs, they will (presumably) be taken up by the cell and metabolized by host kinases to their active NTP form. Then, these compounds should be recognized by the viral replication/transcription machinery and incorporated into a nascent RNA chain. Inhibition can be achieved by one or more mechanisms including premature termination of RNA elongation by RdRp stalling, depletion of cellular NTP pools, or induction of mismatches that lead to accumulation of (deleterious) mutations [101, 102], also referred to as 'lethal mutagenesis' [103].

Some examples of nucleoside analogues previously reported to have antiviral activity against CoVs are listed in Table 1. In general, studies in which CoVs were cultured in the presence of nucleoside analogues demonstrated a relatively high barrier to antiviral drug resistance [34, 39, 104, 105]. To acquire resistance to nucleoside analogues, changes should be acquired in or near the RdRp's active site, which might interfere with its enzymatic activity and consequently viral fitness. For example, the two resistance mutations identified in the RdRp domain of MHV after passaging in the presence of remdesivir conferred partial resistance to the compound and reduced the fitness of MHV or SARS-CoV mutants in competition studies with wt virus [34]. Interestingly, the same mutations alone or together increased CoV sensitivity to B-D-N4-hydroxycytidine (NHC) [42]. Based on the overall conservation of the NTP binding site across CoV subgenera and in other viruses [106], compounds targeting viral RdRps can act as broad-spectrum inhibitors and that is why in the case of a newly emerging pathogen they usually are one of the first drug classes tested in drug re-purposing programs.

In the case of CoVs, the presence of a proofreading enzyme, nsp14-ExoN, may provide resistance or elevated tolerance to antiviral nucleoside analogues. Therefore, in order to efficiently inhibit CoVs, compounds should be incorporated by the RdRp while evading ExoN-mediated excision, or at least be incorporated at a much higher rate than ExoN can use to remove them. NHC displays a high resistance to ExoN excision, introducing an intolerable number of mutations in the viral genome at low micromolar concentrations in cell culture [39, 42]. This suggests that this nucleoside analogue is a mutagenic agent promoting lethal mutagenesis. Structural studies demonstrated that the incorporation of nucleoside analogues like remdesivir results in termination of RNA elongation after a limited chain extension (non-obligate termination; Table 1). In this case, the incorporated nucleotide analogue is buried in

the RdRp's active center and prevents the translocation of RNA (stalling) after the incorporation of 3 additional NTPs. This is explained by remdesivir's chemical structure, in which the cyano-group clashes with the RdRp's thumb domain [107, 108]. This may complicate access by the nsp14/nsp10 complex and could allow remdesivir to escape from ExoN-mediated excision [108]. Moreover, this may explain why remdesivir is less efficient in inhibiting wt virus than ExoN-knockout mutants [34].

In order to increase the efficacy of nucleoside analogues to inhibit CoVs, one could target both the RdRp and the ExoN activity using combination therapy. As demonstrated in cell culture, inactivation of ExoN increases the sensitivity of SARS-CoV and MHV to nucleoside analogues, or abrogates the production of viral progeny of other CoVs, including MERS-CoV and SARS-CoV-2 (**chapter IV)**. This suggests that targeting both the RdRp and ExoN is may be a good antiviral strategy. To date, screening of marketed small molecules identified two compounds (ATA and patulin) that efficiently inhibit ExoN activity in biochemical assays at low-micromolar concentrations (calculated EC_{50} values of 1.25 and 20 µM, respectively). However, a high cytotoxicity and poor inhibitory activity were demonstrated in Vero E6 cells infected with SARS-CoV-2 [109]. The nsp14-ExoN of CoVs and other nidovirus members ([110] and **chapter III**) as well as the Ebolavirus nucleoprotein exonuclease [111, 112] belong to the DEDDh family of exonucleases. Therefore, analysis of compounds that target enzymes belonging to this family can lead to the identification of broad-spectrum inhibitors or help to understand the mode of action of prospective molecules. Structure modelling of another DEDDh exonuclease (CRN-4) with inhibitors like ATA, MES and pontacyl violet 6R elucidated the binding at the compound-enzyme interface and identified the residues involved in this interaction [113]. This suggests that targeting nsp14-ExoN activity directly may be possible, although , on the down side, the lack of a pocket in this domain main will remain a major challenge [114].

Table 1- List of nucleoside analogues with described CoVs antiviral activity in infected cells, animal experiments or clinical trials

Compound Name	Derivatives	Analogue of	Proposed mode of action against CoVs	Antiviral effect*	Ref.
Acyclovir (fleximer)	Ganciclovir CMPD3	Guanosine		HIV; VZV; HSV; MERS-CoV; HCoV-NL63	[3, 115, 116]
AT-527	AT-511, AT-9010	Guanosine	Stops elongation of RNA chain	SARS-CoV-2, HCV	[85]
BCX4430 (Galidesivir)		Adenosine	Stops elongation of RNA chain Binds to RdRp	MERS-CoV, SARS-CoV, SARS-CoV-2, influenza	[117, 118]
B-D-N4-hydroxycytidine (NHC)	MK-4482 (Molnupiravir)/ EIDD-2801	Cytidine	Lethal mutagenesis Resistant to ExoN activity	MERS-CoV, SARS-CoV, SARS-CoV-2, HCoV-NL63, HcoV-OC43, VEEV, CHIKV	[39, 42, 119, 120]
Gemcitabine hydrochloride		Cytidine	Stops elongation of RNA chain	MERS-CoV, SARS-CoV, SARS-CoV-2, ZIKV, Influenza	[121-123]
GS-5734 (Remdesivir)	GS-441524	Adenosine	Stops elongation of RNA chain Competition with ATP for RdRp binding Mutagenic potential	MERS-CoV, SARS-CoV, SARS-CoV-2, HcoV-OC43, EBOV	[34, 35]
Mizoribine		Imidazole		SARS-CoV	[124]
Ribavirin		Guanosine	Reduction of NTP pools	MERS-CoV, SARS-CoV, RSV, HCV	[104, 125]
Sofosbuvir		Uridine	Stops elongation of RNA chain	HCV	[118, 126]
T-705 (Favipiravir)	T-1105	Guanosine	Stops elongation of RNA chain Lethal mutagenesis	SARS-CoV-2, Influenza, WNV, HCV	[106, 127-129]
Tenofovir		Adenosine		HIV, HBV	[130]
5-fluorouracil		Uridine	Lethal mutagenesis	SARS-CoV	[104]
6-Azauridine		Uridine		HcoV-NL63	[131]

VEEV, Venezuelan equine encephalitis virus; HBV, hepatitis B virus; VZV, Varicella zoster virus; Ref., references;

Look at the other side of nsp14: N7-MTase as a target

Coronavirus nsp14 is a bi-functional protein known to perform two activities *in vitro*: excision of nucleotides in a 3'-to-5' direction and methylation of the N7 position of the CoV mRNA cap structure, as described in **chapter V**. Presumably, CoVs are dependent on this cap-structure for translation of their genomes into proteins by cellular ribosomes. This 5' cap structure avoids viral mRNA to be recognized as "non-self" by multiple innate immune sensors and protects it from degradation by host 5'-to-3' exoribonucleases. Characterization of N7-MTase mutants revealed that this protein is important for the viability of different CoVs (**chapter V**) and for replication in cell culture [132]. Thus, the CoV N7-MTase may constitute an attractive target for antiviral drug development.

A comparison of allosteric and catalytic pockets of all viral proteins across different α- and β-CoVs revealed that the nsp14-N7MTase is highly conserved, presenting 60% conservation at the amino acid level and (for example) 100% identity between SARS-CoV and SARS-CoV-2 [114]. In addition, the nsp14-N7-MTase domain presents a unique non-Rossmann fold that distinguishes it from the majority of known cellular and viral MTases. To date, the development of different types of assays for characterization and evaluation of N7-MTase activity has been reported, leading to the identification of potential inhibitors targeting this domain, most of them *in vitro* [133-139]. Thus far, three different approaches have been used for developing nsp14-N7-MTase inhibitors. One strategy is the design of compounds directly targeting the N7-MTase, based on the structure of its catalytic pocket, like aurintricarboxylic acid (ATA) and sinefugin. Another approach is to design analogues of SAM, the main methyl donor used by viral and cellular MTases. Consequently, these compounds will act as competitors of MTase SAM-dependent like SAH, which binds more strongly to CoVs MTases than SAM itself [135]. Alternatively, development of inhibitors that can interfere with the production of SAM by targeting molecules involved in its metabolism may reduce its intracellular levels and block (indirectly) MTase activity, like S-adenosylhomocysteine (SAH) or adenosine analogues such as aristeromycin (**chapter VI**). Challenges for the development of specific viral MTase inhibitors include the lack of specificity, high cytotoxicity and poor bio-availability which may have contributed to the poor correlation between results from structural, biochemical and cell-based screening of N7-MTase compounds. This suggests that improved drug design and more-translatable models that can corroborate enzymatic assays with infected cell-based screenings need to be pursued.

Nsp14: the constant gardener promoting viral fitness and fidelity?

The replication of +RNA virus genomes is generally characterized by high error rates, large viral progeny sizes and short replication times [101]. Consequently, a cloud of closely related viral genomes is generated with variable degrees of fitness, the so-called quasispecies population. The accumulation of mutations can result in loss of fitness or error catastrophe, but on the other hand the adaptation of RNA virus population to changing circumstances depends on the generation and selection of beneficial mutations [103]. Distribution of these mutations is unevenly throughout the genome and different factors may contribute to the frequency of mutations derived from low-fidelity RdRps.

The mutation rate is correlated with RdRp speed (rate at which the polymerase incorporates NTPs into the RNA chain during synthesis) and accuracy (selection of the correct NTP according to the Watson-Crick base pair geometry). For CoVs, RdRp speed *in vitro* using the nsp12-nsp7-nsp8$_2$ complex was estimated to range from 10 to 100 nt per second [127]. Compared to the RdRps from e.g. poliovirus, which displays a similar structural organization, the SARS-CoV-2 RdRp is rather fast, presenting a 3 to 10 times higher speed of NTP incorporation [106, 140, 141]. Taking into account that CoV genomes are around 30 kb long instead of the more common 7-15 kb seen in other RNA viruses, it can be presumed that the CoV RdRp is faster. However, *in vitro* data revealed that if this is the case, this appears to come at a cost: an increased level of mismatch incorporation compared to e.g. DENV and other RNA viruses presenting a shorter genome length [96, 142]. The generally restricted genome size of +RNA viruses, below 15 kb in length, is presumably associated with the lack of proofreading mechanisms. This constraint has been linked to having low genetic complexity [143, 144]. Replication fidelity, genome size and complexity are trapped in a triangular relation known as the Eigen paradox [145], which tries to explain the evolutionary state of +RNA genome sizes. In contrast, most nidoviruses, including CoVs, possess a genome larger than 20 kb. The identification of an ExoN domain in all these large-genome nidoviruses and the attribution of a proofreading function to this protein may explain how they balance their RdRp fidelity and genome size [143, 146, 147]. With some exceptions [110], the ExoN enzyme has been mainly characterized for CoVs, as described in **chapter III**.

For two CoVs, the impact of ExoN knock-out mutations on viral RNA synthesis has provided direct experimental evidence that this enzyme boosts replication fidelity. ExoN-knockout mutants of SARS-CoV and MHV displayed an increased mutation frequency compared to the corresponding wt virus [148-150].In contrast, the equivalent mutants of five other CoVs proved to be non-viable: MERS-CoV, SARS-CoV-2 (described in **chapter IV**), HCoV-229E [98], TGEV [151] and IBV (personal communication by E. Bickerton *et al.*, described in [152]). This

extreme phenotypic difference between SARS-CoV and MHV on the one hand and different α-, β- and γ-CoVs on the other hand suggests that the first two viruses may somehow be exceptions to the rule. Although both the MHV and SARS-CoV ExoN knockouts are somewhat crippled in their replication, they can apparently tolerate the impact of the ExoN knockout on virus replication, fidelity and fitness for many passages.

In-depth analysis of the genome of passaged MHV-ExoN-knockout mutants revealed that acquisition of compensatory mutations in different regions of the genome, including nsp12, is critical for viral fitness in the absence of a functional ExoN [153]. Exchanging nsp12 and nsp14 of this MHV-ExoN knockout mutant (including compensatory mutations) for their wt counterparts was detrimental to viral replication and competitive fitness. As reversion of the mutations in the MHV-ExoN knockout mutant was not observed, this suggests that the mutations acquired during passaging adapted the virus to overcome or tolerate the limitations on viral RNA synthesis and replication posed by the selective pressure of having a non-functional or partially functional ExoN. Analysis of intermediate revertants of this MHV ExoN-knockout mutant (D89A/E91A), obtained by single alanine or conservative substitutions of the first two catalytic residues of the DEDDh motif, demonstrated no increased replication or competitive fitness [153]. In addition, it seems that there is no clear benefit for reversion from MHV ExoN-knockout to wt to occur, which might explain why this was not observed, not even after 250 passages [154]. While for MERS-CoV and HCoV-229E conservative and/or alanine mutations were analyzed for each single residue of the DEEDh motif (**chapter IV** and [98]), for SARS-CoV and MHV only substitutions of the first two catalytic residues were evaluated. This leaves the question if replacement of other residues in MHV and SARS-CoV would lead to the same phenotypic profile. Overall, these observations suggest that nsp14 or nsp14-ExoN plays a more direct and basic role that is critical for RNA synthesis and not only correlated with promoting the fidelity of virus replication.

Recently, CoV ExoN was also proposed to play a role in RNA recombination [155]. In viruses with a non-segmented RNA genome, recombination can occur between two distinct RNA molecules (inter-molecular) or within the same RNA molecule (intra-molecular). Two mechanisms have been hypothesized: recombination by template switching and recombination by non-replicative breakage and rejoining [156]. As part of the discontinuous minus-strand RNA synthesis that CoVs employ during the production of their subgenomic RNAs, a form of recombination occurs for which base pairing between complementary TRS sequences (minus body TRS to plus leader TRS) is a crucial determinant. In addition, similar RdRp template switching behavior may lead to the generation of defective genomes with large deletions, which can be replicated *in* trans by the full-length helper virus if they contain

the signals for initiation of RNA synthesis. Therefore, such defective genomes may interfere with virus replication and if they are packaged this yields defective interfering particles, which may be infectious and/or strong inducers of cellular immune responses [157, 158]. Both these processes, production of sgRNAs and of defective genomes, affect the replication of virus. In order to analyze the occurrence of recombination in CoVs, NGS and full-length direct RNA sequencing was performed, which allows correlation of mutations/recombination occurring in the same RNA strand [155, 159, 160]. In these studies, the occurrence of recombination was identified by the formation of junctions, derived from RdRp template jumping or switching between two non-contiguous sequences. From the recombination events, defective viral particles (containing deletions of genomic sequence while retaining 5' and 3' untranslated regions), canonical sgRNAs and alternative sgRNAs were generated. When analyzing the genetic profile of different β-CoVs, MHV, MERS-CoV and SARS-CoV-2, similarities were observed in terms of the position of junctions in the genome, frequency of junctions (proportion of junctions in a population of genomes) and nucleotide composition of junctions. Strikingly, a higher recombination frequency was observed in SARS-CoV-2 samples when compared to MERS-CoV and MHV, which might promote viral sequence variation and adaptation to selective pressures [155]. In this study, a role for CoV ExoN in recombination was proposed based on the reduced recombination frequency observed for an MHV ExoN knockout mutant [155]. Mainly, an increased abundance of canonical and alternative sgRNA was detected in both intracellular and supernatant RNA of MHV-wt. Already, when MHV ExoN-knockout mutants were characterized previously, a reduced abundance of sgRNA 2 was noticed [148]. Moreover, for non-viable HCoV-229E ExoN knockout mutants an increase of the relative amount of sgRNA 4 to 6 and the appearance of an aberrant sized sgRNA 3 was previously reported [98], suggesting that ExoN inactivation can impact sgRNA production. As a proof-reading enzyme ExoN must interact with the RTC and may interfere with some of its other activities e.g. elongation and backtracking ([94, 161] see above). Thus, ExoN may affect RdRp processivity, as proposed in mechanistic models based on the acquired enzyme structures and *in vitro* experiments [161, 162]. Consequently, this might indirectly influence viral recombination and alter the production of defective viral genomes, canonical or non-canonical sgRNAs which subsequently may affect viral progeny viability and infectivity.

THE NEXT CHAPTER – SOME POINTS OF REFLECTION

The on-going COVID-19 crisis revealed the limitations of our knowledge about CoVs and the lack of preparedness for this scale of events. Thus, in the wake of the SARS-CoV-2 pandemic, efforts to understand how CoVs replicate and interact with their host were increased. Looking

at the latest discoveries in CoV molecular biology, obtained using e.g. refined structural and biochemical techniques, it seems only natural that a synergetic translation of *in vitro* models to the context of the infected cell will be explored. Mechanistic studies that unraveled interactions between different replicase subunits demonstrated that the RTC revolves mainly around a subset of subunits: nsp12-nsp8$_2$-nsp7, nsp13, nsp10/nsp14, nsp16/nsp10 and nsp9. Dynamic interactions between these RTC subunits can be (temporarily) established and coordinate all mechanisms around RNA synthesis and post-transcriptional modifications. The identification of potential structural features that mediate these interactions and genetic markers that define functional domains is important to understand how sequential activities are performed. In addition, this can help to appreciate evolutionary pathways. The mechanisms underlying several processes carried out by the CoV RTC remain to be elucidated, such as initiation of RNA synthesis, RdRp template switching during sgRNA synthesis, proof-reading and viral mRNA capping. Taking into consideration the importance of these mechanisms for viral replication (**chapter IV** and **V**), this might define promising new targets for antiviral drug development.

Trying to create broad(er)-spectrum prophylaxis and therapy remains a major goal to solve the current pandemic and prepare for future emerging coronaviruses. The genetic plasticity of +RNA virus genomes presents a challenge for controlling virus spread, retaining vaccine efficacy and the development of efficient antivirals, as it drives the rapid development of escape variants while preserving overall viral fitness. Already, during recent months, a large number of SARS-CoV-2 'variants' have attracted attention, including B.1.1.7 (also known as the British variant), B.1.351 (South African variant), B.1.1.28.P1 (Brazilian variant) and most recently B.1.617 (Indian variant). Many of these are being monitored and characterized to understand their clinical and epidemiological relevance. In general, besides having several poorly understood mutations elsewhere in the genome, these variants carry spike protein mutations that have been flagged for (presumably) enhancing virion infectivity and/or potentially affecting vaccine efficacy and neutralization by therapeutic monoclonal antibodies [163-165]. This emphasizes the urgent need to invest in preparedness through surveillance of circulating viruses, implementation of broad-spectrum antiviral drugs and other therapies, and development of adaptable platform for vaccine production that can be easily deployed to address new SARS-CoV-2 variants (if necessary), other CoVs or at large other viruses. In sum, *an ounce of prevention is worth a pound of cure.*

REFERENCES

1. Weiss, S.R., *Forty years with coronaviruses.* J Exp Med, 2020. **217**(5).
2. Else, H. *How a torrent of COVID science changed research publishing — in seven charts*. 2020 [cited 2021 03-04-2021]; Available from: https://www.nature.com/articles/d41586-020-03564-y.
3. Peters, H.L., et al., *Design, synthesis and evaluation of a series of acyclic fleximer nucleoside analogues with anti-coronavirus activity.* Bioorg Med Chem Lett, 2015. **25**(15): p. 2923-6.
4. Yoon, J.S., et al., *Design, Synthesis, and Anti-RNA Virus Activity of 6'-Fluorinated-Aristeromycin Analogues.* J Med Chem, 2019.
5. Morens, D.M. and A.S. Fauci, *Emerging Pandemic Diseases: How We Got to COVID-19.* Cell, 2020. **183**(3): p. 837.
6. Organization, W.H. *The top 10 causes of death*. 2020 [cited 2021 05-05-2021]; Available from: https://www.who.int/news-room/fact-sheets/detail/the-top-10-causes-of-death.
7. De Clercq, E. and G. Li, *Approved Antiviral Drugs over the Past 50 Years.* Clin Microbiol Rev, 2016. **29**(3): p. 695-747.
8. Li, G. and E. De Clercq, *Therapeutic options for the 2019 novel coronavirus (2019-nCoV).* Nat Rev Drug Discov, 2020. **19**(3): p. 149-150.
9. Zumla, A., et al., *Coronaviruses - drug discovery and therapeutic options.* Nat Rev Drug Discov, 2016. **15**(5): p. 327-47.
10. Thorlund, K., et al., *A real-time dashboard of clinical trials for COVID-19.* Lancet Digit Health, 2020. **2**(6): p. e286-e287.
11. de Wilde, A.H., et al., *Screening of an FDA-approved compound library identifies four small-molecule inhibitors of Middle East respiratory syndrome coronavirus replication in cell culture.* Antimicrob Agents Chemother, 2014. **58**(8): p. 4875-84.
12. Vincent, M.J., et al., *Chloroquine is a potent inhibitor of SARS coronavirus infection and spread.* Virol J, 2005. **2**: p. 69.
13. Keyaerts, E., et al., *In vitro inhibition of severe acute respiratory syndrome coronavirus by chloroquine.* Biochem Biophys Res Commun, 2004. **323**(1): p. 264-8.
14. Kono, M., et al., *Inhibition of human coronavirus 229E infection in human epithelial lung cells (L132) by chloroquine: involvement of p38 MAPK and ERK.* Antiviral Res, 2008. **77**(2): p. 150-2.
15. Wang, M., et al., *Remdesivir and chloroquine effectively inhibit the recently emerged novel coronavirus (2019-nCoV) in vitro.* Cell Res, 2020. **30**(3): p. 269-271.
16. Yao, X., et al., *In Vitro Antiviral Activity and Projection of Optimized Dosing Design of Hydroxychloroquine for the Treatment of Severe Acute Respiratory Syndrome Coronavirus 2 (SARS-CoV-2).* Clin Infect Dis, 2020.
17. Consortium, W.H.O.S.T., et al., *Repurposed Antiviral Drugs for Covid-19 - Interim WHO Solidarity Trial Results.* N Engl J Med, 2021. **384**(6): p. 497-511.
18. Bansal, P., et al., *Hydroxychloroquine: a comprehensive review and its controversial role in coronavirus disease 2019.* Ann Med, 2021. **53**(1): p. 117-134.
19. Hoffmann, M., et al., *Chloroquine does not inhibit infection of human lung cells with SARS-CoV-2.* Nature, 2020. **585**(7826): p. 588-590.
20. Funnell, S.G.P., et al., *Emerging preclinical evidence does not support broad use of hydroxychloroquine in COVID-19 patients.* Nat Commun, 2020. **11**(1): p. 4253.

21. Hoffmann, M., et al., *SARS-CoV-2 Cell Entry Depends on ACE2 and TMPRSS2 and Is Blocked by a Clinically Proven Protease Inhibitor.* Cell, 2020. **181**(2): p. 271-280 e8.
22. Park, J.E., et al., *Proteolytic processing of Middle East respiratory syndrome coronavirus spikes expands virus tropism.* Proc Natl Acad Sci U S A, 2016. **113**(43): p. 12262-12267.
23. Maisonnasse, P., et al., *Hydroxychloroquine use against SARS-CoV-2 infection in non-human primates.* Nature, 2020. **585**(7826): p. 584-587.
24. Munster, V.J., et al., *Respiratory disease in rhesus macaques inoculated with SARS-CoV-2.* Nature, 2020. **585**(7824): p. 268-272.
25. Rosenke, K., et al., *Hydroxychloroquine prophylaxis and treatment is ineffective in macaque and hamster SARS-CoV-2 disease models.* JCI Insight, 2020. **5**(23).
26. Letko, M., A. Marzi, and V. Munster, *Functional assessment of cell entry and receptor usage for SARS-CoV-2 and other lineage B betacoronaviruses.* Nat Microbiol, 2020.
27. de Wilde, A.H., et al., *MERS-coronavirus replication induces severe in vitro cytopathology and is strongly inhibited by cyclosporin A or interferon-alpha treatment.* J Gen Virol, 2013. **94**(Pt 8): p. 1749-1760.
28. Hou, Y.J., et al., *SARS-CoV-2 Reverse Genetics Reveals a Variable Infection Gradient in the Respiratory Tract.* Cell, 2020. **182**(2): p. 429-446 e14.
29. Dijkman, R., et al., *Isolation and characterization of current human coronavirus strains in primary human epithelial cell cultures reveal differences in target cell tropism.* J Virol, 2013. **87**(11): p. 6081-90.
30. Kindler, E., et al., *Efficient replication of the novel human betacoronavirus EMC on primary human epithelium highlights its zoonotic potential.* mBio, 2013. **4**(1): p. e00611-12.
31. Han, Y., et al., *Identification of SARS-CoV-2 inhibitors using lung and colonic organoids.* Nature, 2021. **589**(7841): p. 270-275.
32. Si, L., et al., *Human organ chip-enabled pipeline to rapidly repurpose therapeutics during viral pandemics.* bioRxiv, 2020: p. 2020.04.13.039917.
33. Cevik, M., et al., *Virology, transmission, and pathogenesis of SARS-CoV-2.* BMJ, 2020. **371**: p. m3862.
34. Agostini, M.L., et al., *Coronavirus Susceptibility to the Antiviral Remdesivir (GS-5734) Is Mediated by the Viral Polymerase and the Proofreading Exoribonuclease.* MBio, 2018. **9**(2).
35. Sheahan, T.P., et al., *Broad-spectrum antiviral GS-5734 inhibits both epidemic and zoonotic coronaviruses.* Sci Transl Med, 2017. **9**(396).
36. de Wit, E., et al., *Prophylactic and therapeutic remdesivir (GS-5734) treatment in the rhesus macaque model of MERS-CoV infection.* Proceedings of the National Academy of Sciences, 2020.
37. Beigel, J.H., K.M. Tomashek, and L.E. Dodd, *Remdesivir for the Treatment of Covid-19 - Preliminary Report. Reply.* N Engl J Med, 2020. **383**(10): p. 994.
38. Spinner, C.D., et al., *Effect of Remdesivir vs Standard Care on Clinical Status at 11 Days in Patients With Moderate COVID-19: A Randomized Clinical Trial.* JAMA, 2020. **324**(11): p. 1048-1057.
39. Agostini, M.L., et al., *Small-Molecule Antiviral beta-d-N (4)-Hydroxycytidine Inhibits a Proofreading-Intact Coronavirus with a High Genetic Barrier to Resistance.* J Virol, 2019. **93**(24).

40. Good, S.S., et al., *Preclinical evaluation of AT-527, a novel guanosine nucleotide prodrug with potent, pan-genotypic activity against hepatitis C virus.* PLoS One, 2020. **15**(1): p. e0227104.
41. Good, S.S., et al., *AT-527, a Double Prodrug of a Guanosine Nucleotide Analog, Is a Potent Inhibitor of SARS-CoV-2 In Vitro and a Promising Oral Antiviral for Treatment of COVID-19.* Antimicrob Agents Chemother, 2021. **65**(4).
42. Sheahan, T.P., et al., *An orally bioavailable broad-spectrum antiviral inhibits SARS-CoV-2 in human airway epithelial cell cultures and multiple coronaviruses in mice.* Sci Transl Med, 2020. **12**(541).
43. Ng, D.L., et al., *Clinicopathologic, Immunohistochemical, and Ultrastructural Findings of a Fatal Case of Middle East Respiratory Syndrome Coronavirus Infection in the United Arab Emirates, April 2014.* Am J Pathol, 2016. **186**(3): p. 652-8.
44. Munster, V.J., E. de Wit, and H. Feldmann, *Pneumonia from human coronavirus in a macaque model.* N Engl J Med, 2013. **368**(16): p. 1560-2.
45. de Wit, E., et al., *Middle East respiratory syndrome coronavirus (MERS-CoV) causes transient lower respiratory tract infection in rhesus macaques.* Proc Natl Acad Sci U S A, 2013. **110**(41): p. 16598-603.
46. Hoffmann, M., et al., *The novel coronavirus 2019 (2019-nCoV) uses the SARS-coronavirus receptor ACE2 and the cellular protease TMPRSS2 for entry into target cells.* bioRxiv, 2020.
47. Zhao, G., et al., *A safe and convenient pseudovirus-based inhibition assay to detect neutralizing antibodies and screen for viral entry inhibitors against the novel human coronavirus MERS-CoV.* Virol J, 2013. **10**: p. 266.
48. Hu, J., et al., *Development of cell-based pseudovirus entry assay to identify potential viral entry inhibitors and neutralizing antibodies against SARS-CoV-2.* Genes Dis, 2020. **7**(4): p. 551-557.
49. Yang, L., et al., *Identification of SARS-CoV-2 entry inhibitors among already approved drugs.* Acta Pharmacol Sin, 2020.
50. Huang, S.W., et al., *Assessing the application of a pseudovirus system for emerging SARS-CoV-2 and re-emerging avian influenza virus H5 subtypes in vaccine development.* Biomed J, 2020. **43**(4): p. 375-387.
51. Gordon, D.E., et al., *Comparative host-coronavirus protein interaction networks reveal pan-viral disease mechanisms.* Science, 2020. **370**(6521).
52. Gordon, D.E., et al., *A SARS-CoV-2 protein interaction map reveals targets for drug repurposing.* Nature, 2020. **583**(7816): p. 459-468.
53. de Wilde, A.H., et al., *A Kinome-Wide Small Interfering RNA Screen Identifies Proviral and Antiviral Host Factors in Severe Acute Respiratory Syndrome Coronavirus Replication, Including Double-Stranded RNA-Activated Protein Kinase and Early Secretory Pathway Proteins.* J Virol, 2015. **89**(16): p. 8318-33.
54. Jiang, H.W., et al., *SARS-CoV-2 Orf9b suppresses type I interferon responses by targeting TOM70.* Cell Mol Immunol, 2020. **17**(9): p. 998-1000.
55. Yang, S., et al., *Control of antiviral innate immune response by protein geranylgeranylation.* Sci Adv, 2019. **5**(5): p. eaav7999.
56. Friesland, M., et al., *Sigma-1 receptor regulates early steps of viral RNA replication at the onset of hepatitis C virus infection.* J Virol, 2013. **87**(11): p. 6377-90.

57. Galindez, G., et al., *Lessons from the COVID-19 pandemic for advancing computational drug repurposing strategies.* Nature Computational Science, 2021. **1**(1): p. 33-41.
58. Ziebuhr, J., E.J. Snijder, and A.E. Gorbalenya, *Virus-encoded proteinases and proteolytic processing in the Nidovirales.* J Gen Virol, 2000. **81**(Pt 4): p. 853-79.
59. Gorbalenya, A.E., et al., *Nidovirales: evolving the largest RNA virus genome.* Virus Res, 2006. **117**(1): p. 17-37.
60. Wolff, G., et al., *Double-Membrane Vesicles as Platforms for Viral Replication.* Trends Microbiol, 2020. **28**(12): p. 1022-1033.
61. Snijder, E.J., E. Decroly, and J. Ziebuhr, *The Nonstructural Proteins Directing Coronavirus RNA Synthesis and Processing.* Adv Virus Res, 2016. **96**: p. 59-126.
62. Ulferts, R. and J. Ziebuhr, *Nidovirus ribonucleases: Structures and functions in viral replication.* RNA Biol, 2011. **8**(2): p. 295-304.
63. Posthuma, C.C., A.J.W. Te Velthuis, and E.J. Snijder, *Nidovirus RNA polymerases: Complex enzymes handling exceptional RNA genomes.* Virus Res, 2017. **234**: p. 58-73.
64. Xu, X., et al., *Molecular model of SARS coronavirus polymerase: implications for biochemical functions and drug design.* Nucleic Acids Res, 2003. **31**(24): p. 7117-30.
65. Kirchdoerfer, R.N. and A.B. Ward, *Structure of the SARS-CoV nsp12 polymerase bound to nsp7 and nsp8 co-factors.* Nat Commun, 2019. **10**(1): p. 2342.
66. Gao, Y., et al., *Structure of the RNA-dependent RNA polymerase from COVID-19 virus.* Science, 2020. **368**(6492): p. 779-782.
67. Peng, Q., et al., *Structural and Biochemical Characterization of the nsp12-nsp7-nsp8 Core Polymerase Complex from SARS-CoV-2.* Cell Rep, 2020. **31**(11): p. 107774.
68. Wang, Q., et al., *Structural Basis for RNA Replication by the SARS-CoV-2 Polymerase.* Cell, 2020. **182**(2): p. 417-428 e13.
69. Hillen, H.S., et al., *Structure of replicating SARS-CoV-2 polymerase.* Nature, 2020. **584**(7819): p. 154-156.
70. Yin, W., et al., *Structural basis for inhibition of the RNA-dependent RNA polymerase from SARS-CoV-2 by remdesivir.* Science, 2020. **368**(6498): p. 1499-1504.
71. Yan, L., et al., *Cryo-EM Structure of an Extended SARS-CoV-2 Replication and Transcription Complex Reveals an Intermediate State in Cap Synthesis.* Cell, 2021. **184**(1): p. 184-193 e10.
72. Yan, L., et al., *Architecture of a SARS-CoV-2 mini replication and transcription complex.* Nat Commun, 2020. **11**(1): p. 5874.
73. Chen, J., et al., *Structural Basis for Helicase-Polymerase Coupling in the SARS-CoV-2 Replication-Transcription Complex.* Cell, 2020. **182**(6): p. 1560-1573 e13.
74. Gorbalenya, A.E., et al., *Coronavirus genome: prediction of putative functional domains in the non-structural polyprotein by comparative amino acid sequence analysis.* Nucleic Acids Res, 1989. **17**(12): p. 4847-61.
75. Lehmann, K.C., et al., *Discovery of an essential nucleotidylating activity associated with a newly delineated conserved domain in the RNA polymerase-containing protein of all nidoviruses.* Nucleic Acids Res, 2015. **43**(17): p. 8416-34.
76. Choi, K.H. and M.G. Rossmann, *RNA-dependent RNA polymerases from Flaviviridae.* Curr Opin Struct Biol, 2009. **19**(6): p. 746-51.
77. Subissi, L., et al., *One severe acute respiratory syndrome coronavirus protein complex integrates processive RNA polymerase and exonuclease activities.* Proc Natl Acad Sci U S A, 2014. **111**(37): p. E3900-E3909.

78. Ahn, D.G., et al., *Biochemical characterization of a recombinant SARS coronavirus nsp12 RNA-dependent RNA polymerase capable of copying viral RNA templates.* Arch Virol, 2012. **157**(11): p. 2095-104.
79. Imbert, I., et al., *A second, non-canonical RNA-dependent RNA polymerase in SARS coronavirus.* EMBO J, 2006. **25**(20): p. 4933-42.
80. te Velthuis, A.J., S.H. van den Worm, and E.J. Snijder, *The SARS-coronavirus nsp7+nsp8 complex is a unique multimeric RNA polymerase capable of both de novo initiation and primer extension.* Nucleic Acids Res, 2012. **40**(4): p. 1737-47.
81. Slanina, H., et al., *Coronavirus replication-transcription complex: Vital and selective NMPylation of a conserved site in nsp9 by the NiRAN-RdRp subunit.* Proc Natl Acad Sci U S A, 2021. **118**(6).
82. Paul, A.V. and E. Wimmer, *Initiation of protein-primed picornavirus RNA synthesis.* Virus Res, 2015. **206**: p. 12-26.
83. Gorbalenya, A.E., et al., *The palm subdomain-based active site is internally permuted in viral RNA-dependent RNA polymerases of an ancient lineage.* J Mol Biol, 2002. **324**(1): p. 47-62.
84. Peersen, O.B., *A Comprehensive Superposition of Viral Polymerase Structures.* Viruses, 2019. **11**(8).
85. Shannon, A., et al., *Protein-primed RNA synthesis in SARS-CoVs and structural basis for inhibition by AT-527.* bioRxiv, 2021: p. 2021.03.23.436564.
86. Sola, I., et al., *Continuous and Discontinuous RNA Synthesis in Coronaviruses.* Annu Rev Virol, 2015. **2**(1): p. 265-88.
87. Hu, X., et al., *Mechanism of duplex unwinding by coronavirus nsp13 helicases.* bioRxiv, 2020: p. 2020.08.02.233510.
88. Ivanov, K.A. and J. Ziebuhr, *Human coronavirus 229E nonstructural protein 13: characterization of duplex-unwinding, nucleoside triphosphatase, and RNA 5'-triphosphatase activities.* J Virol, 2004. **78**(14): p. 7833-8.
89. Lisica, A., et al., *Mechanisms of backtrack recovery by RNA polymerases I and II.* Proc Natl Acad Sci U S A, 2016. **113**(11): p. 2946-51.
90. Dulin, D., et al., *Signatures of Nucleotide Analog Incorporation by an RNA-Dependent RNA Polymerase Revealed Using High-Throughput Magnetic Tweezers.* Cell Rep, 2017. **21**(4): p. 1063-1076.
91. Dulin, D., et al., *Backtracking behavior in viral RNA-dependent RNA polymerase provides the basis for a second initiation site.* Nucleic Acids Res, 2015. **43**(21): p. 10421-9.
92. Nudler, E., *RNA polymerase backtracking in gene regulation and genome instability.* Cell, 2012. **149**(7): p. 1438-45.
93. Epshtein, V., et al., *UvrD facilitates DNA repair by pulling RNA polymerase backwards.* Nature, 2014. **505**(7483): p. 372-7.
94. Malone, B., et al., *Structural basis for backtracking by the SARS-CoV-2 replication-transcription complex.* bioRxiv, 2021: p. 2021.03.13.435256.
95. Hillen, H.S., *Structure and function of SARS-CoV-2 polymerase.* Curr Opin Virol, 2021. **48**: p. 82-90.
96. Ferron, F., et al., *Structural and molecular basis of mismatch correction and ribavirin excision from coronavirus RNA.* Proc Natl Acad Sci U S A, 2018. **115**(2): p. E162-E171.

97. Bouvet, M., et al., *RNA 3'-end mismatch excision by the severe acute respiratory syndrome coronavirus nonstructural protein nsp10/nsp14 exoribonuclease complex.* Proc Natl Acad Sci U S A, 2012. **109**(24): p. 9372-9377.
98. Minskaia, E., et al., *Discovery of an RNA virus 3'->5' exoribonuclease that is critically involved in coronavirus RNA synthesis.* Proc Natl Acad Sci U S A, 2006. **103**(13): p. 5108-5113.
99. Ma, Y., et al., *Structural basis and functional analysis of the SARS coronavirus nsp14-nsp10 complex.* Proc Natl Acad Sci U S A, 2015. **112**(30): p. 9436-9441.
100. Moeller, N.H., et al., *Structure and dynamics of SARS-CoV-2 proofreading exoribonuclease ExoN.* bioRxiv, 2021: p. 2021.04.02.438274.
101. Pruijssers, A.J. and M.R. Denison, *Nucleoside analogues for the treatment of coronavirus infections.* Curr Opin Virol, 2019. **35**: p. 57-62.
102. Robson, F., et al., *Coronavirus RNA Proofreading: Molecular Basis and Therapeutic Targeting.* Mol Cell, 2020. **79**(5): p. 710-727.
103. Eigen, M., *Error catastrophe and antiviral strategy.* Proc Natl Acad Sci U S A, 2002. **99**(21): p. 13374-13376.
104. Smith, E.C., et al., *Coronaviruses lacking exoribonuclease activity are susceptible to lethal mutagenesis: evidence for proofreading and potential therapeutics.* PLoS Pathog, 2013. **9**(8): p. e1003565.
105. Jordan, P.C., S.K. Stevens, and J. Deval, *Nucleosides for the treatment of respiratory RNA virus infections.* Antivir Chem Chemother, 2018. **26**: p. 2040206618764483.
106. Shannon, A., et al., *Favipiravir strikes the SARS-CoV-2 at its Achilles heel, the RNA polymerase.* bioRxiv, 2020.
107. Bravo, J.P.K., et al., *Remdesivir is a delayed translocation inhibitor of SARS-CoV-2 replication.* Mol Cell, 2021. **81**(7): p. 1548-1552 e4.
108. Kokic, G., et al., *Mechanism of SARS-CoV-2 polymerase stalling by remdesivir.* Nat Commun, 2021. **12**(1): p. 279.
109. Canal, B., et al., *Identifying SARS-CoV-2 Antiviral Compounds by Screening for Small Molecule Inhibitors of Nsp14/nsp10 Exoribonuclease.* bioRxiv, 2021: p. 2021.04.07.438812.
110. Durzynska, I., et al., *Characterization of a bafinivirus exoribonuclease activity.* J Gen Virol, 2018. **99**(9): p. 1253-1260.
111. Hastie, K.M., et al., *Structural basis for the dsRNA specificity of the Lassa virus NP exonuclease.* PLoS One, 2012. **7**(8): p. e44211.
112. Yekwa, E., et al., *Arenaviridae exoribonuclease presents genomic RNA edition capacity.* bioRxiv, 2019: p. 541698.
113. Huang, K.W., et al., *Identification of Inhibitors for the DEDDh Family of Exonucleases and a Unique Inhibition Mechanism by Crystal Structure Analysis of CRN-4 Bound with 2-Morpholin-4-ylethanesulfonate (MES).* J Med Chem, 2016. **59**(17): p. 8019-29.
114. Yazdani, S., et al., *The SARS-CoV-2 replication-transcription complex is a priority target for broad-spectrum pan-coronavirus drugs.* bioRxiv, 2021: p. 2021.03.23.436637.
115. Vanpouille, C., et al., *A new class of dual-targeted antivirals: monophosphorylated acyclovir prodrug derivatives suppress both human immunodeficiency virus type 1 and herpes simplex virus type 2.* J Infect Dis, 2010. **201**(4): p. 635-43.

116. Wada-Shimosato, Y., et al., *Effectiveness of acyclovir prophylaxis against varicella zoster virus disease after allogeneic hematopoietic cell transplantation: A systematic review and meta-analysis.* Transpl Infect Dis, 2019. **21**(3): p. e13061.
117. Taylor, R., et al., *BCX4430 - A broad-spectrum antiviral adenosine nucleoside analog under development for the treatment of Ebola virus disease.* J Infect Public Health, 2016. **9**(3): p. 220-6.
118. Elfiky, A.A., *Ribavirin, Remdesivir, Sofosbuvir, Galidesivir, and Tenofovir against SARS-CoV-2 RNA dependent RNA polymerase (RdRp): A molecular docking study.* Life Sci, 2020. **253**: p. 117592.
119. Wahl, A., et al., *SARS-CoV-2 infection is effectively treated and prevented by EIDD-2801.* Nature, 2021.
120. Cox, R.M., J.D. Wolf, and R.K. Plemper, *Therapeutically administered ribonucleoside analogue MK-4482/EIDD-2801 blocks SARS-CoV-2 transmission in ferrets.* Nat Microbiol, 2021. **6**(1): p. 11-18.
121. Dyall, J., et al., *Repurposing of clinically developed drugs for treatment of Middle East respiratory syndrome coronavirus infection.* Antimicrob Agents Chemother, 2014. **58**(8): p. 4885-93.
122. Jang, Y., et al., *Comparison of Antiviral Activity of Gemcitabine with 2'-Fluoro-2'-Deoxycytidine and Combination Therapy with Remdesivir against SARS-CoV-2.* Int J Mol Sci, 2021. **22**(4).
123. Zhang, Y.N., et al., *Gemcitabine, lycorine and oxysophoridine inhibit novel coronavirus (SARS-CoV-2) in cell culture.* Emerg Microbes Infect, 2020. **9**(1): p. 1170-1173.
124. Saijo, M., et al., *Inhibitory effect of mizoribine and ribavirin on the replication of severe acute respiratory syndrome (SARS)-associated coronavirus.* Antiviral Res, 2005. **66**(2-3): p. 159-63.
125. Chan, J.F., et al., *Broad-spectrum antivirals for the emerging Middle East respiratory syndrome coronavirus.* J Infect, 2013. **67**(6): p. 606-16.
126. Liu, S., et al., *Evaluation of 19 antiviral drugs against SARS-CoV-2 Infection.* bioRxiv, 2020: p. 2020.04.29.067983.
127. Shannon, A., et al., *Rapid incorporation of Favipiravir by the fast and permissive viral RNA polymerase complex results in SARS-CoV-2 lethal mutagenesis.* Nat Commun, 2020. **11**(1): p. 4682.
128. de Avila, A.I., et al., *Lethal Mutagenesis of Hepatitis C Virus Induced by Favipiravir.* PLoS One, 2016. **11**(10): p. e0164691.
129. Escribano-Romero, E., et al., *Extinction of West Nile Virus by Favipiravir through Lethal Mutagenesis.* Antimicrob Agents Chemother, 2017. **61**(11).
130. Batalha, P.N., et al., *Drug repurposing for the treatment of COVID-19: Pharmacological aspects and synthetic approaches.* Bioorg Chem, 2021. **106**: p. 104488.
131. Pyrc, K., et al., *Inhibition of human coronavirus NL63 infection at early stages of the replication cycle.* Antimicrob Agents Chemother, 2006. **50**(6): p. 2000-8.
132. Case, J.B., et al., *Mutagenesis of S-adenosyl-l-methionine-binding residues in coronavirus nsp14 N7-methyltransferase demonstrates differing requirements for genome translation and resistance to innate immunity.* J Virol, 2016. **90**(16): p. 7248-7256.

133. Devkota, K., et al., *Probing the SAM Binding Site of SARS-CoV-2 nsp14 in vitro Using SAM Competitive Inhibitors Guides Developing Selective bi-substrate Inhibitors.* bioRxiv, 2021: p. 2021.02.19.424337.
134. Basu, S., et al., *Identification of SARS-CoV-2 Antiviral Compounds by Screening for Small Molecule Inhibitors of the nsp14 RNA Cap Methyltransferase.* bioRxiv, 2021: p. 2021.04.07.438810.
135. Aouadi, W., et al., *Toward the identification of viral cap-methyltransferase inhibitors by fluorescence screening assay.* Antiviral Res, 2017. **144**: p. 330-339.
136. Pearson, L.A., et al., *Development of a High-Throughput Screening Assay to Identify Inhibitors of the SARS-CoV-2 Guanine-N7-Methyltransferase Using RapidFire Mass Spectrometry.* SLAS Discov, 2021: p. 24725552211000652.
137. Sun, Y., et al., *Yeast-based assays for the high-throughput screening of inhibitors of coronavirus RNA cap guanine-N7-methyltransferase.* Antiviral Res, 2014. **104**: p. 156-64.
138. Ahmed-Belkacem, R., et al., *Synthesis of adenine dinucleosides SAM analogs as specific inhibitors of SARS-CoV nsp14 RNA cap guanine-N7-methyltransferase.* Eur J Med Chem, 2020. **201**: p. 112557.
139. Krafcikova, P., et al., *Structural analysis of the SARS-CoV-2 methyltransferase complex involved in RNA cap creation bound to sinefungin.* Nat Commun, 2020. **11**(1): p. 3717.
140. Gohara, D.W., J.J. Arnold, and C.E. Cameron, *Poliovirus RNA-dependent RNA polymerase (3Dpol): kinetic, thermodynamic, and structural analysis of ribonucleotide selection.* Biochemistry, 2004. **43**(18): p. 5149-58.
141. Jin, Z., et al., *Assembly, purification, and pre-steady-state kinetic analysis of active RNA-dependent RNA polymerase elongation complex.* J Biol Chem, 2012. **287**(13): p. 10674-10683.
142. Sanjuan, R., et al., *Viral mutation rates.* J Virol, 2010. **84**(19): p. 9733-9748.
143. Nga, P.T., et al., *Discovery of the first insect nidovirus, a missing evolutionary link in the emergence of the largest RNA virus genomes.* PLoS Pathog, 2011. **7**(9): p. e1002215.
144. Lauber, C., et al., *The footprint of genome architecture in the largest genome expansion in RNA viruses.* PLoS Pathog, 2013. **9**(7): p. e1003500.
145. Eigen, M., *Selforganization of matter and the evolution of biological macromolecules.* Naturwissenschaften, 1971. **58**(10): p. 465-523.
146. Bukhari, K., et al., *Description and initial characterization of metatranscriptomic nidovirus-like genomes from the proposed new family Abyssoviridae, and from a sister group to the Coronavirinae, the proposed genus Alphaletovirus.* Virology, 2018. **524**: p. 160-171.
147. Saberi, A., et al., *A planarian nidovirus expands the limits of RNA genome size.* PLoS Pathog, 2018. **14**(11): p. e1007314.
148. Eckerle, L.D., et al., *High fidelity of murine hepatitis virus replication is decreased in nsp14 exoribonuclease mutants.* J Virol, 2007. **81**(22): p. 12135-12144.
149. Eckerle, L.D., et al., *Effects of mutagenesis of murine hepatitis virus nsp1 and nsp14 on replication in culture.* Adv Exp Med Biol, 2006. **581**: p. 55-60.
150. Eckerle, L.D., et al., *Infidelity of SARS-CoV Nsp14-exonuclease mutant virus replication is revealed by complete genome sequencing.* PLoS Pathog, 2010. **6**(5): p. e1000896.
151. Becares, M., et al., *Mutagenesis of coronavirus nsp14 reveals its potential role in modulation of the innate immune response.* J Virol, 2016. **90**(11): p. 5399-5414.

152. Ogando, N.S., et al., *The enzymatic activity of the nsp14 exoribonuclease is critical for replication of MERS-CoV and SARS-CoV-2.* J Virol, 2020.
153. Graepel, K.W., et al., *Fitness barriers limit reversion of a proofreading-deficient coronavirus.* J Virol, 2019. **93**(20): p. e00711-19.
154. Graepel, K.W., et al., *Proofreading-deficient coronaviruses adapt for increased fitness over long-term passage without reversion of exoribonuclease-inactivating mutations.* MBio, 2017. **8**(6): p. e01503-01517.
155. Gribble, J., et al., *The coronavirus proofreading exoribonuclease mediates extensive viral recombination.* PLoS Pathog, 2021. **17**(1): p. e1009226.
156. Graham, R.L. and R.S. Baric, *Recombination, reservoirs, and the modular spike: mechanisms of coronavirus cross-species transmission.* J Virol, 2010. **84**(7): p. 3134-46.
157. Sun, Y., et al., *Immunostimulatory Defective Viral Genomes from Respiratory Syncytial Virus Promote a Strong Innate Antiviral Response during Infection in Mice and Humans.* PLoS Pathog, 2015. **11**(9): p. e1005122.
158. Vasilijevic, J., et al., *Reduced accumulation of defective viral genomes contributes to severe outcome in influenza virus infected patients.* PLoS Pathog, 2017. **13**(10): p. e1006650.
159. Gribble, J., et al., *The coronavirus proofreading exoribonuclease mediates extensive viral recombination.* bioRxiv, 2020: p. 2020.04.23.057786.
160. Viehweger, A., et al., *Direct RNA nanopore sequencing of full-length coronavirus genomes provides novel insights into structural variants and enables modification analysis.* Genome Res, 2019. **29**(9): p. 1545-1554.
161. Bera, S.C., et al., *The nucleotide addition cycle of the SARS-CoV-2 polymerase.* bioRxiv, 2021: p. 2021.03.27.437309.
162. Seifert, M., et al., *Inhibition of SARS-CoV-2 polymerase by nucleotide analogs: a single molecule perspective.* bioRxiv, 2021.
163. Planas, D., et al., *Sensitivity of infectious SARS-CoV-2 B.1.1.7 and B.1.351 variants to neutralizing antibodies.* Nat Med, 2021.
164. Wang, P., et al., *Increased resistance of SARS-CoV-2 variant P.1 to antibody neutralization.* Cell Host Microbe, 2021.
165. Hoffmann, M., et al., *SARS-CoV-2 variants B.1.351 and P.1 escape from neutralizing antibodies.* Cell, 2021.

Abbreviation	Meaning
+RNA	positive-sense single-stranded RNA
5-FU	5-fluoro-uracil
aa	amino acid
ACE2	angiotensin-converting enzyme 2
APN	aminopeptidase N
ARDS	acute respiratory distress syndrome
ATA	aurintricarboxylic acid
BCoV	bovine coronavirus
BwCoV	Beluga whale coronavirus
CCoV	canine coronavirus
cDNA	complementary DNA
CEACAM	carcinoembryonic antigen-related adhesion molecules
CHO	chloroquine
CL^{pro}	chymotrypsin-like protease
CNI	calcineurin inhibitors
CoV	coronavirus
COVID-19	coronavirus disease 2019
CPE	cytopathic effect
Cryo-EM	cryo-electron microscopy
CsA	cycloporine A
CTD	C-terminal domain
Cyp	cyclophilin
DENV	Dengue virus
DFA	6’,6’-difluoro-aristeromycin
DMV	double-membrane vesicles
dpi or d p.i.	days post infection
DPP4	dipeptidyl peptidase 4
dpt or d p.t.	days post transfection
ds	double-stranded
E	envelope protein
EAV	equine arteritis virus
EBOV	Ebola virus
EMA	European Medicines Agency
EMC	Erasmus Medical Center
EndoU	endoribonuclease
EqCoV	equine coronavirus
ER	endoplasmic reticulum
ERGIC	endoplasmic reticulum-Golgi intermediate compartment
EVL	everolimus
ExoN	exoribonuclease
FeCoV	feline enteric coronavirus
FIPV	feline infectious peritonitis virus
GMP, GDP, GTP	guanosine mono-, di-, triphosphate

gRNA	genomic RNA
GTase	guanylyltransferase
HAE	human airway epithelial cells
HBV	hepatitis B virus
HCoV-229E	human coronavirus 229E
HCoV-HKU1	human coronavirus HKU1
HCoV-NL63	human coronavirus NL63
HCoV-OC43	human coronavirus OC43
HCV	hepatitis C virus
HEL	helicase
HIV	human immunodeficiency virus
hpi or h p.i.	hours post infection
HR	heptad repeat
HTS	high-throughput screening
IBV	infectious bronchitis virus
ICTV	International Committee on Taxonomy of viruses
IFN	interferon
k/d	knockdown
k/o	knockout
kb	kilobase
kDa	kilodalton
KTR	kidney transplant recipients
LUMC	Leiden University Medical Center
M	membrane protein
MERS	Middle East respiratory syndrome
MHV	mouse hepatitis virus
MMF	mycophenolate mofetil
MoA	mode of action
MOI	multiplicity of infection
Mpro	main protease
MPA	mycophenolic acid
mRNA	messenger RNA
N	nucleocapsid protein
N7-Mtase	N7-guanine methyltransferase
NGS	next generation sequencing
NHC	N4-hydroxycytidine
NiRAN	Nidovirus RdRp-associated nucleotidyl transferase domain
nsp	non-structural protein
nt	nucleotide
NTD	N-terminal domain
NTP	nucleoside triphosphate
O2-Mtase or 2'-O-MTase	2'-O-methyltransferase
ORF	open reading frame
PDB	Protein Data Bank

PDCoV	porcine deltacoronavirus
pDFA	monophosphoramidate 6',6'-Difluoro-aristeromycin
PEDV	porcine epidemic diarrhea virus
PFU	plaque forming unit
PhCoV	pheasant coronavirus
PHEV	porcine hemagglutinating encephalomyelitis virus
PL^{pro}	papain-like protease
pp	polyprotein
PSCNV	planarian secretory cell nidovirus
RbCoV	rabbit coronavirus
RBD	receptor binding domain
RCoV	rat coronavirus
RdRp	RNA-dependent RNA polymerase
RDV	remdesivir
RNA	ribonucleic acid
RO	replication organelle
RSV	respiratory syncytial virus
RTC	replication and transcription complex
rwt	recombinant wild-type virus
S	spike protein
SAH	S-adenosylhomocysteine
SAM	S-adenosylmethionine
SARS	severe acute respiratory syndrome
SARS-CoV-2	severe acute respiratory syndrome coronavirus 2
sg	subgenomic
ss	single-stranded
TAC	Tacrolimus
TGEV	transmissible gastroenteritis virus
TMPRSS2	transmembrane protease serine 2
TPase	triphosphatase
TRS	transcription-regulating sequence
TuCoV	turkey coronavirus
UMP, UDP, UTP	uridine mono-, di- triphosphate
VCS	voclosporin
VEEV	Venezuelan equine encephalitis virus
VZV	Varicella zoster virus
WNV	West Nile virus
wt	wild type
ZBD	zinc binding domain
ZF	zinc finger
ZIKV	Zika virus

ENGLISH SUMMARY

Up to the present time, seven coronavirus (CoVs) that can infect humans have been identified: four endemic human CoVs (229E, NL63, OC43 and HKU1), responsible for common cold symptoms, and three zoonotic CoVs (SARS-CoV, MERS-CoV and SARS-CoV-2) that can cause severe disease. The latter viruses emerged in the last 20 years. The potential for zoonotic transmission and global spread demonstrated by the pandemic SARS-CoV-2, and its burden on public health, have emphasized the critical need to develop highly efficacious strategies for prophylaxis and therapy of infections with CoVs at large. In **chapter I**, a timeline of CoV discovery and a broader overview of their biology, replication cycle, and pathogenesis are presented. Furthermore, some findings regarding vaccine development and antiviral and antibody therapies are highlighted.

The research described in this PhD thesis was largely dedicated to the quest for broad-spectrum CoV inhibitors. In the beginning of this project, compounds were tested mainly in cells infected with MERS-CoV, whereas after February 2020 the evaluation of antiviral activity against SARS-CoV-2 was also included. **Chapter II** describes the characterization of some of the first SARS-CoV-2 isolates and the adaptation of *in-house* phenotypic screening assays to determine the sensitivity of SARS-CoV-2 to different inhibitors such as remdesivir, alisporivir, chloroquine, and pegylated interferon alpha. This type of assays was used in **chapters VI** and **VII** to evaluate the inhibitory effect of 6',6'-difluoro-aristeromycin (DFA) and FDA-approved compounds, respectively. In **chapter VI**, DFA, a small molecule originally designed to target S-adenosylhomocysteine (SAH) hydrolase was characterized by phenotypic studies and genotyping of drug-resistant mutants. This compound can strongly inhibit MERS-CoV replication and completely abrogate the production of viral progeny at low-micromolar concentrations. Based on our results, we hypothesize that this small molecule may affect intracellular levels of the methyl donor S-adenosylmethionine, which is used by the two CoV methyltransferases involved in the processing of the cap that is present at the 5'-end of all viral mRNAs. The cap structure is important for translation of viral mRNAs by host ribosomes, protection of these RNAs from exoribonuclease hydrolase activity, and escape from immune sensors. In **chapter VII,** calcineurin inhibitors (CNI) that possess antiviral activity against RNA viruses were tested against SARS-CoV-2. Cyclosporine A (CsA, a known broad-spectrum inhibitor of human and zoonotic CoVs) and voclosporin (VCS, a novel CNI structurally similar to CsA), were demonstrated to have antiviral activity against SARS-CoV-2. In particular, VCS reduced the SARS-CoV-2 load in lung cells at concentrations that are safe in humans and at lower concentrations than CsA and tacrolimus (TAC). The efficacy of approved vaccines is yet uncertain in kidney transplant recipients (KTRs), in which immunosuppressive and non-

immunosuppressive therapies like CsA and TAC are commonly administered to prevent rejection of the transplant. Based on our *in vitro* experimental data, we argue that there may be a potential benefit of the use of VCS to treat COVID-19 in KTRs undergoing an immunosuppressive regimen. These data warranted the further clinical investigation of VCS in SARS-CoV-2-infected KTRs, which is currently in progress.

The development of antiviral therapies requires a detailed understanding of CoV replication and its interplay with host cells. SARS-CoV and SARS-CoV-2 belong to the same CoV species, showing a limited genetic distance and essentially the same genome organization. In order to understand potential differences between SARS-CoV and SARS-CoV-2 replication in infected cells, a comparison of various replication features was performed, including RNA synthesis, the production of viral progeny, and cytopathology upon infection (using electron microscopy and immunolabelling), which is described in **chapter II**. One important difference between these two viruses is the presence of a "furin-like cleavage site" in the region connecting the S1 and S2 domains of the SARS-CoV-2 Spike (S) protein. Adaptative mutations in this S region evolved upon passaging of SARS-CoV-2 in Vero E6 cells (the most common cell line used), resulting in phenotypic changes. According to other studies, the change or loss of this site can potentially affect infection efficiency in other (more relevant) cell lines, e.g., lung cells. Over the past three decades, CoV replicase proteins have been characterized using a combination of bioinformatics, biochemistry, structural biology, and (reverse) genetics. **Chapters III** to **V** describe the in-depth characterization of CoV nsp14, one of the enzymatic components of the replication and transcription complex (RTC), which provided evidence for its importance for virus viability and fitness, while also establishing that nsp14 might be a good target for drug design. This bifunctional protein contains 3'-to-5' exoribonuclease (ExoN) and guanine-N7-methyltransferase (N7-MTase) domains that are described in **chapters IV** and **V,** respectively. Supported by the increasing availability of structural information for SARS-CoV nsp14, key residues of both nsp14 domains were identified and their importance was probed by site-directed mutagenesis. Phenotypes of engineered mutant CoVs, launched from cloned cDNA templates, were analyzed, as well as enzymatic activities of corresponding recombinant proteins using *in vitro* assays. The data in **Chapter IV** demonstrate that CoV nsp14 ExoN activity is critical for primary viral RNA synthesis and apparently has an additional role in viral replication, besides mediating error-correction (proofreading) of mismatches incorporated by the viral polymerase during genome replication. It was found that both MERS-CoV and SARS-CoV-2 cannot tolerate an ExoN knockout mutation, in contrast to what was previously reported for MHV and SARS-CoV. In **Chapter V,** evidence is presented that also the nsp14 N7-MTase domain/activity is important for *Betacoronavirus* viability and that there might be

structural differences between MHV, SARS-CoV, SARS-CoV-2, and MERS-CoV, despite the strong conservation of the N7-MTase amino acid sequence. Three substitutions led to the same phenotypic profile and they define key residues of the N7-MTase catalytic pocket that can be targeted to design inhibitors with a potential pan-coronaviral activity spectrum. Mechanistic hypotheses on how nsp14 interacts with other subunits of the RTC during RNA synthesis and post-transcriptional processes are described in **chapter VIII**. Additionally, in this concluding chapter, the history of unsuccessful CoV-targeting antivirals is briefly summarized, together with possible new approaches in antiviral research. Lastly, some prospects for future research are outlined.

NEDERLANDSE SAMENVATTING

Tot op heden zijn zeven coronavirussen (CoV's) geïdentificeerd die mensen kunnen infecteren: vier endemische humane CoV's (229E, NL63, OC43 en HKU1), verantwoordelijk voor verkoudheidssymptomen, en drie zoönotische CoV's (SARS-CoV, MERS- CoV en SARS-CoV-2) die ernstige ziekte kunnen veroorzaken. De laatstgenoemde virussen zijn in de afgelopen 20 jaar ontstaan. Het potentieel voor zoönotische overdracht en wereldwijde verspreiding, aangetoond door de SARS-CoV-2 pandemie, en de belasting voor de gezondheidszorg die dit heeft veroorzaakt, benadrukken de noodzaak van de ontwikkeling van zeer effectieve strategieën voor profylaxe en de behandeling van CoV infecties in het algemeen. In **hoofdstuk I** wordt een tijdlijn van de ontdekking van CoV's gegeven, samen met een breder overzicht van hun biologie, replicatiecyclus en pathogenese. Verder worden enkele bevindingen met betrekking tot de ontwikkeling van vaccins en therapieën met virusremmers en antilichamen benadrukt.

Het onderzoek beschreven in dit proefschrift was grotendeels gewijd aan de zoektocht naar breed-spectrum CoV-remmers. In het begin van dit project werden verbindingen voornamelijk getest in cellen die waren geïnfecteerd met MERS-CoV, terwijl vanaf februari 2020 ook de evaluatie van antivirale activiteit tegen SARS-CoV-2 in deze zoektocht werd opgenomen. **Hoofdstuk II** beschrijft de karakterisering van enkele van de eerste SARS-CoV-2-isolaten en het geschikt maken van een zelf-ontwikkelde fenotypische screeningsassay om de gevoeligheid van SARS-CoV-2 voor verschillende remmers te bepalen, zoals remdesivir, alisporivir, chloroquine en gepegyleerd interferon alfa. Dit type assay is gebruikt in **hoofdstukken VI** en **VII** van dit proefschrift om het remmende effect van respectievelijk 6',6'-difluor-aristeromycine (DFA) en FDA-goedgekeurde verbindingen te evalueren. In **hoofdstuk VI** werd DFA, een klein molecuul dat oorspronkelijk ontworpen was om S-adenosylhomocysteïne (SAH) hydrolase te remmen, gekarakteriseerd door middel van fenotypische studies en de genotypische karakterisering van resistente mutanten. Deze verbinding is in staat MERS-CoV-replicatie sterk te remmen en de productie van viraal nageslacht volledig te blokkeren bij laag-micromolaire concentraties. Op basis van onze resultaten veronderstellen we dat dit kleine molecuul de intracellulaire concentraties kan beïnvloeden van de methyldonor S-adenosylmethionine, die wordt gebruikt door de twee coronavirale methyltransferases die betrokken zijn bij het genereren van de cap-structuur die aanwezig is op het 5'-uiteinde van alle virale mRNA's. De cap-structuur is belangrijk voor de translatie van virale mRNA's door de ribosomen van de gastheer, bescherming van deze RNA's tegen hydrolase-activiteit van exoribonucleases en ontsnapping aan immuunsensoren. In **hoofdstuk VII** werden calcineurineremmers (CNI) met antivirale activiteit tegen RNA-virussen

getest tegen SARS-CoV-2. Van cyclosporine A (CsA, een bekende breedspectrumremmer van humane en zoönotische CoV's) en voclosporine (VCS, een nieuwe CNI die structureel vergelijkbaar is met CsA) werd aangetoond dat ze antivirale activiteit hebben tegen SARS-CoV-2. In het bijzonder verminderde VCS de SARS-CoV-2 replicatie in longcellen bij concentraties die veilig zijn voor mensen en bij lagere concentraties van dan CsA en tacrolimus (TAC). De werkzaamheid van goedgekeurde vaccins is nog onzeker bij ontvangers van niertransplantaties (KTR's), bij wie immunosuppressieve en niet-immunosuppressieve therapieën zoals CsA en TAC vaak worden toegediend om afstoting van het donororgaan te voorkomen. Op basis van onze in vitro experimentele data stellen we dat er een mogelijk voordeel kan zijn van het gebruik van VCS voor de behandeling van COVID-19 in KTR's onder een immunosuppressief regime. Deze gegevens rechtvaardigen verder klinisch onderzoek van VCS in met SARS-CoV-2 geïnfecteerde KTR's, dat momenteel in gang is gezet.

De ontwikkeling van antivirale therapieën vereist een gedetailleerd begrip van CoV-replicatie en het samenspel van het virus met gastheercellen. SARS-CoV en SARS-CoV-2 behoren tot dezelfde CoV-soort, staan op beperkte genetische afstand van elkaar en hebben in essentie dezelfde genoomorganisatie. Om mogelijke verschillen tussen SARS-CoV- en SARS-CoV-2-replicatie in geïnfecteerde cellen te begrijpen, werd een vergelijking gemaakt van verschillende replicatiekenmerken, waaronder RNA-synthese, de productie van nieuwe virusdeeltjes en de cytopathologie na infectie (met behulp van elektronenmicroscopie en immunolabeling), beschreven in **hoofdstuk II**. Een belangrijk verschil tussen deze twee virussen is de aanwezigheid van een "furine-achtige klievingsplaats" in het gebied dat de S1- en S2-domeinen van het SARS-CoV-2 Spike (S)-eiwit verbindt. Adaptieve mutaties in dit S-gebied ontstonden na passage van SARS-CoV-2 in Vero E6-cellen (de meest gebruikte cellijn), wat resulteerde in fenotypische veranderingen. Uit andere onderzoeken blijkt dat de verandering of het verlies van deze site mogelijk van invloed zijn op de infectie-efficiëntie in andere (relevantere) cellijnen, bijvoorbeeld longcellen. In de afgelopen drie decennia zijn CoV-replicase-eiwitten gekarakteriseerd met behulp van een combinatie van bio-informatica, biochemie, structuurbiologie en (reverse) genetica. **Hoofdstukken III tot V** beschrijven de diepgaande karakterisering van CoV nsp14, één van de enzymatische componenten van het replicatie- en transcriptiecomplex (RTC), die bewijs leverde voor het belang van nsp14 voor de levensvatbaarheid en de fitness van het virus, terwijl ook werd vastgesteld dat nsp14 een goed doelwit zou kunnen zijn voor het ontwerpen van virusremmers. Dit bifunctionele eiwit bevat 3’-naar-5’ exobonuclease (ExoN) en guanine-N7-methyltransferase (N7-MTase) domeinen die respectievelijk worden beschreven in **hoofdstuk IV en V**. Ondersteund door de toenemende beschikbaarheid van structurele informatie voor SARS-CoV nsp14, werden

sleutelresiduen van beide nsp14-domeinen geïdentificeerd en onderzocht door plaatsgerichte mutagenese. Het fenotype van mutante CoV's, gelanceerd vanaf gekloonde cDNA-templates, werd geanalyseerd, evenals de enzymatische activiteit van de overeenkomstige recombinante eiwitten met behulp van in vitro-assays . De gegevens in **Hoofdstuk IV** laten zien dat CoV nsp14 ExoN-activiteit cruciaal is voor de primaire virale RNA-synthese en blijkbaar een extra rol speelt, naast het corrigeren van mismatches (proofreading) die tijdens genoomreplicatie door het virale polymerase zijn ingebouwd. Bovendien bleek dat zowel MERS-CoV als SARS-CoV-2 een ExoN-knockout-mutatie in het genoom niet kunnen verdragen, in tegenstelling tot wat eerder is beschreven voor MHV en SARS-CoV. In **Hoofdstuk V** wordt bewijs gepresenteerd dat ook het nsp14 N7-MTase domein/activiteit belangrijk is voor de levensvatbaarheid van bètacoronavirussen en dat er structurele verschillen kunnen zijn tussen N7-MTase van MHV, SARS-CoV, SARS-CoV-2 en MERS-CoV, ondanks de sterke conservering van de aminozuursequentie. Drie substituties leidden tot hetzelfde fenotypische profiel en zij definiëren de belangrijkste residuen van de N7-MTase katalytische pocket die kunnen worden gebruikt bij het ontwerpen van remmers met een potentieel pan-coronaviraal activiteitsspectrum. Mechanistische hypothesen over hoe nsp14 interacteert met andere subeenheden van het RTC tijdens RNA-synthese en post-transcriptionele processen worden besproken in **hoofdstuk VIII**. Bovendien wordt in dit afsluitende **hoofdstuk** de geschiedenis van minder- of niet-succesvolle antivirale middelen tegen CoV’s kort samengevat, samen met mogelijke nieuwe benaderingen in antiviraal onderzoek. Tot slot worden enkele vooruitzichten voor toekomstig onderzoek geschetst.

LIST OF PUBLICATIONS

(presented in chronological order)

Jing-Wen Lin[#], Chao Tang[#], Han-Cheng Wei[#], Baowen Du[#], Chuan Chen[#], Minjin Wang[#], Yongzhao Zhou[#], Ming-Xia Yu[#], Lu Cheng[#], Suvi Kuivanen, **Natacha S Ogando**, Lev Levanov, Yuancun Zhao, Chang-Ling Li, Ran Zhou, Zhidan Li, Yiming Zhang, Ke Sun, Chengdi Wang, Li Chen, Xia Xiao, Xiuran Zheng, Sha-Sha Chen, Zhen Zhou, Ruirui Yang, Dan Zhang, Mengying Xu, Junwei Song, Danrui Wang, Yupeng Li, ShiKun Lei, Wanqin Zeng, Qingxin Yang, Ping He, Yaoyao Zhang, Lifang Zhou, Ling Cao, Feng Luo, Huayi Liu, Liping Wang, Fei Ye, Ming Zhang, Mengjiao Li, Wei Fan, Xinqiong Li, Kaiju Li, Bowen Ke, Jiannan Xu, Huiping Yang, Shusen He, Ming Pan, Yichen Yan, Yi Zha, Lingyu Jiang, Changxiu Yu, Yingfen Liu, Zhiyong Xu, Qingfeng Li, Yongmei Jiang, Jiufeng Sun, Wei Hong, Hongping Wei, Guangwen Lu, Olli Vapalahti, Yunzi Luo, Yuquan Wei, Thomas Connor, Wenjie Tan, Eric J Snijder, Teemu Smura, Weimin Li, Jia Geng, Binwu Ying, Lu Chen (2021). Genomic monitoring of SARS-CoV-2 uncovers an Nsp1 deletion variant that modulates type I interferon response. Cell Host Microbe 29(3): 489-502.

Ilaria Manfredonia, Chandran Nithin, Almudena Ponce-Salvatierra, Pritha Ghosh, Tomasz K Wirecki, Tycho Marinus, **Natacha S Ogando**, Eric J Snijder, Martijn J van Hemert, Janusz M Bujnicki, Danny Incarnato (2020). Genome-wide mapping of SARS-CoV-2 RNA structures identifies therapeutically-relevant elements. Nucleic Acids Res. 48(22): 12436-12452.

Natacha S Ogando, Jessika C Zevenhoven-Dobbe, Yvonne van der Meer, Peter J Bredenbeek, Clara C Posthuma[#], Eric J Snijder[#] (2020). The enzymatic activity of the nsp14 exoribonuclease is critical for replication of MERS-CoV and SARS-CoV-2. J. Virol. 94(23):e01246-20.

Natacha S Ogando, Tim J Dalebout, Jessika C Zevenhoven-Dobbe, Ronald W A L Limpens, Yvonne van der Meer, Leon Caly, Julian Druce, Jutte J C de Vries, Marjolein Kikkert, Montserrat Bárcena, Igor Sidorov, Eric J Snijder (2020). SARS-coronavirus-2 replication in Vero E6 cells: replication kinetics, rapid adaptation and cytopathology. J. Gen. Virol. 101(9):925-940.

Clarisse Salgado-Benvindo[#], Melissa Thaler[#], Ali Tas, **Natacha S Ogando**, Peter J Bredenbeek, Dennis K Ninaber, Ying Wang, Pieter S Hiemstra, Eric J Snijder, Martijn J van Hemert (2020). Suramin inhibits SARS-CoV-2 infection in cell culture by interfering with early steps of the replication cycle. Antimicrob. Agents Chemother. 64(8):e00900-00920.

Simon Dirmeier, Christopher Dächert, Martijn van Hemert, Ali Tas, **Natacha S Ogando**, Frank van Kuppeveld, Ralf Bartenschlager, Lars Kaderali, Marco Binder, Niko Beerenwinkel (2020). Host factor prioritization for pan-viral genetic perturbation screens using random intercept models and network propagation. PLoS Comput. Biol. 16(12):e1007587.

Natacha S Ogando, Francois Ferron, Etienne Decroly, Bruno Canard, Clara C Posthuma[#], Eric J Snijder[#] (2019). The curious case of the nidovirus exoribonuclease: its role in RNA synthesis and replication fidelity. Front. Microbiol. 10:1813.

Ji-Seong Yoon, Gyudong Kim, Dnyandev B Jarhad, Hong-Rae Kim, Young-Sup Shin, Shuhao Qu, Pramod K Sahu, Hea Ok Kim, Hyuk Woo Lee, Su Bin Wang, Yun Jeong Kong, Tong-Shin Chang, **Natacha S Ogando**, Kristina Kovacikova, Eric J Snijder, Clara C Posthuma, Martijn J van Hemert, Lak Shin Jeong (2019). Design, synthesis, and anti-RNA virus activity of 6'-fluorinated-aristeromycin analogues. J. Med. Chem. 62(13):6346-5362.

Cláudia I Pereira, João A Graça, **Natacha S Ogando**, Ana M P Gomes, F Xavier Malcata (2010). Influence of bacterial dynamics upon the final characteristics of model Portuguese traditional cheeses. Food Microbiol. 27(3):339-346.

Cláudia I Pereira, João A Graça, **Natacha S Ogando**, Ana M P Gomes, F Xavier Malcata (2009). Bacterial dynamics in model cheese systems, aiming at safety and quality of Portuguese-style traditional ewe's cheeses. J. Food Prot. 72(11):2243-51.

[#] These authors contributed equally to this work.

Natacha Ogando was born in Porto (Sé), Portugal, on January 13th, 1988. In 2005, she started her Bachelor studies in Bioscience with specialization in Microbiology at the Faculty of Biotechnology of the Catholic University of Portugal, where she obtained her degree in 2008. Subsequently, between 2009 and 2012, she studied Virology at the same University and developed a Master project on detection of enteric viruses in environmental and biological samples using molecular biological techniques under the supervision of Prof. Dr. São José Nascimento and Prof. Dr. Ana Gomes. Her Master project included an internship at the Virology department of the Biological Research Center of the University of Santiago de Compostela. While writing her Master thesis, she contributed as a researcher to the identification and study of microorganisms in the development of ectomycorrhizas at the Centre of Biotechnology and Fine Chemistry of the Catholic University of Portugal. In 2012, she performed an internship at the Molecular Biology Department of Genentech, working on the identification of targets of lung adenocarcinoma using *in vivo* models. Next, she accepted a position at MedImmune where she worked in the research department, developing seasonal influenza live-attenuated vaccines. In 2015, she was awarded a PhD fellowship integrated in the Marie Skłodowska-Curie ANTIVIRALS Training Network, supported by the European Union's Horizon 2020 program. Since then, she has been working at the Leiden University Medical Center under the supervision of Dr. Clara Posthuma and Prof. Dr. Eric Snijder, and performed the research described in this thesis. Natacha Ogando's research has focused on the search for coronavirus inhibitors targeting host factors or viral functions that are important for viral replication. Between May 2020 and July 2021, she joined the Swift COronavirus therapeutics REsponse (SCORE) project funded by the European Union's Horizon 2020 program. From July 2021 onwards, Natacha will look for new challenges to continue her scientific career.